Proactive and Social navigation of autonomous vehicles in shared spaces

Maria Kabtoul

Université Grenoble Alpes

THÈSE

Pour obtenir le grade de

DOCTEUR DE L'UNIVERSITE GRENOBLE ALPES

Spécialité: Informatique

Arrêté ministériel: 25 mai 2016

Présentée par

Maria KABTOUL

Thèse codirigée par **Anne SPALANZANI,** MCF, UGA
et par **Philippe MARTINET,** DR, INRIA

préparée au sein du **Laboratoire Institut National de Recherche en Informatique et en Automatique**
dans **l'École Doctorale Mathématiques, Sciences et technologies de l'information, Informatique**

Navigation sociale et proactive de véhicules autonomes dans des espaces partagés

Proactive and social navigation of autonomous vehicles in shared spaces

Thèse soutenue publiquement le **02/12/2021,**
devant le jury composé de:

Rachid Alami
Directeur de Recherche, LAAS-CNRS, Rapporteur
Alberto Sanfeliu
Professeur des Universités, Universitat Politècnica de Catalunya, Rapporteur
Xavier Alameda-Pineda
Chargé de Recherche, INRIA, Examinateur
Marie Babel
Maître de Conférences, INSA de Rennes, Examinatrice
Vincent Fremont
Professeur des Universités, École Centrale de Nantes, Président
Philippe Martinet
Directeur de Recherche, INRIA, Directeur de thèse
Anne Spalanzani
Maître de Conférences, Université Grenoble Alpes, Directrice de thèse

Abstract

The current trend in electric autonomous vehicles design is based on pre-existing models of cities which have been built for cars. The carbon footprint of cities cannot be reduced until the overall requirement for vehicles is reduced and more green and pedestrianized zones are created for better livability. However, such green zones cannot be scaled without providing autonomous mobility solutions, accessible to people with reduced mobility. Such solutions need to be capable of operating in spaces shared with pedestrians, which makes this a much harder problem to solve as compared to traditional autonomous driving. This thesis serves as a starting point to develop such autonomous mobility solutions. The work is focused on developing a navigation system for autonomous vehicles operating around pedestrians. The suggested solution is a proactive framework capable of anticipating pedestrian reactions and exploiting their cooperation to optimize the performance while ensuring pedestrians safety and comfort.

A cooperation-based model for pedestrian behaviors around a vehicle is proposed. The model starts by evaluating the pedestrian tendency to cooperate with the vehicle by a time-varying factor. This factor is then used in combination with the space measurements to predict the future trajectory. The model is based on social rules and cognitive studies by using the concept of the social zones and then applying the deformable virtual zone concept (DVZ) to measure the resulting influence in each zone. Both parts of the model are learnt using a data-set of pedestrians to vehicle interactions by manually annotating the behaviors in the data-set.

Moreover, the model is exploited in the navigation system to control both the velocity and the local steering of the vehicle. Firstly, the longitudinal velocity is proactively controlled. Two criteria are considered to control the longitudinal velocity. The first is a safety criterion using the minimum distance between an agent and the vehicle's body. The second is proactive criterion using the cooperation measure of the surrounding agents. The latter is essential to exploit any cooperative behavior and avoid the freezing of the vehicle in dense scenarios. Finally, the optimal control is derived using the gradient of a cost function combining the two previous criteria. This is possible thanks to a suggested formulation of the cooperation model using a non-central chi distribution for the distance between the vehicle and an agent.

A smooth steering is derived using a proactive dynamic channel method for the space exploration. The method depends on evaluating the navigation cost in a channel (sub-space) using a fuzzy cost model. The channel with the minimum cost is selected, and a human-like steering is affected using a Quintic spline candidate path between channels. Finally, the local steering is derived using a sliding mode path follower.

The navigation is evaluated using PedSim simulator under ROS in pedestrian-vehicle interaction scenarios. The navigation is tested with different pedestrian density and sparsity. The proactive framework managed to navigate the vehicle producing smooth trajectories while maintaining the pedestrians' safety and reducing the travel time in comparison with traditional reactive methods (Risk-RRT).

Résumé

La tendance actuelle dans la conception des véhicules électriques autonomes est basée sur des modèles préexistants de villes qui ont été construits pour les voitures. L'empreinte carbone des villes ne peut être réduite tant que les besoins globaux en véhicules ne sont pas réduits et que davantage de zones vertes ne soient créées pour une meilleure habitabilité. Cependant, Le nombre de ces zones ne peuvent être augmentées sans fournir des solutions de mobilité autonomes et accessibles à tous. De telles solutions doivent être capables de fonctionner dans des espaces partagés avec les piétons, ce qui rend ce problème beaucoup plus difficile par rapport à la conduite autonome traditionnelle. Comme point de départ pour développer de telles solutions, cette thèse pose des jalons pour développer de telles solutions et se focalise sur la navigation pour les véhicules autonomes à proximité des piétons. La solution proposée est un cadre proactif capable d'anticiper les réactions des piétons et d'exploiter leur coopération pour optimiser la performance tout en assurant leur sécurité.

Dans un premier temps, un modèle de comportement des piétons est proposé. Le modèle commence par évaluer la tendance des piétons à coopérer avec le véhicule par un paramètre dépendant du temps. Cette tendance est ensuite utilisée combinée à des mesures spatiales pour prédire la trajectoire future. Le modèle est basé sur des règles sociales et des études cognitives en utilisant le concept de zones sociales. Il intègre ensuite le concept de zone virtuelle déformable (ZVD) pour mesurer l'influence résultante dans chaque zone. Les deux parties du modèle sont entrainées grâce à un corpus de données vidéos annoté où des piétons interagissent avec un véhicule.

Dans un second temps, La vitesse et les manœuvres du véhicule sont étudiées. Premièrement, deux critères sont considérés pour contrôler la vitesse longitudinale. Le premier est un critère de sécurité qui utilise la distance minimale entre un agent et le châssis du véhicule. Le second est un critère proactif qui utilise la mesure de coopération des agents environnants. Ce dernier est indispensable pour exploiter tout comportement coopératif et éviter le gel du véhicule dans des scénarios denses. Enfin, le contrôle optimal est dérivé en utilisant le gradient d'une fonction de coût combinant les deux critères précédents. Ceci est possible grâce à une formulation suggérée du modèle de coopération utilisant une distribution Chi non centrale pour la distance entre le véhicule et un agent.

Un cadre de canaux dynamiques et proactifs est suggéré pour la manœuvre locale. La méthode dépend de l'évaluation du coût de navigation dans un canal (sous-espace) à l'aide d'un modèle de coût flou. Le canal avec le moindre coût est sélectionné et une transition douce est réalisée à l'aide d'une spline Quintique entre les canaux. Enfin, la control local est calculé à l'aide d'un contrôleur de mode glissant.

La navigation est évaluée à l'aide du simulateur PedSim sous ROS dans des scénarios d'interaction piéton-véhicule. La navigation est testée avec différentes densités et parcimonie de piétons. Le cadre proactif a produit des trajectoires de véhicules fluides tout en maintenant la sécurité des piétons et en réduisant le temps de trajet par rapport aux méthodes réactives traditionnelles (Risk-RRT).

Acknowledgement

I would like to thank my supervisors, Anne Spalanzani and Philippe Martinet for their guidance and advice throughout this thesis. Thank you Anne and Philippe for your time, support and kindness.

I would also like to thank the two research teams that hosted me during my PhD: CHROMA team at Inria Grenoble, and ACENRAURI team at Inria Sophia Antipolis. Many thanks to my colleagues from both teams and to both team leaders: Olivier Simonin and Ezio Malis for their valuable support.

Special thanks to all the members of the french national HIANIC project who supported and funded this work. This work would not have been possible without the collaboration with the different project members. Thanks to our colleagues from LIG Grenoble: Julie Dugdale and Manon Predhumeau for their valuable collaboration on the pedestrian simulation. Thanks to our colleagues from LS2N Nantes for their support and collaboration in realising the tests and in the data collection: thank you Salvador Dominguezquijada, David Perez Morales, Arnaud Hamon, Gaêtan Garcia and all the rest of the LS2N members.

Finally, I would like to thank my family and friends for their love and support: you all made this journey much easier...

Contents

List of Figures

List of Tables

List of Algorithms

Acronyms

AD* Anytime Dynamic A*. 40

AV Autonomous Vehicle. 35, 36, 45, 49, 157, 158, 174, 175

AVs Autonomous Vehicles. 17, 19, 20, 35, 170

CA Cellular Automata. 54

CC Cross-Correlation. 62, 74

CF Cooperation Factor. 60, 77

DVZ Deformable Virtual Zone. 41, 56, 57, 61

ESFM Extended Social Force Model. 34, 35

FRP Freezing Robot Problem. 84, 85, 101

GP Gaussian Processes. 55

HATEB Human-Aware Timed Elastic Bands. 104

HC Highly Cooperative. 61, 62

HRI Human-Robot Interaction. 1, 31, 32, 33, 34, 36, 49, 170

IB Inverse Behavior. 74

ICF Inner Cooperation Factor. 76, 78

KF Kalman Filter. 55

MAD Minimum Approach Distance. 4, 68, 163, 165

MPC Model Predictive Control. 35, 104

MPDMP Markov Decision Process Motion Prediction. 55

MSE Mean Square Error. 75, 76

NLP Nonlinear Optimization Problem. 72

ORCA Optimal Reciprocal Collision Avoidance. 154

PDC Proactive Dynamic Channel. xi, 4, 110, 111, 113, 165, 166, 176

PF Particle Filter. 55

POC Probability Of Collision. 91, 92, 94

PVI Pedestrian-Vehicle Interaction. 1, 32, 33, 36, 37, 49, 71, 154, 160, 167, 170, 174, 175

PVO Probabilistic Velocity Obstacle. 43

Risk-RRT Risk Rapidly-exploring Random Trees. 84, 154, 165, 166, 167, 173

RL Reinforcement Learning. 104

ROS Robot Operating System. 3, 28, 55, 153, 155, 156, 166, 173, 174

RRT Rapidly-exploring Random Trees. 154, 167

SB Similar Behavior. 74

SC Somewhat Cooperative. 61

SFM Social Force Model. 54, 55

SI Safety Index. 87

TEB Timed Elastic Bands. 41

TTC Time To Collision. 141, 142, 143, 144

UC Uncooperative. 61, 62

VO Velocity Obstacle. 43

Mathematical Notations

V_{max}	The maximum allowed speed for the vehicle in the shared space
V_{Pmax}	The maximum allowed speed for a pedestrian in the shared space
T_F	The interaction (or simulation) time period
t_0	The interaction (or simulation) start time moment
$\boldsymbol{X_j} = [x_j, y_j]^T$	The center position of the pedestrian j
$\boldsymbol{V_j}$	The velocity of pedestrian j
$\boldsymbol{X_V} = [x_v, y_v]^T$	The position of center of the vehicle's body
$\boldsymbol{X_R}$	The position of center of the vehicle's rear axis
$\boldsymbol{V_V}$	The velocity of the vehicle
v	The longitudinal velocity of the vehicle
a	The longitudinal acceleration of the vehicle
θ	The orientation of the vehicle
δ	The steering angle of the vehicle
L	Wheelbase length of the vehicle
W	Wheelbase width of the vehicle
L_V	Length of the vehicle's body
W_V	Width of the vehicle's body
s	The traveled arc length along a curve
e_l	The lateral displacement error with respect to a reference curve
$\kappa(s)$	The curvature of a curve at the traveled arc length s
S_p	The shape matrix of the pedestrian footprint
S_V	The shape matrix of the vehicle's footprint
T_h	Prediction future time horizon
R_{ped}	The pedestrian circular footprint radius
R_P	The pedestrian circular personal zone radius
R_C	The pedestrian circular cooperation zone radius
I_V^j	The deformation of the pedestrian's j cooperation zone due to vehicle intrusion
Θ_V^j	The deformation angle of the pedestrian's j cooperation zone due to vehicle intrusion
I_P^j	The deformation of the pedestrian's j personal zone due to pedestrian intrusion
Θ_P^j	The deformation angle of the pedestrian's j personal zone due to pedestrian intrusion

$d(\alpha, t)$	The DVZ deformation radius at angle α and time t
$d_h(\alpha)$	The DVZ undeformed radius at angle α and time t
CF_j	The cooperation factor of pedestrian j
$\boldsymbol{P_{cf}^j}$	The cooperation model input parameters of agent j
$\mathbb{P}_{[j,veh]}$	The probability of collision between a pedestrian j and the vehicle
$\mathcal{D}^j(t)$	The relative occupancy of the cooperation space surrounding a pedestrian j
$V_m^j(t)$	The average speed of a pedestrian j from the start of the interaction until time t
$CF_m(j)$	The average value of the cooperation factor of agent j during an interaction
$CF_m(s, j)$	The average value of the cooperation factor of agent j during the interaction s
R_{CC}	The cross-correlation factor
R_{GT}	The ground truth value of R_{CC}
R_{CC}^d	The discretized values of R_{CC}
$\boldsymbol{G_j}$	The position of pedestrian j goal point
D_{goal}^j	The euclidean distance between pedestrian j and the goal point
Θ_{goal}^j	The orientation of the pedestrian j goal point with respect to his/her current position
$\bar{V}_V$	The average speed of the vehicle during an interaction
V_V^{max}	The maximum speed of the vehicle during an interaction
$\bar{a}_V$	The average longitudinal acceleration of the vehicle during an interaction
a_V^{max}	The maximum longitudinal acceleration of the vehicle during an interaction
d_{min}	The minimum approach distance of the vehicle to all pedestrians
d_{min}^j	The minimum approach distance of the vehicle to a pedestrian j
t_{MAD}^j	The time of the minimum approach distance of the vehicle to a pedestrian j
V_{MAD}^j	The vehicle's speed at the time of the minimum approach distance to a pedestrian j
a_{MAD}^j	The vehicle's longitudinal acceleration at the time of the minimum approach distance to a pedestrian j
V_{MAD}	The vehicle's average minimum approach speed
a_{MAD}	The vehicle's average minimum approach longitudinal acceleration
Φ	The pedestrian cooperation model parameters
Ψ	The cooperation-based trajectory planning model parameters

$MSE\%$	Mean square error
$A(k)$	Total number of pedestrians in an interaction k
$T(k)$	Time period of an interaction k
$X_{real}^{j,k}$	The real position of a pedestrian j in an interaction k
$X_{model}^{j,k}$	The model predicted position of a pedestrian j in an interaction k
SI_j	A safety index for a pedestrian j
$\mathcal{N}(\mu, \sigma)$	The normal distribution with a mean μ and variance σ^2
$\mathcal{X}(2, \lambda)$	Two degree of freedom non-central chi distribution
$TT_[veh/ref]$	The vehicle's travel time relative to its reference travel time
$TT_[veh/peds]$	The vehicle's travel time relative to the pedestrians reference travel time
PI	Safety based performance index
CH_i	A channel i
$\mathcal{D}_P$	Perception range radius of the vehicle
w_{local}	Channel navigation cost model local weight
w_{global}	Channel navigation cost model global weight
w_{fuzzy}	Channel navigation cost model fuzzy weight
$D(t)$	Space density at time t
ΔD	Space density change
$N_{uc\%}$	Percentage of uncooperative pedestrians
$e_q(s)$	the Quintic spline value at arc length s
E_{lat}	Path following lateral displacement error
E_θ	Path following orientation error
E	Path following total error
σ	The sliding surface
δ_{eq}	Equilibrium steering control
δ_s	Sliding steering control
GI	Space sparsity measure with a Gini index
E_P	Path energy
$\bar{I}_{ucf}$	The uncomfortableness index
TTC_{Danger}	TTC-based danger estimate
E_T	Trajectory energy
C_L	Relative traveled distance
TT_G	Relative time to reach goal
a_C	Centripetal acceleration
X^g	Point X expressed in the global coordinates frame
X^v	Point X expressed in the vehicle's local coordinates frame

1 Introduction

Autonomous driving systems have the potential to transform cities planning and urban lifestyle. Autonomous Vehicles (AVs) can reduce human losses and injures caused by traffic accidents, and they are accessible equally to all (families, elderly, infirm). Furthermore, they are predicted to reduce the harmful emissions by optimizing travel times. However, these driver-less vehicles cannot be fully integrated into our daily lives without the capability to navigate safely and efficiently around vulnerable road users. Studying the interaction between vehicles and pedestrians is becoming increasingly more interesting with the growing influence of the "Shared Space" concept in city planning. Shared spaces introduce extra constraints and challenges to the navigation task. Insuring both pedestrians' and passengers' comfort and safety while navigating efficiently is a highly challenging task, especially in a shared, dynamic and dense environment.
This thesis is mainly focused on developing a robust navigation system suitable for close interactions with pedestrians in an unstructured environment (no markings on the floor, no traffic signs, etc). The proposed solution is a proactive navigation framework which exploits the cooperative nature of human behavior. Thus, enabling the autonomous vehicle to engage in the environment as an active agent and to deploy natural and legible driving patterns.

In this chapter, we present the motivation behind this work and the general context on automated vehicles, their advantages and challenges. The main problem addressed in this thesis is presented. Furthermore, the general framework of the proposed method is explained. Finally, the main contributions of this thesis along with the manuscript outline are detailed.

1.1 Motivation: Future Cities and Autonomous Vehicles

The quality of urban life is negatively affected by the increasing levels of road traffic and congestion. High inner-city traffic levels produce both air and noise pollution, along with a less safe neighborhood environment and reduced sense of local communities [Env04]. Consecutively, cities around the world started converting large spaces into green and pedestrian-friendly zones to improve the quality of air and the quality of life in general [MV21]. We can see examples of such initiatives across the world such as the pedestrianization of the Times Square, NYC in 2014 (Fig. 1.1).

Fig. 1.1.: Pedestrianization of the Times Square, NYC

This approach achieves a reduction in overall vehicle traffic which is a major cause of greenhouse gas emissions. However, the size to which cities can expand these green zones is limited due to lack of transport options for goods and people with reduced mobility, such as the elderly, families and the infirm. This is compounded by the fact that the elderly population is expected to double over the next 20 years in Europe [Boo20]. Shared spaces are presented in city planning as a solution to this issue. They are considered a way to balance mobility requirements and economic growth, while respecting the environment and providing an improved quality of urban life [Ham08]. This is a new design concept that is spreading across the world and changing the way cities look and function. Such shared spaces can be seen in London's Oxford Circus 'X-crossing'[1] and Exhibition Road (Fig. 1.2), or Sonnenfelsplatz square in Graz, Austria [Hoe11], to mention a few.

[1] http://news.bbc.co.uk/2/hi/8337341.stm

Fig. 1.2.: Turning London's Exhibition Road into a shared space

The transition from the traditional road structure and the vision of open, pedestrian-friendly city spaces is becoming a reality. Specially with more cities joining the green initiatives and plans. This year only, 50 new cities joined the European Commission's Green City Accord[2], including the city of Grenoble where this research is based. The goal is reducing harmful gas emissions by 55% by 2030 as compared to its levels in 1990, with the vision of promoting smart cities where people and robots (including AVs) can interact in daily life [Ccr20]. These green cities are not a mere vision for the far future but are becoming a near reality, specially with the new announced projects and planning trends. The city of Paris, for example, recently released its vision for 2030[3] to transform the famous Champs-Élysées area to a greener pedestrian-friendly area (Fig. 1.3), with the Place de la Concorde to be ready in less than 3 years from now (by 2024). However, current AVs are not ready to operate in these green, pedestrian-friendly cities.

Classical autonomous vehicles navigation is adapted to simple, structured and predictable environments. When encountering an obstacle, these vehicles either stop or a collision is avoided by handling control back to drivers. Furthermore, the current incumbents in the automotive industry are designing AVs which mostly operate on road infrastructure, sparsely interacts with pedestrians and follows stipulated traffic rules. On top of not closely interacting with pedestrians, these systems relay heavily on the traditional road structure, which makes it incapable of operating unstructured spaces. However, with this increased push towards greener and more livable spaces it becomes even more imperative to develop models of autonomous mobility for shared spaces with pedestrians.

[2]https://ec.europa.eu
[3]https://hubinstitute.com

Fig. 1.3.: An aspect of the 2030 Champs-Élysées vision by Philippe Chiambaretta & Co

This vision of the future pedestrian-friendly cities is the main motivation behind this work and the french ANR project HIANIC [4]. The project addresses the different problems related to autonomous driving in a shared space. As a part of the project, this work is focused on the navigation aspect to develop a socially compliant, efficient and safe navigation system for AVs. With the goal of being capable of navigating the shared pedestrian-friendly spaces which are anticipated to grow over the coming years.
To address autonomous driving in this thesis, let's start with an overview of autonomous driving systems, their categories, latest advancements and ongoing challenges.

1.2 Autonomous Driving Systems

Autonomous mobility has many advantages over traditional mobility solutions. One of the main advantage autonomous solutions can bring to society is the improved road safety. Studies show that 94% of road accidents are attributed to human factor [Adm18]. They are also expected to reduce harmful gas emission by 60% by optimizing travel times and energy consumption therefore dampening traffic waves [Ste+19; ET21]. Moreover, autonomous mobility can positively impact the environment by reducing the overall requirement for privately owned vehicles. This is according to a study in Germany which showed that autonomous shared mobility could help dispense of around 85% of the current vehicles on the roads [Hei+17].

All these promising prospects have created a flourishing market and pushed automakers and stack-holders in the field to introduce new autonomous driving technologies. The

[4] Human Inspired Autonomous Navigation In Crowds, https://project.inria.fr/hianic/

first autonomous driving technologies date back to the 1970s when the anti-lock braking system was introduced [Gal19]. This type of technology is known as ADAS which stands for Advanced Driver-Assistance Systems. The past 50 years have witnessed major advancement in ADAS technologies. The newly developed systems took advantage of the wide range of available sensors and perception algorithms to estimate not only the vehicle's state, but also to estimate and understand the state of the surrounding environment. Some ADAS systems are only designed to warn or inform the driver to take a corrective action, such as lane departure warning. Whereas, other ADAS can directly take partial or full control over a sub-system in the vehicle, like the automatic emergency braking system [Zie+17].

Based on the degree of autonomy, autonomous driving systems are classified to 6 levels as shown in Fig. 1.4. Systems of levels 0-2 are considered driver's support features where the driver is responsible of monitoring the system performance. In level 0, the human driver is responsible of all the aspects of the driving task (i.e. no autonomy). In this level the driving is enhanced by warnings such as the blind spot warning but the driver is mainly responsible of steering/braking to maintain safety. In Level 1, the driver assistance system can provide steering **OR** acceleration/braking actions support to the driver such as the lane centering system or the adaptive cruise control system. When the ADAS provides both steering **AND** acceleration/braking assistance, the system is considered of level 2. Therefore, a system providing both lane centering and adaptive cruise control at the same time is considered of level 2. On the other hand, systems of levels 3-5 are considered automated driving features, where the driver does not need to be continuously engaged when these features are in action. In levels 3 and 4, the system can take full control of the vehicle but only when specific conditions are met. The main difference between these two levels, is that in level 3 the driver must be ready to take over when requested to intervene by the system. Finally, level 5 provides a full-time control of the vehicle under all conditions that can be managed by a human driver. [Int18]

1.2.1 Latest Development and Current Challenges

Despite the ongoing developments and achievements in the automotive industry, the current technologies are still not ready for mass deployment or higher levels of autonomy. Many autonomous driving companies had promised the public with fully autonomous vehicles by 2020, from General Motors to Googl's Waymo, Toyota and Tesla. However, when it comes to autonomous driving, the community had greatly underestimated the complexity of the driving task in a variety of environments and scenarios.

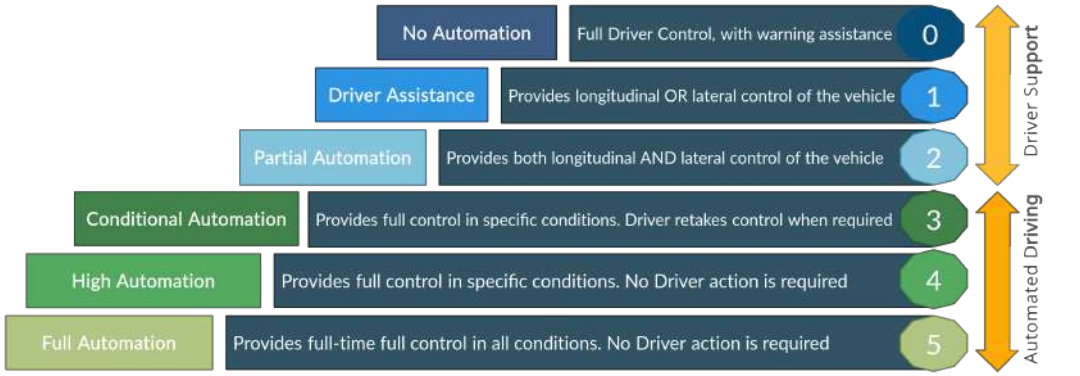

Fig. 1.4.: The 6 levels of autonomy in driving systems

Most autonomous driving technologies on the market today are offering up-to level 2 or 3 autonomy. However, several fatal crashes involving these levels have been reported in the past years[5]. We can identify a large spectrum of challenges related to autonomous vehicles control, perception or navigation depending on the working scenario and environment [Yaq+20]. In the context of this work, let's identify the main challenges and milestones on the way to full autonomous navigation in shared spaces with pedestrians:

- **Planning Challenges:** It is highly challenging to find a valid path in a dynamic human-populated and unstructured space, while ensuring safety and efficiency. One main reason is the coupled nature of the human-vehicle planning imposed by the shared space. Ignoring this cooperation between the two parties can lead to the freezing of the vehicle and not just in highly dense spaces. The study in [Mav+21] argues that this problem can occur even with one human interactions if the agent is navigating in close proximity. **This makes the coupled behavior problem a core concern and not just a limit problem**. This coupled behavior results in complex, non-convex planning objective functions. This computational complexity starts becoming obvious even in a simple collision avoidance cooperative objective, such as the one in [TP20] where the problem is tackled locally. Since tools for global non-convex multi-objectives analysis do not exist, then frameworks such as RRT[RSL11] are expected to fail in such scenarios, as well.

- **Behavioral Challenges:** One of the biggest challenges in navigating shared spaces is understanding human behavior, specially around vehicles. Despite the huge body of research on human motion modeling in crowds [Rud+20], modeling human behavior and reactions in close proximity with autonomous vehicles remains an open research question. Moreover, the vehicle should abide by human expectations

[5] Tesla's level 2 crash, Level 3 accidents

by deploying a behavior similar to that of experienced drivers, or what is referred to as producing legible motion [MTK18; Sto18]. The vehicle should also produce natural driving patterns, which means that it should be able to blend in the environment as an active and not just a responsive agent.

- **Evaluation Challenges:** Evaluating the navigation performance and qualifying a navigation systems in shared spaces is not a straightforward task. The challenges arise when evaluating the performance both in simulations and in real-world experiments. Firstly, the limitations of the currently available spared spaces simulators make testing and validating the navigation in simulations more limited. The study in [FL20] shows that the available crowd simulators suffer from a limited performance due to unrealistic assumptions of the real-world such as behavior homogeneity and agents omniscience. Additionally, the issue of simulating autonomous vehicles around crowds is still not addressed in most simulators. Whereas, setting up real-world experiments to evaluate the navigation around humans is highly challenging. It is even more challenging in the case of an autonomous vehicle that can be potentially harmful. In addition to the simulation or testing environment challenges, the evaluation methods, criteria and metrics should be well-defined and adapted to the particular targeted case of shared spaces social navigation [Mav+21].

- **Societal and Legislative Challenges:** A main issue in the field of autonomous driving is that the technology is in general more advanced that the regulatory processes. These legislative challenges are even more prominent for the case of navigating in close proximity with pedestrians [Bar+17]. Furthermore, the social acceptability of autonomous vehicles, specially around pedestrians, is a major concern in the community. A recent study in [Jin+20] summarized the main points that affect the social acceptability. According to the study, multiple factor which are not related to the navigation performance can affect the social acceptance. Such factors include the performance-to-price value, the ease of use and the environmental impact. However, the main identified factors contributing to the social acceptability are navigation performance related such as the perceived risk, the safety concerns and the compatibility with social norms. Meaning that a robust, safe and socially-aware navigation system is the key to the social acceptability and to raising the public trust of autonomous vehicles.

We focused here on the challenges related to the navigation behavior of the vehicle, as it is the core subject of this thesis. However, the task of full autonomous driving in shared spaces faces furthermore challenges related to the sensory and perceptive system of the

vehicle for example. More on the perception challenges for autonomous vehicles can be viewed in [LI20; Ros+19; KJD18; Shi+17].

1.3 Targeted System And Problem Definition

The targeted system in this thesis is an automated vehicle equipped with the necessary sensory system for pedestrian identification and tracking. The vehicle's perception system can make advantage of the wide range of available sensors from LiDARs to cameras, to achieve the pedestrian tracking task. An example of an instrumented automated vehicle is shown in Fig. 1.5 with the automated Renault Zoe we use in out laboratory experiments.

Fig. 1.5.: The automated Renault Zoe vehicle

As illustrated in Fig. 1.6, the vehicle information pipeline starts with the raw sensor information to localize the vehicle and to identify and track the dynamic objects (which are the pedestrians in our case). This is followed by the prediction of the agents behavior and the environment dynamics. The previous predictions are used to plan an appropriate vehicle path and the necessary vehicle control commands (longitudinal velocity and steering angle) are generated. The highlighted modules on the figure represent the parts included in the scope of this thesis. Meaning that the pedestrian tracking is provided as a system input.

Problem Definition: Consider a navigation space $\mathcal{C} \in \mathbb{R}^2$ which does not contain any special markings, signals or driving rules. All areas in the space are open equally to the pedestrians and the vehicles. Moreover, the space imposes low speed limits of the navigating vehicles. This speed is limited to $V_{max} = 20km/h$, as this the maximum

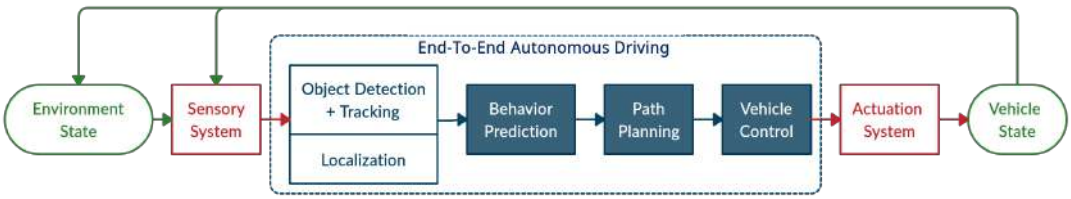

Fig. 1.6.: Information flow diagram in an autonomous driving system

allowed speed for vehicles circulating shared spaces[6].
Consider a set of $N \in \mathbb{N}$ pedestrians $\{a_j\}_{j \leq N}$ in the space. The positions and the velocities of each pedestrian are provided by the perception system as $\{X_j(t)\}_{j \leq N} \in \mathcal{C}$, $\{V_j(t)\}_{j \leq N} \in \mathbb{R}^2$, respectively. The pedestrians navigate towards their goal destinations $\{G_j\}_{j \leq N}$ while abiding by the social norms and avoiding collisions with other agents. Assuming an autonomous vehicle of dimensions $L \times W$ needs to navigate through the shared space $\mathcal{C}$ to reach a final destination $G_V \in \mathbb{R}^2$ according to a global path provided by a higher level path planner.
Find the vehicle's lower level control commands which are the longitudinal velocity control $v(t)$, and the steering angle $\delta(t)$ such that the following criteria are met:

- **Success**: The vehicle succeeds in navigating the shared space and reaches its goal G_V within an infinite time $T_F \in \mathbb{R}_+$.

- **Safety**: The vehicle navigates the space while avoiding collisions with the pedestrians.

- **Efficiency**: The resulting trajectory is efficient in terms of optimizing the traveled time and the traveled distance.

- **Naturalness**: The vehicle navigates the space actively while cooperating and exchanging trajectories with the surrounding agents, i.e. the freezing of the vehicle is avoided.

- **Comfort**: The vehicle produces a legible behavior and navigate while maintaining the comfort of the surrounding pedestrians, and the comfort of its possible passengers.

- **Scalability**: The proposed solution should meet the previously mentioned criteria in interactions with both high and low pedestrian densities.

[6]Article R.110-2 du code de la route, www.audiar.org

1.4 Proposed Solution: A Proactive Social Navigation Framework

The suggested solution is a proactive social navigation framework. The system is based on the idea of the coupled navigation behavior between the pedestrian and the vehicle in shared spaces. The system takes into account the cooperative nature of human behavior and exploits it to explore new navigation options, and navigate the shared space "proactively".

Proactive behaviours are natural behaviours applied by drivers in everyday scenarios. Expert drivers interact, cooperate and influence other road users to navigate in an optimal manner. Applying this kind of proactivity in autonomous driving systems is key to a natural and socially acceptable behaviour. Moreover, the advantages of a proactive navigation is particularly prominent in dense pedestrians-vehicle interaction scenarios. A reactive controller cannot consider the cooperation of the pedestrians in the scene and their reactions to the vehicle. This leads to over penalizing the vehicle's navigation options. Subsequently, the reactive controller would have a poor performance in such scenarios [VMO17a], leading to suboptimal navigation solutions or even the freezing of the vehicle in some cases.

Although the term "Proactivity" is not used explicitly in the literature very often, the concept is considered in several applications. These applications include tasks which require influencing the work space. To cite a few Example, this can be a leader/follower task such as the work in [Clo+06], or minimizing the social effect of the navigation policy in [FS14a]. In this work, the proactivity is considered as an invitation to the pedestrians to cooperate with the vehicle and change their planned paths. Meaning that the system does not merely awaits for an obstacle-free path to emerge in the shared navigation space. The proactive system takes an action (proaction) to produce such obstacle-free paths in an anticipated future horizon.

Finally, the suggested proactive navigation framework components and information flow are illustrated in Fig. 1.7. The proposed system starts by estimating the cooperation of the pedestrians in the scene, or how much would they be willing to compromise their trajectories with the vehicle. Based on the cooperation level estimation the future navigation behavior of each agent in predicted. Following this step, a decision is made on the magnitude and direction of the proactive action. The decision is made using the pedestrian behavior estimation and prediction information, as well as, the current state of the navigation space. This step can be viewed as selecting a general direction of the navigation within the shared space. Based on the decided proactive action, the global

path of the vehicle is modified locally and the exact longitudinal and lateral control commands are derived to follow the planned trajectory. The selected longitudinal-lateral control architecture is a cascading architecture where first the longitudinal control is derived using a stand-alone system, then the output of this system is used to compute the lateral control (more on the control architecture is provided in 2.5).

Fig. 1.7.: Suggested proactive navigation system components and information flow

1.5 Contributions

The main contributions of this thesis are the following:

A first implementation of a complete proactive navigation system. The following system components are integrated and a complete proactive navigation system is implemented. This is, to our knowledge, the first attempt to formulate, implement and test a proactive navigation system around pedestrians.

- **A cooperation-based behavioral model for pedestrians around vehicles.** The proposed model is a 2-layer behavioral model using social concepts. In the first layer the cooperative behavior of a pedestrian is estimated and modeled by a time-varying factor. In the second layer, this cooperation factor is used in combination with the space state measurements and the vehicle influence to predict the pedestrian behavior. **Chapter 3**

- **A method for proactive longitudinal velocity control.** The longitudinal velocity is controlled by exploiting the cooperative nature of pedestrian behavior. The control is derived by influencing the pedestrians proactively to maximize their cooperation, while maintaining their safety. **Chapter 4**

- **A proactive navigation cost model.** The model can be used to measure the cost of navigating through a specific sub-space. The model is based on the travelled distance cost in combination with a fuzzy logic based pedestrian disturbance cost.

The model is exploited in the manoeuvring system but can be used independently and integrated into other pre-existing systems. **Chapter 5**

- **A proactive dynamic channel method for manoeuvring pedestrian crowds.** The proposed method integrates multiple concepts and frameworks to build a proactive manoeuvring system. The system is based on exploring the different navigation options in the space (channels) and selecting the optimal channel with the least navigation cost. The exploration of the space channels is done using a segment of the global path. Whereas, the selection of a channel is done with the previous cost model. The transition between the channels or the local path modification is done using a human-like transition function. Moreover, a sliding mode controller is suggested to perform the path following. **Chapter 5**

The testing and evaluation of the proactive navigation around pedestrians under ROS[7]

- **The formalization of the evaluation metrics necessary for performance validation in shared spaces.** The metrics necessary for performance evaluation around pedestrians are presented. The algorithm for each metric calculation is provided and the success/fail criteria for the case of autonomous vehicle navigation is discussed. **Chapter 6**

- **The collection of a pedestrian-vehicle interaction dataset.** An experiment of pedestrian-vehicle interaction is performed and the pedestrian tracking information is collected on-board of the vehicle. The experiment provides data on pedestrian behavior in a shared space with a vehicle and their reactions to both aggressive and yielding driving patterns. The collected data is used in this work for model validation and as reference for performance evaluation. **Chapter 7**

[7] The Robot Operating System, https://www.ros.org/

1.6 Manuscript Outline

This manuscript starts in **Chapter 2** with a general background on the different components of a proactive and socially-aware navigation system. The chapter provides a general overview, whereas, the more detailed background and related works on each sub-system are found in the corresponding chapters.

Part II: Proactive Navigation Framework

In this part, the three components of the proactive navigation system shown previously in Fig. 1.6 are discussed in a similar order:
In **Chapter 3** the behavioral modeling of pedestrians around autonomous vehicles is discussed. The proposed cooperation-based model is presented and evaluated. The chapter further entails the presentation of a pedestrian-vehicle interaction dataset.
In **Chapter 4** the proactive longitudinal velocity control of the vehicle is discussed. The proposed control method is calibrated and tested in a simulated pedestrians-vehicle interaction using the previously developed pedestrian behavioral model.
In **Chapter 5** the steering control of the vehicle is discussed. The proactive dynamic channel method for space exploration is presented and the corresponding steering control is derived. The calibration and analysis of the proposed system is also provided.

Part III: Implementation and Validation

In this part, the three components presented in the previous part are integrated to test and validate the entire system performance:
In **Chapter 6** the performance metrics used to validate the different performance aspects of a navigation system around pedestrians are presented and discussed.
In **Chapter 7** the proactive navigation system is integrated and tested in a simulated shared space environment under ROS. The performance is analysed in different pedestrian-vehicle interaction scenarios, and the navigation is evaluated using the previously defined performance metrics.

Finally, in **Chapter 8** a global conclusion is derived on the work presented in this thesis. The main contribution are summarized. Furthermore, A discussion on the potential future avenues and prospects of this thesis is given.

Background and Related Work

2

Building a proactive and socially-aware navigation system is a multidisciplinary challenge. This chapter gives a background on the different components required for such systems. These components include understanding the interaction between the navigating robot and its surrounding environment, how is this new understanding used in the navigation and the corresponding planning and control aspects. We start by placing this work in the global framework of human-robot interaction and explaining how does this serve as a starting point to establish the desired socially-aware navigation policy. The chapter further entails a background on proactive navigation and modeling dynamic shared spaces. Finally, a background on the verification of autonomous navigation systems is given, with a focus on our special case of vehicle navigation in shared spaces.

2.1 From Human-Robot Interaction to Social Vehicle Navigation

Studying robotic systems which require an interaction with a human agent to perform a task is critical for applications in many emerging fields, ranging from simple domestic applications to industrial applications and tasks in more undetermined environments such as search and rescue operations. Studies have shown that human reactions to machines are different from their reactions to other humans when performing the same task [HRJ04]. This feature was the motivation for several studies aiming to understand HRI. The main challenge in HRI applications is the fact that its a multidisciplinary task, requiring developments in perception, AI, psychology and robotics.

Traditional robotic navigation systems were not viewed as HRI systems. The navigation task was approached in a purely mathematical way to find the shortest path to a goal point, for example, or to avoid static and dynamic obstacles [ZLC18; ABM11; FSL07a]. However, with the evolution of the field, robotic applications became increasingly more present in human populated environments and the limitations of the previously developed navigation methods became more prominent. Stakeholders in the field started classifying navigation problems around humans as HRI applications under the category of social navigation. Social Navigation (or socially-aware navigation) are navigation

methods developed specifically for human populated environments. Meaning that the navigation framework includes extra layers to deal with interpreting human intention, decision making and producing human-like behaviors which are socially-acceptable [Kru+13]. The term itself includes a wide range of applications and can be interpreted in different ways based on what is considered "socially acceptable". However, some ground rules are established in the community to give a minimum qualification for a robot behavior to be considered socially-aware [RSL15].

Social navigation is a HRI problem whether the goal is to perform a task with a minimal effect on the surrounding environment or to engage the surrounding agents in a desired manner. In other words, whether the interaction with humans during the navigation is preferred or not, it is present, and any navigation solution that does not consider this interaction, is ill-defined. In some navigation applications the HRI aspect of the task is very prominent and clear, such as evacuation or guidance tasks where there is a leader-follower situation with the robot being the former. Here the interaction is a straightforward main piece of the puzzle, similar to previously studied types of HRI. This does not remain the case in other navigation applications, such as navigation in spaces shared with pedestrians, where the goal is to reach a destination with an optimal trajectory regardless of the other agents in the space. In such applications, the HRI becomes an underlying layer that governs the dynamics of the space and drives the solution to our puzzle. The navigation space and time both become common resources between the robot and the other human agents in the environment. Understanding HRI in this case means understanding how these resources are pooled and shared, and how can these processes be manipulated to optimize the navigation task. In such case, and in the specific application of autonomous vehicles we study PVI as a sub-category of HRI (Fig. 2.1).

Understanding PVI enables us to develop autonomous vehicles which are capable of navigating urban and pedestrian populated environments such as busy city centers, shared spaces, parking lots, etc. The benefits of PVI research can also be extended to any mobile robot navigating a pedestrian space, such as airports, universities and shopping malls, for example. However, different adaptations are required for PVI case not only due to the size of the vehicle, but also due to the different social rules and human reactions in the case of a vehicle.

Finally, to move from general HRI to a social framework for navigation among human crowds, two concepts should be taken into account: cooperation and proactivity. The former two terms are qualities of any social interaction, therefore, navigating socially cannot be established without them [JSM20]. Cooperative means that the navigation is viewed as a shared task, and the burden of the task falls equally on both parties (the

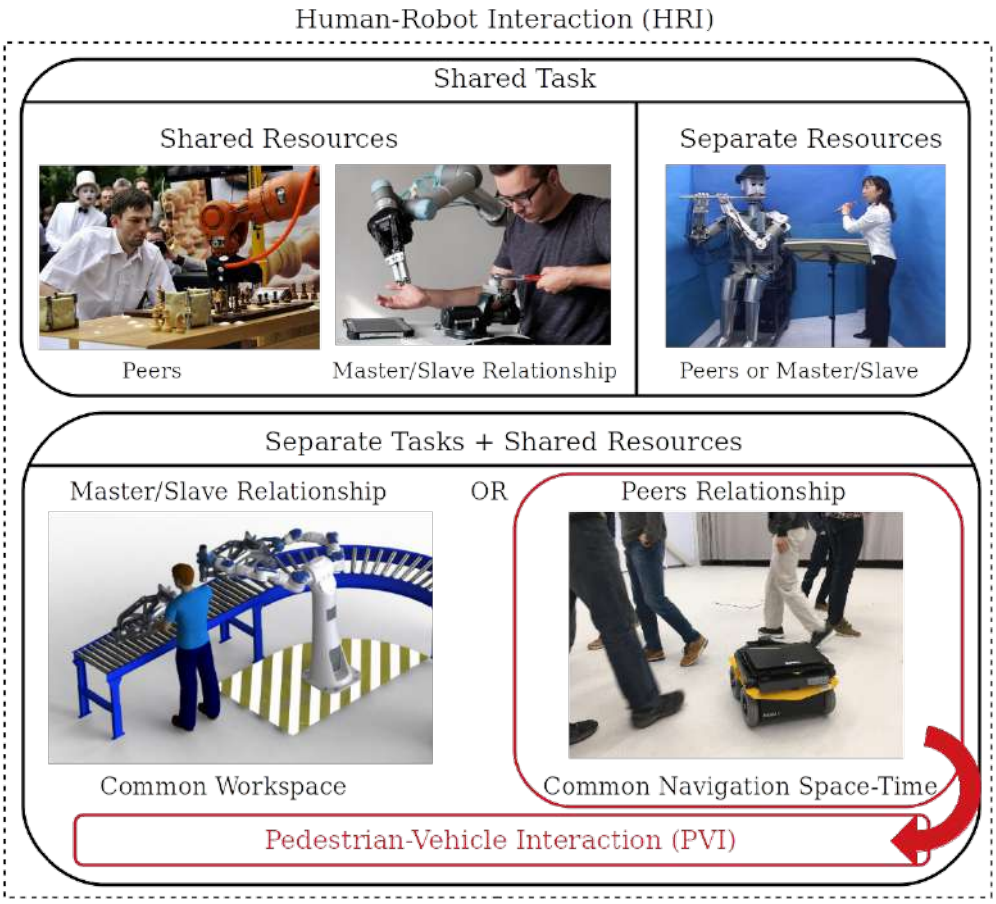

Fig. 2.1.: PVI as a sub-category of HRI

robot and the human). This concept on its own, opened the door to more sociable and efficient robotic navigation systems [KA17]. Proactivity, on the other hand, is a quality of the agent performing the cooperative navigation.

PVIs (and more generally HRIs) can be split into two main categories: reactive interactions and proactive interactions. Neuroscientists define reactive agents as the agents who "learn during their lifetime how to react to environmental stimuli", while proactive agents are more evolved inductive agents which "are able to make generalizations about learned stimuli, and to react to new stimuli based on these generalizations" [SMT20]. In robotics, reactive translates to the type of systems which can interpret their surrounding environment and take actions only as a response to an external influence. While proactive robotics are those able to anticipate the evolution of the environment and take actions without a proceeding influence (Fig. 2.2). Furthermore, in proactive interactions the robot can take an initiative that influences the surrounding agents, similarly to how an experienced conscious being would behave.

Reactive	Stimuli → Reaction → New Stimuli
Proactive	Anticipated Stimuli → Proaction → Stimuli

Fig. 2.2.: Reactive vs. proactive actions

In the problem of navigation around humans, some solutions took the reactive approach such as the works studying the dynamic obstacle avoidance problem [FSL07b; SW14]. However, treating all the surrounding agents as dynamic obstacles that should be avoided has its limitations and drawbacks, specially in more dense and complex spaces [LS13]. To account for this aspect without moving to a proactive approach, some works solve the navigation problem by following an optimal leader through the space [Ste+16a; SN08; Jun+16]. In this case the robot remains a reactive agent following another more experienced and more proactive agent. The goodness of such solutions depends on finding a group of agents with aligned goals or sub-goals, selecting the best agent to follow, and on the experience of the selected agent. All these factors limit the feasibility and scope of such approaches, and the evolution towards proactive robotics becomes inevitable for social navigation frameworks.

2.2 Proactivity in the Literature

Proactivity translates to creating or controlling a situation when performing a task, and not just reacting to pre-existing situations. Motivated by the rowing number of applications HRI applications, researchers recently started exploring proactive robotic behavior. The study in [Gar+17] discussed providing a Tibi mobile robot with proactive capabilities to establish an engagement with people through verbal and non-verbal cues. The study concluded that providing the robot with the ability to take initiative improved the overall human-robot communication, provided that the robot abides to the social norms. Even thought the study is applied to an application which is not navigation specific, the insights of this work on the importance of proactivity in social robotics can be extended to socially-aware navigation. Few works in the literature targeted the navigation task around humans proactively. One approach is presented in [FS14b] where the Extended Social Force Model (ESFM) is exploited in a proactive kinodynamic planner. The proposed planner aims at minimizing the robot disturbance to other pedestrians (or its social work). The proactivity here is prominent in considering the robots effect on its environment and propagating the pedestrian state accordingly. This study demonstrates the advantages of having a proactive behavior in the social planner, over a reactive

one. Although the system is only tested in low-density interaction, the results and insight provided by the method are a motivation to implement proactive behaviors in more socially-aware navigation system. In a more recent study, the work in [JSM20] proposed a proactive-cooperative planner with a switching strategy to pass to a reactive planner depending on the interaction situation. The proposed method integrated Model Predictive Control (MPC) and the ESFM with Collision Prediction. The method was only tested in a constrained one-pedestrian interactions. However, the idea of having a decision making system to switch from proactive to reactive behavior is quite inspiring and can be exploited in developing social navigation systems.

Finally, works on proactive robotic behavior in the literature are very few and limited. However, the studies which discussed proactive behavior, or more specifically proactive navigation, all demonstrate the advantages and importance of deploying robotics proactively. This has been a major motivation for us to develop a proactive and socially-aware navigation system for autonomous vehicles around pedestrians.

Working towards proactive robotics is working towards more "intelligent" or advanced robotics with a more human-like abilities. Moreover, in the case of safety-critical robotic application, such as autonomous vehicles, proactive behavior can be regarded as a necessity and not just an extra improvement. Although this is a new direction in the community, but several opinions argue in favor of this necessity. In a recent article on "Intuition Robotics" by Natalie Hoke titled "5 Times Our Cars Should Proactively Interact with Us"[1], the writer argues the importance of proactive vehicle behavior for the case of in-car voice assistance. According to the study in [Sem+19], 78% of participated drivers where in favor of more proactive voice assistance interventions. This was the result of a poll after a 50 minutes test drive. Furthermore, Lance Eliot[2] argues that today's reactive AVs drive (at best) similarly to novice teenage drivers. He suggests a very simple example scenario of a driver arriving at a traffic light when the light turns yellow. In this situation some novice drivers might not consider the consequences of their actions and brake regardless of the situation. However, more experienced drivers would act proactively and consider their effect on other road agents. This might lead them to deciding to cross the yellow light if they notice that the driver behind them is too close and doesn't seem to be slowing down, for example. In such case, if an autonomous vehicle stops to follow the traffic rules and a human driver crashes into the vehicle from behind, the automakers would blame the human driver. Where in fact this is a matter of over-reactive behavior on the Autonomous Vehicle (AV)'s side and a lack of proactivity. Imagine another example of an AV trying to insert into a busy

[1] https://blog.intuitionrobotics.com/5-times-our-cars-should-proactively-interact-with-us
[2] https://lance-eliot.medium.com/proactive-defensive-driving-for-driverless-cars-missing-link-must-have-88530f19a92d

round-about on a Monday morning (Fig. 2.3a). An over-reactive behavior would lead the AV to keep freezing on the roundabout entry, blocking not just its passengers but the whole traffic flow. Whereas, an experienced driver would act proactively finding the appropriate moment to insert himself. A similar scenario can be imagined when navigating human crowds as driving through a busy campus (Fig. 2.3b), for example.

(a) Busy roundabout, photo by bloomberg.com

(b) Campus top-shot, photo source [Yan+19]

Fig. 2.3.: Examples of situations requiring proactive behavior

In the following, we move to talking about the main challenges in developing the different components of a proactive navigation system. From the challenge of understanding pedestrian behavior in section 2.3 to the navigation system structure and the different planning and control challenges in section 2.4.

2.3 Perceiving Intentions For Proactive Decision Making

Perceiving and understanding intentions is a major challenge in any HRI problem, including PVI. In the case of PVI, the main interest is to model the human behavior during an interaction with the vehicle (Fig. 2.4). The vehicle (or the robot in general) should be able to infer the underlying intention behind a human action in order to respond in an appropriate human-like manner. HRI research resulted in several works on modeling human intention using their movement [Wan+13; Sha12]. This is based on the hypothesis that humans move according to goal-oriented policies [FR11]. The advancement in sensors and perception enabled robotic systems with improved scene understanding capabilities. Robots became capable of using body posture and gaze detection to interpret engagement and even human feelings, as the works in [MKV20; Xu+19; LT19] to mention a few. However, the problem of understanding human behavior cannot be solved globally and solutions are context and environment oriented. For example, the same action made by a pedestrian should be interpreted differently in the case of an adult as compared to a child. Furthermore, the same person might respond

differently to the same stimuli made by a robot in a lab environment as compared to a vehicle on the street. Therefore, the previous works cannot be applied directly to the case of PVI. The new environment outside the lab doors and the different dimensions of a vehicle requires separate treatment.

Fig. 2.4.: Understanding intentions in PVI scenarios inside a shared space

Recent studies in the field addressed the problem of intention prediction in the case of PVI. Several works targeted the problem of pedestrian intention estimation around urban roads, and more specifically addressed the crossing intention at signalized crosswalks [Rid+18a]. Data-driven approaches had a major share in the used methods as they can combine our knowledge about human behavior with other visual and spatial information, such as the works in [Has+15; Völ+16; Ras+19; CMF19; AA20]. According to [SF09] a visual information of the pedestrian such as gaze or body movement detection is imperative to predict the intention. While a more recent study in [DT17b] argues that the detection of explicit body or gaze communication between the pedestrian and the vehicle is not significant in the intention prediction process. Their study showed that this type of communication only occurs when a social or a safety rule was violated, and that the main driver of the pedestrian motion is the behavior of the vehicle itself. Finally, all the previous works and most recent studies address the problem of pedestrian intention estimation in structured urban scenarios. Therefore, understanding pedestrian intention in unstructured spaces shared with vehicles remains an open question on the cutting edge of today's research to develop socially-aware autonomous driving systems.

2.4 The Navigation Task in Shared Spaces

The problem of autonomous navigation becomes increasingly challenging in environments including interactions with vulnerable road users (pedestrians, bikers, etc.) [Ado16; Bel+19]. These scenarios present the challenge of navigating in a dynamic environment governed by specific social rules. In pedestrian-vehicle interaction scenarios, the navigation policy should take into account the agents comfort and acceptance of the autonomous vehicle on top of the strict safety measures.

The navigation and control system is in charge of performing the path planning and computing the low level controls of the vehicle (acceleration and steering) using the output of the perception systems, as shown in Fig. 2.5.

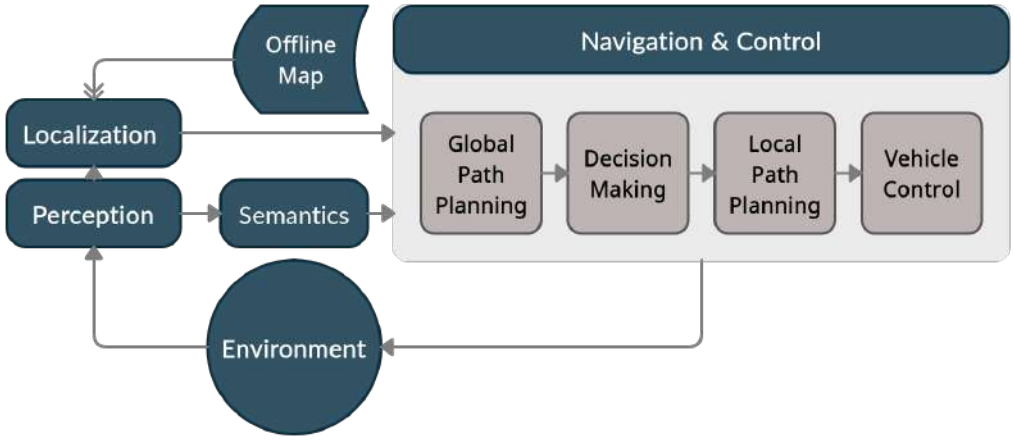

Fig. 2.5.: The autonomous vehicle system components

2.4.1 Global path planning

The first component of the navigation and control system is the global path planner. Global planning is focused on finding the best route to the long term goal. This is done by using a prior knowledge of the space (maps) along with the accumulated sensor data. The global planner doesn't usually deals with the smaller sized dynamic obstacles such as pedestrians and bikers, this is left instead to the local planner and control system. Global path planning is a standing field of research with several algorithms developed over the years from A* to RTT and different generic and data-driven algorithms [CS19]. We will not further explore the topic of global path planning as the scope of this research targets the local planning and control aspects.

2.4.2 Decision making

The decision making is the layer in charge of establishing a behavior policy for the vehicle based on the perceived situation and the surrounding agents intentions. This is key to defining the driving patterns and the social gestures of the vehicle, therefore, it is essential for the social navigation framework. When vehicles navigate structured environments such as highways or urban roads, the related traffic rules help guide the decision making system. Traffic signals, floor markers, sidewalks and pedestrian crossings are all indicators to how the driving pattern should be. However, shared spaces usually lack such indicators. This combined with the uncertainty in pedestrian behavior prediction makes the decision making process in shared spaces much more challenging. Some works in robotics try to tackle this problem by using a context oriented multi-policy decision making process [Cun+20]. In a first step, the system identifies the navigation context and then the corresponding policy is selected. In the case of autonomous vehicles navigation , this works well in situations where it is possible to identify the navigation context, such as lane-change or parking [Cun+15; Gal+17]. The same technique is used for navigating shared zones with pedestrians with human-sized robots. The context is mostly identified based on the existence of a pedestrian-free path where the robot makes a decision with a stop-or-go behavior, or with a follower behavior [MFO16]. However, this limits the performance in more dense spaces where the bigger sized vehicle cannot simply follow a pedestrian or keep stopping.

2.4.3 Local path planning and control

Local path planning allows the system to adapt the previously planned global path to the perceived dynamics of the environment. The goal is to find the best feasible path to drive the vehicle through the dynamic space from the current to the goal configuration. While finding a feasible path for the vehicle is proven to be NP-complete problem, the research community focused on solving the problem approximately or partially rather than trying to find a global solution [Pad+16]. The local planning can use the sensory information to either to build a local map and re-plan a local path or to modify the previously planned global path. This path is then passed to a path tracker responsible for providing the necessary vehicle controls to follow the planned path. Alternatively, both the local planner and the path tracker can be replaced by a single sensor-based controller. Therefore, we get three different categories of solutions to the planning and control problem, as shown in Fig. 2.6.

The first two categories both use the same global planning and control techniques and differ in the way the local path is produced.

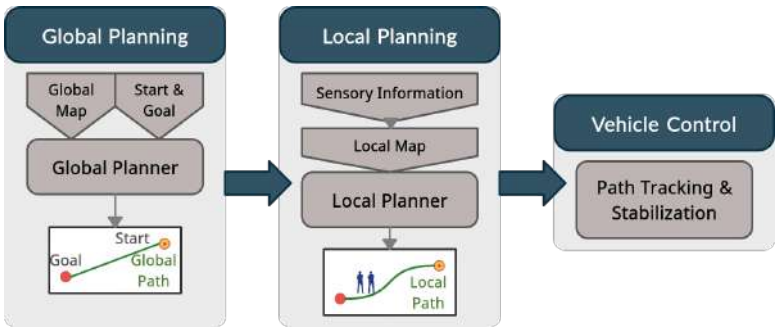

(a) Plan → Re-plan → Control

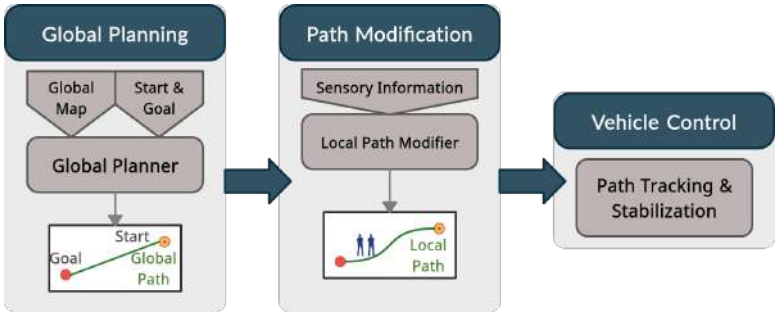

(b) Plan → Adjust → Control

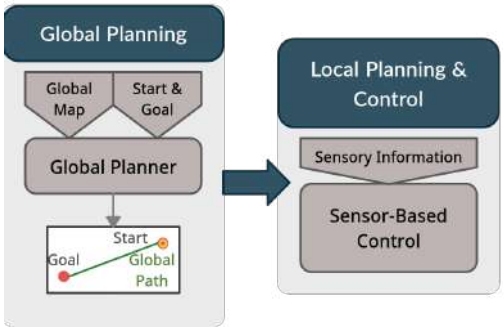

(c) Plan → Control

Fig. 2.6.: Three different methods for using planning and control in autonomous navigation systems

The local planners used in the first category are based on finding an optimal path in a local map generated using the sensory information (Fig. 2.6a). These planners are usually based on search-based methods such as Dijkstra and D* algorithms (or their variations) and sampling-based methods such as the RTT algorithm. A significant body of research is devoted to optimizing these methods for dynamic and fast changing environments which led to new algorithms such as D* Lite, Anytime Dynamic A* (AD*) and several others [LL18]. These new algorithms improved the performance specially in more dense and dynamic environments. However, the performance in these methods remains limited due to the necessity of planning, then generating a local map and

re-planning and finally computing the vehicle controls through a path follower or a path stabilizer. This led to the development of alternative methods of planning where no local map is generated and no search or sampling is required. Instead, the local path is generated by locally modifying segments of the global path using the sensory information (Fig. 2.6b). The most famous and well studies method for local path modification is the Timed Elastic Bands (TEB) method. TEB was first introduced almost a decade ago in [Roe+12], and has been improved and implemented in many works over the years [SXV20; Sun+21]. In TEB the path is modified by solving a non-linear least square optimization problem while taking into account both the non-holonomic and the kinodynamic constraints. A main advantage of TEB and similar path modification approaches is that it provides a balanced trade-off between avoiding local dynamic obstacles and producing a goal oriented motion.

The third and final category of systems introduce a one step local planning and control system when the vehicle controls are provided directly using the sensory information without the need to build a local map or search for a local path (Fig. 2.6c). These techniques also modify the global path, but the modification happens directly on the level of the vehicle control. Such techniques are a necessity specially with the growing need for efficient navigation systems suitable for highly dynamic environments where fast-reactive and even proactive behaviors are needed. Sensor-based control techniques are used in a wide range of robotic applications and can work with any type of perception system (visual sensors, proximity sensors, LiDAR, etc.) [CN21]. One example of such methods which are used for navigation in dynamic spaces are potential-based algorithms. This includes nature-inspired techniques which depend on drawing a movement driven by a group of fields or forces, such as the potential fields [Kha80] and the Deformable Virtual Zone (DVZ) [ZLT94] algorithms. In the potential field approach, every object in the environment produces an attractive or a repulsive force and the motion of the system is driven towards the goal destination as a result of these forces. On the other hand, DVZ method is based on surrounding the body of the robot with a virtual zone which gets deformed due to external intrusions of dynamic and static obstacles, and the robot is driven in the direction minimizing this deformation. The Although these methods are fast and efficient, their main drawback is the problem of convergence towards a local minima [Vic+17].

Local planning and control systems and their integration with the proactive and socially-aware navigation framework are explored in more detail in Chapter 4 and Chapter 5.

2.5 Longitudinal–lateral Vehicle Control Architectures

The navigation problem reduces to finding two system controls: the longitudinal and the lateral. The longitudinal control aims at finding the acceleration or speed control (v) to accomplish the specified system's task. For example, if the task is navigating a dynamic human-populated environment, this means finding the longitudinal control to reach a goal point while avoiding collisions and maintaining the surrounding agents safety and comfort. Whereas, if the task is agent following, for example, the longitudinal control problem can be formulated as a reference speed tracking problem. On the other hand, the lateral control is controlling the steering angle of the system (δ). If the targeted system is based on re-planning or local path modification (see Fig. 2.6), then the lateral control problem reduces to following a previously planned path. Whereas, if the local planning and control are merged in one system, such as sensor-based control systems, then the lateral control aims at finding the exact steering commands to perform the targeted task (reach goal, for example) while avoiding static and/or dynamic obstacles. The longitudinal and lateral control systems can be designed in one of the three architectures shown in Fig. 2.7.

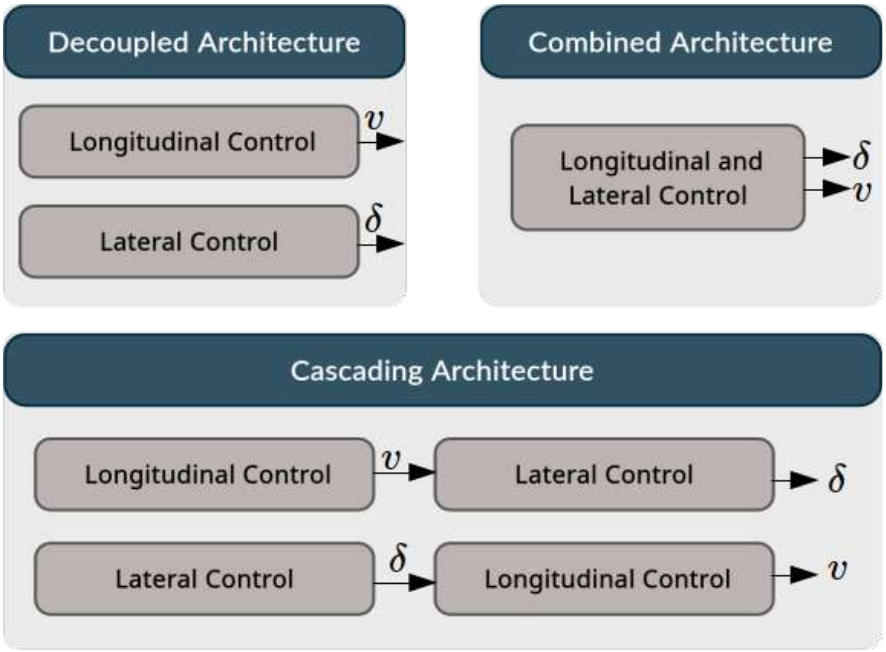

Fig. 2.7.: Longitudinal–lateral Control Architectures

Early works on vehicle control designed a **decoupled control architecture**, where the longitudinal and the lateral controls were addressed in two separate independent systems [HTV95; GL94]. Since the two independent systems architecture simplifies the task, many works in robotics focused on studying decoupling approaches [ABO99; BL01].

However, the decoupling of the two controls can be straightforward in some cases, such as when using a kinematic vehicle model in low velocities [Thu+04]. Therefore, even recent works which manly assumes zero-slip vehicle models used the decoupled architecture to solve the navigation problem [BMM05; Zha+12].

Many works used the decoupling while using the longitudinal control as an input to designing the lateral control system. This **cascading control architecture** was used to solve the path planning or tracking problem while assuming a constant longitudinal input [Pas+14; Dom+16; MT00]. This architecture was also used to design a stand-alone longitudinal control system, then cascade it with a lateral control system which considers the coupled nature of the two, such as the system architecture in [AOB14]. Similarly, the cascading architecture can be used such that the lateral control is computed in an independent system, then used an an input to compute the longitudinal control [Urd+07].

On the other hand, a **combined control architecture** can be used to consider the coupled dynamics or to design a single longitudinal-lateral control system [LH99]. This structure is commonly used in trajectory tracking control applications in the presence of sliding and slippery surfaces [Fan+05], or in higher speed applications. The combined architecture can also be used in shared control scheme to produce both the longitudinal and lateral assistance commands, such as the work in [NSB16]. Moreover, Velocity Obstacle (VO) based methods, such as Probabilistic Velocity Obstacle (PVO) [FSL07b], can also be classified under the combined longitudinal-lateral architecture.

Finally, in this work, a cascading longitudinal–lateral vehicle control architecture is used. This architecture is selected since having two sub-systems simplifies the planning task. Working with low vehicle velocities within shared spaces, allows using a kinematic vehicle model which facilitates designing two control systems instead of one coupled system. Moreover, using the cascading architecture where the longitudinal control is provided as an input to the lateral control system produces more natural and speed adapted steering maneuvers.

2.6 Validation of Autonomous Navigation Systems in Shared Spaces

The process of evaluating and validating an autonomous navigation system translate to making sure the system is functional, efficient and above all safe in all possible working scenarios. This is essential for any system and specially robotic systems that

can potentially be harmful due to the size of the robot and its proximity to humans. Autonomous vehicles navigating shared spaces with vulnerable road users fall in this category of systems with a very high potential risk. It is therefore essential to validate their performance before letting such a system share a space with pedestrians in a fully autonomous way. The most important aspect in the validation process is validating the safety of the navigation system.

This issue of motion safety is a key aspect in any mobile robot application. Researchers in robotics started taking a special interest in studying and formalizing motion safety standards with the increasing number of applications for robots in safety critical environments [Fra07]. There are multiple sources of motion safety failure for an autonomous systems. The failure can be a hardware failure such as a fault in the braking system. It can also accrue due to a perception error, where the perception system leads to an incorrect assumption about the environment. This brings to mind the accident that happened with Tesla's autopilot in 2016 on a highway in Florida, USA. The perception system of the autopilot mode failed to identify a white tractor-trailer on the highway and instead drove in full speed assuming that the path is free of any obstacle which led to the death of the driver [YT16]. Furthermore, the safety motion failure can occur due a software failure. This can either be a software bug or a reasoning error by taking the wrong decision or by encountering a scenario without a valid behavior policy [FK12]. It is critical to validate all the previously mentioned aspects to run the system autonomously around pedestrians. However, for the purpose of this work, we are focused on validating the reasoning and software failures associated with the navigation algorithm and the control system.

The validation process in shared spaces is much more challenging than any other structured environment. The more free and open nature of the shared space creates a wide range of possible working scenarios to test and validate. While in more structured environment, such as a highways, the structure of the space itself and the strict driving roles limits the number of possible user cases. Furthermore, working in proximity with humans with variable ages and physical abilities increases the validation difficulty. The validation process should account for all possible interaction scenarios with pedestrians. This includes all the different interaction types (frontal, lateral, etc.) with all the different possible velocities, accelerations, goals and even space properties than can exist in a shared space. The validation should also include the variable patterns for human behavior and even unmodeled and unpredicted behavior patterns.

2.6.1 Performance Validation Methodology and Criteria

The process of performance validation for an autonomous vehicle in a shared space starts with the Testing Cases Identification. This aim to design a set of tests and identify the parameters and the conditions in each test case. Firstly, the set of testing environments should be identified. This includes the static shared space and its characteristics, such as the entering/exiting points of the space, the shape of the space and the possible pedestrian attraction points or gathering spots. Secondly, the set of parameters of interest to be varied in each environment should be identified. Each parameter should be assigned a range of possible values and a limited set of testing values within that range. For example, if the parameter of interest is the speed of a pedestrian in the space, the possible range of values can be assigned based on the known limits of human speed which does not exceed $13m/s$ for the top world athletes [GN11]. While the set of testing values can be chosen closer to the range of expected normal people's speed in shared spaces. The number of identified testing environments, testing parameters and the size of the selected testing sets will result in the number of required test cases. The identification of the size and nature of the testing set is highly dependant on experience and reasoning. Any case that can accrue in the end application and that was not taken into consideration in the testing set can be a high source of risk.

The second step is the design of the actual tests to be ran in each test case scenario. Each test consists of a performance metric along with a success/failure criterion and performance quality measure. The set of tests should be sufficient to encounter for both the application purpose and all its possible effects on the environment. In our case for AVs navigating shared spaces the purpose of the application will result in metrics for travel time, number of collisions, trajectory smoothness, etc. On the other hand, the designed tests should also account for the possible effect of our AV on the surroundings, such as the comfortableness of the nearby pedestrians and the passengers within the AV.

After the testing cases have been identified and the performance tests have been designed the actual testing can begin, and the tests in each of the identified cases should be repeated for a sufficient number of tries for the results to be qualified. This leads us to a very important requirement in the validation process: a reliable testing environment. The used testing environments, the design and the implementation of the appropriate performance metrics is explored in detail in Chapter 6 and Chapter 7.

2.7 General Context and Notations

In the following we show the general notation and models used for both the vehicle and the pedestrians in the shared space across this thesis:

2.7.1 Coordinate Frames

Let $(O, \vec{X}_G, \vec{Y}_G)$ be the **Global Cartesian Coordinates map frame**. Three additional local coordinate frames are used in this work: two vehicle-centered frames (Fig. 2.8), and one pedestrian-centered frame (Fig. 2.9). The first is the the **vehicle's local Cartesian Coordinates frame** $(O_R, \vec{X}_V, \vec{Y}_V)$, where O_R is the center of the rear wheels axes of the vehicle and $\vec{X}_V$ is in the direction of the longitudinal velocity of the vehicle $\vec{V}_V$. Similarly, $(O_i, \vec{X}_i, \vec{Y}_i)$ is **the pedestrian local Cartesian frame** of a pedestrian i where O_i is the 2D center of mass of the pedestrian and $\vec{X}_i$ is in the direction of the pedestrian velocity vector $\vec{V}_i$. The second local vehicle-centered frame is a **Frenet frame** attached to the vehicle's path [Fre52]. This frame is defined by the tangential and normal vectors at a certain point of the reference curve. In the case of degenerate curves, the tangential is defined in parallel to the curve.

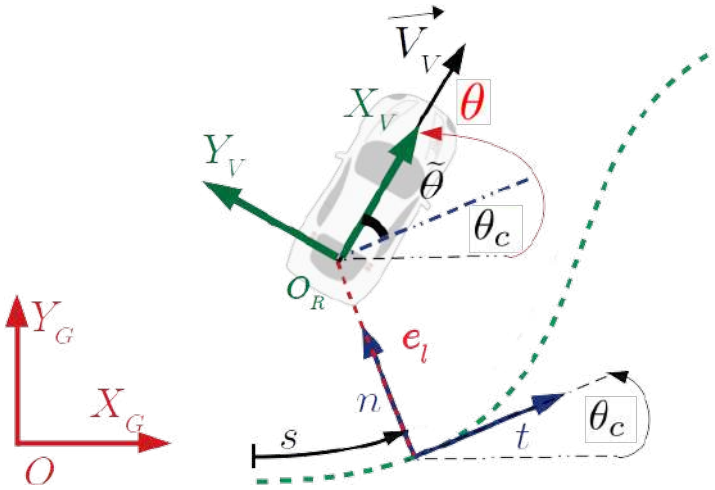

Fig. 2.8.: Vehicle-centered local frames

In the following: the symbols X^g, X^v, X^i and $X^{\mathcal{F}_\mathbf{C}}$ denotes the coordinates of a point X expressed in the global frame, the vehicle frame, the pedestrian i frame ($i \in \mathbb{N}_+$) and the Frenet frame of a curve $\mathbf{C}$ respectively.

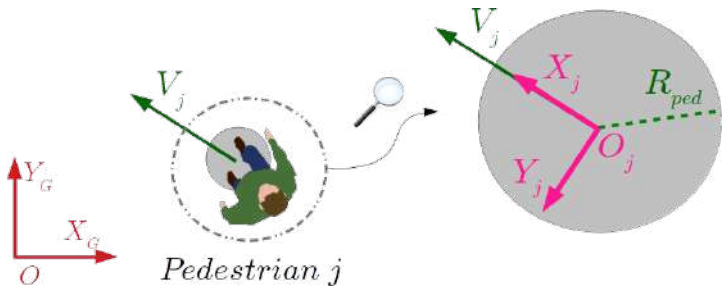

Fig. 2.9.: Pedestrian-centered local frame

2.7.2 System Model

Pedestrians Model

A pedestrian is modelled as a point in the $2D$ plane. The position of a pedestrian j at time t is $\boldsymbol{X_j}(t) = [x_j(t), y_j(t)]^T$ and its velocity is $\boldsymbol{V_j}(t) = [v_{x_j}(t), v_{y_j}(t)]^T$. The pedestrian space occupancy or the footprint of a pedestrian in the 2D plane is considered circular with a radius R_{ped} (Fig. 2.9). We can define the footprint of a pedestrian j at time t and position $\boldsymbol{P_j^g}$ with the function f_{fp}:

$$\begin{aligned} f_{fp}: \quad & \mathbf{R}^2 \to \mathbf{R}^2 \\ & f_{fp}(x; \boldsymbol{P_j^g}, S_p) = (x - \boldsymbol{P_j^g})^T S_p (x - P_j^g) - 1 \end{aligned} \tag{2.1}$$

where S_p is the shape matrix defined as:

$$S_p = \frac{1}{R_{ped}^2} \begin{bmatrix} 1 & 0 \\ 0 & 1 \end{bmatrix} \tag{2.2}$$

Vehicle Model

Navigating among pedestrians imposes low velocities and acceleration limits on the vehicle. In this case, the vehicle is modelled using the kinematic bicycle model with a zero slip assumption [Pol+17]. The position of the center of mass of the vehicle and its orientation at time t is $\boldsymbol{X_V}(t) = [x_v(t), y_v(t)]^T$ and $\theta(t)$ respectively. The steering angle is $\delta(t)$ and the longitudinal velocity and acceleration controls are $v(t)$, $a(t)$ respectively. The vehicle's body is assumed to be a rectangle of length L and width W.

The differential bicycle model of the vehicle can be written at its center of mass in the global coordinates frame as follows:

$$\dot{\boldsymbol{X}}_{\boldsymbol{V}}^{\boldsymbol{g}}(t) = \begin{bmatrix} v(t)\cos\theta(t) \\ v(t)\sin\theta(t) \end{bmatrix} \tag{2.3}$$

$$\dot{\theta}(t) = \frac{v(t)}{L}\tan\delta(t) \tag{2.4}$$

For control purposes the vehicle's model can also be written in the Frenet frame of a path $\mathbb{C}$. This is done using:

- The lateral displacement and the traveled arc length (e_l and s in Fig. 2.8 respectively)
- The heading error angle between the vehicle and the tangential vector to the path: $\tilde{\theta} = \theta - \theta_C$

Assuming $\kappa(s)$ is the curvature of the path $\mathbb{C}$, the vehicle model can be written at O_R as follows [CSB96]:

$$\begin{cases} \dot{s} = vcos(\tilde{\theta})\frac{1}{1-e_l\kappa(s)} \\ \dot{e_l} = vsin(\tilde{\theta}) \\ \dot{\tilde{\theta}} = \dot{\theta} - vcos(\tilde{\theta})\frac{\kappa(s)}{1-e_l\kappa(s)} \\ \dot{v} = a \end{cases} \tag{2.5}$$

The **vehicle's footprint** is approximated with the outer Löwner-John ellipse of the rectangle [Joh14] as shown in Fig. 2.10. This ellipse can be written in the local vehicle frame as:

$$\frac{X'^2}{a^2} + \frac{Y'^2}{b^2} = 1 \tag{2.6}$$

and (X', Y') can be written in the global frame as:

$$X' = (x^g - x_v^g)\cos(\theta) + (y^g - y_v^g)\sin(\theta) \tag{2.7}$$

$$Y' = -(x^g - x_v^g)\sin(\theta) + (y^g - y_v^g)\cos(\theta) \tag{2.8}$$

and the ellipse dimensions (a, b) can be derived from the length and width of the vehicle (L, W) as:

$$a = \tfrac{\sqrt{2}}{2}L, \quad b = \tfrac{\sqrt{2}}{2}W \tag{2.9}$$

Finally, the footprint of the AV can be expressed in quadratic form using the function f_{fp} (Eq. 2.1) as:

$$f_{fp}(x; \boldsymbol{P}_{\boldsymbol{V}}^{\boldsymbol{g}}, S_V) = (x - \boldsymbol{P}_{\boldsymbol{V}}^{\boldsymbol{g}})^T S_p (x - \boldsymbol{P}_{\boldsymbol{V}}^{\boldsymbol{g}}) - 1 \tag{2.10}$$

with the shape matrix S_V:

$$S_V = \frac{1}{a^2 b^2} \begin{bmatrix} b^2 \cos^2(\theta) + a^2 \sin^2(\theta) & (b^2 - a^2)\cos(\theta)\sin(\theta) \\ (b^2 - a^2)\cos(\theta)\sin(\theta) & b^2 \sin^2(\theta) + a^2 \cos^2(\theta) \end{bmatrix} \tag{2.11}$$

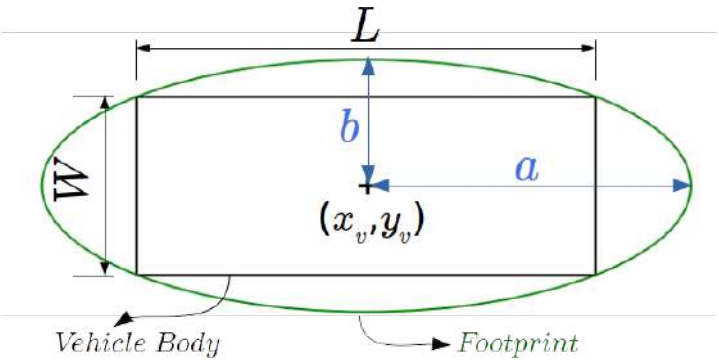

Fig. 2.10.: The vehicle footprint Löwner-John ellipse approximation

2.8 Conclusion

In this chapter we broadly explored the concept of PVI as a sub-category of HRI. As well as, the concept of proactive behavior and its application to the field of robotics and more specifically autonomous navigation. The main behavioral, planning, control and evaluation challenges related to the shared spaces navigation was generally presented. Finally, the models and notations used to describe the autonomous vehicle and the pedestrians across this thesis were detailed.

In the following chapters, we explore in detail the problems of understanding human behavior and proactively controlling the vehicle within a shared space.

Part I

Proactive Navigation Framework

"Treat a man as he is and he will remain as he is. Treat a man as he can and should be and he will become as he can and should be."

– Ralph Waldo Emerson

3 Understanding Pedestrian Behavior Around Vehicles

Developing autonomous vehicles capable of navigating safely and socially around pedestrians is a major challenge in intelligent transportation. This challenge cannot be met without understanding pedestrians' behavioral response to an autonomous vehicle, and the task of building a clear and quantitative description of the pedestrian to vehicle interaction remains a key milestone in autonomous navigation research. This chapter includes the model developed for predicting pedestrian behavior in shared spaces with an autonomous vehicle. The proposed model is based on estimating the cooperation of a pedestrian in interaction with the vehicle. This cooperation estimate is then used to predict the short-term trajectory of the pedestrian. Firstly, the chapter presents the formulation of the pedestrian behavior prediction problem and the related work in the literature. Secondly, a background is given on the main tools and concepts used to build the model. Finally, the proposed model is presented in section 3.4 along with the estimation of the model parameters in section 3.6. The Analysis of the pedestrian behavior prediction results using the proposed cooperation-based model is found in section 3.9. Furthermore, this chapter includes an experiment of pedestrian-vehicle interaction in a shared space. The data of pedestrian and vehicle trajectories is collected during the experiment to further tune and validate the proposed model. The description of the experiment, the collected data and its analysis is presented in section 3.5 of this chapter.

3.1 Problem Definition

Shared spaces introduce new dimensions to the navigation task making it an interdisciplinary challenge, which requires a study of the interaction between the vehicle and its conscious surrounding. Understanding and anticipating pedestrian behavior is crucial for the proactive navigation frame (Fig. 3.1)

The problem of pedestrian behavioral modeling is summarized as follows: Assuming a shared space with M pedestrians and a vehicle, where both the vehicle and the pedestrians follow the models proposed in 2.7. Knowing the state of the space (i.e.

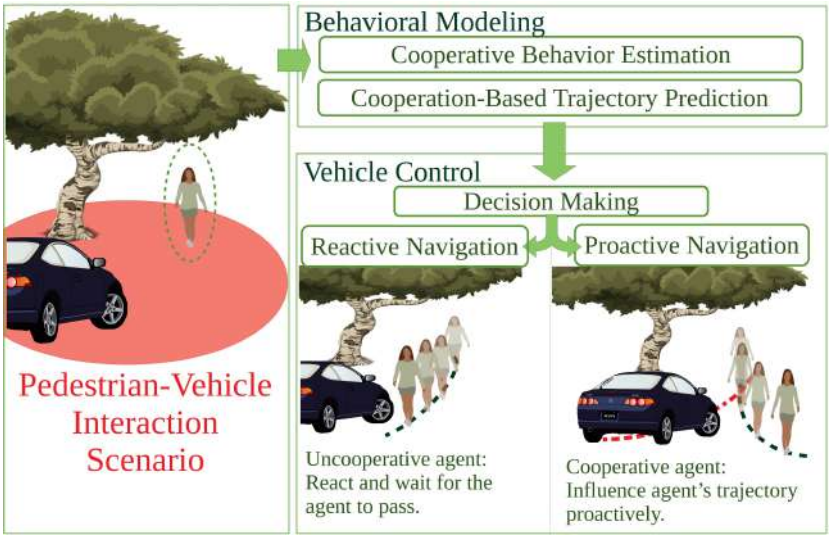

Fig. 3.1.: Pedestrian behavioral modeling as part of a global work scheme for proactive navigation

Pedestrian positions and velocities), what is the reaction of a pedestrian to a specific driving pattern of the vehicle:

$$
\begin{aligned}
&\text{Knowing the state of the space: } \{\boldsymbol{X_j}(t), \boldsymbol{V_j}(t)\}_{1\leq j\leq M} \ : t \in [t_0, t_1] \\
&\text{Given a vehicle behavior: } \boldsymbol{X_V}(t_1), \boldsymbol{V_V}(t_1) \\
&\forall i \leq M : \\
&\text{Find: } \boldsymbol{X_i}(t) \ \forall t \in [t_1, t_1 + T_h]
\end{aligned}
$$

where T_h is the prediction time horizon.

3.2 Related Work

Understanding how humans explore a complex environment has been a topic of spatial cognitive studies for decades [MG76]. Researchers built on these concepts to develop physical-based models for agents navigation around other dynamic agents and static obstacles. The main two types of models are Social Force Model (SFM) [HM95] and the Cellular Automata (CA) Models [NS92]. SFM models the agents in the space of interest as particles moving according to a driving force. This force is the outcome of all forces resulting from the individual interactions in the space. On the other hand, CA models the space as a set of cells and the agents can move between cells based

on a probability of choosing a specific cell. This probability is usually computed using predefined navigation rules. Many works built on top of these two models over the years to optimize the performance based on experience [Far+17; Zha+17], or to consider different types of agents and environment [Zho+21]. Most of the recent studies started optimizing the model for a specific scenario or environment rather than trying to find one global model for pedestrian navigation [CFD21; IA17]. Several studies presents pedestrian positions prediction models through a Kalman Filter (KF) or a Particle Filter (PF) [MTM15; Ber+04; Rid+18b]. Moreover, many works developed Machine Learning based models for the aim of motion prediction. This can be achieved using Markov Decision Process Motion Prediction (MPDMP), such as the model presented in [Vas16]. Other works based their predictions on Gaussian Processes (GP), such as the models proposed in [DT17a; VMO17b; Ful+08].

With the advancements in AV systems, the case of shared spaces started getting more attention in the recent years, to include the interactions with vehicles and cyclists in the model [AS20; Che+21]. However, there is an obvious lack of literature on studying human-vehicle interaction, cooperation and social rules, compared to that of human-robot interaction in general [GS07]. While the former falls under the same category, it is important to consider the particularity of the situation when working with an autonomous vehicle governed by its special properties and social conventions.

Some recent works have tackled the challenge of understanding and modeling the behavior of pedestrians around an autonomous vehicle. [Ran+19] formulates a model for pedestrians interaction based on social and psychological traits. This is done by assigning a dominance percentage to each pedestrian in an interaction scenario. The main limitation of this approach is basing the model on pedestrian-pedestrian interaction and assuming that it applies to pedestrian-vehicle interaction. However, the use of the social and psychological traits to build the model is inspiring and we construct our pedestrian behavioral model in a similar manner. A different method to model pedestrian-vehicle interaction is based on extending the classical SFM. The work in [Pré21] presents a SFM extension to include the vehicle effect in a ROS-based simulation environment. Moreover, [YOR18] also extends the glssfm by adding a repulsive force specific to the vehicle's influence. This resulted in a promising model, simulating several interaction scenarios in a shared space, however it was not validated on real-life data.

3.3 Background

The pedestrian-vehicle interaction model in a shared space is built using special interaction zones. The concept is based on dividing the space around the pedestrian into special areas specific to describing him/her interaction with other pedestrians or with the vehicle. These pedestrian areas are defined using the concepts of the social zones from Proxemics theory. Whereas, the intensity of the interactions within these zones is described using the deformable virtual zone method (DVZ).

3.3.1 The Pedestrian Social Zones

The concept of the pedestrian social zones was introduced in robotics from social behavior and psychological studies on the human management of space, or what is called Proxemics theory [RSL15]. The theory is based on the observations that individuals try to maintain certain distances from others during social interactions [Hal66]. Therefore, a socially-aware robotic system navigating among humans should respect these distances to maintain human safety and comfort. The theory defines different types of zones relative to individual interactions, group interactions or human-object interactions. To study pedestrian behavior in shared spaces we require two types of pedestrian zones: one related to pedestrian-pedestrian interaction, and one related to pedestrian-vehicle interaction.

For modeling the interactions between the pedestrians, the concepts of the personal and intimate zones are used. **The personal zone** (zone P in Fig. 3.2) is a space around the pedestrian in which any human intrusion would cause discomfort. Such zones are used in pedestrian force-based models (such as glssfm) to activate the repulsive force of pedestrian influence, for example. **The intimate zone** (zone N in Fig. 3.2) is usually contained in the personal zone. It is also related to pedestrian-pedestrian interactions but represents a much lesser tolerant to intrusion than the personal zone. On the other hand, to model the interactions between the pedestrians and the vehicle, different zone dimensions and adaptations are required. This is a result of the increased size and possible danger of a vehicle as compared to human-sized robots. Therefore, inspired by the concept of the personal zone, we introduce **the cooperation zone**, which is a new zone specific to the pedestrian's interactions with a vehicle (zone C in Fig. 3.2). As a pedestrian tends to clear the personal zone from human intrusion, (s)he tends to clear the cooperation zone of any vehicle intrusion.

Different works consider different shapes for the the previous zones around a pedestrian. These shapes vary from concentric circles or ellipses to other asymmetric shapes

dependant on personal factors such as the walking speed or the dominant side of the pedestrian [Gér+08]. In this work, concentric circular shapes are considered for all the zones.

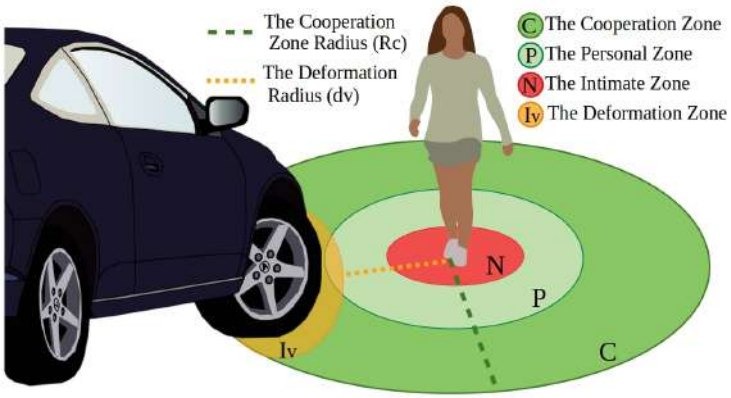

Fig. 3.2.: The Deformation of the cooperation zone due to vehicle intrusion

3.3.2 Deformable Virtual Zone Method

The DVZ method was first introduced by R. Zapata in 1994 [ZLT94] and it has been used since to model systems' maneuvers in both 2D and 3D spaces [CZ01; Amo+11; BMM06]. The idea is to surround the system under study with a virtual zone, and any body entering that zone will cause a deformation. Then, the system can be driven in the direction minimizing this deformation or changing it in a desired way. The system is first surrounded by an *undeformed glsdvz*. The shape of this zone corresponds to the optimal obstacle free case. The intrusion of obstacles is expressed by two scalars: the deformation quantity and the deformation mean angle.

By applying this concept to the previous personal and cooperation zones, we can express, for each pedestrian, the intrusion of other pedestrians and the intrusion of the vehicle respectively.

Assuming a pedestrian i at a position (x_i, y_i) with a heading θ_i. Let $\Gamma_i = (O_i, X_i, Y_i)$ be pedestrian i local coordinates frame which is given by:

$$\Gamma_i = T_G^i \Gamma_G \tag{3.1}$$

where Γ_G is the global coordinates frame and T_G^i is a transformation matrix given by a rotation θ_i and a translation $[x_i, y_i]$ as shown in Fig. 3.3. Let R_P and R_C be the

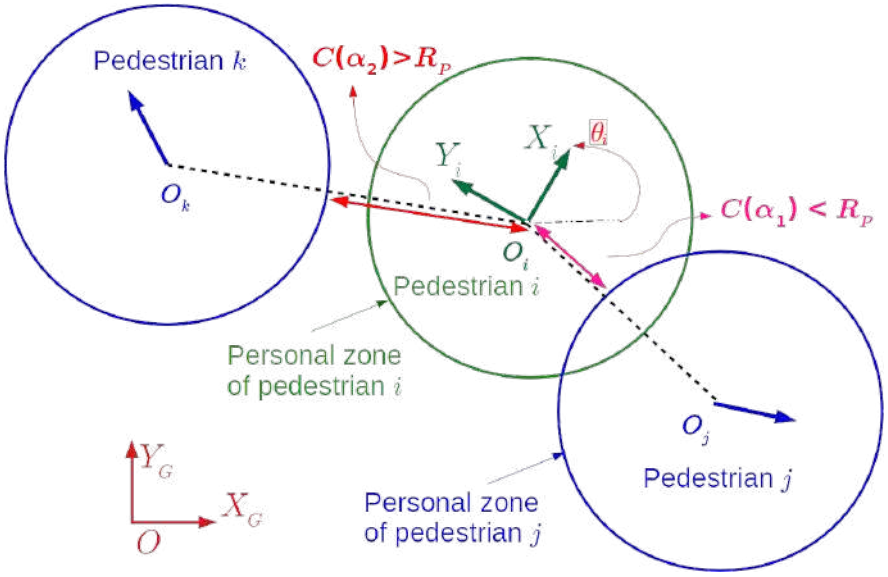

Fig. 3.3.: Example of the deformation radius of the personal zone due to pedestrian intrusion at two angle α_1 and α_2

radius of the circular personal and cooperation zones centered at the pedestrian position $X_P = [x_p, y_p]$. Then the undeformed glsdvz radius at angle α:

$$d_h(\alpha) = \begin{cases} R_P & \text{for the personal zone} \\ R_C & \text{for the cooperation zone} \end{cases} \tag{3.2}$$

and the deformed DVZ radius for both zones is given in the local frame Γ_i by:

$$d(\alpha) = \begin{cases} C(\alpha) & \text{if } C(\alpha) < d_h(\alpha) \\ d_h(\alpha) & \text{Otherwise} \end{cases} \tag{3.3}$$

where $c(\alpha)$ is the distance between the pedestrian i and the personal zone of the closest pedestrian at the angle α for the pedestrian zone (Fig. 3.3), and the distance between the pedestrian and the vehicle's body at angle α for the cooperation zone.

Hence, the deformation of the cooperation zone due to vehicle intrusion (zone I_V in Fig. 3.2) is written as:

$$I_V^i(t) = \frac{1}{2\pi} \int_{\alpha=0}^{2\pi} \frac{R_C - d(\alpha, t)}{R_C} d\alpha \tag{3.4}$$

where $d(\alpha, t)$ is the deformation radius at angle α and time t. Moreover, the cooperation zone weighted deformation angle is defined as:

$$\Theta_V^i(t) = \frac{\frac{1}{2\pi} \int_{\alpha=0}^{2\pi} (R_C - d(\alpha, t))\, \alpha d\alpha}{I_V^i(t)} \tag{3.5}$$

Finally, in a similar manner, $I_P^i(t)$ and $\Theta_P^i(t)$ are defined as the deformation of the personal zone and the deformation angle respectively, of an agent i due to pedestrian intrusion:

$$I_P^i(t) = \frac{1}{2\pi} \int_{\alpha=0}^{2\pi} \frac{R_P - d(\alpha, t)}{R_P} d\alpha \tag{3.6}$$

$$\Theta_P^i(t) = \frac{\frac{1}{2\pi} \int_{\alpha=0}^{2\pi} (R_P - d(\alpha, t))\, \alpha d\alpha}{I_P^i(t)} \tag{3.7}$$

3.4 Model Description

Cooperation has been shown to be a natural behavior in human societies on different scales [BR82], [Now06], and the task of navigating in a shared space can be viewed as a cooperative task, as it involves pooling and sharing of resources (space and time) between the pedestrians and the vehicle.

The proposed method deals with the navigation task as a cooperative task between the vehicle and the pedestrians and models the pedestrian behavior in a two-step process:

- The cooperation behavior of the pedestrian is described with a time-varying factor during the interaction with the vehicle.
- The future trajectory of the pedestrian is predicted based on its level of cooperation and the state of the surrounding space.

3.4.1 Pedestrian-Vehicle Cooperation Modeling

The cooperation of a pedestrian in a glspvi scenario is defined as the tendency of the pedestrian to modify his optimal trajectory around the vehicle to facilitate its navigation. Fig. 3.4 shows an example of the cooperative behavior levels where an agent is navigating around a vehicle from start to goal according to the green dashed path. In Fig. 3.4a the agent is considered uncooperative as the planned path is the optimal shortest path which assumes that the vehicle will move out of the way. On the other hand, in both Fig. 3.4b and Fig. 3.4c the optimal path is modified due to the existence of the vehicle. However, in case b the agent assumes some cooperation on the vehicle's side, therefore, the agent is considered somewhat cooperative. Whereas, in case c the planned path drives the agent completely out the vehicle's way and does not assume any cooperation on the vehicle's side. Therefore, the agent Fig. 3.4c is considered to be highly cooperative.

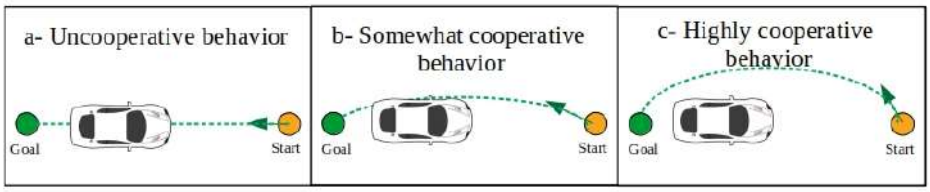

Fig. 3.4.: Example of the cooperative behavior annotation.

To model this cooperative behavior, a **Cooperation Factor (CF)** is assigned to each agent a throughout an interaction $CF_a(t)$. A larger CF indicates a more cooperative behavior from the vehicle's point of view, and vise versa.

The cooperation model of an agent a is designed as follows:

$$CF_a(t) = f_c(\boldsymbol{P^a_{cf}}(t)) \tag{3.8}$$

where f_c is a first order linear function:

$$\begin{aligned} f_c: \quad & [0,1]^{4\times 1} \rightarrow [0,1] \\ & x \longmapsto Ax + B \end{aligned} \tag{3.9}$$

$A \in \mathbb{R}^{1\times 4}$, $B \in \mathbb{R}$. the cooperation model **input parameters** of agent a (P^a_{cf}) are the following:

$$\boldsymbol{P^a_{cf}}(t) = \left[\mathbb{P}_{[a,veh]}(t), \mathcal{D}^a(t), I^a_P(t), \frac{V^a_m(t)}{V_{Pmax}}\right]^T \tag{3.10}$$

- $\mathbb{P}_{[a,veh]}(t)$: the probability of collision of agent a with the vehicle. The method for calculating the probability of collision is discussed in Chapter 4.

- $\mathcal{D}^a(t)$: the relative occupancy of the cooperation space surrounding the agent:

$$\mathcal{D}^a(t) = \sum_{j=1}^{N} d^a_j \times \frac{R^2_{ped}}{R^2_C} \tag{3.11}$$

$$d^a_j = \begin{cases} 1 & \text{if } ||\boldsymbol{P^a_j}||_2 \leq R_C \\ 0 & \text{Otherwise} \end{cases} \tag{3.12}$$

  with R_{ped} the pedestrian footprint radius, N the total number of pedestrians in the scene, and $\boldsymbol{P^a_j}$ the position of pedestrian j expressed in the local frame of pedestrian a. $||.||_2$ is the $\mathcal{L}_2$ Norm.

- $I^a_P(t)$: the deformation of the personal zone of the agent defined in (3.6)

- $\frac{V_m^a(t)}{V_{Pmax}}$: the relative preferred speed of the agent. V_{Pmax} the maximum possible speed of a pedestrian in the shared space. $V_m^a(t)$ is the average speed of the pedestrian a since the start of the interaction at time t_0:

$$V_m^a(t) = \frac{1}{t - t_0} \int_{\tau=t_0}^{t} V_a(\tau) d\tau \ \in [0, V_{Pmax}] \tag{3.13}$$

Our choice of input parameters can be viewed as a time-varying extension to the case of a human-vehicle interaction, and a new adaptation of the motion parameters proposed in [Guy+11] for modeling pedestrian dominance. The choice of $\mathbb{P}_{[a,veh]}(t)$ is based on the straightforward correlation between a cooperative behavior of a pedestrian in interaction with a vehicle and the estimated threat of the situation. Moreover, $I_P^a(t)$ represents the social concepts on the tendency of humans to maintain their personal zone clear of interference [RSL15] using the concept of the DVZ method [ZLT94]. In the same time, $\mathcal{D}^a(t)$ and $\frac{V_m^a(t)}{V_{Pmax}}$ are scaled representations of the parameters proposed in [Guy+11].

Deriving the model parameters

The model parameters: $\Phi = [A, B]$ (in (3.9)) are found by using a number of recorded interactions between a group of pedestrians and a vehicle. First, a manual annotation is performed where a mean cooperation value is assigned to each agent in each simulation depending on the agent's behavior. This is done by observing the agent's trajectory and knowing each agent's goal destination in the simulation; one of the four descriptions is selected:

- Uncooperative (UC) Agent: The agent took the optimal path to the goal point, without cooperating with the vehicle.

- Somewhat Cooperative (SC) Agent: The agent modified the optimal path, assuming some cooperation on the vehicle's side.

- Highly Cooperative (HC) Agent: The agent modified the optimal path, taking most of the burden in the pedestrian-vehicle cooperation task.

- Unidentified: cannot assign a clear cooperation description to the specific interaction case.

After discarding the unidentified cases, a mean cooperation value over the simulation period ($[t_0, t_0 + T_F]$) is assigned to each agent:

$$CF_m(a) = \frac{1}{T_F} \int_{t=t_0}^{t_0+T_F} CF_a(t) = \begin{cases} 0.25 & \text{if agent } a \text{ is UC} \\ 0.50 & \text{if agent } a \text{ is SC} \\ 0.75 & \text{if agent } a \text{ is HC} \end{cases} \tag{3.14}$$

These annotations are used as the ground truth for the mean value of the cooperation factor profiles. However, if only this criteria is used the optimization problem will clearly be under-constrained. This is because a time-varying profile of the cooperation is extracted using a single value (the mean value of the function). Therefore, the problem is further constrained by exploiting the fact that in each scenario the agents exhibiting similar behaviors (i.e. similar trajectory variations) are assigned similar nominal values. Meaning that the optimal CF model should result in highly correlated profiles for agents with similar mean cooperation values in one simulation, and similarly, highly uncorrelated profiles for agents with contradicting cooperation behaviors (HC and UC).

Finally, the pedestrian-vehicle cooperation model is obtained by finding the optimal value for the model parameters Φ such that they minimize both $J_1(\Phi)$ and $J_2(\Phi)$:

- J_1 is the term minimizing the error between the average value of the cooperation factor and the ground-truth annotations:

$$J_1(\Phi) = \sum_{s=1}^{M} \left[\sum_{a=1}^{A(s)} ||CF_m(s,a) - \frac{1}{T} \int_{t=t_0(s)}^{t_0(s)+T_F(s)} f_c(P_{cf}^a(t), \Phi)||_2 \right] \tag{3.15}$$

  with M being the total number of simulations, and $A(s)$, $[t_0(s), t_0(s) + T_F(s)]$ the total number of agents and the period of a simulation s.

- J_2 is the term that minimizes the Cross-Correlation (CC) error between the identically annotated profiles and maximizes it between the contradicting annotations in one simulation:

$$J_2(\Phi) = \sum_{s=1}^{M} \sum_{k=1}^{A(s)} \sum_{l=1}^{A(s)} R_{CC}[CF_k, CF_l] \lambda(k,l) \tag{3.16}$$

where $R_{CC}[CF_k, CF_l]$ is the cross-correlation factor between the cooperation factor profiles of agents (l, k):

$$R_{CC}[CF_k, CF_l] = \frac{\int_{t=t_0}^{t_0+T} CF_k(t) * CF_l(t)}{\sqrt{\int_{t=t_0}^{t_0+T} CF_k(t)^2 * \int_{t=0}^{T} CF_l(t)^2}} \tag{3.17}$$

and:

$$\lambda(k,l) = \begin{cases} -1 & \text{if } k \neq l \text{ and } CF_m(k) = CF_m(l) \\ 1 & \text{if } k \neq l \text{ and } CF_m(k) = inv(CF_m(l))^* \\ 0 & \text{Otherwise} \end{cases} \tag{3.18}$$

$^*HC = inv(UC), UC = inv(HC)$

3.4.2 Cooperation-Based Pedestrians Trajectory planning model

The main idea behind the model is that the trajectory of an agent can be predicted by knowing: the state of the space surrounding the agent, the influence of the vehicle, and how cooperative this particular agent is.

The trajectory planning model is of the form:

$$\boldsymbol{V_a}(t+1) = f_T(\boldsymbol{V_a}(t), \boldsymbol{P_m}(t)) \tag{3.19}$$

$$\boldsymbol{V_a} = \begin{bmatrix} V_a \\ \angle \boldsymbol{V_a} \end{bmatrix} \tag{3.20}$$

where $\angle \boldsymbol{X}$ indicated the orientation of the vector $\boldsymbol{X}$, $\boldsymbol{V_a}(t+1)$ and $\boldsymbol{V_a}(t) \in \mathbb{R}^2$ are the predicted and current velocity of agent a respectively, and f_T is a C^1 smooth function:

$$\begin{aligned} f_T : \quad \mathbb{R}^N &\rightarrow [0, V_{Pmax}] \times [0, 2\pi] \\ X &\longmapsto f_T(X) \end{aligned} \tag{3.21}$$

and the model **input parameters** or the motion parameters are the following:

$$\boldsymbol{P_m}(t) = \begin{bmatrix} CF_a(t).I_V^a(t) \\ CF_a(t).\Theta_V^a(t) \\ [1 - CF_a(t)].\Theta_{goal}^a(t) \\ [1 - CF_a(t)].D_{goal}^a(t) \\ I_P^a(t) \\ \theta_P^a(t) \end{bmatrix} \tag{3.22}$$

- I_V^a, Θ_V^a: the deformation parameters of the cooperation zone of agent a due to vehicle intrusion (found in (E.6) and (E.8))
- I_P^a, Θ_P^a: the deformation parameters of the personal zone of agent a due to pedestrian intrusion (found in (3.6) and (3.7))
- $D_{goal}^a, \Theta_{goal}^a$: the distance and the orientation of agent's a goal point. Assuming $\boldsymbol{G_a^a}(t)$ is the position of the agent's goal point written in the local frame of the agent, then:

$$D_{goal}^a(t) = ||\boldsymbol{G_a^a}||_2 \tag{3.23}$$

$$\Theta_{goal}^a(t) = \angle \boldsymbol{G_a^a} \tag{3.24}$$

- CF_a: the cooperation factor of the agent.

Multiplying the parameters resulting from the vehicle's influence (I_V, Θ_V) by the cooperation factor in the first two inputs refers to the fact that the more cooperative the agents are, the more their trajectories are influenced by the vehicle. Similarly, the less cooperative the agents are, the more their trajectories are influenced by the goal destination. Hence, the destination parameters (Θ_{goal}^a, D_{goal}^a) are weighted by the inverse of the cooperation factor in the third and fourth inputs. The remaining inputs present the effect of the surrounding pedestrians and the change in the agent's cooperation.

3.5 Pedestrians-Vehicle Interaction Data Generation: for Parameters Estimation and Model Verification

Collecting real-life pedestrian trajectory data is essential to model and understand pedestrian navigation behavior. Pedestrian datasets have been widely used in the literature to train, calibrate and verify pedestrian motion models. Multiple datasets of pedestrian interactions exist in the literature such as the Stanford university campus drone dataset [Rob+16], and the New York Grand Central Station dataset [ZWT12]. However, there is an obvious lack in pedestrian data collection for the case of shared spaces with vehicles. Pedestrian-vehicle interaction data is required to model pedestrian motion in shared spaces and to describe the vehicle's influence on a pedestrian or a group of pedestrians. The VCI CITR is the only dataset recently made public, which provides a set of pedestrian trajectories in a shared space with a golf-cart vehicle [Yan+19]. The dataset includes a top-view trajectories of a group of volunteers navigating a parking

lot in four interaction scenarios: frontal crossing, back crossing, lateral and bi-lateral crossing. The scenarios in the dataset include two driving modes. In the yield mode, the vehicle stops giving the priority to the pedestrians. While in the aggressive mode, the vehicle keeps accelerating taking over the pedestrians. However, more diverse driving patterns and the interactions with a real-sized vehicle is required to accurately model pedestrian behavior in shared spaces. To verify the suggested pedestrian cooperation model and to analyse pedestrian behavior in shared space, we designed a pedestrian-vehicle interaction experiment and collected the corresponding trajectory data.

3.5.1 Experimental Setup and Data Collection

The experiment took place at the parking lot of the LS2N lab on the École Centrale de Nantes campus (Fig. 3.5c). The experiment involved 17 volunteers (lab members and students):

- 2 female volunteers
- 15 male volunteers
- 1 male volunteer with reduced mobility

The volunteers in the experiment interact with a Renault Fluence vehicle with a driver behind the wheel (Fig. 3.5a). The data is collected on board of the vehicle using a perception system consisting of: 4 Camera, 1 Velodyne (VLP-16), 1 IMU and 1 GPS (Fig. 3.5b). The experiment is comprised of 5 different interaction scenarios: Frontal, Back, Frontal-Back, Lateral, Bi-lateral and Shared Space scenarios. The definition of the pedestrian-vehicle interaction scenarios is based on the interaction angle as shown in Fig. 3.6. The scenario called "Shared space" is simply a mixture of more than one interaction scenario (frontal crossing with lateral crossing, for example). The interactions included pedestrian groups, pedestrians in motion and standing pedestrians. Each volunteer is given a start and goal point in the space and is asked to move in a free and natural way. The driver is asked to move to a goal point as well with one of two driving patterns: an aggressive driving pattern and a more yielding driving pattern where the priority is given to the pedestrians.

3.5.2 Data Processing and Statistics

The total scenarios acted in the experiment and the number of interactions tested in each scenario are shown in Tab. 3.1.

(a)

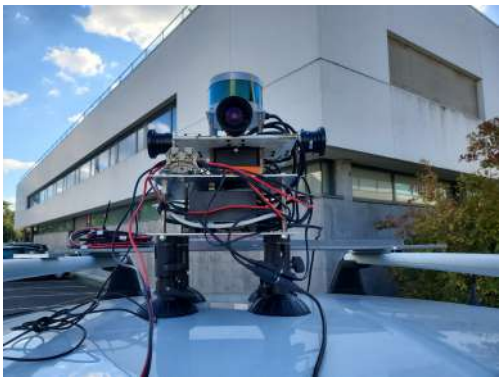

(b)

(c)

Fig. 3.5.: (a) The Renault Fluence vehicle used in the experiment (b) The perception system used for the data collection (c) Top-view of the parking lot

The resulting trajectories in the recorded interactions are visualized in detail in Appendix A.

Vehicle statistics

The behavior of the vehicle in the collected data is divided into two main modes: aggressive driving and a yield driving. The driving pattern of the vehicle in each mode can be described by knowing the speed, heading and acceleration limits during the various interactions. Furthermore, recent studies emphasises the link between the behavior of the vehicle at the minimum approach distance, and the pedestrian safety [Yim+20].

Assuming an interaction between a vehicle and N pedestrians, recorded over a period of $[t_0, t_0 + T_F]$, and assuming $(x_v(t), \theta_v(t), v_v(t), a_v(t))$ to be the position, heading, speed and acceleration of the vehicle at time t respectively, then the vehicle's behavior main parameters relative to studying PVI are the following:

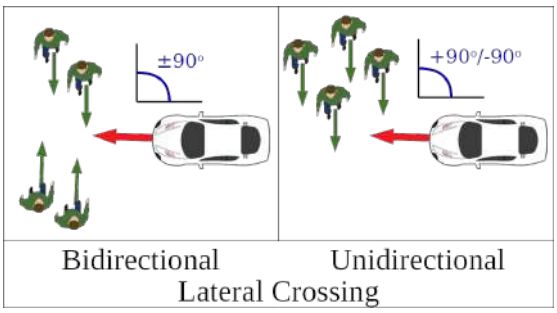

(a) PVI angle $= \pm 90^o$ for Lateral Crossing

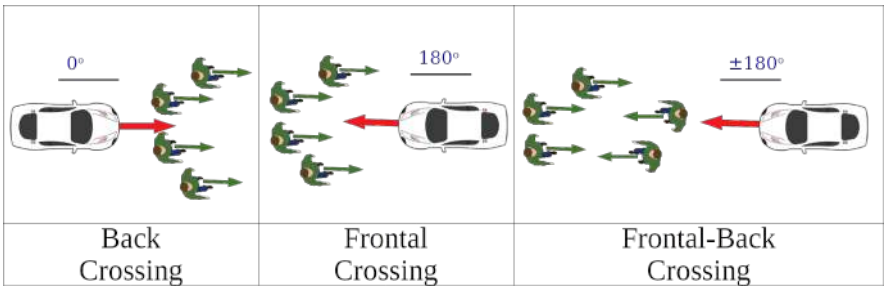

(b) PVI angle $= \pm 180^o$ for Frontal and Back Crossing

Fig. 3.6.: PVI scenarios based on the interaction angle

Interaction Scenario	Number Of Interactions	
	Aggressive Driver	Yielding Driver
Frontal Crossing	5	4
Back Crossing	1	1
Frontal-Back Crossing	1	1
Lateral Crossing	3	2
Bi-Lateral Crossing	2	1
Shared Space	2	3

Tab. 3.1.: Number of interaction scenarios in the experiment

- Average and max vehicle speed:

$$\bar{V}_V = \frac{1}{T_F} \sum_{t=t_0}^{t_0+T_F} v_v(t) \tag{3.25}$$

$$V_V^{max} = max_{t_0 \leq t \leq t_0+T_F} v_v(t) \tag{3.26}$$

- Average and max vehicle acceleration:

$$\bar{a}_V = \frac{1}{T_F} \sum_{t=t_0}^{t_0+T_F} a_v(t) \tag{3.27}$$

$$a_V^{max} = max_{t_0 \leq t \leq t_0+T_F} a_v(t) \tag{3.28}$$

- Average MAD to a pedestrian:

$$d_{min} = \frac{1}{N}\sum_{i=1}^{N} d^i_{min} \ : d^i_{min} = \min_{t_0 \leq t \leq t_0+T_F} D(v,i,t) \tag{3.29}$$

  where $D(v,i,t)$ denotes the distance between the vehicle and pedestrian i at time t and d^i_{min} is the vehicle's min approach distance to pedestrian i during the interaction.

- Average vehicle's speed and acceleration at min approach distance. let t^i_{dmin} be the time of the minimum approach to pedestrian i:

$$t^i_{MAD} = \{t \in [t_0, t_0 + T_F] : D(v,i,t) = d^i_{min}\} \tag{3.30}$$

  then the average speed and acceleration at MAD are:

$$V_{MAD} = \frac{1}{N}\sum_{i=1}^{N} V^i_{MAD} \ : V^i_{MAD} = v_v(t^i_{MAD}) \tag{3.31}$$

$$a_{MAD} = \frac{1}{N}\sum_{i=1}^{N} a^i_{MAD} \ : a^i_{MAD} = a_v(t^i_{MAD}) \tag{3.32}$$

The statistics of the previous parameters in the recorded data is summarized in Tab. 3.2 for both the aggressive driving and the yield driving interactions. The statistics shows the Mean, Maximum (Max), Median and Standard Deviation (Std. Dev.) of each value.

The vehicle's speed in the collected data is within the limit of the speed in a shared space ($< 5.5m/s$). The values of the average speed and acceleration of the vehicle does not differ much between the aggressive mode and yield mode. However, the distinction between the two modes is reflected more in the distribution of the vehicle's max speed and max acceleration during the interaction, where higher values are observed is the aggressive case. The driving pattern difference is also reflected in the vehicle acceleration at the minimum approach distance to a pedestrian. This can be noticed in Fig. 3.7, where in the yield mode the acceleration of the vehicle at the minimum approach distance is always limited ($< 0.45m/s^2$). Whereas in the aggressive mode the vehicle can experience higher acceleration values for a number of pedestrians in each interaction.

Parameter	Behaviour	Mean	Max	Median	Std. Dev.
Avg. Speed (m/s)	Aggressive	1.54	2.58	1.47	0.52
	Yield	1.20	2.14	1.15	0.54
Max. Speed (m/s)	Aggressive	3.33	5.58	2.89	1.27
	Yield	2.79	4.54	2.60	1.26
Avg. Acceleration (m/s^2)	Aggressive	0.30	0.54	0.29	0.13
	Yield	0.22	0.45	0.20	0.14
Max. Acceleration (m/s^2)	Aggressive	2.08	4.70	1.71	1.35
	Yield	1.20	2.61	0.94	0.87
Min. Approach Distance (m)	Aggressive	1.89	17.78	0.68	3.24
	Yield	1.43	10.26	0.94	2.05
Min. Approach Speed (m/s)	Aggressive	1.89	4.68	1.60	1.16
	Yield	1.65	4.35	1.61	1.10
Min. Approach Acceleration (m/s^2)	Aggressive	0.18	1.19	0.11	0.20
	Yield	0.14	0.44	0.88	1.30

Tab. 3.2.: Vehicle statistics in the collected PVI data

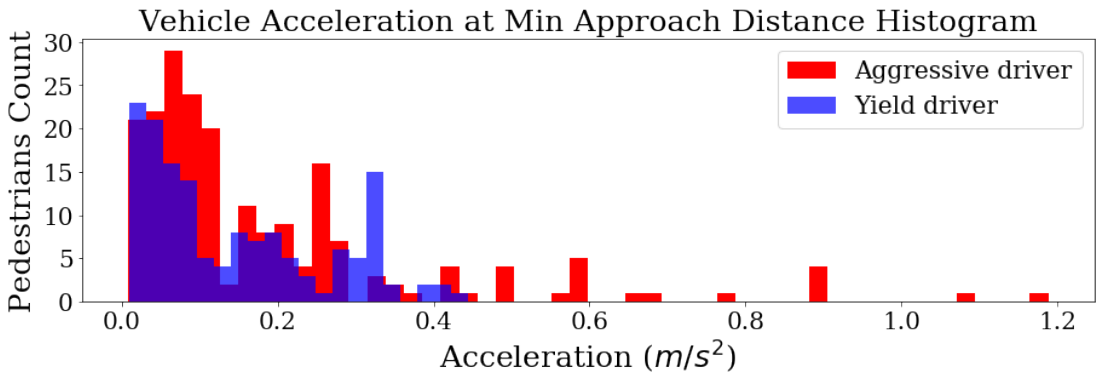

Fig. 3.7.: Histogram of the vehicle acceleration at the min. approach distance to a pedestrian in the collected data

More details on the collected vehicle data statistics can be found in Appendix B.

Pedestrians statistics

The pedestrian data is processed in a similar manner to that of the vehicle to compute the distribution of: the pedestrian average and max speed, the pedestrian average and max acceleration, and the pedestrian speed and acceleration limits the minimum approach distance. The values of the previous parameters are shown in Tab. 3.3. Opposite to the vehicle, the pedestrians experienced slightly higher levels of speed and acceleration in the yielding mode. By observing the values of the acceleration at the glsmad in more detail (Fig. 3.8), it is noted that pedestrians experience higher acceleration levels in the

aggressive mode for the lateral (uni and bi directional). Whereas, they experience higher acceleration levels in the yielding mode for the frontal and back crossing interactions.

Parameter	Behaviour	Mean	Max	Median	Std. Dev.
Avg. Speed (m/s)	Aggressive	0.70	1.33	0.75	0.30
	Yield	0.70	3.42	0.72	0.35
Max. Speed (m/s)	Aggressive	1.41	3.24	1.36	0.46
	Yield	1.48	3.83	1.44	0.45
Avg. Acceleration (m/s^2)	Aggressive	0.94	1.63	0.98	0.26
	Yield	0.87	1.90	0.80	0.29
Min. Approach Speed (m/s)	Aggressive	0.63	1.75	0.68	0.44
	Yield	0.65	3.83	0.68	0.51
Min. Approach Acceleration (m/s^2)	Aggressive	0.95	1.33	0.45	0.84
	Yield	0.99	2.26	0.33	0.23

Tab. 3.3.: Pedestrians statistics in the collected PVI data

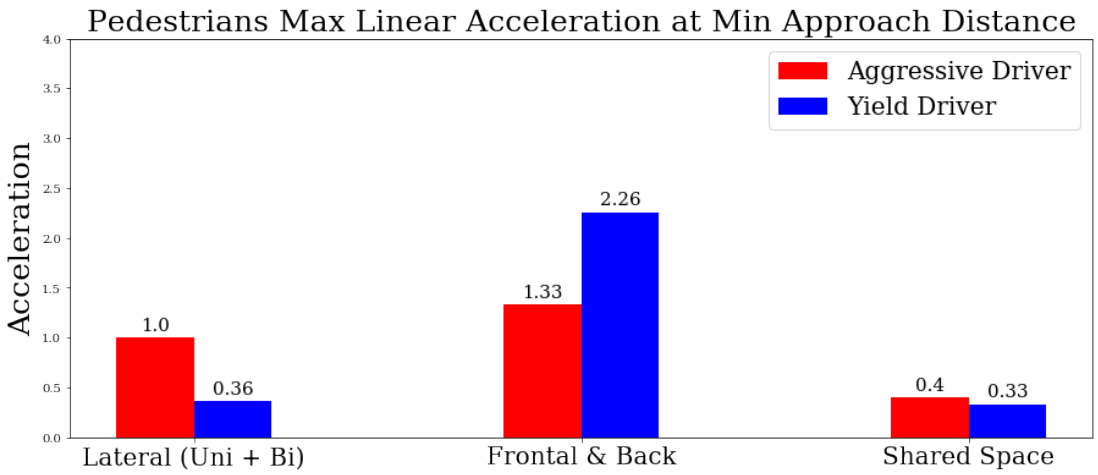

Fig. 3.8.: Maximum pedestrian acceleration at the min. approach distance to the vehicle in the collected data

The previous statistics on the collected data will be used in chapter 7 to analyse the performance of the proactive navigation framework, and to study the effect of the navigation of the safety and comfort of the pedestrians.

More details on the collected pedestrian data statistics can be found in Appendix B.

3.6 Model Parameters Estimation

The model parameters are estimated and evaluated using the VCI-CITR[1] data-set [Yan+19] and the previous École Centrale dataset. The considered scenarios in the VCI-CITR dataset include interactions between a vehicle and a group of pedestrians (7 to 10 in each interaction). The recorded interaction scenarios are frontal crossing and lateral crossing (uni-directional and bi-directional). These two types present the most basic interactions of a shared space which still occur frequently in most shared spaces.

The set of scenarios used in this work consists of 22 simulations divided as follows:

- Frontal Crossing: 4 simulations.
- Lateral Crossing: 10 bidirectional, 4 unidirectional with a yield driving mode and 4 unidirectional with a normal driving mode.

Each one of the four previous types is divided into two sets. An estimation set with 75% of the total number of simulations in each type, and a validation set with the remaining 25%. For the École Centrale dataset, the data is divided based on the driver's behavior (aggressive or yield). Then each type is split into 75% for the estimation set and 25% for the validation set. This is to include the two behaviors in both the estimation and the evaluation sets.

3.6.1 Pedestrian cooperation model parameters estimation

To estimate the cooperation model parameters: $\Phi = [A, B] \in \mathbb{R}^{1\times 5}$ (in (3.9)), the following steps are performed:

First, using all the PVI scenarios selected from the VCI-CITR dataset (both the estimation and validation sets), a mean cooperation value is assigned to each agent in each interaction depending on its behavior, as explained in section 3.4.1.

Second, using only the data from the estimation set, a first order linear regression is used to fit the model in (3.8) to the annotated pedestrian cooperation data. Meaning that the model parameters are found using only the first optimization criterion, J_1 in (3.15):

$$\Phi' = arg \min_{\Phi'} J_1(\Phi') \in \mathbb{R}^{1\times 5} \tag{3.33}$$

[1]Vehicle-Crowd Interaction data-set - CITR lab: `https://github.com/dongfang-steven-yang/vci-dataset-citr`

This optimization problem is solved and the value Φ' of the model parameters is found using scikit-learn Python.

The value Φ' of the parameters is considered as an average estimation. A search for the optimal value of the modal parameters is performed in a neighborhood of Φ' using the cross-correlation based second optimization criterion (J_2 in (3.16)). The search neighborhood is selected to be 20% of the average estimation. Hence, the resulting search set is:

$$\mathcal{N}(\Phi') = \prod_{j=1}^{5} [0.8 \times \phi'_j, 1.2 \times \phi'_j] \ : \Phi' = [\phi'_1, ..., \phi'_5] \tag{3.34}$$

Subsequently, the optimal model parameters are:

$$\Phi = arg \min_{\Phi \in \mathcal{N}(\Phi')} J_1(\Phi) \tag{3.35}$$

The problem in (3.35) is a bounded smooth Nonlinear Optimization Problem (NLP). Therefore, a derivative-free optimization method is used to solve it. Based on previous study on the performance of available derivative-free solvers, the TOMLAB solver (Matlab) is selected [RS12]. The selected solver performs searches using a local NLP solver from starting points chosen by a scatter search algorithm within the bounds $\mathcal{N}(\Phi')$.

3.6.2 Cooperation-based trajectory planning model parameters estimation

The cooperation-based trajectory planning model is estimated using linear regression, such that:

$$\boldsymbol{V_a}(t+1) = f_T(\boldsymbol{V_a}(t), P_m(t)) \tag{3.36}$$

with:

$$\boldsymbol{V_a} = \begin{bmatrix} V_a \\ \angle \boldsymbol{V_a} \end{bmatrix} \tag{3.37}$$

$$\begin{aligned} f_T : \quad \mathbb{R}^N &\rightarrow [0, V_{Pmax}] \times [0, 2\pi] \\ X &\longmapsto C_1 X + C_2 \end{aligned} \tag{3.38}$$

with: $C_1 \in \mathbb{R}^{2\times 6}$, $C_2 \in \mathbb{R}^2$. The model parameters Ψ are optimized to minimize the error between the predicted trajectory and the ground truth pedestrian trajectories in the estimation set.

$$\Psi = \begin{bmatrix} C_1[0] & C_2[0] \\ C_1[1] & C_2[1] \end{bmatrix} = [\Psi_0, \Psi_1]^T \in \mathbb{R}^{2\times 8} \tag{3.39}$$

The model is learnt for short term prediction, such that:

$$\Psi = \left[arg \min_{\Psi_0} J_V(\Psi_0),\ arg \min_{\Psi_1} J_\theta(\Psi_1) \right]^T \tag{3.40}$$

where J_V and J_θ are the linear velocity and orientation short-term prediction errors respectively.
Assuming T_h is the prediction horizon, $[t_0(s), t_0(s)+T_F(s)]$ is the period of an interaction s, and t_k is the time discretization step, then the number of time iterations in the interaction is: $K(s) = int(\frac{T_F(s)}{t_k})$.
Let $A(s)$ be the number of pedestrians in an interaction s, and M the total number of interactions in the estimation set. Moreover, lets call $V^{l,m}_{real}$ the ground truth value of the linear velocity for agent m in an interaction l, and $V^{l,m}_{model}$ its predicted value. Then, the linear velocity prediction error is written as:

$$J_V(\Psi_0) = \sum_{s=1}^{M} \sum_{i=1}^{A(s)} \sum_{j=1}^{K(s)} J_v(s,i,j;\Psi_0) \tag{3.41}$$

with:

$$J_v(s,i,j;\Psi_0) = \sum_{t=t_0+it_k}^{t_0+it_k+T_h} ||V^{s,j}_{real}(t) - V^{s,j}_{model}(t;\Psi_0)||_2 \tag{3.42}$$

Similarly, the orientation prediction error is:

$$J_\theta(\Psi_1) = \sum_{s=1}^{M} \sum_{i=1}^{A(s)} \sum_{j=1}^{K(s)} J_o(s,i,j;\Psi_1) \tag{3.43}$$

with:

$$J_o(s,i,j;\Psi_1) = \sum_{t=t_0+it_k}^{t_0+it_k+T_h} ||\angle \boldsymbol{V^{s,j}_{real}}(t) - \angle \boldsymbol{V^{s,j}_{model}}(t;\Psi_1)||_2 \tag{3.44}$$

Finally, The optimization problem is solved and the value of the model parameters Ψ is learnt using the scikit-learn[2] library in Python.

[2] `https://scikit-learn.org/`

3.7 Models Evaluation

The evaluated model parameters are shown in Appendix G.

3.7.1 Pedestrian cooperation model evaluation

To evaluate the accuracy of the cooperation model, a cross-correlation test is implemented. Where for each pair of agents in each simulation, the cross-correlation factor between their cooperation profiles is computed.

First, the ground-truth values of the CC factors (R_{GT}) is obtained using the earlier annotations as shown in Table 3.4.

Cross-Correlation Factors Ground Truth	
Agent Pair Annotation	R_{GT}
Similar Behavior (SB): [UC, UC] or [HC, HC] or [SC, SC]	1
Inverse Behavior (IB): [HC, UC] or [UC, HC]	0
Unidentified Cases: [Nan, -] or [-, Nan]	Nan

Tab. 3.4.: Obtaining the ground-truth values of the agents CC factors

After discarding the unidentified cases, the CC factors of all the agent pairs (R_{CC}) are computed using (3.17). These continuous values are then discretized to be compared with the ground truth values:

$$R^d_{CC}[CF_k, CF_l] = \begin{cases} 1 & \text{if } R_{CC}[CF_k, CF_l] \geq 0.5 \\ 0 & \text{otherwise} \end{cases} \tag{3.45}$$

and the behavior of the agent pair is predicted to be similar (SB) if $R^d_{CC} = 1$, and inverse (IB) if $R^d_{CC} = 0$.

Finally, the confusion matrix [Hos15] is computed as illustrated in Tab. 3.5.

	Actual SB	Actual IB
Predicted SB	True Similar (ts)	False Inverse (fi)
Predicted IB	False Similar (fs)	True Inverse (ti)

Tab. 3.5.: Obtaining the confusion matrix of the predicted CC factors

The accuracy of the model is evaluated using:

$$Accuracy = \frac{ts + ti}{ts + fs + ti + fi} \times 100\% \tag{3.46}$$

The result of evaluating the confusion matrices and the accuracy of the model is shown in Tab. 3.6 for each type of the interaction scenarios in the VCI-CITR data-set, and in Tab. 3.7 for the École Centrale data-set.

	Frontal Crossing	Lateral Crossing	All Scenarios
Confusion Matrix	41 | 1 7 | 4	220 | 6 64 | 48	261 | 7 71 | 52
Accuracy	85%	79%	80%

Tab. 3.6.: The cooperation model accuracy against the VCI-CITR data-set based on the CC test

	Frontal Crossing	Lateral Crossing	All Scenarios
Confusion Matrix	38 | 0 7 | 5	25 | 4 9 | 10	63 | 4 16 | 15
Accuracy	86%	73%	79%

Tab. 3.7.: The cooperation model accuracy against the École Centrale data-set based on the CC test

The cooperation model is able to predict the similarities in agents' behaviors with a good accuracy in both lateral and frontal crossing scenarios. The prediction accuracy was lower for the École Centrale data-set's lateral cases due to the more limited available sample of agent's pairs. Noting that the available scenarios in the data-set provided a small sample of agent pairs with inverse behaviors in the frontal crossing simulations, which leads to an unreliable evaluation of the accuracy for the frontal crossing cases.

3.7.2 Cooperation-based trajectory planning model evaluation

To evaluate the model, the Mean Square Error (MSE) between the trajectories predicted by the model and the real trajectories in the validation set is computed. Tab. 3.8 shows the $MSE\%$ in the linear velocity and the orientation for each type of interaction scenarios computed using:

$$MSE\% = \frac{1}{M}\sum_{s=1}^{M}\frac{1}{A(s)}\sum_{a=1}^{A(s)}\frac{1}{T(s)}\sum_{t_k=t_0}^{T(s)+t_0}\frac{||X_{real}^{a,s}(t_k) - X_{model}^{a,s}(t_k)||_2}{||X_{real}^{a,s}(t_k)||_2} \times 100\% \quad (3.47)$$

where M is the total number of simulations, $A(s)$, $T(s)$ are the total number of agents and the period of simulation s respectively. $X_{real}^{a,s}$, $X_{model}^{a,s}$ are the real and the model output values respectively for agent a in simulation s, which is replaced by either the linear velocity or the orientation.

The model predicts the agents trajectories with a good accuracy for both the linear velocity and the orientation. A higher orientation MSE value is observed is the frontal

	Frontal Crossing	Lateral Crossing	All Scenarios
Linear Velocity	18.42%	22.61%	21.91%
Orientation	2.66%	1.5%	1.69%

Tab. 3.8.: $MSE\%$ between the model output and the real trajectories in the validation set

crossing scenarios. Whereas, a higher linear velocity MSE is observed for the lateral crossing. This is caused by the agents experiencing more frequent orientation variations in a frontal crossing interaction, and more linear velocity variations in a lateral crossing interaction.

3.8 Towards A More Generalized Model

One drawback of the proposed pedestrian cooperation model is that the model is impersonal. Meaning that any two pedestrians existing in the same situation with the same goal destination will act similarly. Which is an incorrect assumption in real life situations. Multiple other factors can affect the behaviour of a pedestrian. These factors can include the age, physical and psychological state of the pedestrian for example [Dur+16]. Excluding these factors would lead to errors or biases in the trajectory prediction. To account for these factors, a new parameter is added to the cooperation model. We call it the Inner Cooperation Factor (ICF) which is unique to each agent. The ICF replaces the additive parameter B in the cooperation model (3.9) and the generalized cooperation model is written as:

$$CF_a(t) = f'_c(P^a_{cf}(t)) \tag{3.48}$$

where f'_c is a first order linear function:

$$\begin{aligned} f'_c : \quad & [0,1]^{4\times 1} \to [0,1] \\ & X \longmapsto AX + ICF(t) \\ & \text{with } ICF(t_0) = B \end{aligned} \tag{3.49}$$

where t_0 is the initial time of the interaction.

During an interaction scenario, the ICF of each detected pedestrian is updated over consecutive time intervals (Fig. 3.9). First, an initial value is assumed ($ICF(t_0) = B$). Then, the trajectory of the agent is predicted for a fixed prediction horizon T_h using the cooperation-based trajectory planning model. The predicted trajectory is then compared with the actual observed trajectory. ICF is updated using a simple gradient descent method to minimize the trajectory prediction error. The computation of the prediction

error gradient is straightforward since both the modified cooperation model and the trajectory planning model are linear. The derivation of the trajectory error gradient in shown in Appendix D.

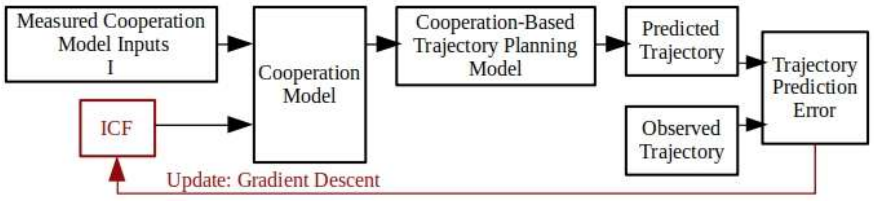

Fig. 3.9.: Updating the inner cooperation factor of an agent based on the trajectory prediction error

3.9 Results Analysis

The cooperation model and the cooperation-based trajectory planning model are implemented to predict the behavior and trajectories of the pedestrians in the evaluation set of the data. Fig. 3.10 shows an example of the cooperation factor profiles for a group of agents in one of the lateral crossing scenarios. It can be observed in the figure that agents $1, 6, 7, 8$ show high cooperation factor values towards the end of the simulation ($CF > 0.75$) as these agents did not pass in front of the vehicle, but waited for it to pass instead. Agents $3, 5$ show low CF values ($CF < 0.3$) when passing in front of the vehicle while it is approaching. On the other hand, agent 2 shows higher CF values than agents $3, 5$ as it passed in front of the vehicle earlier in the simulation when it was further away, hence the passing behavior was also cooperative. Finally, agent 4 would be expected to have a CF profile more similar to agent 6, but its somewhat stable cooperation may be attributed to the fact that it experienced less overall acceleration and was further away from the vehicle than agent 6.

3.9.1 Generalized vs. basic cooperation model

The cooperation-based trajectory planning model is tested with the two proposed versions of the cooperation model in (3.8) and (3.49). The goal is to show the effect of incorporating an additional personal parameter (ICF) in the cooperation model (3.49) on the trajectory prediction error. The trajectories of the pedestrians in the validation set is predicted using the model over a $T = 10s$ prediction horizon with both versions of the cooperation model. In the case of the generalized version, ICF is set to the initial value similar to the basic model: $ICF(t_0) = B$ and updated to minimize the trajectory

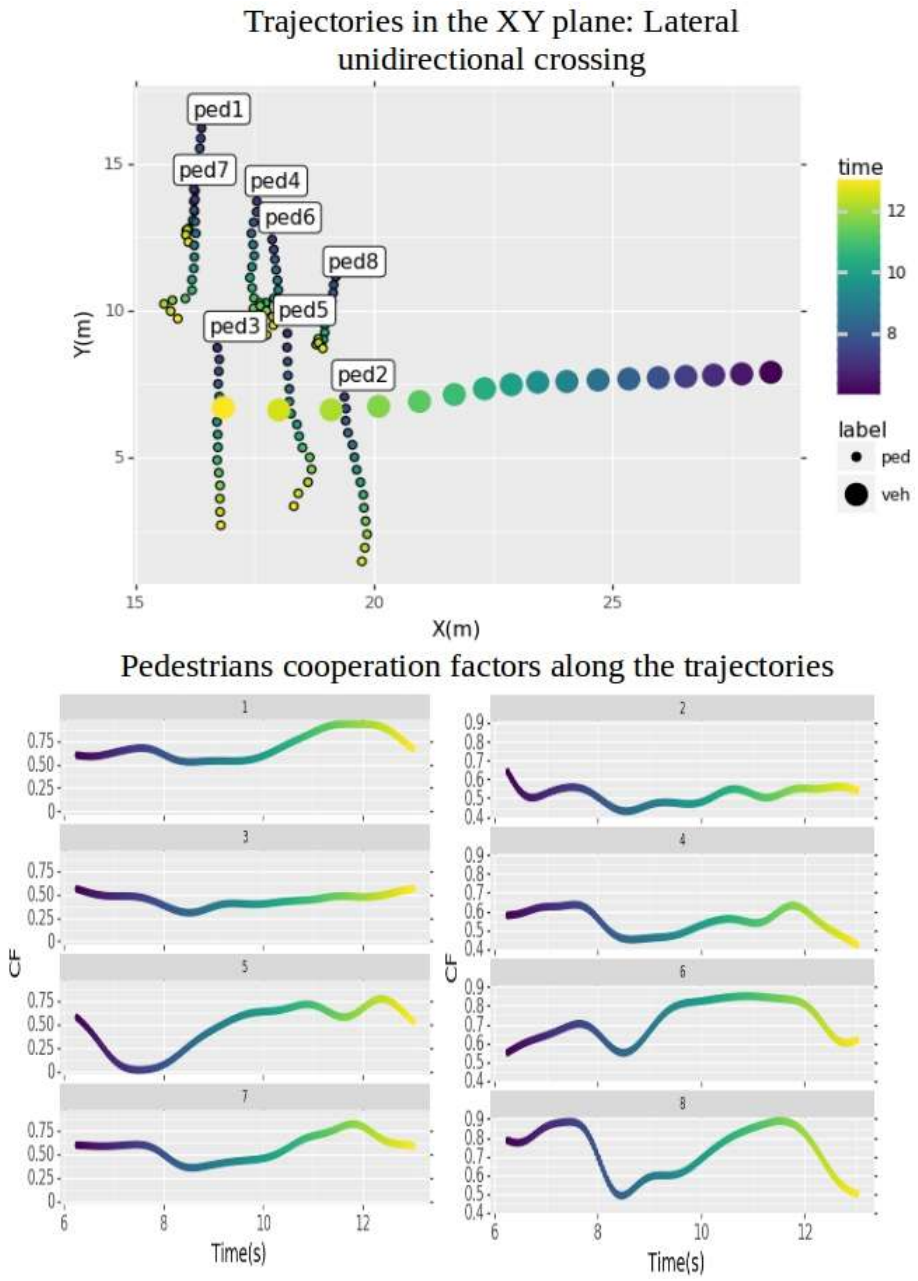

Fig. 3.10.: The cooperation factor profiles of the agents in a lateral crossing scenario

prediction error over $T_h = 2s$ time horizon. The $MSE\%$ between the predicted and the ground-truth trajectories is calculated according to (3.47). Tab. 3.9 shows the $MSE\%$ in the linear velocity and the orientation for each type of interaction scenarios with and without the additional personal parameter (titled ICF, Basic respectively). Fig. 3.11 shows an example of the model output for the trajectory prediction in one of the frontal interactions with both versions of the cooperation model.

Interaction Scenario	Frontal Crossing		Lateral Crossing		All Scenarios	
	Basic	ICF	Basic	ICF	Basic	ICF
Linear Velocity	18.42%	17.31%	22.61%	20.35%	21.91%	19.79%
Orientation	2.66%	2.11%	1.50%	0.07%	1.69%	0.44%

Tab. 3.9.: $MSE\%$ between the model output and the real trajectories in the validation set using the basic cooperation model (3.8) (Basic), and the extended version in (3.49) (ICF)

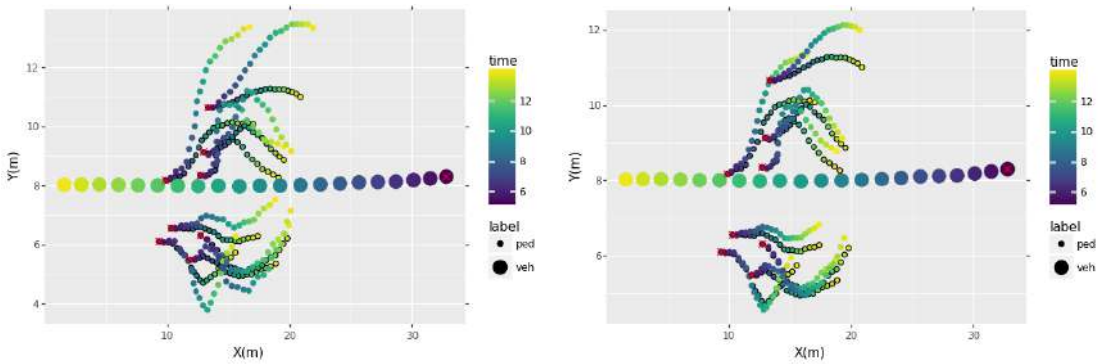

(a) With the basic cooperation model (3.8) **(b)** With the modified cooperation model (3.49)

Fig. 3.11.: Trajectory prediction model output in a frontal interaction scenario. Black contour: Real. No contour: Predicted. X: starting point

The additional online estimated parameter ICF in the generalized cooperation model helped reduce the prediction error of the cooperation-based trajectory planning model. A more significant reduction of $MSE\%$ is noticed for the orientation estimation specially for the case of lateral interactions.

More on the model output visualization is found in Appendix C.

3.9.2 Effect of changing the cooperation factor

To visualize the effect of changing the cooperation factor of a group of agents in an interaction scenario, a reference frontal interaction simulation is generated using the cooperation model in (3.8). Afterwards, two other simulations are generated using two modified versions of the cooperation model: one with a 50% increment, and the other with a 50% decrements of the cooperation factor. Fig. 3.12 shows the three resulting simulations, where it can be observed that the simulation with an increased cooperation factor resulted in a more cooperative behavior on the agents side, moving out of the vehicle's way. Fig. 3.13 also shows the cooperation factors of the agents corresponding to the three simulations. Note that even-though an increment/decrement

on the cooperation model is applied, the cooperation factor is still computed based on the evolution of the simulation.

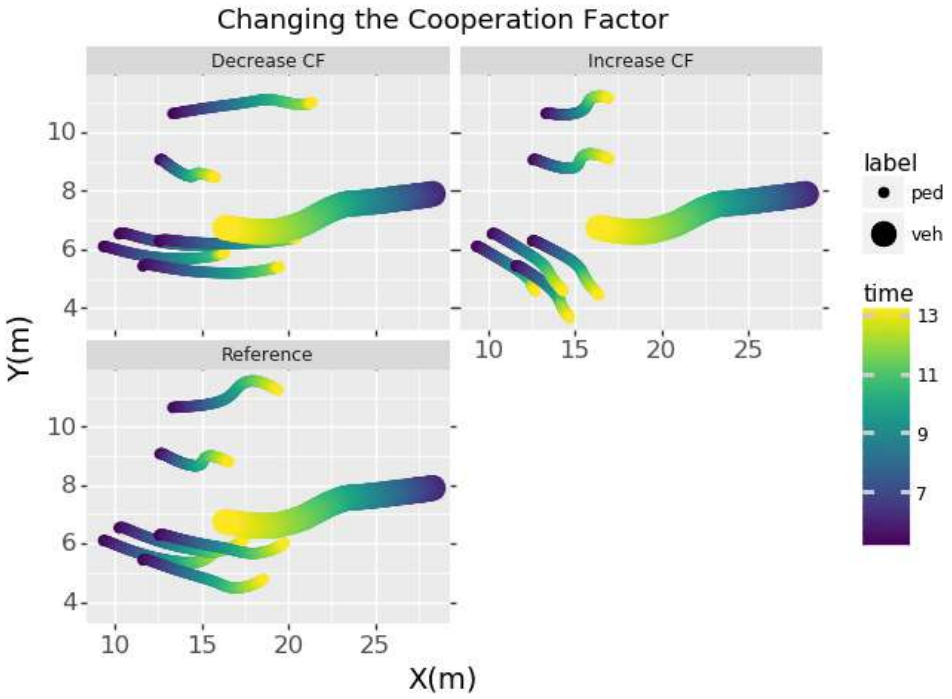

Fig. 3.12.: Trajectories in the XY plane of the two simulations generated with increased/decreased cooperation factor values vs. the original reference simulation

3.10 Conclusion and Prospects

This chapter provides a study on pedestrian-vehicle cooperation through modeling and data collection. The work in this chapter presents a pedestrian-vehicle interaction model based on the concept of cooperative navigation, which can be exploited in autonomous navigation systems to ensure safe and socially-accepted behavior of the vehicle. The proposed model estimates the pedestrian reaction in two steps. In a first step a cooperation factor is estimated to present the cooperative behavior of an agent from the vehicle's point on view. The suggested cooperation measure is based on personal factors of the agent (goal and preferred speed) and on the state of the space surrounding the agent. This state includes both the pedestrian the vehicle influence. After estimating the pedestrian cooperation, a cooperation-based trajectory prediction can be performed. The proposed trajectory planning model presents the trade-off in pedestrian planning between the goal destination's influence and the vehicle's influence. This trade-off is

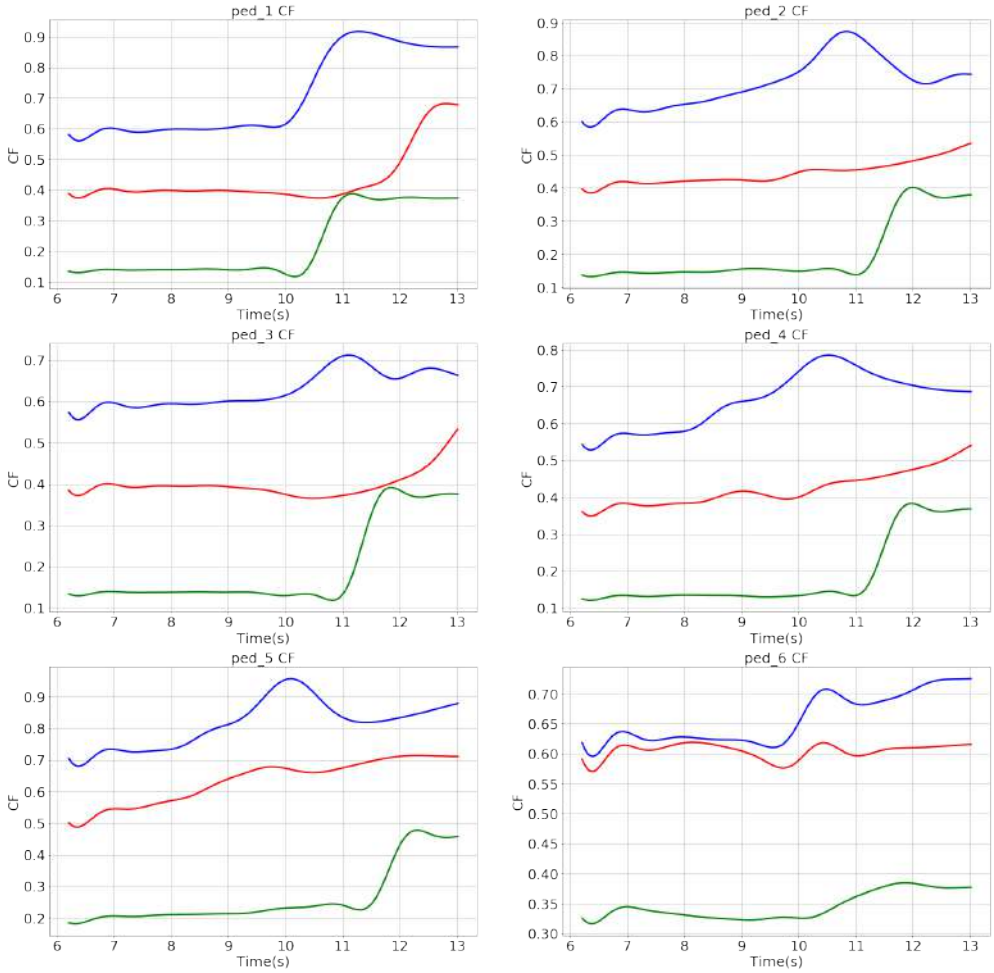

Fig. 3.13.: The cooperation factors of the agents corresponding to the three simulations in Fig. 3.12. Red: reference simulation, blue: simulation generated with a 50% increment on CF, green: simulation generated with a 50% decrement on CF.

based on the cooperation of the specific pedestrian. The model developed in this chapter and the corresponding results were the basis for the following publication:

"***M. Kabtoul, A. Spalanzani and P. Martinet. Towards Proactive Navigation: A Pedestrian- Vehicle Cooperation Based Behavioral Model. IEEE International Conference on Robotics and Automation (ICRA), May 2020, Paris, France. pp.6958-6964. hal-02509637***"

The cooperation estimation part of the model performs well in scenarios including a group of pedestrians in interaction with a vehicle, and its output describes the change in the pedestrian's behavior using a time-varying factor ranging between zero (highly uncooperative) to one (highly cooperative). In future works, the ability of the cooperation model to identify groups of agents in dense spaces can be tested. This is because

the cooperation model is built to maximize the cooperation factor's cross-correlation between agents with similar behavior patterns. Therefore, agents in a group would be expected to have highly correlated cooperation profiles.

The cooperation model is further generalized by adding a personal parameter to the model. This parameter is unique to each pedestrian and can be evaluated online to minimize the trajectory prediction error. This is done to account for not considering other personal factors which cannot be measured directly from the state of the space, but can affect an individual's cooperation in real scenarios. In future development of the model, visual information (age, physical state, .. etc) can be incorporated to the model trough this parameter.

Additionally, the chapter presented the collected data from a pedestrian-vehicle interactions experiment performed on the site of *École Centrale de Nantes*. The experiment included two types of driving behaviors: aggressive and yield driving. The experiment enriches the limited available pedestrian-vehicle interaction data in the literature, specially in shared spaces. This is a step towards developing and validating more accurate pedestrian behavior models around vehicles. Moreover, the statistics provided show an analysis of pedestrian state in the cases of aggressive and yielding driving. Which can be used to evaluate the performance of navigation systems by analysing the safety and comfort of pedestrians against the values provided by our statistics.

Last but not least, using the cooperation-based trajectory planning model, scenarios of pedestrian-vehicle interaction can be simulated. The model will be used for pedestrian behavior prediction as part of the proactive navigation framework. The model is tested and verified using a set of real-life recorded scenarios. To our knowledge, this is the first attempt to validate a pedestrian-vehicle behavioral model on real data, thanks to the release of the VCI-CITR data-set and our collected data.

4 Proactive Longitudinal Velocity Control

The number of mobile robot applications in human-populated environments has increased significantly in the past years: applications at airports, hotels, hospitals, factories, etc. This large spectrum of applications motivated researches to put considerable efforts into the development of trajectory generation methods both for path planning and trajectory tracking in the presence of dynamic obstacles.

The problem of navigation around pedestrians in addressed in this work using a cascading longitudinal-lateral control system. The longitudinal velocity control will be used as an input to the lateral control system presented in the coming chapter (Ch. 5). The selected architecture allows decomposing the two available degrees of freedom of the proactive command. Therefore, a stand-alone system for the longitudinal control is designed to explore the possibility of a proactive influence using only a one degree of freedom control.

The problem is formulated as an optimal control problem and solved by exploiting the cooperative nature of human behavior. The proposed control framework drives the vehicle proactively and safely along a pre-defined global path, while avoiding the freezing of the vehicle in dense environments. The system is implemented and tested in pedestrian-vehicle lateral interaction scenario using the previously developed cooperation-based pedestrian planning model (in Ch.3). The results are analysed and compared with a reactive method in terms of safety and efficiency.

4.1 Related Work

Many works in the literature targeted the longitudinal control during navigation applications. The goal is mostly to keep a safe distance from dynamic obstacles in the environment (vehicles, pedestrians, etc.), to avoid collisions or to maintain a relatively constant speed with braking in emergency situations.

In early works, the independent longitudinal vehicle control was mostly used in platooning operations [CG76; Hed+91; GL94; SD90]. In such applications, the common inputs

of the system would be the desired safety distance and a preferred constant speed. The longitudinal velocity of the vehicle is controlled to keep the inter-vehicle distancing close to the desired safety space, within the preferred speed limits. The longitudinal control is also addressed in works targeting a similar problem to the car-following in a platoon, which is the vehicle merging [CH99; LH00]. In these cases, the goal is to control the speed of the vehicle when joining a platoon or a new lane in order to reach the merging point at the appropriate time moment.
Despite the wide range of works on longitudinal control in platooning, car-following or merging applications, theses system remain unsuitable for dynamic pedestrian-populated environment. This is a direct result of the highly reactive and even subservient robotic behavior that is required in the platooning case.

Works on the longitudinal control are also found in the collision avoidance literature. The probabilistic framework used for collision and risk assessment is in terms used for the longitudinal control [Lam+08; KS20]. This is done such that the speed is increased in more safe environments and decreased or nulled with high probability or risk of collision. Moreover, probabilistic risk-based trajectory generation methods, such as Risk Rapidly-exploring Random Trees (Risk-RRT), can also fall under this category [RSL11]. Since the time-based part of the planned trajectory to be followed is computed based on the estimated collision risk. However, in dynamic or more cluttered environments such strategies can be highly penalizing to the system and can often lead to the famous Freezing Robot Problem (FRP) [TK10].

FRP arises when an environment surpasses a certain level of density and complexity. This happens when the robot planning system deems all the possible navigation possibilities unsafe and freezes in place to avoid collisions. A specific portion of research is concentrated to solving FRP in dynamic or cluttered environments. However, what can be noted in general, is that the problem is mostly handled by adjusting the manoeuvring or the space search methods [Fan+19]. In [Sat+20], for example, the problem is solved by predicting a potential freezing zone around pedestrians and the velocity command is derived to steer away from this zone. Meaning that the potential of solving FRP using a longitudinal controller have not been addressed yet in the literature.

The longitudinal control was not viewed only as a way to avoid collisions but also as a way to increase the efficiency and safety of the navigation overall [KZ86]. Works on robot navigation in dynamic environments targeted the longitudinal control as a way to optimize the navigation time while copping with unexpected events. Examples of this can been seen in early works on navigating dynamic spaces, such as the fuzzy logic controller proposed in [Man+97].

Finally, weather the aim is to solve FRP, maintain safety or improve the navigation efficiency, we can identify one main limitation in the case of pedestrian-populated environments: the lack of proactivity. Meaning that the potential of avoiding the FRP or improving the efficiency by using a proactive longitudinal control to invoke new collision-free navigation options has not been yet explored in the literature. The advantages of a proactive longitudinal controller is particularly prominent in dense pedestrian interaction scenarios. A reactive controller cannot consider the cooperation of the pedestrians and does not attempt to influence their behavior. This leads to over penalizing the navigation options. Subsequently, any reactive controller would have a poor performance in such scenarios [VMO17a], leading to inefficient and unnatural navigation solutions and even the freezing of the robot in some cases.

4.2 System Model

Reminder: The vehicle and the pedestrians in the scene are modelled as explained in 2.7.2. The linear velocity limit is assumed equal to the speed limit in shared spaces $V_{max} = 20km/h = 5.5m/s$ which justifies the vehicle's model choice. The position, orientation and velocity of the vehicle are $\boldsymbol{X_V} = [x_V, y_V]^T$, $\boldsymbol{V_V} = [v, \theta_v]^T$ respectively. On the other hand, a pedestrian is modelled as a point in the $2D$ plane. The position of a pedestrian j at time t is $\boldsymbol{X_j}(t) = [x_j(t), y_j(t)]^T$ and its velocity is $\boldsymbol{V_j}(t) = [v_{x_j}(t), v_{y_j}(t)]^T$.

The pedestrians in the scene are assumed to plane their trajectories according to the cooperation-based trajectory planning model suggested in Chapter 3, as illustrated in Fig. 4.1.

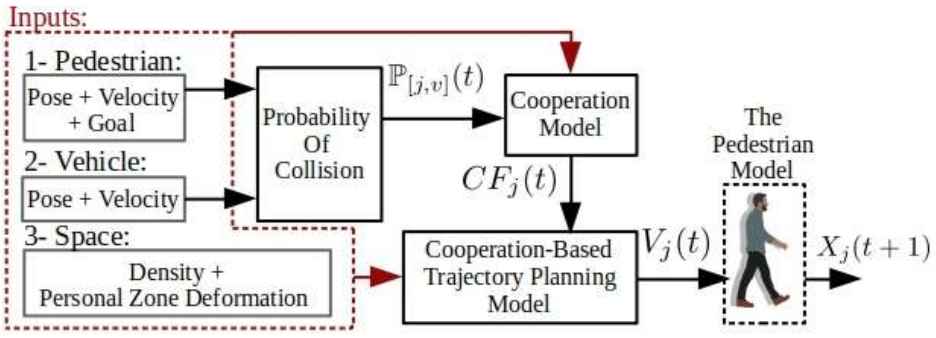

Fig. 4.1.: The pedestrian's cooperation-based trajectory planning model

4.2.1 Minimum pedestrian-vehicle distance

As explained in 2.7.2, the footprints of all pedestrians are circles with radius R_{ped} and the footprint of the vehicle is the outer Löwner-John ellipse of the rectangular vehicle body. The minimum distance between a pedestrian j and the vehicle body is approximated with the minimum distance between the two footprints. As explained earlier the ellipse of the vehicle's footprint can be written as:

$$f_{fp}^{v}(\boldsymbol{X}; S_V) = (\boldsymbol{X} - \boldsymbol{X_V})^T S_p (\boldsymbol{X} - \boldsymbol{X_V}) - 1 = 0 \tag{4.1}$$

Similarly the circle of a pedestrian j footprint is written as:

$$f_{fp}^{v}(\boldsymbol{X}; j, S_P) = (\boldsymbol{X} - \boldsymbol{X_j})^T S_p (\boldsymbol{X} - \boldsymbol{X_j}) - 1 = 0 \tag{4.2}$$

where S_V, S_P are the shape matrices of the vehicle and the pedestrian respectively (in (2.11) and (2.2)).

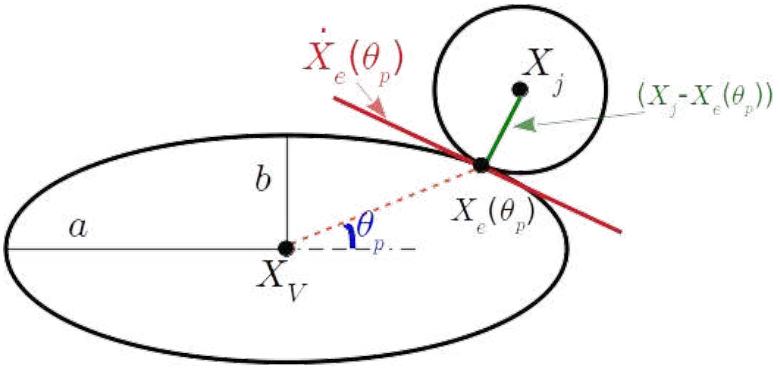

Fig. 4.2.: Estimating the closest distance between a pedestrian j and the vehicle's footprints

Assuming $\boldsymbol{X_e}$ is a point on the ellipse at an angle θ_p: $f_{fp}^{v}(\boldsymbol{X_e}(\theta); S_V) = 0$, then the square distance function between the pedestrian position and this point is:

$$F_D(\theta) = (\boldsymbol{X_e}(\theta) - \boldsymbol{X_j})^2 \tag{4.3}$$

for $\theta \in [0, 2\pi]$, F_D is a non-negative, periodic and differentiable function. Therefore, it has a global minimum occurring at an angle θ_p for which the first-order derivative is zero:

$$\dot{F}_D(\theta_p) = 2\,(\boldsymbol{X_e}(\theta_p) - \boldsymbol{X_j})\,\dot{\boldsymbol{X}}_{\boldsymbol{e}}(\theta_p) = 0 \tag{4.4}$$

this implies that $(\boldsymbol{X_e}(\theta_p) - \boldsymbol{X_j})$ is perpendicular to $\dot{\boldsymbol{X}}_{\boldsymbol{e}}(\theta_p)$:

$$\nabla\,(\boldsymbol{X_e}(\theta_p) - \boldsymbol{X_j})\,.\nabla\dot{\boldsymbol{X}}_{\boldsymbol{e}}(\theta_p) = 0 \tag{4.5}$$

and the vector $\dot{\boldsymbol{X}}_{\boldsymbol{e}}(\theta_p)$ is tangent to the ellipse at $\boldsymbol{X}_{\boldsymbol{e}}(\theta_p)$ (Fig. 4.2).

$$f_{fp}^{v}(\boldsymbol{X}_{\boldsymbol{e}}(\theta_p); S_V) = 0 \tag{4.6}$$

The coordinates of $\boldsymbol{X}_{\boldsymbol{e}}(\theta_p)$ cam be obtained by solving equations (4.4) and (4.6). However, there are no general analytical methods to solve it. Therefore, the solution is obtained using the Newton-Raphson iterative root-finding algorithm [Ebe06]. Finally, the closest distance between a pedestrian j and the vehicle is:

$$\boxed{D_j^{min} = ||\boldsymbol{X}_{\boldsymbol{j}} - \boldsymbol{X}_{\boldsymbol{e}}(\theta_p)||_2 - R_{ped}} \tag{4.7}$$

4.3 Background

To develop a proactive linear velocity controller, it is important to exploit the cooperation of pedestrians while maintaining their safety. Ensuring the safety of the pedestrians in the scene remains the main priority of the navigation system. Invoking more cooperative pedestrian behaviours is desired providing that it does not compromise the safety at any time. To estimate pedestrian safety during the navigation, a safety index in defined. The suggested **Safety Index (SI)** is a quantitative measure based on a minimal distance between the vehicle's body and the pedestrian. Using the concepts of the personal and the cooperation zones (discussed in Section 3.3.1), the safety index for a pedestrian j at time t is evaluated as follows:

$$\boxed{SI_j(t) = \frac{D_j^{min}(t) - R_P}{R_C - R_P}} \tag{4.8}$$

where: D_J^{min} is the minimum distance between the pedestrian j and the body of the vehicle estimated as explained in 4.2.1, R_P is the radius of the personal zone and R_C is the radius of the cooperation zone. As shown in Fig. 4.3, SI takes negative values when the vehicle enters the personal zone of the pedestrian indicating a failed navigation. Entering the cooperation zone results in $SI_j < 1$ expressing a possible discomfort of the pedestrian. A better navigation policy results in larger SI values.

Moreover, to reduce the complexity of the navigation task, a **Zone of Vehicle's Influence** is defined. In the navigation policy, only the cooperation for pedestrians detected within this zone is taken into consideration. The influence zone proposed in this work is a 180^o zone with the same orientation as the vehicle. The radius of the zone is proportional to the linear velocity of the vehicle. This ensures a larger influence margin in higher

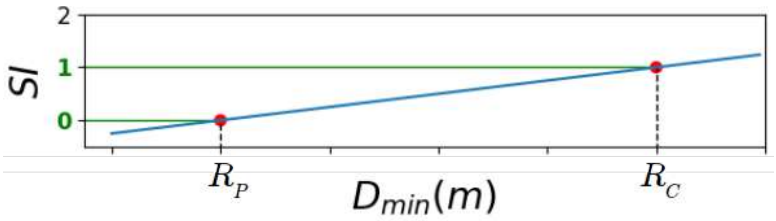

Fig. 4.3.: Safety Index (SI) values against the minimum distance between a pedestrian and the vehicle's body (D_{min})

velocities. The parameters of the influence zone (center $\boldsymbol{X_I} = [x_I, y_I]^T$ and radius R_I) are found as follows:

$$\boldsymbol{X_I}(t) = \boldsymbol{X_V}(t) - \frac{L_V}{2}\boldsymbol{V_V}(t), \quad R_I(t) = r_{min}(1 + u(t)) \tag{4.9}$$

with: L_V the length of the vehicle, $r_{min} \geq 0$, and $\boldsymbol{V_V}(t) = [u(t)\cos\theta_V(t), u(t)\sin\theta_V(t)]^T$.

Fig. 4.4 shows multiple examples of the influence zone with different velocities of the vehicle.

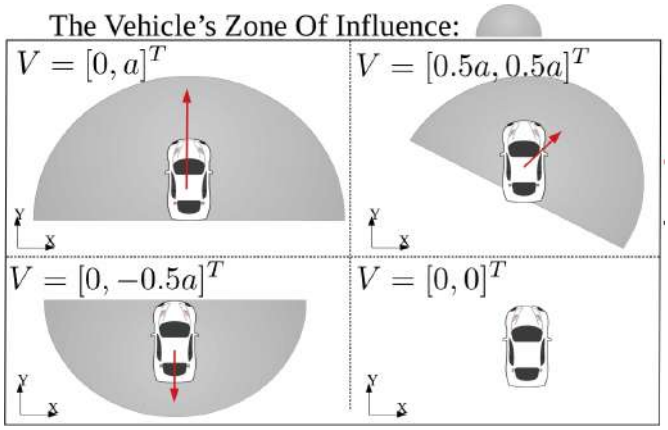

Fig. 4.4.: The zone of influence of the vehicle with different vehicle velocities, where $a \in \mathbf{R}_+$

In the following, the problem of proactive navigation is presented in a pedestrians-vehicle interaction scenario. The problem is formulated as an optimal control problem to find the longitudinal velocity control of the vehicle. The solution is then found based on the pedestrian-vehicle cooperation model.

4.4 Problem Formulation

The problem of longitudinal velocity control around pedestrians is formulated in a proactive and social manner. The control we are attempting to find allows the vehicle (or the robot) to actively engage in the space and not merely react to the surrounding agents. Moreover, the desired control should not lose its reactive nature but rather build on top of it. The vehicle is expected to engage in the space exploiting the pedestrian cooperation, while maintaining their safety.

Given an interaction scenario between a vehicle and N pedestrians, the problem of longitudinal control is formulated as follows:

System Inputs:

- $M \in \mathbb{N}$: $M \leq N$ is the number of pedestrians detected in the influence zone of the vehicle
- $X_P(t) = [X_1(t), ..., X_M(t)]$ and $V_P(t) = [V_1(t), ..., V_M(t)]$: the perceived positions and velocities of the M pedestrians in the influence zone at time t respectively
- The steering angle of the vehicle is provided from a higher level global planner

Problem: Find the longitudinal velocity control $u(t)$ of the vehicle, such that:

$$u(t) = \min_{u(t) \in [-v_{max}, +v_{max}]} J_{reg}\left(u(t), V_P(t), X_P(t), X_V(t)\right) \tag{4.10}$$

$$J_{reg} = \frac{1}{T_h} \int_{t=t_0}^{t_0+T_h} J\left(u(t), V_P(t), X_P(t), X_V(t)\right) + T\left(u(t)\right) \tag{4.11}$$

where v_{max} is the speed limit of the vehicle and J is a cost function that aims to maximize the cooperation of the influenced agents while ensuring their safety:

$$J = \frac{1}{M} \sum_{j=1}^{M} \alpha_1 \left(1 - CF_j(t)\right) - \alpha_2 SI_j(t) \tag{4.12}$$

with $(\alpha_1, \alpha_2) \in \mathbb{R}_+^2$, and $T\left(u(t)\right)$ is a Tikhonov regularization function [Tik43] added to penalize infinite solutions and prefer solutions with smaller L_2 norms:

$$T\left(u(t)\right) = \alpha_3 ||u(t)||_2^2 \; ; \quad \alpha_3 \in \mathbb{R}_+ \tag{4.13}$$

4.5 Solving the Control Problem

The solution for the optimization problem in (4.10) derived using the Hamilton–Jacobi–Bellman (HJB) equation has the form:

$$\boxed{u(t) = \frac{1}{2M\alpha_3} \sum_{j=1}^{M} \alpha_1 \partial_u CF_J\,(t) + \alpha_2 \partial_u SI_j\,(t)} \tag{4.14}$$

the symbol $\partial_y x$ is equivalent to $\frac{\partial x}{\partial y}$; $\forall x, y$.

The problem is then reduced to finding the gradient of the cooperation factor and the safety index with respect to the vehicle's control.

The gradient of the safety index of agent j depends only on the gradient of the distance to the vehicle $D_j^{min}(t)$:

$$\boxed{\partial_u SI_j\,(t) = \frac{1}{R_C - R_P} \partial_u D_j^{min}\,(t)} \tag{4.15}$$

To derive the gradient of the distance, let's rewrite both the pedestrian's and the vehicle's differential models. Using the same parameter assumptions used in section 2.7.2 for both the pedestrian and the vehicle, let's write: $X_u^V = \partial_u X_V$ and $X_u^j = \partial_u X_j$. Then, the gradient of the Euclidean distance can be written as:

$$\boxed{\partial_u D_j^{min}(t) = \partial_{X_P} D_j^{min}(t) \partial_u X_j + \partial_{X_V} D_j^{min}(t) \partial_u X_V} \tag{4.16}$$

This can be obtained by knowing the two gradients: $\partial_u X_j$ and $\partial_u X_V$.

- **Obtaining** $\partial_u X_V$: The vehicle's model is the following:

$$\dot{X_V}(t) = \begin{bmatrix} v(t)\cos\theta(t) \\ v(t)\sin\theta(t) \end{bmatrix} \tag{4.17}$$

$$\dot{\theta}(t) = \frac{v(t)}{L}\tan\delta(t) \tag{4.18}$$

With a partial differentiation of the vehicle's bicycle model and by adding the control $u(t) = v(t)$, we get:

$$\begin{aligned} \frac{d}{dt}\left(\partial_u X_V(t)\right) &= \begin{bmatrix} cos\theta(t) - u(t)sin\theta(t)\partial_u\theta(t) \\ sin\theta(t) + u(t)cos\theta(t)\partial_u\theta(t) \end{bmatrix} \\ \frac{d}{dt}\left(\partial_u\theta(t)\right) &= \frac{1}{L}\tan\delta(t) \end{aligned} \tag{4.19}$$

Finally, the term $\partial_u X_V$ is obtained by solving the previous model numerically.

- **Obtaining** $\partial_u X_j$: This term can be evaluated using the pedestrian cooperation-based trajectory planning model with:

$$\dot{X}_j(t) = V_j(t) \tag{4.20}$$

$$\frac{d}{dt}\left(\partial_u X_j(t)\right) = \partial_u V_j(t) \tag{4.21}$$

Similarly to the previous case, $\partial_u X_j$ is evaluated with a numerical solution of the previous model, where the term $\partial_u V_j(t)$ which can be determined using the cooperation-based pedestrian trajectory planning model (in 3). The following two gradients can be derived by simple calculations:

$$\boxed{\partial_u V_j(t) = \mathbf{F}_1\left(\partial_u V_j(t-1), CF_j(t), \partial_u \mathbb{P}_{[j,v]}(t), \partial_u D_j^{min}(t)\right)} \tag{4.22}$$

$$\boxed{\partial_u CF_j(t) = \mathbf{F}_2\left(\partial_u V_j(t-1), \partial_u \mathbb{P}_{[j,v]}(t)\right)} \tag{4.23}$$

where: $\mathbf{F}_1 : \mathbb{R}^3 \to \mathbb{R}^2$, $\mathbf{F}_2 : \mathbb{R}^2 \to \mathbb{R}$ are linear functions. The derivation of these functions is provided in Appendix E.

If we can express the gradient of the probability of collision. Then, the optimal velocity control $u(t)$ can be computed. This is done by substituting (4.22) and (4.19) in (4.16) and then in (4.15) we can compute the gradient $\partial_u SI_j(t)$. Whereas the gradient $\partial_u CF_J$ is obtained from (4.23).

In the following we explore the method for computing the probability of collision and its gradient.

4.5.1 The Probability Of Collision

The Probability Of Collision (POC) between the vehicle and a pedestrian is the main parameters expressing the effect of the vehicle's behaviour on the cooperation of the pedestrian in the interaction model (as shown in Section 3.4.1). Therefore, the gradient of the POC is an important factor in deriving the proactive control used to convey a desired vehicle's influence.

Most of the methods used to compute the POC between two entities are numerical and evaluating the gradient is not straightforward [Che+17], which is a drawback in our case. Therefore, our selected method depends on using an analytical form with a differentiable function to compute the POC. The method is based on using a probability

distribution to describe the trajectory of each agent. This is used to derive a probability density function (PDF) of the Euclidean distance between the two agents. Finally, the POC is equal to the probability of the distance falling below a threshold minimum distance.

Given a pedestrian j with a position $\boldsymbol{X_j} = [x_j, y_j]^T \in \mathbb{R}^2$ and velocity $\boldsymbol{V_j} = (v_j, \theta_j) \in \mathbb{R}^2 \times [0, 2\pi]$, and a vehicle with a position $\boldsymbol{X_V} = [x_v, y_v]^T \in \mathbb{R}^2$ and velocity $\boldsymbol{V_V} = (v_v, \theta_v) \in \mathbb{R}^2 \times [0, 2\pi]$. Assuming that each of the position parameters for both the pedestrian and the vehicle follow a natural distribution with a variance $\sigma_x^2(t)$:

$$
\begin{aligned}
&X_j(t) \sim \mathcal{N}(\mu_{X_j}(t), \Sigma_X(t)) \\
&\text{with: } \mu_{X_j}(t) = [\mu_{x_j}(t), \mu_{y_j}(t)]
\end{aligned}
$$

$$
\begin{aligned}
&X_V(t) \sim \mathcal{N}(\mu_{X_V}(t), \Sigma_X(t)) \\
&\text{with: } \mu_{X_V}(t) = [\mu_{x_v}(t), \mu_{y_v}(t)]
\end{aligned}
$$

Where:

$$
\Sigma_X = \begin{bmatrix} \sigma_x & \sigma_x^2 \\ \sigma_x^2 & \sigma_x \end{bmatrix} \tag{4.24}
$$

and the symbol $\mu_{[X]}$ denotes the mean value of the parameter $[X]$.

Then the distance between two points on the same axis has a natural distribution as well:

$$
E_x(t) = x_j(t) - x_v(t) \sim \mathcal{N}(\mu_{x_j}(t) - \mu_{x_v}(t), 2\sigma_x(t)) \tag{4.25}
$$

$$
E_y(t) = y_j(t) - y_v(t) \sim \mathcal{N}(\mu_{y_j}(t) - \mu_{y_v}(t), 2\sigma_x(t)) \tag{4.26}
$$

The weighted distance between the pedestrian and the vehicle follows a two degrees of freedom non-central $\mathcal{X}$ distribution [Cha11]:

$$
\begin{aligned}
&Z(t) = \frac{\sqrt{E_x^2(t) + E_y^2(t)}}{2\sigma_x(t)} \sim \mathcal{X}(2, \lambda(t)) \\
&\text{with: } \lambda(t) = \frac{D(t)}{2\sigma_x(t)}
\end{aligned}
$$

where $D(t)$ is the Euclidean distance between the mean values of the positions of the pedestrian and the vehicle at time t:

$$
D(t) = \sqrt{\left(\mu_{x_v}(t) - \mu_{x_j}(t)\right)^2 + \left(\mu_{y_v}(t) - \mu_{y_j}(t)\right)^2} \tag{4.27}
$$

The probability of collision at a time instant t_k is computed for a fixed prediction horizon T_h. First, the trajectories of both agents are predicted over the fixed time interval $[t_k, T_h + t_k]$. Then, the distribution of the weighted distance between the two agents (Z) is estimated over this time interval. The probability of collision is estimated as the probability of the weighted distance Z falling below a minimum limit distance d_{lim}:

$$\mathbb{P}_{[j,v]}(t_k) = \frac{1}{T_h} \int_{t=t_k}^{t_k+T_h} \mathbf{P}(Z(t) \leq d_{lim}) dt \tag{4.28}$$

This can be expressed using the cumulative distribution function (CDF) of Z:

$$\mathbf{P}(Z(t) \leq d_{lim}) = F_Z(x; 2, \lambda(t)) \tag{4.29}$$

$$\mathbb{P}_{[j,v]}(t_k) = \frac{1}{T_h} \int_{t=t_k}^{t_k+T_h} F_Z(d_{lim}; 2, \lambda(t))\ dt \tag{4.30}$$

where the CDF of a non central $\mathcal{X}$ distribution is:

$$F_Z(x; k, \lambda) = 1 - Q_{\frac{k}{2}}(\sqrt{\lambda}, \sqrt{x}) \tag{4.31}$$

with $Q_K(a, b)$ the Marcum Q-function [Mar50]. The previous CDF can be estimated using Wilson-Hilferty approximation [Abd54] and this is easily implemented using Python Scipy library[1].

Deriving the probability of collision using the previous method allows to compute its gradient using the probability density function of the distance:

$$\partial_u \mathbb{P}_{[j,v]}(t_k) = \frac{1}{T_h} \int_{t=t_k}^{t_k+T_h} \partial_u \lambda(t) F_Z(d_{lim}; 2, \lambda) \tag{4.32}$$

$$\partial_u \mathbb{P}_{[j,v]}(t_k) = \frac{1}{T_h} \int_{t=t_k}^{t_k+T_h} \frac{1}{2\sigma_x(t)} \partial_u D_j^{min}(t) F_Z(d_{lim}; 2, \lambda(t)) dt \tag{4.33}$$

Assuming the variance on the position and the velocity estimation at time t_k are σ_p^2, σ_v^2 respectively. Then:

$$\sigma_x(t_k + kt_s) = \sigma_{pos} + kt_s^2 \sigma_v \tag{4.34}$$

where $k \in \mathbb{N}_+$ and $t_s \in \mathbb{R}_+^*$ is the time step. finally:

$$\partial_u \mathbb{P}_{[j,v]}(t_k) = \frac{1}{T_h} \int_{t=t_k}^{t_k+T_h} \frac{1}{2(\sigma_{pos} + kt_s^2 \sigma_v)} \partial_u D_j^{min}(t) F_Z(d_{lim}; 2, \lambda(t)) dt \tag{4.35}$$

[1] `https://www.scipy.org/`

We can summarize the steps of computing the probability of collision and its gradient as follows:

- Predict the mean trajectories of the positions of both the pedestrian and the vehicle with a constant velocity prediction μ_{X_V}, μ_{X_j} over $[t_k, t_k + T_h]$.
- Predict the position variance $\sigma_x(t)$ over $[t_k, t_k + T_h]$ as in (4.34).
- Compute the minimum distance: $D_j^{min}(t) : \ \forall t \in [t_k, t_k + T_h]$ using (4.27).
- Compute: $\lambda(t) = \frac{D_j^{min}(t)}{2\sigma_x(t)} : \ \forall t \in [t_k, t_k + T_h]$
- Estimate the CDF of the weighted distance $F_Z(d_{lim}; 2, \lambda(t)) : \ \forall t \in [t_k, t_k + T_h]$
- Compute the probability of collisions:

$$\mathbb{P}_{[j,v]}(t_k) = \frac{1}{T_h} \int_{t=t_k}^{t_k+T_h} F_Z(d_{lim}; 2, \lambda(t)) \, dt \tag{4.36}$$

- Compute the POC gradient as in (4.35)

Finally, Algorithm 1 shows the steps of finding the optimal proactive control. Note that all the steps include only fast simple linear calculations. The only heavier calculation is computing the gradient of the probability of collision in step 6.

Algorithm 1. Proactive Linear Velocity Control

Input: Poses and Velocities of the vehicle $[X_V, V_V]$, and the agents in the influence zone: $X_P = [X_1 \dots X_M]^T$, $V_P = [V_1 \dots V_M]^T$
Output: longitudinal velocity control: $u(t)$

Initialize: $\partial_u V_P \leftarrow 0$
while $M > 0$ **do**
  for $j \leftarrow 1$ to M **do**
    Update the gradient of the pedestrians positions: X_u^P
    Update the gradient of the vehicle's position: X_u^V
    Update the gradient of the distance: $\partial_u D_j(t)$
    Predict the trajectories over future horizon T_h
    Compute the gradient of POC: $\partial_u \mathbb{P}_{[j,v]}(t)$
    Update the gradient of the security index: $\partial_u SI_j(t)$
    Update: $\partial_u CF_j(t)$, $\partial_u V_P(t)$
    Update the gradient of the pedestrian velocity: $\partial_u V_P$
  end for
  Update the control: $u(t) = \frac{1}{2M\alpha_3} \sum_{j=1}^{M} \alpha_1 \partial_u CF_J(t) + \alpha_2 \partial_u SI_j(t)$
end while

4.6 Implementation

The test simulations include interactions between the vehicle and a group of pedestrians. The lateral crossing scenario is selected to test and tune the controller parameters. This is because in this scenario the steering options are more limited and the main contribution in the navigation comes from the velocity control. The pedestrians in the simulations plan their trajectories using the cooperation-based trajectory planning model with the modified cooperation factor, as illustrated in Chapter 3. In every simulation, the pedestrians are initialized with random inner cooperation factors ($ICF \in [0, 1]$) and random goal points within a defined workspace.

On the other hand, the vehicle is modelled as explained in 2.7.2. The vehicle's steering angle is provided by a global A^* planner, while the linear velocity is controlled using the previous proactive control method. Fig. 4.5 shows the overall structure of the vehicle's proactive navigation system. Required pedestrian information include their positions and velocities which can be provided by the vehicle's perception system.

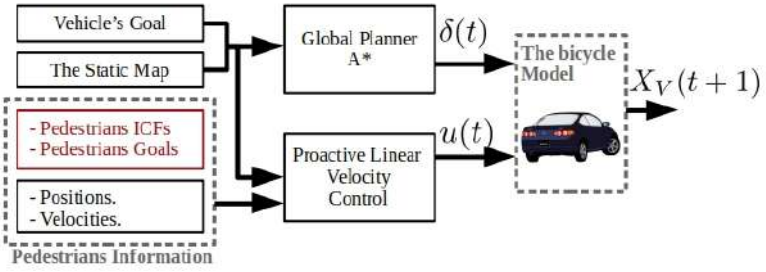

Fig. 4.5.: The Proactive Navigation Policy

4.6.1 A reactive method for comparison purposes

The same previous structure is used to run the simulations with a reactive linear velocity controller. The reactive control is computed using the same method as the proactive one, with a modified cost function. This modified cost function includes only a reactive term based on the safety index:

$$J_{reactive}(t) = \frac{1}{M}\sum_{j=1}^{M} -\alpha_2^{'} SI_j(t) \tag{4.37}$$

where $\alpha_2^{'} \in \mathbb{R}_+$, M is the total number of pedestrians detected in the influence zone and SI_j is the same safety index defined in (4.8).

To compare the two methods, the same simulation is ran twice. With the same initial positions and goals for both the vehicle and the pedestrians. As well as, the same inner cooperation factors (ICFs) for the pedestrians. The only difference is the local velocity controller (proactive or reactive).

4.7 Results Analysis

The resulting trajectories from one example simulation is shown in Fig. 4.6. The simulation includes a lateral crossing scenario between a vehicle and a flow of $N = 66$ pedestrians. The maximum velocity allowed in the space is $4m.s^{-1}$ for the vehicle and $3m.s^{-1}$ for the pedestrians. The ICFs for the pedestrians are assigned randomly between $[0, 1]$ to simulate variable pedestrian behaviors. The figure shows the resulting trajectories in the XY plane with the two control modes: proactive and reactive. In each mode, four different screenshots of the simulation are shown for a better visualization of its progress. The time interval present in each screenshot is noted on the right of the figure. The figure clearly shows that in the proactive mode the vehicle successfully crosses the pedestrians flow by anticipating their cooperation. While in the reactive mode, the vehicle stops to ensure the safety margins. Once the vehicle stops, the pedestrians continue their crossing and the reactive mode will not be able to find a valid solution. This results in the freezing of the vehicle in the reactive mode until the flow of pedestrians ends.

4.7.1 The Vehicle's Travel Time

The travel time of an agent (vehicle or pedestrian) is the time required to travel from the initial position to the goal destination. To compare the travel time between the proactive mode and the reactive mode in relative terms, we define two parameters. These two parameters serve as reference travel times. The first parameter is the reference pedestrian crossing time (TT_{peds}): the time required for all the pedestrians in the simulation to complete their crossing without a vehicle interference. This time is measured by running a reference simulation which contains the same pedestrian configuration, but without the vehicle. The second parameter is the vehicle's reference travel time (TT_{ref}): the time required for the vehicle to reach its final destination without any pedestrian interference. In the same manner, this time is measured by running a simulation which does not contain any pedestrians but has the same vehicle initialization and goal.

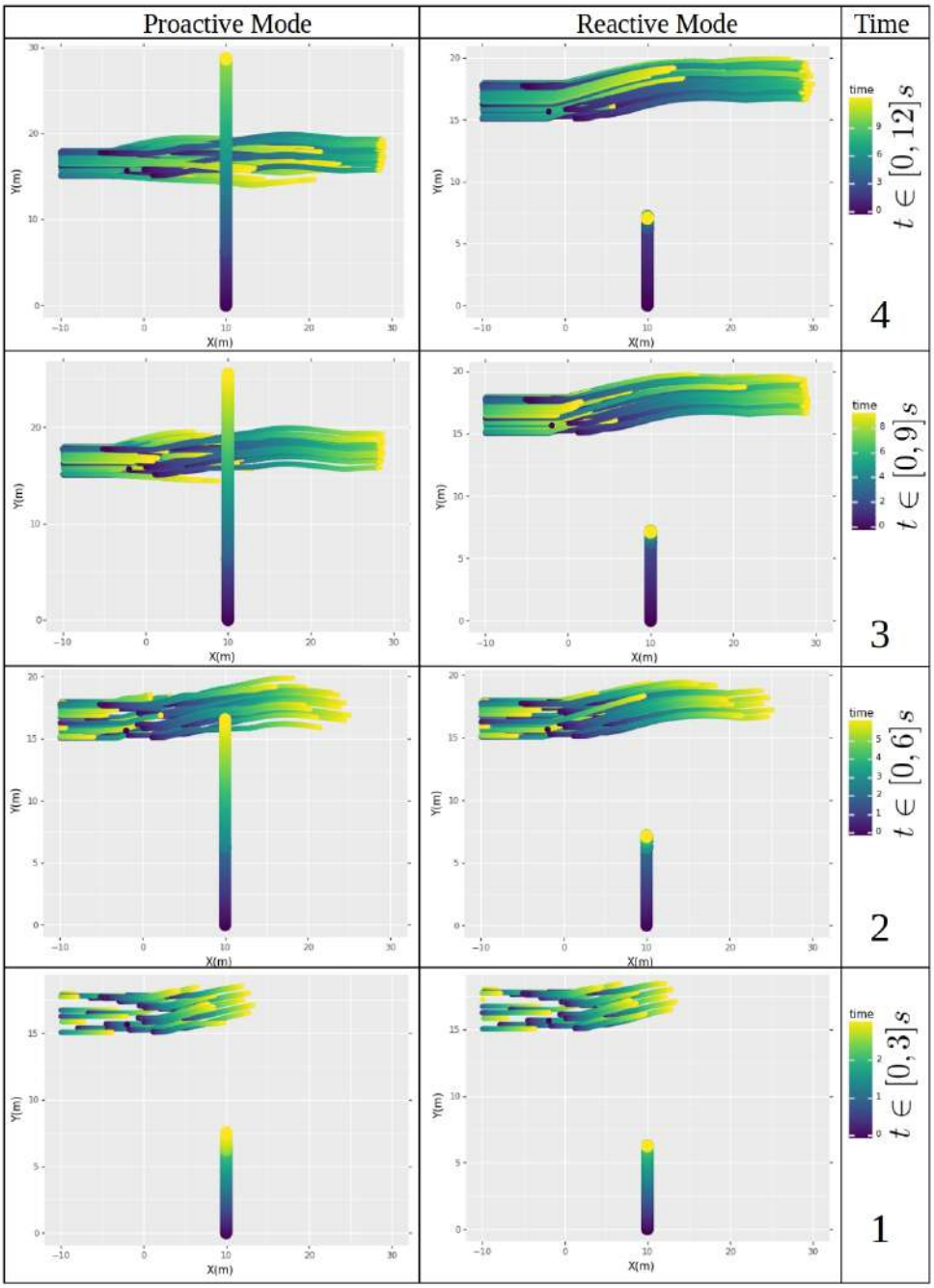

Fig. 4.6.: Pedestrian-vehicle lateral crossing simulation (two modes)

Let $TT(s)$ be the travel time of the vehicle in a simulation s regardless of the navigation mode. Then, we can define two relative travel times for the vehicle in this simulation:

- The vehicle's travel time relative to its reference travel time:

$$TT_{[veh/ref]}(s) = \frac{TT_{ref}(s) - TT(s)}{TT_{ref}} \times 100\% \tag{4.38}$$

- The vehicle's travel time relative to the pedestrians' reference crossing time:

$$TT_{[veh/peds]}(s) = \frac{TT_{peds}(s) - TT(s)}{TT_{peds}} \times 100\% \tag{4.39}$$

Using these two relative terms instead of the original vehicle travel time in seconds ($TT(s)$), allows us to compare the performance of the proactive and reactive modes independently of the pedestrians' configuration in a set of test simulations.

A total of 200 simulations are run (100 pair) with a random initialization. Each pair consists of the same simulation with a different navigation mode (reactive / proactive). The number of pedestrians in each simulation is chosen randomly between $30 - 100$ pedestrians. The rest of the initialization parameters are also assigned randomly (initial positions, initial velocities, goals, ICFs). The two previous relative travel times are computed for every simulation.

Fig. 4.7.A shows the histogram of the vehicle's travel time relative to its reference travel time, where the two modes are shown in different colors. $TT_{[veh/ref]}$ takes negative values in both modes. Which shows that even the proactive mode slows down the vehicle or even immobilise it sometimes to cross the pedestrian flow. However, this delay is much smaller in the proactive case. The proactive mode yields a navigation $10 - 50\%$ slower than the reference crossing. While the reactive mode can results in very high delays (can be over 250% slower).

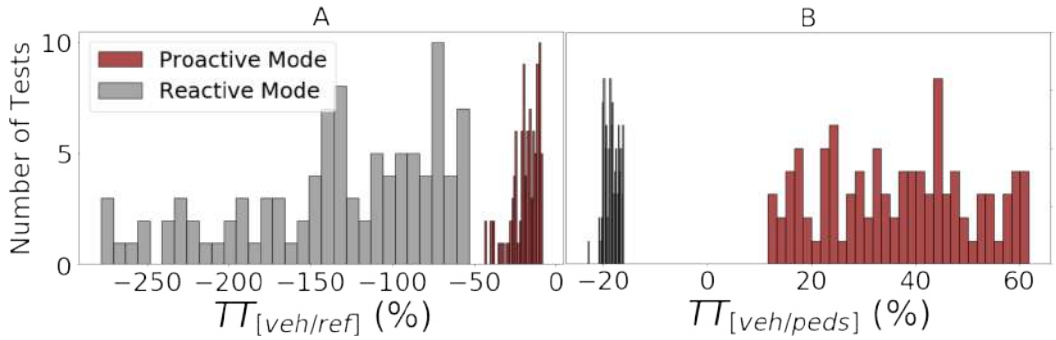

Fig. 4.7.: Histogram of the vehicle's relative travel time. A: $TT_{[veh/ref]}$, B: $TT_{[veh/peds]}$

The histogram of the vehicle's travel time relative to the pedestrians reference crossing time is shown in Fig. 4.7.B $TT_{[veh/peds]}$ takes positive values for the proactive mode and negative values for the reactive mode. This means that the proactive mode finds a solution while the pedestrians are still crossing. Therefore reaching the goal destination before all the pedestrians have crossed. While in the reactive mode the vehicle is frozen for some time due to the detection of nearby pedestrians. The important point to notice here is the range of values existent in the histogram of $TT_{[veh/peds]}$. In the reactive

mode, the histogram is extended over a very small range (all values are around -20%). This shows that there is a high correlation between the pedestrian crossing time and the vehicle's travel time in the reactive mode. On the other hand, $TT_{[veh/peds]}$ in the proactive mode takes a large range of values ($[15\%, 60\%]$). This shows that the proactive mode does not depend on the crossing time of the pedestrian flow. It also shows that the travel time gain in the proactive mode differs depending on the particular interaction situation. Because the proactive action is only taken when the safety of the pedestrians is ensured. In other words, in the proactive mode a solution is always found regardless of the crossing time of the pedestrian flow. However, a large gain in the travel time cannot always be ensured. A more detailed analysis of our simulation results show that the gain in the travel time is larger with larger crowds of pedestrians.

4.7.2 Pedestrians' safety test

To evaluate the navigation method from a safety perspective, a global performance index (PI) is defined in a simulation of period T with N pedestrians as:

$$\boxed{PI = \min_{j\in[1,\dots,N]} \min_{t\in[0,T]} SI_j(t)} \tag{4.40}$$

where $SI_j(t)$ is the safety index defined in (4.8) for a pedestrian j at time t.

In other words, the performance of the vehicle is judged by the minimum safety margin it has with a pedestrian over the simulation time (i.e. worst case margin).

Fig. 4.8 shows the histogram of the performance index. PI is evaluated over the same previous 100 simulations with the proactive mode. The histogram shows that most PI values are in $[0, 1]$. This means that in the proactive mode the vehicle enters the cooperation zone of at least one pedestrian at a certain time. However, the histogram does not contain any negative values. This mean that the proactive mode maintained the imposed safety margins and the vehicle did not enter the security zone of any pedestrian. Therefore, the navigation was successful in terms of safety.

However, the current safety measure uses only the position of the pedestrian with the assumption of equal safety margins around the pedestrian. This is a strict measure in comparison with real behaviours of pedestrians. A safety measure that considers the velocity of the pedestrian along with a different security zone (ellipses instead of a circle for example [RSL15]) is required for a more realistic estimation.

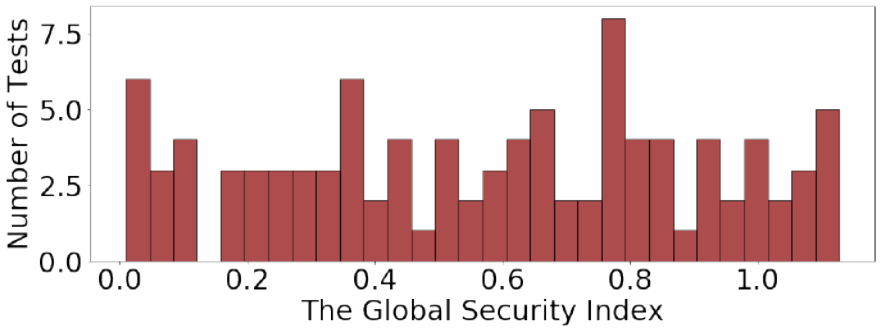

Fig. 4.8.: The histogram of the global security index PI

4.7.3 Results with more/less cooperative crowds

In the proactive mode, the linear velocity is optimized to increase the cooperativeness of the pedestrians in the scene. Therefore, the nature of the crowd should effect the performance of the proactive navigation.

To investigate the effect of the cooperativeness of the crowd, the internal cooperation factor (ICF) parameter is manipulated. By initializing the pedestrians' ICFs values in $[0.5, 1]$, a more cooperative crowd is simulated. Whereas, a less cooperative crowd is simulated by initializing it in $[0, 0.5]$. In the previous test, the ICFs for the pedestrians are chosen randomly in $[0, 1]$ to simulate a normal mixed crowd.

200 more simulations are ran in the proactive mode of pedestrians-vehicle lateral crossing scenario. Combined with the previous tests, this results in a total of 300 proactive mode simulations: 100 with a normal mixed crowd, 100 with a cooperative crowd and 100 with an uncooperative crowd.

The vehicle's travel time relative to its reference travel time $TT_{[veh/ref]}$ is computed for every simulation. Fig. 4.9 shows the normal distribution fit to the histogram of $TT_{[veh/ref]}$ for each type of the simulated crowd. The figure shows that the proactive mode does depend on the cooperativeness of the simulated crowd. A better performance is obtained with more cooperative crowds. Whereas, longer time delays can occur with highly uncooperative crowds.

4.8 Conclusion

This chapter addressed the aspect of longitudinal velocity control or the trajectory following within the framework of the proactive navigation. The work explored the possibility of a proactive behavior without modifying the pre-planned path and by using only the

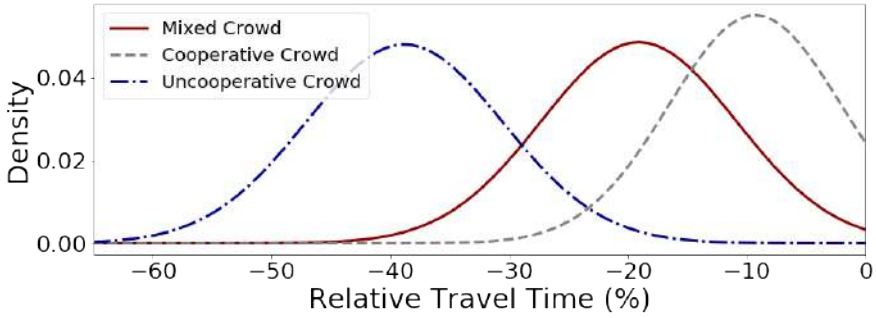

Fig. 4.9.: Normal distribution of the vehicle's relative travel time $TT_{[veh/ref]}$ in a number of simulations with different crowd cooperativeness

longitudinal control. The proposed method derives a longitudinal velocity control capable of navigating dense pedestrian crowds. The method exploits the cooperative social behavior of pedestrians while ensuring the necessary safety margins. The controller was tuned and tested in lateral crossing simulations and the method was compared with the performance of a reactive controller. The development of the method presented in this chapter and the corresponding conclusions resulted in the following publication:

"***M. Kabtoul, P. Martinet and A. Spalanzani. Proactive Longitudinal Velocity Control In Pedestrians-Vehicle Interaction Scenarios. 23rd IEEE International Conference on Intelligent Transportation Systems (ITSC, Sep 2020, Rhodes, Greece. pp.1-6. hal-02944369***"

The results showed that even this one-degree of proactive control improves the navigation performance significantly. The main advantages of the method include: avoiding the freezing robot problem in dense scenarios, major efficiency gains in terms of the travel time, navigating socially by incorporating the pedestrian cooperation behavioral model and maintaining pedestrian safety. This result provides us with a new perspective on solving the FRP around pedestrians. The capability of using a longitudinal control to avoid the freezing around dynamic obstacles opens the door to new works and implementations which do not only focus on solving FRP using path planning and steering. However, a system which does not modify its local steering to cope with the dynamic environment would remain highly limited. Although the proactive longitudinal control on its own is highly beneficial, it is necessary to integrate it with a lateral control. This would allow to modify the pre-planned global path to drive the system in appropriate directions based on the dynamic evolution of the space. This lateral control part of the proactive navigation system is explored in the following chapter.

Proactive manoeuvring Control

5

Pedestrian-friendly manoeuvring requires an understanding of both pedestrian reaction and intention. Merely safety based reactive manoeuvring can lead to sub-optimal navigation solutions resulting in the freezing of the vehicle in dense scenarios. Moreover, a strictly reactive method results in an unnatural driving behavior which cannot guarantee the legibility or social acceptance of the automated vehicle. This chapter is focused on the lateral control system of the proactive navigation framework. The lateral control sub-system uses the longitudinal control developed in the previous chapter (Ch. 4) as a system input in the cascading longitudinal-lateral control architecture. The work presents a human-inspired manoeuvring method adapted to navigation in close interaction with pedestrians using a dynamic channel approach. The method allows to proactively explore the navigation options based on anticipating pedestrians reactions and cooperation. The navigation is tested in pedestrian-vehicle interactions in both frontal and lateral scenarios with variable space density and sparsity. The chapter further entails the evaluation of the simulation results based on the safety and comfort of the pedestrians, the quality of the vehicle's trajectory and the time to reach its goal destination.

5.1 Related Work

Adapting the lateral control to navigate among dynamic and static obstacles is a topic widely addressed in the literature. Different approaches are used for manoeuvring control depending on the targeted application from path planning, to local path modification or sensor based lateral control. When navigating pedestrian populated environments or dynamic environments, the navigation task is addressed either by adapting a collision avoidance strategy or a behavior imitation strategy. In collision avoidance solutions, the aim is to find an obstacle-free path considering both the static obstacle and the dynamic evolution of the space. Whereas in imitation strategies, the problem of planning or re-planning is eliminated by imitating the behavior of an agent capable of navigating the environment.

A great deal of research targeted the lateral control to solve the collision avoidance problem. As this is considered a main requirement to operate around pedestrians and

maintain their safety. One Type of the methods developed for pedestrian collision avoidance manoeuvring control is potential fields based algorithms where the steering control results from a set of artificial potential attractive/repulsive forces. Such techniques can be found in [FFB19; ZMK21; Sch18], to cite a few. However, the problem of local minima remains a main concern when using such methods.
Another type of manoeuvring strategies are grid-based algorithms. These methods aim to finding and following the shortest and safest path between the start and goal points. Recent works developed these algorithms to be more suitable for dynamic environments, such as [Fra+20; Aje+20; Bai+21]. These techniques may perform well on roads and structured environments. However, they remain limited in dynamic and unstructured environments. As the open nature of such spaces and the huge range of navigation options risk generating unnatural and illegible vehicle trajectories.
Discrete optimization methods are also applied for collision avoidance manoeuvring control, such as the methods proposed in [Gra+19; Oli+20; RKS18]. Learning techniques has also shown some potential in the field of autonomous navigation for collision avoidance as in [Li+20a] or in [BK21]. However, all the previously mentioned collision avoidance based methods are not suitable to highly dynamic environments. Moreover, these techniques are over-reactive and would fail in more dense spaces where an obstacle-free path simply does not exist.

A different approach to solving the manoeuvring problem is to adapt an imitation strategy. Such methods address the planning problem in a highly complex environment by a leader-follower solution. In such cases the autonomous system does not perform a search for the optimal path but rather a search for an optimal leader. Then, the system navigates the space by following this optimal leader through the environment. Such methods are found in [Mül+08; Ste+16b], for example. Although such have the problem of the existence and search for the optimal leader, they are still beneficial for human-sized robot navigation in complex environments. They are highly limited for autonomous vehicles navigation in shared spaces. This is due to the size difference between a vehicle and a human, which makes it mostly impossible to follow the same path as a pedestrian in a dense space. Additionally, a path that is natural and socially acceptable for a pedestrian, will mostly be not the same for a vehicle.

The manoeuvring problem around humans has also been addressed as a cooperative problem between the human and the robot. For example, [SFA21] proposed a Human-Aware Timed Elastic Bands (HATEB) planner which anticipates the cooperative behavior of humans in navigation tasks. Another method in [Bri+21] also considers the cooperation of a pedestrian in developing a MPC planner based on a recommended sub-goal and using deep Reinforcement Learning (RL). A different implementation of the cooperation concept is shown in [Ran+19] where the dominance of e pedestrian in an interaction

scenario is measured and the navigation policy is adapted to deploy a complementary dominant behavior. The works on cooperative navigation takes the social aspects of human motion into account and reduces the over-reactive behavior of the collision avoidance systems. However, these systems still lack the proactive property of a natural navigation strategy. Moreover, all the previous works are shown effective in interactions with few pedestrians and are not suitable to more dense and dynamic spaces.

5.2 Problem Formulation

The problem of the proactive manoeuvring control is translated to finding the steering commands of the vehicle which guarantee a safe, efficient and natural driving. The efficiency of the steering comes from exploiting the pedestrian cooperative behavior to explore non pedestrian-free navigation options and avoid the freezing of the system in dense scenarios. Moreover, the resulting vehicle path should resemble the driving patterns performed by experienced drivers to ensure the legibility and social compliance of the vehicle, or what is referred to as natural driving.

In an interaction scenario between a vehicle and N pedestrians, the problem is formulated as a proactive local path modification as follows:

System Inputs:

- $X_P(t) = [X_1(t), ..., X_N(t)]$ and $V_P(t) = [V_1(t), ..., V_N(t)]$: the perceived positions and velocities of the N pedestrians at time t respectively
- $v(t)$: a linear velocity control from the external proactive longitudinal controller
- The global path for the vehicle, provided by a global path planner

Problem: Find the steering control $\delta(t)$ of the vehicle, such that:

- $\delta(t) \in [\delta_{min}, \delta_{max}]$
- The resulting path is smooth, natural and legible.
- The resulting path minimizes the deviation from the global path, while maintaining pedestrian comfort.

5.3 Background and Global Overview

The previous requirements are met by using a proactive dynamic channel method. The method is based on exploring the look-ahead navigation space of the vehicle and partitioning it to a set of possible navigation options (channels). Then a navigation cost is computed for each option (channel). This cost is based on the travel distance cost to satisfy the previous efficiency and minimum global path deviation requirements. The navigation cost is also dependent on the space occupancy and the pedestrian cooperative behavior, this ensures the previous pedestrian safety/comfort requirement. Then, a transition path is constructed to drive the vehicle along the selected navigation channel. This transition path is built to resemble the smooth lane change paths conducted by experienced drivers. The latter step is to establish a smooth, natural and legible path. Finally, the steering command is derived to track the previous transition path.

In this section, we provide a background on the different previous techniques and concepts used to build the suggested manoeuvring framework. This includes autonomous lane changing and path tracking methods. As well as, a background on fuzzy logic systems which will be used later to construct the channel cost model.

5.3.1 Fuzzy Logic Systems

Fuzzy logic is a computational method that can be used for decision making, modeling or control to offer flexibility under uncertainty. The first paper on fuzzy sets was published by Lotfi A. Zadeh in 1965 [Zad65]. Fuzzy logic can be seen as an extension of the binary logic, or in Bart Kosko's words "The binary logic of modern computers often falls short when describing the vagueness of the real world. Fuzzy logic offers more graceful alternatives". The difference is that fuzzy logic is based on the "degree of truth" of linguistic variables, rather than the binary true/false. [KI93]

A fuzzy system has the structure shown in Fig. 5.1. The Rule Base is a set of "If-Then" rules built based on experience and personal knowledge of the system under study. To process a numerical (crisp) input to the system: firstly, the input is processed by a Fuzzifier to be transformed into fuzzy sets, where each set is represented by a membership function. Then the Inference Engine establishes the best-fit rule from the Rule Base and generates a fuzzy output. This is in terms treated by the Defuzzifier to generate an explicit numerical output. [Men95]

Fuzzy logic has many automotive applications as it enables the inclusion of human assessments in computing problems. Fuzzy logic is used in this work to build a model

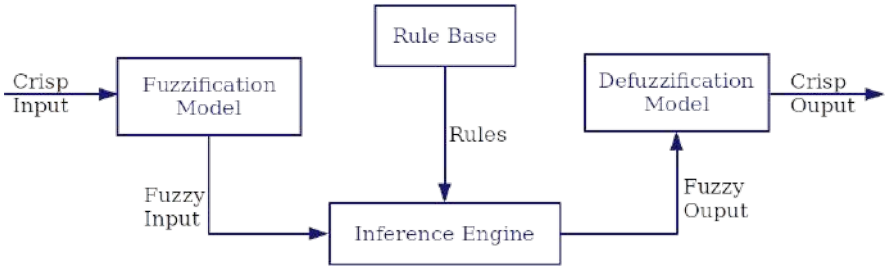

Fig. 5.1.: Fuzzy Logic system overview

capable of estimating the navigation cost in a sub-space based on the state of that space.

5.3.2 Autonomous Lane Change

Autonomous Lane change is a problem widely studied in the literature since the early 90s [CT94; HRO97]. Lane change is a manoeuvre which aims to move the non-holonomic vehicle system between two parallel paths. This can be summarized as follows: generate the appropriate steering angle so that the vehicle travels the distance between two lanes along its local lateral axis and aligns itself with the adjacent lane at the end of the manoeuvre such that a lane keeping task can be resumed safely and smoothly. The previous lane change problem can be formulated in a temporal frame (Fig. 5.2a) by defining a finite time period to perform the desired lateral displacement between the two lanes. The problem can also be formulated in a spacial frame (Fig. 5.2b) by defining a look-ahead travel distance to perform the desired lateral displacement regardless of the required time. The latter definition is more appropriate to dynamic spaces as in such scenarios the displacement time depends on the evolution of the dynamic environment and cannot be guaranteed.

Many techniques have been developed over the years for the purpose of autonomous lane change on highways and roads. We explore these techniques to deploy a lane-change-like manoeuvre between the imaginary channels in the open unconstrained shared space. The first category of techniques developed for the purpose of lane changing are optimization methods. These methods depend on a designed cost-function with a set of constraints, such as the vehicle kinematics and road dimensions [Zho+19]. However, the optimization problem in this case is multi-objective, non-convex with multiple nonlinear constraints. Therefore, a global optimal solution cannot always be found in real-time [Li+20b].
The second category are sampling-based methods [Zen+19]. In such methods, a number of candidate lane changing paths are sampled and an optimal candidate is selected.

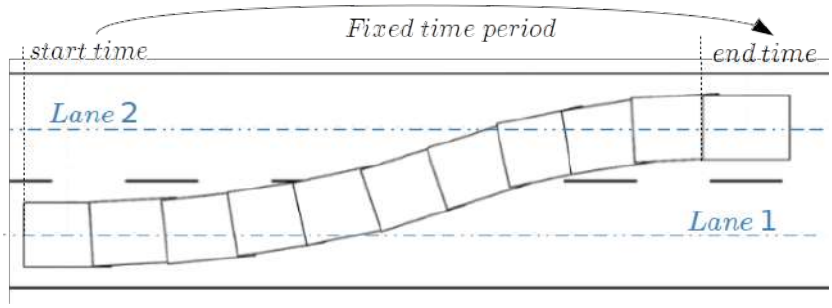

(a) Temporal Frame

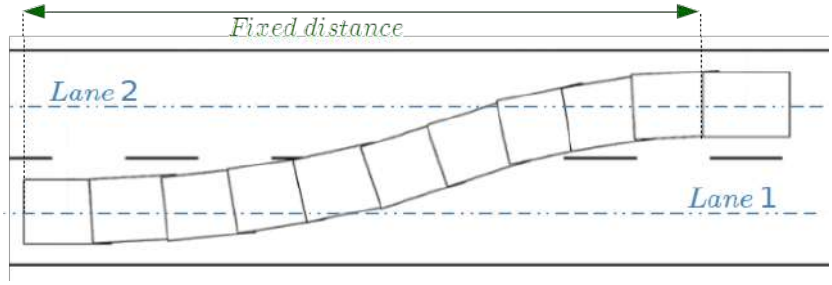

(b) Spacial Frame

Fig. 5.2.: Lane change maneuver

However, these techniques can generate many additional candidate paths that are not feasible or do not fulfill the safety constraints when navigating in close interaction with pedestrians. Several other works suggests constructing a lane-change candidate path analytically [Din+21]. Then using a path following steering controller to generate the desired vehicle steering commands. This method allows to join the goal lane (or channel in our case), while guaranteeing the exact transition behavior at all times. One of the most famously used path candidates for lane changing is the Quintic spline for the lateral movement with respect to a local Frenet Frame [Li+20c]. A Quintic spline candidate can guarantee a C2-continuous path and it has the form:

$$\boxed{e_q(x) = a_5x^5 + a_4x^4 + a_3x^3 + a_2x^2 + a_1x + a_0 \ : \{a_i\}_{0\leq i\leq 5} \in \mathbb{R}^*} \tag{5.1}$$

5.3.3 Path Following

Path following control is generating the lower-level steering control of the vehicle to follow a pre-defined path. This path can either be a path generated offline a priori, or online by the local planner. The main performance aspects of a path following system are the accuracy and the smoothness. The accuracy means maintaining a low displacement (lateral + heading) from the reference path. Whereas, the smoothness is maintaining this accuracy without any aggressive steering commands [Pad+16].

Several techniques are present in the literature for the purpose of path following [Dom+16]. The survey in [XP20] divides path followers into three main categories. The first category is Geometric concept based control, where the kinematics of the system is used to compute the control such as the pure pursuit controller developed in the DARPA challenge. The main advantage of this category is the simplicity and efficiency at low velocities. However, such technique does not perform well with high curvature paths. At higher velocities, the dynamics of the system should also be considered. This leads us to the second category which uses Feedback control and can be implemented with a more accurate system model. Such methods include H_∞ [Mit+20], adaptive control [Pou+17] or sliding mode control. The third category of path followers are model predictive control (MPC) path followers, which add to the previous category a forward prediction of the system state [Ye+19]. However, MPC path follower are challenging to implement in real-time, as the optimization may fail and the computation time at each iteration cannot be guaranteed [May14]. Learning-based approaches has also made an advancement in path following controllers, such methods can be seen in [Sha+20; Liu+20].

For the case of path following in a shared space, the imposed low speed limits justifies using a kinematic based controller. The method selected for the path following in this work uses a feedback-based sliding mode controller (SMC) [HYH18]. SMC is selected to follow the Quintic spline during a channel transition as it is robust and easily implemented in real-time. Furthermore, the closed-loop performance becomes insensitive to system uncertainties [Bar+18]. SMC is a nonlinear control technique that drives the target system to a designed surface in the state space, then keeps the system in a close neighborhood of this surface in a sliding (switching) manner (Fig. 5.3).

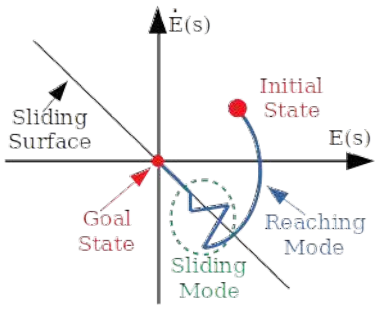

Fig. 5.3.: The sliding surface and the two control modes in SMC

5.4 The Proactive Dynamic Channel (PDC)

Let $\mathcal{D}_P \in \mathbb{R}_+$ be the perception range of the vehicle, then space perceived in the direction of the vehicle or the forward perception space (Fig. 5.4) $\mathbf{S}$ is:

$$\mathbf{S} = \{||X^v||_2 \leq \mathcal{D}_P; X^v \in (\mathbb{R}_+ \times \mathbb{R})\} \tag{5.2}$$

and let P_G be the global vehicle's path provided by a higher level path planner:

$$P_G = \{(x_i, y_i) \in \mathbb{R}^2 : \ i \in \mathbb{N}_+\} \tag{5.3}$$

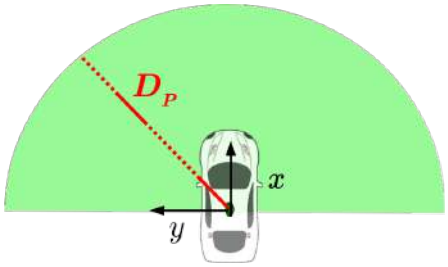

Fig. 5.4.: The sub-space perceived in the vehicle movement direction

We call a channel every sub-space of $\mathbf{S}$ defined by a center point, width, length and orientation:

$$CH_i^g = \{(x_i, y_i), \theta_i, (W_i, L_i)\} \in \{\mathbb{R}^2, [0, 2\pi], \mathbb{R}_+^2\} \tag{5.4}$$

Assuming we wish to partition the space $\mathbf{S}$ into a set of channels with a constant channel width W_C, then it can be divided into a set of K channels using the global path P_G, where:

$$K = \frac{2\mathcal{D}_P}{W_i} \tag{5.5}$$

The partitioning of the space into a set of K channels is done based on the global path of the vehicle P_G. If p_j is the next waypoint on the global path, and (p_j, t, n) is the Frenet frame at this point ($\mathcal{F}_\mathbf{P}$), then the channels can be written in this Frame as:

$$CH_i^{\mathcal{F}_\mathbf{P}} = \{(\pm iW_C, 0), 0, W_C, L_C\}; i \in [0, nint(\frac{K}{2})] \tag{5.6}$$

where $nint(.)$ is the nearest integer function, and with a constant width and length for all the channels: $(W_C, L_C) \in \mathbb{R}_+^2$.

Fig. 5.5a shows the resulting channels with width W_C and length L_C for a point p_j on the global path. This process in repeated at consecutive time moments when a new channel

is reached or over fixed time steps. If this process is repeated over the consecutive waypoints on the global path, we end up with the sequence of channels enveloping the global path and parallel to it. Fig. 5.5ba and Fig. 5.5bb show an example of the resulting channels in the space at two different instants of the navigation. Whereas, Fig. 5.5bc shows the overall channels sequence resulting after a number of iterations.

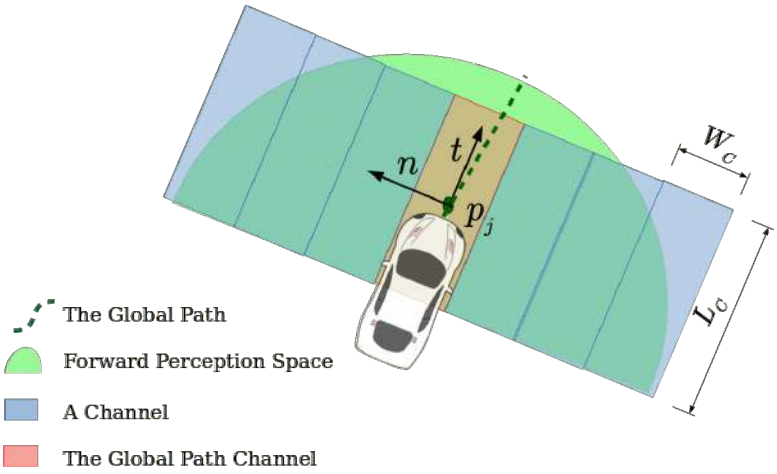

(a) The resulting channels within the forward perception range for a path waypoint p_j

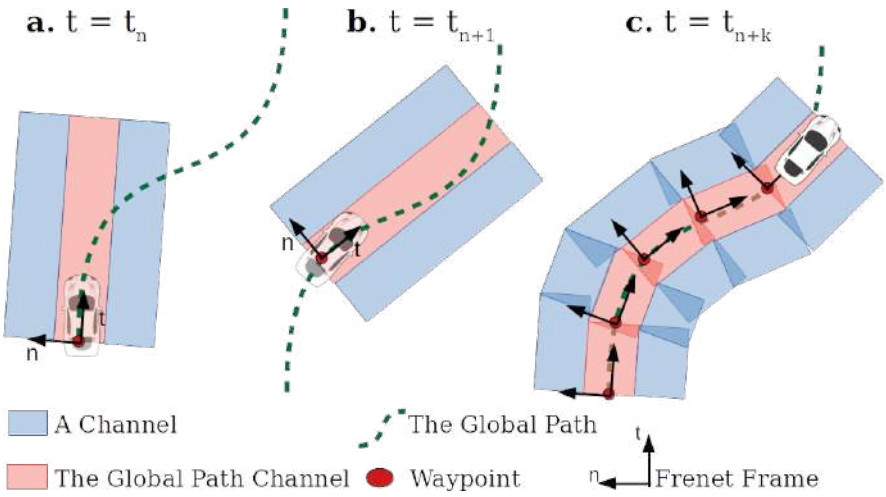

(b) The resulting channels at different time instances

Fig. 5.5.: The proactive dynamic channel: space partitioning

By computing the set of channels present in the navigation space, the task of finding a valid path is reduced to selecting the optimal navigation channel. This decision making step is essential in the proactive navigation framework, as it defines the general direction of the vehicle in the space.

The navigation cost of each channel is evaluated by assigning a weight to each channel w_C. The higher the weight w_C the more costly is to navigate in this channel in terms of pedestrian discomfort and travel/time cost.

5.4.1 The navigation cost of a dynamic channel

The first navigation cost weight w_{fuzzy} is based on the state of the channel itself to minimize the discomfort caused to pedestrians navigation in the channel under evaluation. This criteria is necessary but not sufficient, as the navigation cost to a channel depends on the pose of the vehicle, it's goal or global path as well. To account for this cost, two additional channel cost weights are defined: the travel cost from the vehicle's current pose to the channel (w_{local}), and the travel cost from the channel back to the global path (w_{global}). This allows penalizing travelling far distances from the current position of the vehicle or from its reference global path, over minor advantages in terms of pedestrian discomfort.

Let $X_{CH}(t)$ be the center point of the channel, D_P the perception range, and $p_j(t)$ the next waypoint on the global path at time t, then:

$$w_{local}(t) = \frac{1}{D_P}||X^v_{CH}(t)||_2 \in [0,1] \tag{5.7}$$

$$w_{global}(t) = \frac{1}{D_P}||X^v_{CH}(t) - p^v_j(t)||_2 \in [0,1] \tag{5.8}$$

Thus, the final navigation cost to a channel C can be written as:

$$w_C(t) = \beta_0 \left[w_{fuzzy}(t) + \beta_1 w_{local}(t) + \beta_2 w_{global}(t)\right] \tag{5.9}$$

where: $\beta_k \in [0,1] \ : k \in \{0,1,2\}$.

This formulation allows to select the channel with the optimal state while adding a penalty on travelling to further away channels. Therefore, distant channels are only selected if this selection results in a significant advantage in terms of the navigation cost.

The only cost left to compute is w_{fuzzy}. This weight aims to measuring the cost based on the channel state itself. Therefore, it is based on the state of the pedestrians within the channel under evaluation. A fuzzy logic model based on the pedestrian state is proposed in the following to compute the channel state cost w_{fuzzy}.

5.4.2 The channel state cost - fuzzy model

To comply with the principals of pedestrian safety and human aware navigation, channels with less pedestrians and more cooperative pedestrians should be preferred. Therefore, the first measure used to estimate the channel state cost weight is the pedestrian density in a channel. The second measure is the expected density change in the channel over a future navigation horizon T_H. This allows to prioritize channels with a predicted reduce in density over T_H. The third measure is based on the cooperation of the pedestrians in the channel. Proactive navigation is a common task that requires cooperation between the pedestrians and the vehicle. This means that the navigation system should manoeuvre in directions containing more cooperative pedestrians who are willing to compromise their paths and facilitate the vehicle's navigation. However, there is no straightforward way to construct a weight function using the previous three measures. But it is possible to construct a set of navigation rules based on experience. Therefore, Fuzzy logic is used to compute the navigation cost of a channel.

The fuzzy model Inputs/Output

The three inputs of the fuzzy cost model are: Pedestrian density in the channel (D), the expected change in the channel's density over T_h (ΔD) and the percentage of uncooperative agents in the channel ($N_{UC\%}$) These three inputs are computed as follows:

$$D(t) = \frac{\pi R_{ped}^2 M(t)}{L_C W_C} \times 100\% \ \in [0, 100]\% \tag{5.10}$$

$$\Delta D(t) = D(t + T_H) - D(t) \ \% \ \in [-100, 100]\% \tag{5.11}$$

$$N_{UC\%}(t) = \frac{M_{UC}(t)}{M(t)} \times 100\% \ \in [0, 100]\% \tag{5.12}$$

where M is the total number of pedestrians in the channel, R_{ped} is the radius of the pedestrian's footprint, and M_{UC} is the number of agents with a low cooperation factor ($CF \leq 0.5$).

The output of the fuzzy model is a channel weight $w_{fuzzy} \in [0, 1]$.

Triangular functions are used as membership functions for both the inputs and the output. The fuzzy values of the inputs and the corresponding membership functions are shown in Fig. 5.6.

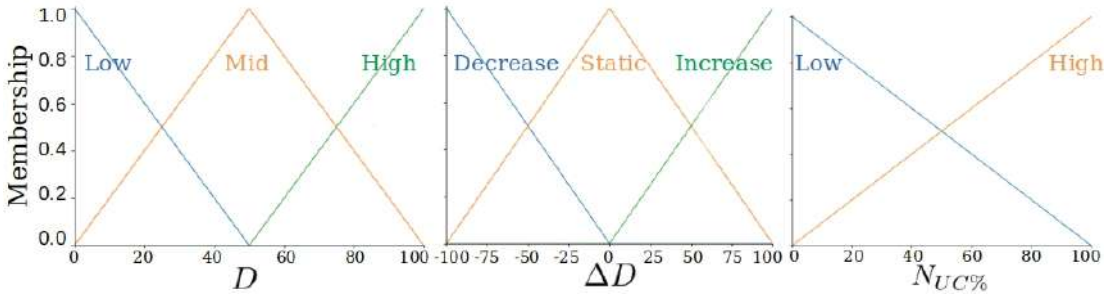

Fig. 5.6.: The membership functions of the navigation cost fuzzy model inputs

Fuzzy model description

The model rules are constructed to prioritize channels with smaller weights. Therefore, lower weights are assigned to channels with lower densities, with a decrease in their densities over the navigation horizon and/or with a lower percentage of uncooperative pedestrians in the channel. The list of adapted navigation cost rules is shown in detail in Appendix G.

The fuzzification of the values is done using the g-Fuzzification method, while the defuzzification is done using the center of gravity method [Ros00].

Fig. 5.7a shows a visualization of the channel weight membership function and a defuzzification output example when: $D = 40\%, \Delta D = 30\%, N_{UC\%} = 30\%$. The output of the fuzzy model output is plotted in Fig. 5.7b with two different channel density levels.

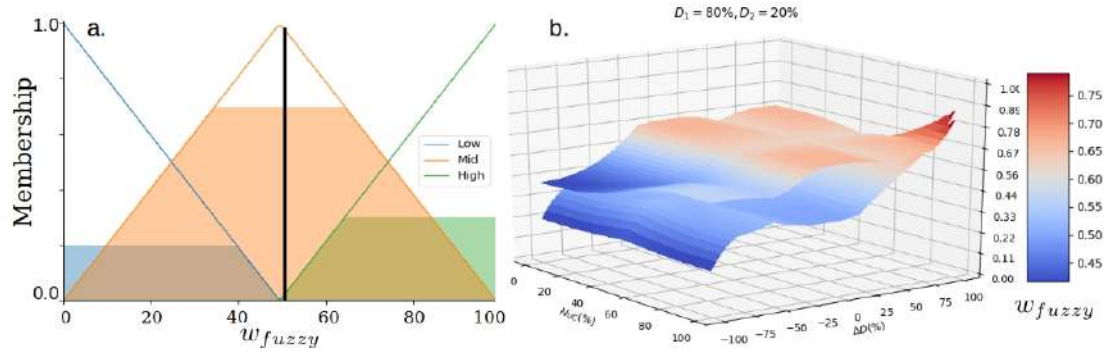

Fig. 5.7.: a: The membership functions of the channel fuzzy weight (w_{fuzzy}). b: The fuzzy model output with two different density levels

Finally, after calculating the navigation cost for each channel, the channel with the least cost is selected as the goal navigation channel. The task of the navigation turns into transitioning to the selected channel and navigating within it, until a new channel is selected. In the following, we explore how the global path is modified locally to transition between and navigate within the selected channels.

5.5 Proactive Channel-Based Local Path Modification

Selecting a navigation channel results in a goal navigation sub-space. The task of constructing an exact path to move between the selected channels is considered a local modification of the global path. This is because the proactive channels themselves are built based on the global path. To maintain a vehicle behavior similar to the driving patterns of experienced drivers, a lane change like steering is adapted to perform the channel transition. Lane change manoeuvring generates natural and legible vehicle trajectories.

Constructing a lane-change candidate path analytically allows to join the goal channel, while guaranteeing the exact transition behavior at all times [Din+21]. Quintic Splines are often selected for such maneuvers, as they can guarantee a C2-continuous path is used as a transition candidate.

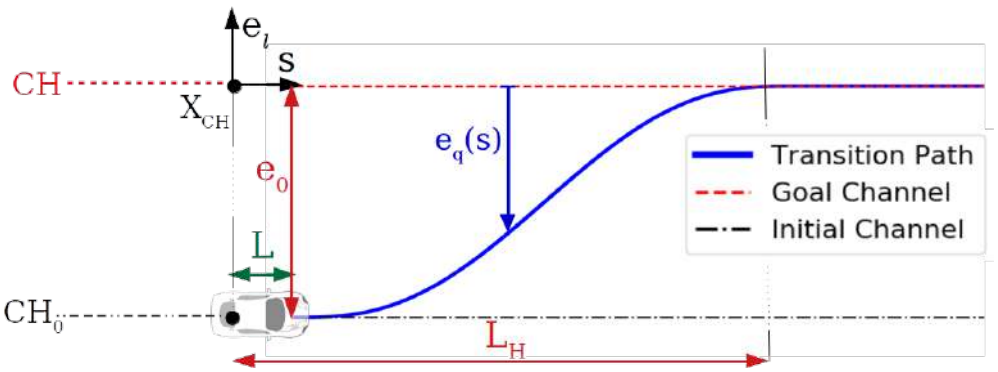

Fig. 5.8.: Constructing a Quintic path between two channels

Lets assume we want to construct a Quintic transition path from a current channel CH_0 and a goal channel CH, as shown in Fig. 5.8. Let $X_{CH}(t)$ be the center of the goal channel, and let $\mathcal{F}_{\mathcal{X}_{\mathcal{CH}}}$ be the Frenet frame with respect to the channel center line. Supposing the vehicle state in this frame is $(e_l, s, \tilde{\theta})$, then the transition Quintic path can be written as:

$$e_q(s) = a_5 s^5 + a_4 s^4 + a_3 s^3 + a_2 s^2 + a_1 s + a_0 \tag{5.13}$$

The parameters of this function ($a_i \in \mathbb{R} \;\; : i \in \{0, \ldots, 5\}$) can be easily derived by applying the motion constraints in (5.14), the only variable that needs to be chosen is the look-ahead navigation horizon L_H.

$$\begin{aligned} e_q(L_0) = e_0 \quad \dot{e}_q(L_0) = 0 \quad \ddot{e}_q(L_0) = 0 \\ e_q(L_H) = 0 \quad \dot{e}_q(L_H) = 0 \quad \ddot{e}_q(L_H) = 0 \end{aligned} \tag{5.14}$$

where $L_0 = L, e_0$ are the length of the vehicle and the initial lateral displacement of the vehicle respectively. The conditions in (5.14) yields:

$$\begin{pmatrix} a_5 \\ \vdots \\ a_0 \end{pmatrix} = \begin{pmatrix} e_0 \\ 0 \\ 0 \\ 0 \\ 0 \\ 0 \end{pmatrix} \times \begin{pmatrix} L_0^5 & L_0^4 & L_0^3 & L_0^2 & L_0 & 1 \\ 5L_0^4 & 4L_0^3 & 3L_0^2 & 2L_0^1 & 1 & 0 \\ 20L_0^3 & 12L_0^2 & 6L_0 & 2 & 0 & 0 \\ L_H^5 & L_H^4 & L_H^3 & L_H^2 & L_H & 1 \\ 5L_H^4 & 4L_H^3 & 3L_H^2 & 2L_H^1 & 1 & 0 \\ 20L_H^3 & 12L_H^2 & 6L_H & 2 & 0 & 0 \end{pmatrix}^{-1} \tag{5.15}$$

Finally, the overall path that the vehicle would follow is the integration of the center lines of the selected channels, along with the transition candidates between these channels.

5.5.1 Local steering control for path following

The goal from the controller is to transition to the goal channel using the constructed Qunitic path, then follow the center of the goal channel. Since the goal of the controller is to drive the system to the goal channel, the control is derived by expressing the system in the Frenet Frame of the goal channel center $\mathcal{F}_{\mathcal{X}_{\mathcal{CH}}}$. This selecting greatly simplifies the design, since the channel center always has a zero curvature.

This is done by finding the closest point between the vehicle's rear axis center O_R and the channel CH. As shown in Fig. 5.9, at a certain arc length s_1, we call this point $M(s_1)$. The goal channel is simply shifted to the projection of this point on the Qunitic path, which yields a new channel at the arc length s which is $CH(s_1) = CH'$. Then, as shown in Fig. 5.10, the system is controlled based on the error between the vehicle's current location and the new shifted channel CH'.

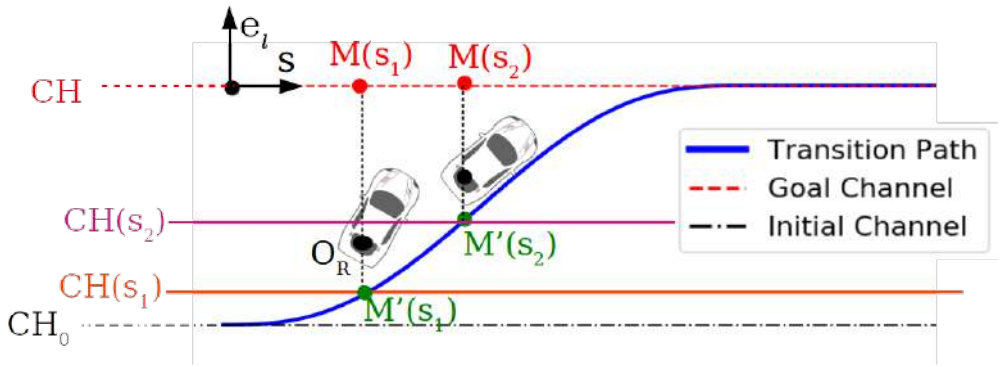

Fig. 5.9.: Goal channel center shifting using the Quintic transition path

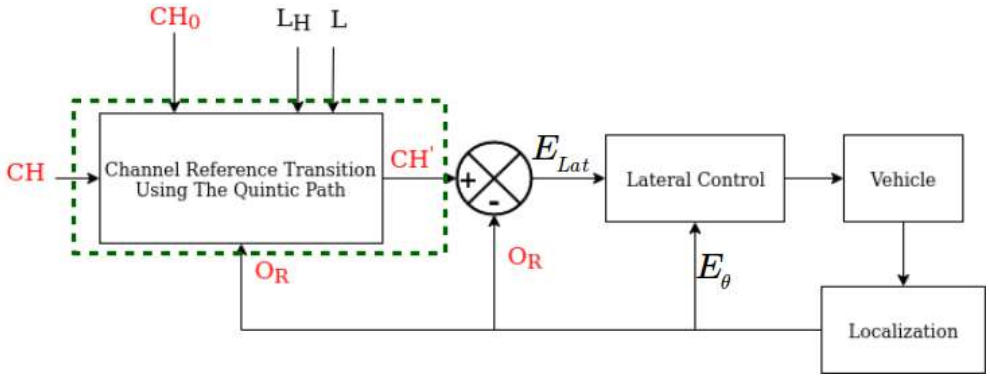

Fig. 5.10.: Lateral control diagram using the shifted channel

The previous lateral sliding mode steering controller is constructed using two tracking errors: the lateral displacement error (E_{lat}) and the heading error (E_θ), shown in Fig. 5.11. This ensures the tracking of the path and the natural manoeuvre while satisfying the smoothness in the vehicle heading as well. This can also contribute to the comfort of the vehicle's passengers. These two heading errors, as well as, the global tracking error (E) can be written with respect to the vehicle model in the Frenet frame of the goal channel $\mathcal{F}_\mathcal{C}$ as follows (Fig. 5.12):

$$E_{lat}(s) = e_q(s) - e_l(s) \tag{5.16}$$

$$E_\theta(s) = \theta(s) \tag{5.17}$$

$$E(s) = E_{Lat}(s) + d_s E_\theta(s) \quad : d_s \in \mathbb{R}^*_+ \tag{5.18}$$

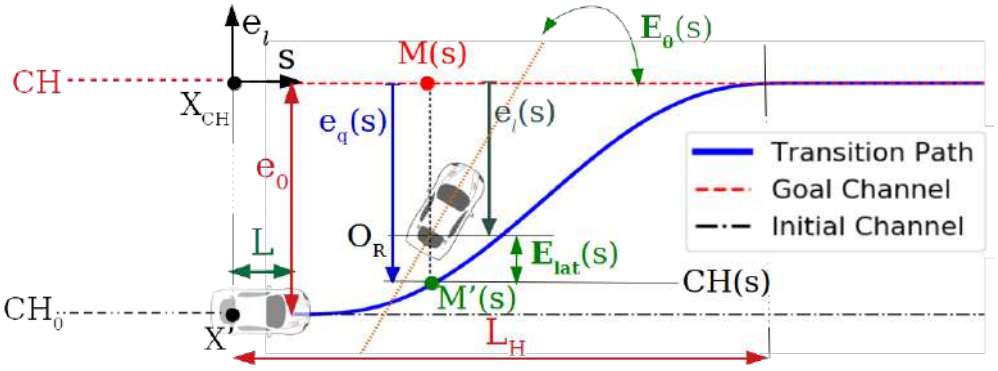

Fig. 5.11.: The vehicle tracking errors

Since the relative input-output degree of our system is two, a first degree sliding surface σ is selected:

$$\sigma = \left(\frac{d}{dt} + \lambda\right) E(s) \tag{5.19}$$

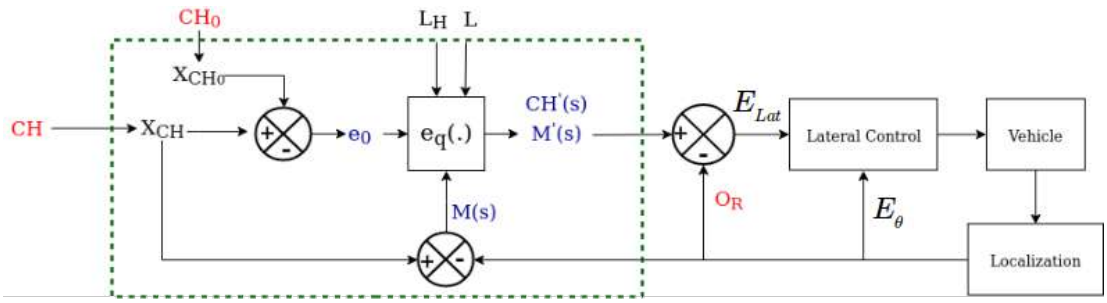

Fig. 5.12.: Lateral error computation using the Quintic path

where $\lambda \in \mathbb{R}_+^*$ defines the unique pole of the reduced dynamics system resulting in the closed loop.

The control required to reach the goal state ($E(s) = 0, \dot{E}(s) = 0$) is composed of two parts. These two modes are an equilibrium control which drives the system to the sliding surface (δ_{eq}), and a sliding control δ_s. The sliding control part keeps the system close to the sliding surface until the goal state is reached.

The previous equilibrium control is achieved when σ is constant:

$$\delta_{eq} = \delta|_{\dot{\sigma}=0} \tag{5.20}$$

This is solved by substituting the error derivatives in (5.18) and by using the vehicle's state space model $\left(\dot{s}, \dot{e}_l, \dot{\tilde{\theta}}\right)$. With a zero-curvature assumption for the center channel path and by assuming small steering variations $\dot{\delta} \ll 1$, the equilibrium control is derived as a function of the state variables, and the control parameters:

$$\begin{gathered} \delta_{eq} = F_\delta(\tilde{\theta}, s, v, a, \lambda, d_s) \\ F : [0, 2\pi] \times \mathbb{R}^{*5} \rightarrow [-\delta_{max}, \delta_{max}] \end{gathered} \tag{5.21}$$

with $\delta_{max} = \pi/6$. The exact form and derivation of the previous function for the equilibrium control is shown in Appendix F.

The second part of the control is the sliding mode steering δ_s, which insures keeping the system on the sliding surface until reaching the optimal state. Several methods are used in the literature to derive the sliding mode control part. To avoid the chattering phenomena which occurs in simpler first order SMC, we use the "Super Twisting" second order algorithm [SU16]. The "Super Twisting" can be seen as a nonlinear version of the classic PI controller, where the sliding control is chosen as:

$$\delta_s = -\gamma_1 \sqrt{|\sigma|} sign(\sigma) + c \tag{5.22}$$

$$\text{with: } \dot{c} = -\gamma_0 sign(\sigma) \tag{5.23}$$

with the constants: $\gamma_1 = U, \gamma_0 = 1.1U$, where $U \in \mathcal{R}_+$ is a constant to be tuned.

Finally, given an initial state of the vehicle (s, e_l, θ, v, a) and a goal channel C, the steering control is computed as:

$$\delta = \delta_{eq} + \delta_s \tag{5.24}$$

The flowchart for our navigation scheme is shown in Fig. 5.13. As shown in the figure, a new exploration of the space is performed in two cases. Either a new channel have been reached, or a time period of T_H have passed without successfully reaching the goal channel. Reaching a channel is when the displacement error E from the goal channel and its variation are smaller than the limit displacement error ϵ_1 and the limit displacement variation error ϵ_2. The values of ϵ_1 and ϵ_2 are tuned experimentally to the values shown in Appendix G.

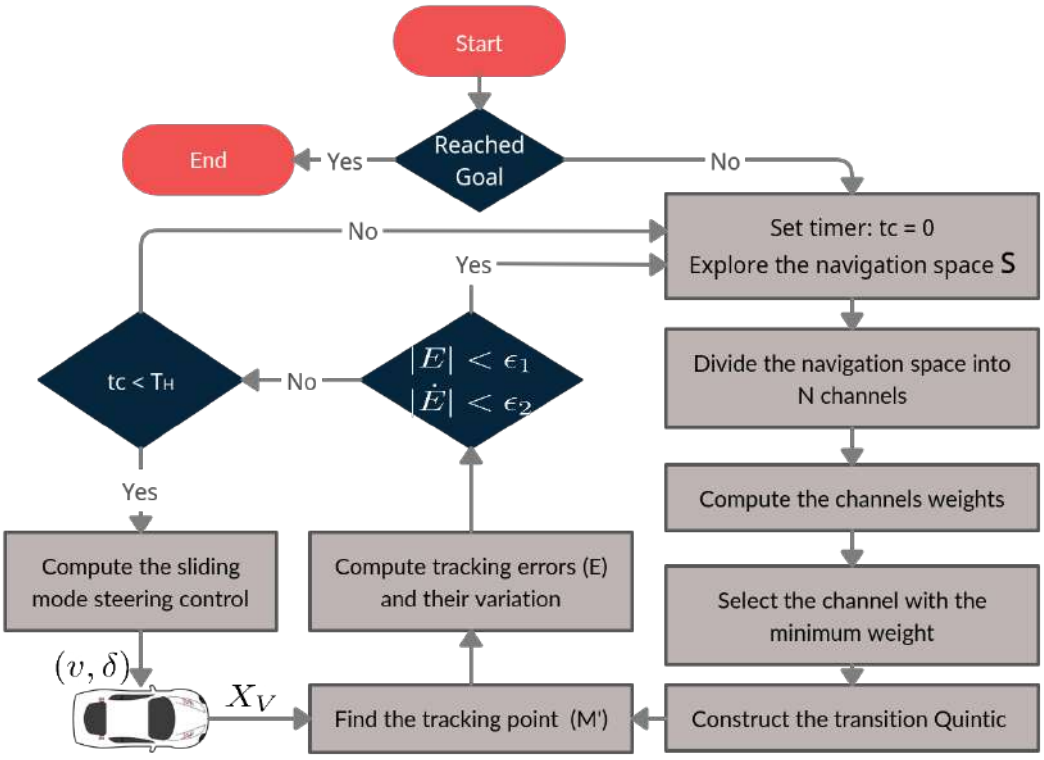

Fig. 5.13.: The proactive and smooth manoeuvring algorithm

5.6 Parameters Calibration

5.6.1 Calibrating the SMC parameters

To use the steering controller defined earlier, several parameters need to be tuned. The first is the lookahead distance used to define the transition Quintic spline in (5.14). The lookahead distance is computed depending on the speed of the vehicle: $L_H = vK_F$ where $K_F = 10$. Fig. 5.14b shows the closed-loop system (trajectory and steering) response with different values of K_F, which is selected to achieve a fast closed-loop response with minimal overshooting ($< 5\%$). The rest of the steering control parameters are tuned in a similar manner to achieve a smooth steering and avoid trajectory overshooting. The weight between the lateral and heading tracking errors in (5.18) is selected as $d_s = 2$. While, the sliding surface constant in (5.19) is set to $\lambda = 10$. Finally, the "Super-twisting" parameter in (5.23) is tuned to $U = 10$.

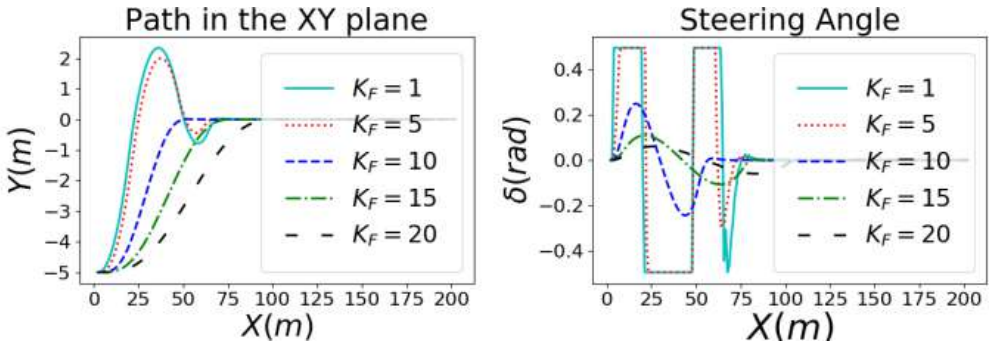

Fig. 5.14.: Tuning the lookahead distance factor

5.6.2 Calibrating the channel dimensions

Calibration Criteria

To calibrate the channel dimensions, three average performance measures are used: the average travel time of the vehicle to reach its goal, it's average path energy, and the average uncomfortableness index of the pedestrians. The vehicle time to reach goal is the time measured in seconds between the start of the simulation and the moment of reaching the goal destination.

Secondly, the path energy [BN90] is a qualitative measure used to evaluate the quality of the vehicle's trajectory or its smoothness. Let $X_j = (x_j, y_j)\ j \in [0, .., M]$ be the overall

path of the vehicle during the simulation, then the equivalent path energy is evaluated as:

$$E_T = \sum_{j=1}^{M} \left(\frac{y_j - y_{j-1}}{x_j - x_{j-1}} \right)^2 \tag{5.25}$$

where $E_T \in \mathcal{R}_+$ increases when a path contains more frequent and sharp maneuvers ($E_T = 0$ for a straight path).

Finally, the uncomfortableness index is used to evaluate the *pedestrian comfort* during the interaction with the vehicle [Hel+01]. This index reflects the degree and frequency of the velocity change a pedestrian can experience during the interaction. In each simulation, the uncomfortableness index is evaluated as:

$$\bar{I}_{ucf} = \frac{1}{N} \sum_{i=1}^{N} \frac{\bar{y}_i}{\bar{h}_i} \tag{5.26}$$

$$\begin{aligned} &\bar{h}_i = \tfrac{1}{T_F} \textstyle\sum_{t=t_0}^{t_0+T_F} v_i^2(t) \quad \bar{y}_i = \tfrac{1}{T_F} \textstyle\sum_{t=t_0}^{t_0+T_F} (v_i(t) - \bar{g}_i)^2 \\ &\bar{g}_i = \tfrac{1}{T_F} \textstyle\sum_{t=t_0}^{t_0+T_H} v_i(t) \end{aligned} \tag{5.27}$$

where: N is the total number of pedestrians in the simulation, $\bar{h}_i$, $\bar{y}_i$ are the mean square velocity and the deviation of the average velocity of agent i respectively, and $\bar{g}_i$ the average velocity of agent i over the simulation period $[t_0, t_0 + T_F]$.

More details on these metrics are shown in Chapter 6.

Calibration

Firstly, a group of 540 simulations are ran to study the effect of the channel length on the performance. The simulations contained three levels of pedestrian density ($D \in 30, 50, 70\%$), with a sparsity range of $GI \in [55, 75]\%$. Additionally, the maximum velocity of the vehicle, the simulation duration and the channel width are constant across all simulations ($v_{max} = 4m/s, T_F = 60s, W = 3m$ respectively). The simulations are grouped based on the density level and the channel length, each group containing 30 simulations where six different channel lengths in $[5, 120]m$ are tested.

Secondly, different width values of the dynamic channels are tested in a similar manner to the previous test. Another group of 540 simulations are ran using the same previous configuration with a fixed channel length of $40m$ and four different width value in $[1, 10]m$.

Fig. 5.15 shows the results of the three average performance measures with the different channel lengths, widths and the three levels of density. Each point on the graph represents the average value for one group of simulations. The results show that larger channel lengths reduce the vehicle travel time and increase the comfort of pedestrians. Moreover, larger channel lengths significantly reduce the vehicle's path energy resulting in smoother trajectories with less channel change along the simulation. This is a result of anticipating a larger space horizon to plan and select the best manoeuvring option. However, the relationship between the channel length and it's effect on the navigation is not linear. The results show that a minimum channel length is required to obtain a high performance gain. This minimum length is equal to around $20m$ in our case. Whereas, increasing the length beyond that limit results in smaller performance gains. Moreover, large loss in efficiency in terms of the travel time and pedestrian comfort occurs when using a large channel width. On the other hand, a large channel width results in a more smooth path as less partitions of the space are explored thus resulting in less steering options. Finally, a channel length of $40m$ and a small channel width equal to approximately half the vehicle width ($1m$) are selected to maintain a smooth path while maximizing pedestrian comfort and minimizing the vehicle travel time.

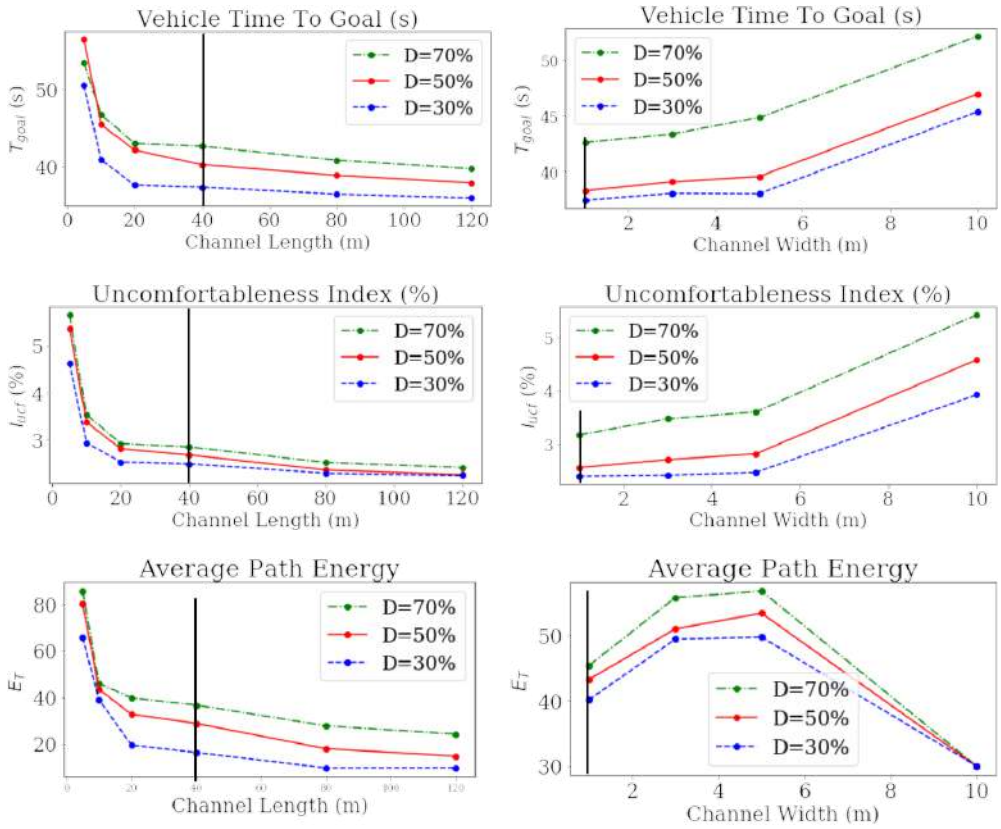

Fig. 5.15.: Effect of channel dimensions on the steering performance

5.7 Results Analysis

The navigation is tested using the PedSim simulator presented in [Pré21] under ROS (Fig. 5.16a). The tests included frontal and lateral crossing interaction scenarios with a group of pedestrians. The method is tested with a range of different average pedestrian density and sparsity in the space. To measure sparsity in a particular interaction, we use a Gini Index measure which represents how equitably a resource is distributed among entities in a group [GMD16]. In our case, the Gini index measures the distribution of pedestrians among the interaction space partitions. Let T_F be the simulation duration, N_{max} the maximum number of pedestrians in the space, and $N(t)$ be the total number of pedestrians in the space at time t. Then, the average pedestrian density and sparsity are measured as follows:

$$D = \frac{1}{T_F} \sum_{t=t_0}^{t_0+T_F} \frac{N(t)}{N_{max}} \times 100\% \tag{5.28}$$

$$GI = \frac{1}{T_F} \sum_{t=t_0}^{t_0+T_F} \sum_{j=1}^{N(t)} \frac{|1 - N_j(t)|}{N(t) + 1} \times 100\% \tag{5.29}$$

where the interaction space is first divided into a grid of $N(t)$ equal cells. Then, N_j is the number of pedestrians in a cell j of the grid (Fig. 5.16b). If the distribution of the pedestrians in the space is homogeneous, then there is one pedestrian in each of the equal grid cells, yielding $GI = 0\%$. On the other hand, if the distribution has a maximum sparsity, then all the pedestrians are in one cell k resulting in $N_k = N(t), N_{j \neq k} = 0 => GI = 100\%$. Note that these extreme cases are not feasible in most scenarios.

5.7.1 The proactive channel weight model

To investigate how the channel selection and weight assigning is working, let's observe the model output for some test cases. In the following tests, the case of three possible channel options is presented. The width of each channel equals the width of the vehicle $W_C = 2m$, whereas the length of the channel is $L_C = 40m$. Having the width of the channel equal to the width of the vehicle means that the existence of only one pedestrian in a channel yields it a non obstacle-free choice. Each test case is a snapshot of a moment in the navigation at time t_k. The snapshot shows the positions and velocities of both the pedestrians and the vehicle, as well as, the pedestrian's cooperation factors. For each case we show the fuzzy weight model inputs at t_k: Density D, Predicted change of density over $T_h = 5s$ (ΔD) and the percentage of uncooperative pedestrians $N_{UC\%}$. The resulting channel weights are calculated: fuzzy weight w_{fuzzy}, local weight w_{local},

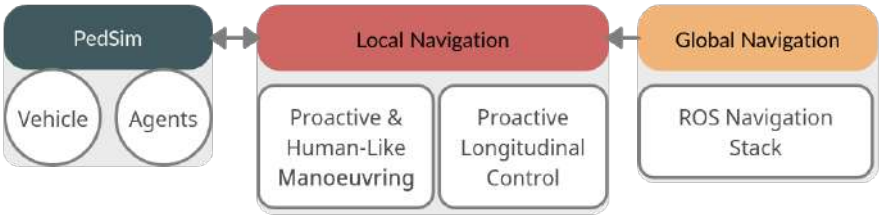

(a) The testing framework under ROS

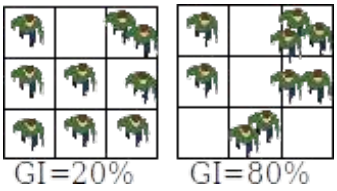

(b) Two exmamples of the GI sparsity measure

Fig. 5.16.: The testing framework and the GI measure

global weight w_{global}, along with the total channel weight w_C. The global path of the vehicle is shown as a dashed green line in each case.

Example Cases 1-3: The first three example cases are shown in Tab. 5.1. In all three cases the pedestrians maintain the same density distribution along the three channels. A pedestrian free path does exist at the moment of the screen shot through channel $Ch\ 3$. However, this channel is not always selected. In all three cases we notice that the fuzzy weight of channel $Ch\ 3$ is the smallest. This weight is then adjusted by the additional cost of traveling from the vehicle's position to the channel (w_{local}) and the cost of travelling from the channel back to the global path (w_{global}). In both Case 1 and Case 2, the pedestrian in $Ch\ 2$ is predicted to stay there for the upcoming prediction horizon T_h. However, the pedestrian in Case 1 is highly cooperative. This makes the fuzzy weight of the channel smaller in Case 1 than in Case 2. Consequently, in Case 1 the advantage of travelling to the pedestrian free channel is not enough compared to navigating in $Ch\ 2$ which is slightly denser but much less energy consuming. Whereas, in Case 2, the uncooperative pedestrian in $Ch\ 2$ yields its navigation cost higher, which makes travelling to channel $Ch\ 3$ worth the additional cost. Finally, Case 3 is similar to Case 1, with the difference of expecting that the pedestrian in $Ch\ 2$ is going to leave it towards $Ch\ 3$. Therefore, channel $Ch\ 2$ is selected for the navigation.

Example Cases 4-6: Three more examples are shown in Tab. 5.2. Example Case 4 shows the advantage of of adjusting the channel state weight w_{fuzzy} with the local and global costs. Since the state of all channels is similar, the global path channel $Ch\ 2$ is

	Case 1			Case 2			Case 3		
	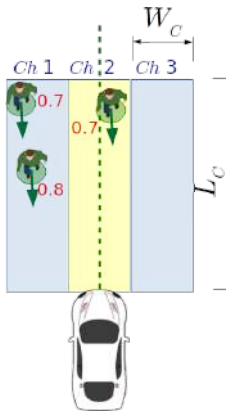			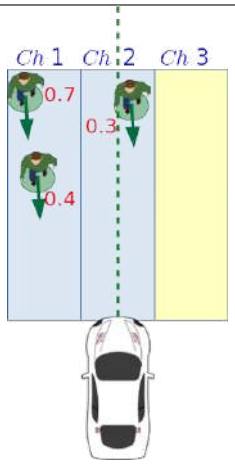			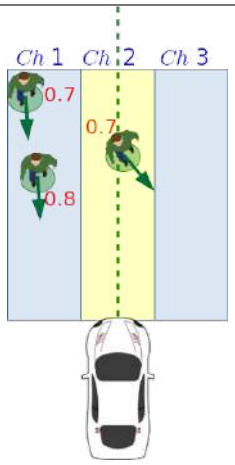		
Channel	$Ch\ 1$	$Ch\ 2$	$Ch\ 3$	$Ch\ 1$	$Ch\ 2$	$Ch\ 3$	$Ch\ 1$	$Ch\ 2$	$Ch\ 3$
D	1.26%	0.63%	0%	1.26%	0.63%	0%	1.26%	0.63%	0%
ΔD	0%	0%	0%	0%	0%	0%	0%	−0.78%	+0.78%
$N_{UC\%}$	0%	0%	0%	50%	100%	0%	0%	0%	0%
w_{fuzzy}	0.06	0.04	0.01	0.19	0.18	0.01	0.06	0.03	0.025
w_{local}	$\frac{1}{3}$	0	$\frac{1}{3}$	$\frac{1}{3}$	0	$\frac{1}{3}$	$\frac{1}{3}$	0	$\frac{1}{3}$
w_{global}	$\frac{1}{3}$	0	$\frac{1}{3}$	$\frac{1}{3}$	0	$\frac{1}{3}$	$\frac{1}{3}$	0	$\frac{1}{3}$
w_C	0.12	0.04	0.07	0.25	0.18	0.07	0.12	0.03	0.085

Tab. 5.1.: Example Cases 1-3 for the navigation cost computation and the proactive channel selection

selected. In Case 5 an example is shown where the local and global navigation costs (w_{local}, w_{global}) are not similar. Finally, in Case 6 a higher density example is shown.

	Case 4			Case 5			Case 6		
	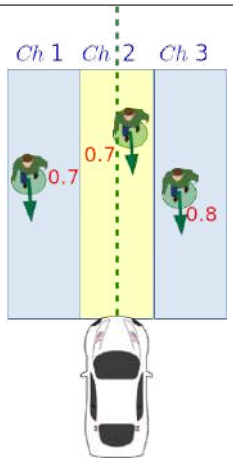			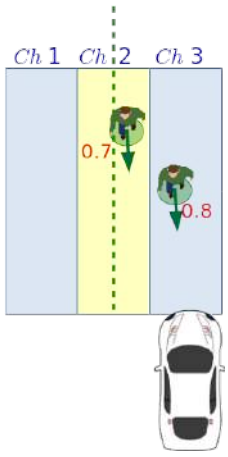			A More Dense Case Example		
Channel	$Ch\ 1$	$Ch\ 2$	$Ch\ 3$	$Ch\ 1$	$Ch\ 2$	$Ch\ 3$	$Ch\ 1$	$Ch\ 2$	$Ch\ 3$
D	0.63%	0.63%	0.63%	0%	0.63%	0.63%	25.1%	55.3%	24.5%
ΔD	0%	0%	0%	0%	0%	0%	+9%	−10%	+11%
$N_{UC\%}$	0%	0%	0%	0%	0%	0%	50%	60%	50%
w_{fuzzy}	0.04	0.04	0.04	0.01	0.04	0.04	0.305	0.427	0.311
w_{local}	$\frac{1}{3}$	0	$\frac{1}{3}$	$\frac{2}{3}$	$\frac{1}{3}$	0	$\frac{1}{3}$	0	$\frac{1}{3}$
w_{global}	$\frac{1}{3}$	0	$\frac{1}{3}$	$\frac{1}{3}$	0	$\frac{1}{3}$	$\frac{1}{3}$	0	$\frac{1}{3}$
w_C	0.1	0.04	0.1	0.09	0.06	0.08	0.365	0.427	0.3715

Tab. 5.2.: Example Cases 4-6 for the navigation cost computation and the proactive channel selection

5.7.2 Steering performance analysis

Low density interactions

Let's start by examining the performance of the system in interactions with very low density (i.e. interactions with few pedestrians). The case of frontal interaction is explored in detail, as this case allows more efficient steering options (as opposite to the lateral crossing case).

A frontal interaction scenario is initialized between two pedestrians and the vehicle using PedSim. The goals of the pedestrians lay behind the vehicle and vise-versa, to test an exact frontal interaction. Fig. 5.17 shows the resulting paths in the XY plane at different times of the interaction. The vehicle avoids the pedestrians by transitioning to a different channel, and no cooperation is detected on the pedestrians side. Once the pedestrians are avoided, the vehicle moves back to the original global path channel. Noting the difference in the security margins between the front and the side of the vehicle. On the frontal side, the vehicle starts avoiding the pedestrians at about $20m$ distance. Whereas, only around $2m$ distance is maintained when the pedestrians are safely passing on the vehicle's side and no collision could occur. This is a result of considering the probability of collision in our system model rather than relying directly on the distance to the vehicle's body. The resulting smooth steering control command along with the vehicle's orientation, and the corresponding angular velocity and acceleration are shown in Fig. 5.19. The channel selection in this example is yielding two transitions. Therefore, the reference path to be followed is given by the two channels center lines along with two Quintic transition paths as shown in Fig. 5.18. Overall, the reference path is followed with small lateral and orientation errors. However, a static lateral displacement error is observed. This is a result of considering maintaining the vehicle within a channel and avoid steering efforts over the very small lateral displacements.

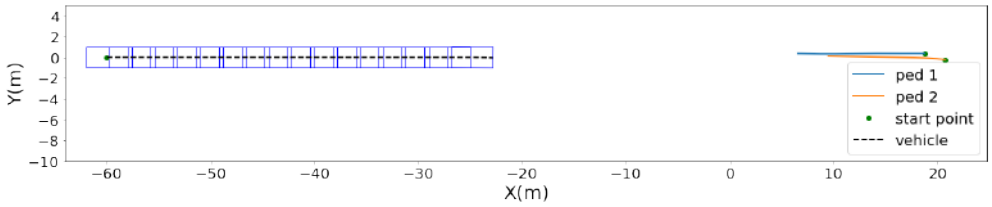

(a) time = 6.2s

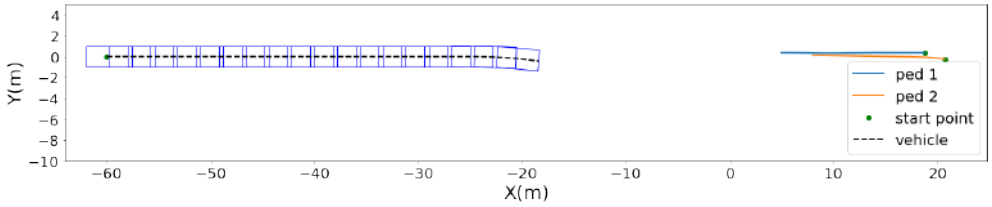

(b) time = 7s

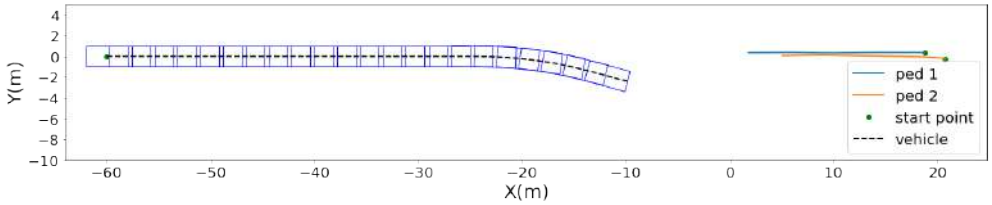

(c) time = 8.6s

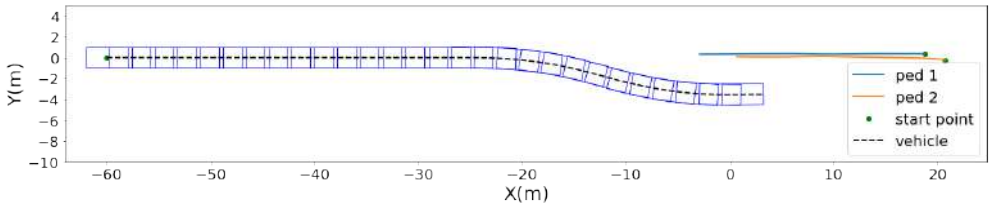

(d) time = 11s

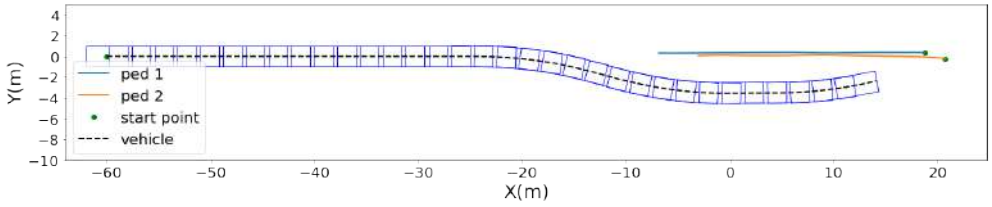

(e) time = 14s

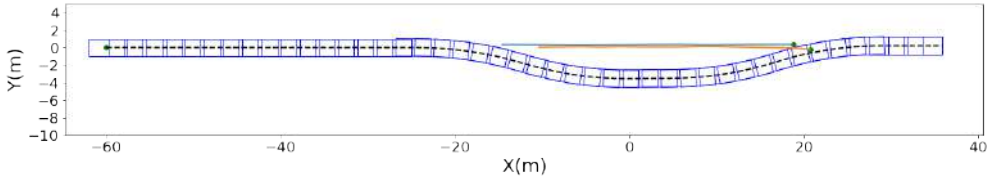

(f) time = 17s

Fig. 5.17.: Resulting paths in the XY plane in a low-density frontal interaction scenario

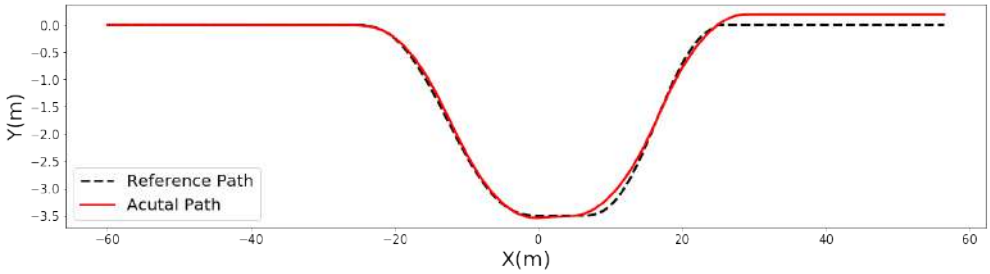

(a) Reference and actual paths

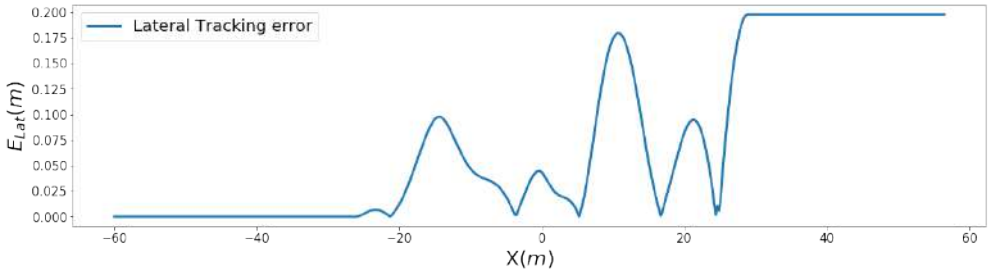

(b) Lateral tracking error

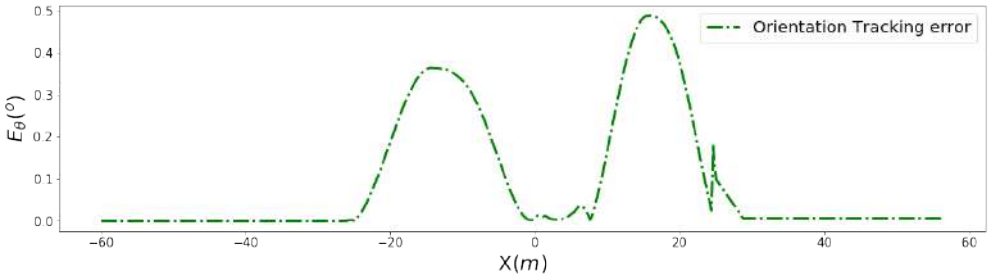

(c) Orientation tracking error

Fig. 5.18.: Path following errors in the frontal interaction scenario in Fig. 5.17

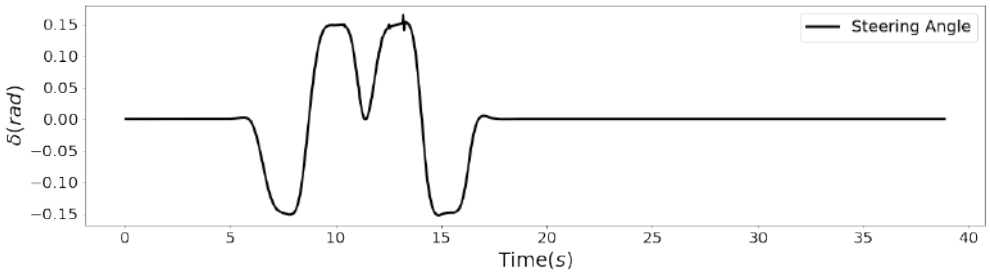

(a) Steering Angle

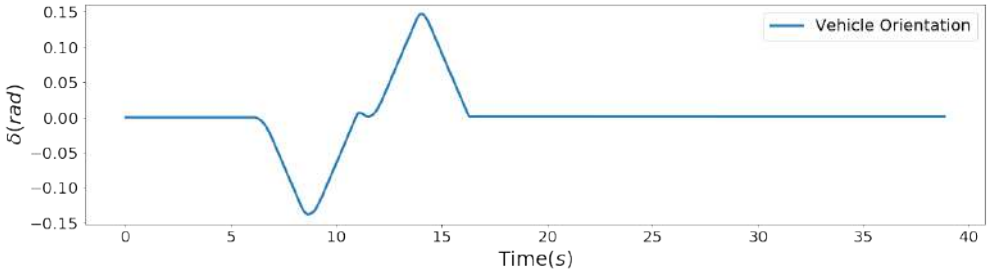

(b) Orientation

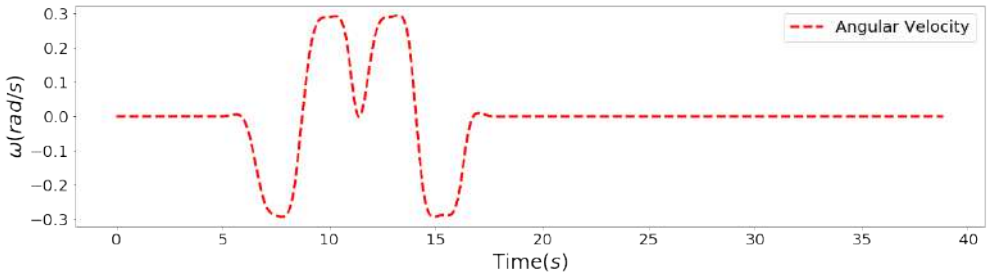

(c) Angular Velocity

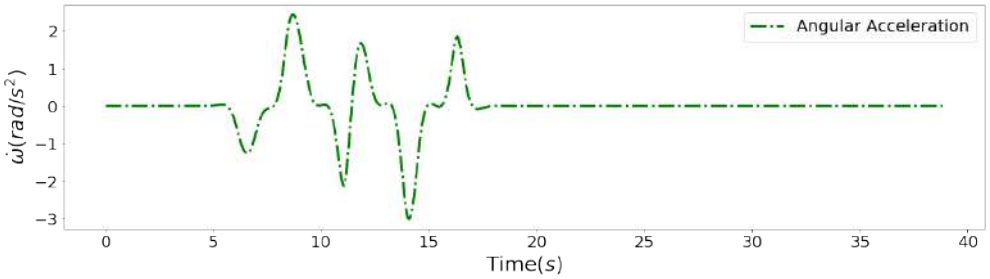

(d) Angular Acceleration

Fig. 5.19.: Resulting steering commands and orientation in the frontal interaction scenario in Fig. 5.17

Higher density interactions

A total of 840 simulations are ran (520 frontal and 320 lateral) with over $10K$ pedestrian trajectories. The simulations included pedestrian crowds with average density ranging between $D \in [20, 90]\%$ and with average sparsity in $GI \in [35, 93]\%$. The maximum speed of the vehicle, the simulation duration and the channel width/length are constant across all the simulations ($v_{max} = 4m/s, T_F = 60s, W = 1m, L = 40m$ respectively).

Fig. 5.20 shows six examples of the resulting trajectories for both the vehicle and the pedestrians in the XY plane.

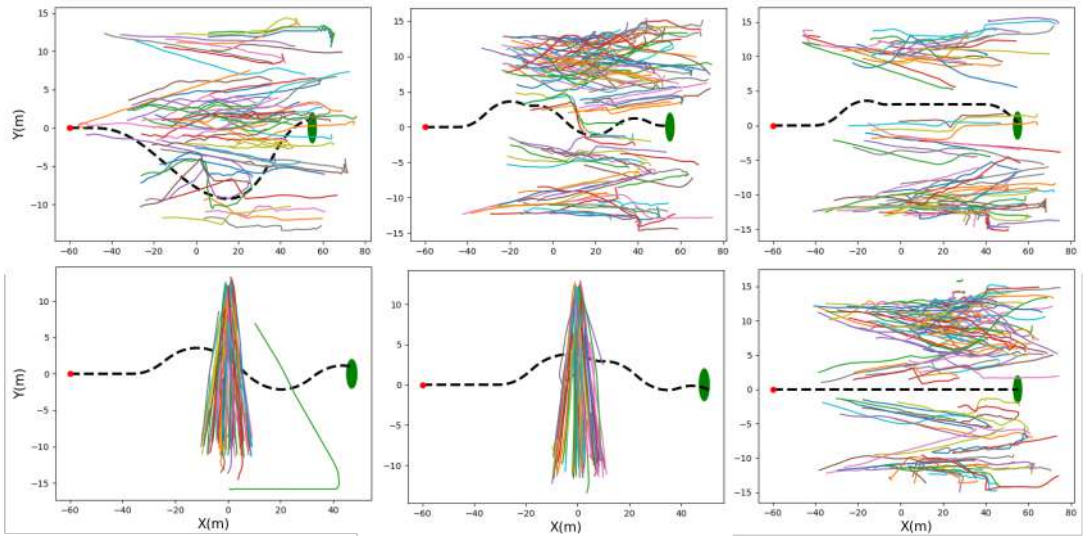

Fig. 5.20.: The resulting trajectories in 6 different interaction tests. Black dashed line: vehicle path, colored lines: pedestrians paths, red circle: vehicle start point, green ellipse: vehicle goal.

Another visualization of one frontal interaction scenario on PedSim is shown in Fig. 5.21 at different time instances. The global path channel is plotted in blue, while the selected navigation channel is in red. In (a) the space is explored proactively and the optimal navigation channel is selected. Then, the human-like transition to the channel is executed in (b,c,d). Next, the same process is repeated again in (e,f,g), until the goal destination is reached.

The steering commands along with the resulting angular velocity and acceleration is observed over the simulated tests. The average and max value for each quantity is evaluated in each simulation as follows:

- Maximum and average value of the steering commands in a simulation:

$$\begin{aligned} \delta_{max} &= \max_{t\in[t_0,t_0+T_F]} |\delta(t)| \\ \delta_{avg} &= \frac{1}{T_F}\sum_{t=t_0}^{T_F} |\delta(t)| \end{aligned} \tag{5.30}$$

- Maximum and average value of the angular velocity in a simulation:

$$\begin{aligned} \omega_{max} &= \max_{t\in[t_0,t_0+T_F]} |\omega(t)| \\ \omega_{avg} &= \frac{1}{T_F}\sum_{t=t_0}^{T_F} |\omega(t)| \end{aligned} \tag{5.31}$$

- Maximum and average value of the angular acceleration in a simulation:

$$\begin{aligned} \dot{\omega}_{max} &= \max_{t\in[t_0,t_0+T_F]} |\dot{\omega}(t)| \\ \dot{\omega}_{avg} &= \frac{1}{T_F}\sum_{t=t_0}^{T_F} |\dot{\omega}(t)| \end{aligned} \tag{5.32}$$

The statistical results of the previous quantities over the simulated tests group (both frontal and lateral) is shown in Tab. 5.3. The average values of the three quantities gives an idea about the steering effort over the simulation. Whereas, the maximum values are shown to express the worse case scenario (with the highest steering or steering rate).

Parameter	Unit	Mean	Max	75%	Std. Dev.
δ_{avg}	rad	0.03	0.11	0.05	0.02
δ_{max}		0.06	0.23	0.10	0.05
ω_{avg}	rad/s	0.12	0.32	0.21	0.10
ω_{max}		0.27	0.77	0.39	0.20
$\dot{\omega}_{avg}$	rad/s^2	0.73	2.18	1.23	0.61
$\dot{\omega}_{max}$		1.43	4.19	2.97	0.89

Tab. 5.3.: Steering, angular velocity and angular acceleration across the tested interactions

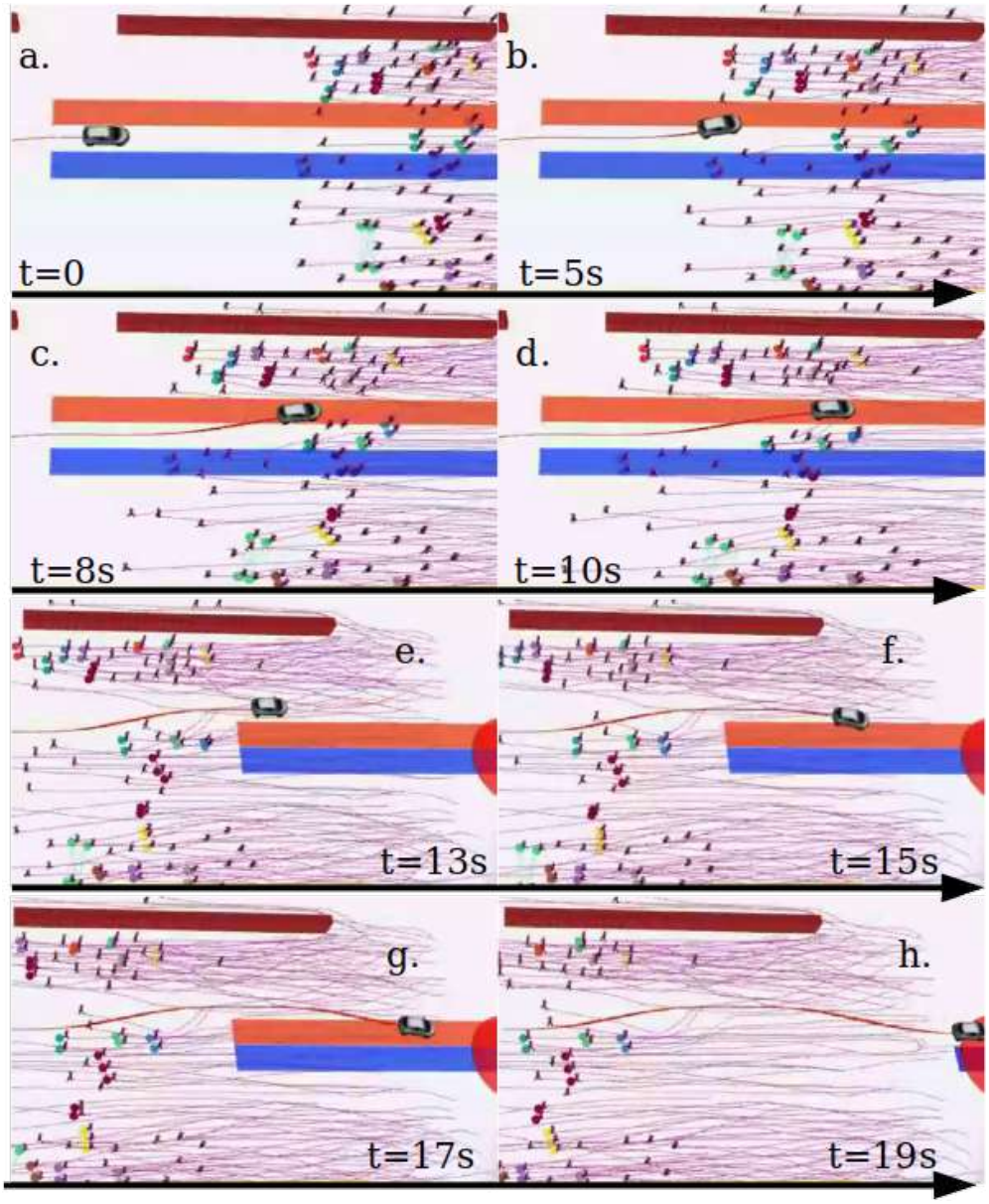

Fig. 5.21.: Visualization of a frontal interaction in PedSim. The global path channel is shown in blue, whereas, the selected channel is shown in red. The destination of the vehicle is the red semi circle.

5.8 Conclusion

This chapter included the manoeuvring system development of the proactive navigation framework. The work presents a local manoeuvring technique adapted to autonomous vehicles navigation in shares spaces with pedestrians. The suggested method integrates multiple concepts and frameworks to perform a natural and smooth local path modification and steering in the shared space. The main idea was to imagine a structure for the open shared space to deploy the known driving rules and produce natural driving patterns. The developed proactive dynamic channel method starts with dividing the shared space into a set of possible navigation options, which we call channels. These channels are constructed using the global path of the vehicle as a reference which yields a local path modification system. The cost of navigating in each channel is computed based on the vehicle travel effort and the state of the pedestrians within the channel. A lowest cost channel (or best case navigation option) is selected. The global path of the vehicle is modified using Quintic splines segments to transitions between the channels and back to the global path. The method presented in this chapter resulted in the following publication:

"***M. Kabtoul, A. Spalanzani and P. Martinet. Proactive And Smooth manoeuvring For Navigation Around Pedestrians. IEEE International Conference on Robotics and Automation (ICRA), May 2022, Philadelphia, USA. Under Review***"

The method was tested using the PedSim simulator under ROS. The test simulations included frontal and lateral crossing interactions between a vehicle and a group of pedestrians. The steering commands and the corresponding angular velocity and acceleration of the vehicle is evaluated in each test. The tests showed that the method enables the vehicle of navigating variable density spaces while maintaining a smooth manoeuvring of the vehicle. Moreover, the proactive quality of the system enabled the vehicle of navigating high density spaces where a pedestrian-free path does not exist, therefore avoiding the freezing robot problem.

The suggested framework was implemented with a kinematic-based sliding mode path follower. However, the same framework can be implemented with other path following steering controllers to be implemented with higher vehicle speed limit, for example.

The performance of the steering system within the complete proactive navigation framework is going to be further tested and evaluated in Part III.

Part II

Implementation and Validation

"'The universe exists independent of the anthropic principle. . . so does overspace," continued Krigisa. There was a significant difference between existence and understanding, between reaction and proaction—or were intelligence and planning merely illusions? Were we genetically programmed to respond, merely rationalizing our actions after the facts?"

– L.E. Modesitt Jr., *Gravity Dreams*

6 Performance Measures For Navigation Around Pedestrians

Developing fully autonomous vehicles navigation system which can operate around pedestrians is becoming an increasingly critical issue, especially with the growing influence of the shared space concept in cities planning [MM14]. This growing interest is motivated by the premise of more green and pedestrian-friendly cities where vehicles and pedestrians share public spaces in a safe and efficient way [ET21; Ski16]. However, building, testing and validating autonomous navigation systems in shared spaces with pedestrians are highly challenging tasks, each task being a standalone multidisciplinary problem. These steps of the development process (Build $\rightarrow$ Test $\rightarrow$ Validate) are equally crucial before letting a potentially harmful system navigate around humans.

This chapter presents the performance metrics adapted for validating the navigation performance of an autonomous vehicle (or a mobile robot) in close interaction with pedestrians. The computation method of each metric is explained using the trajectory-based information only. Moreover, a success criteria is estimated for each metric based on social studies.

6.1 Problem Definition

Validating the navigation system in shared spaces with pedestrians requires a set of adapted performance measures. The metrics traditionally used for autonomous robot to validate the navigation is necessary but not sufficient. The validation process should consider the safety and comfort of pedestrian around the navigating system, and of the passengers who could be on-board of the vehicle.

The problem can be summarized in selecting and/or designing a set of performance metrics which:

- Evaluate the system's motion safety in proximity with pedestrians.
- Evaluate the efficiency of the resulting motion in terms of the traveled distance and traveled time.

- Evaluate the comfort and safety of the possible vehicle's passengers.
- Evaluate the social compliance and the comfort of the pedestrians around the vehicle.

Inputs: The available inputs for calculating the metrics are the trajectory information for both the pedestrians and the vehicle during an interaction.

Outputs: a scalar value, and the success/fail criteria for each metric.

6.2 Related Work

The problem of autonomous vehicle navigation around pedestrians has started getting researchers attention only in the past recent years. Therefore, not many works in the literature arrived at the performance validation step of an AV system in shared spaces with pedestrians. However, works in robotics in general targeted the issue of navigation systems validation around humans. We can divide the metrics used in such cases into three main categories: motion safety, trajectory quality and pedestrian comfort metrics.

The **motion safety** of a navigation system is mostly evaluated by reporting the collision rate or the near missed rate between the humans and the navigating system, as in [Luo+18] and [Bai+15]. A more continuous metric that can also be used is the minimum and mean distance between pedestrians and the robot [MVL07]. Other studies depend on estimating the safety by the distance or the temporal proximity to the collision when the evasive action starts by the robotic system. For example, the Time To Collision (TTC) is proposed in some studies [Kap+13; Pas20; TS16]. Whereas, the Post Encroachment Time (PET) corresponding to the TTC at the minimal approach distance have been used in other works [Pas20; TS16]. Another metric proposed by [Pas20] for the collision severity is the AV speed before the AV starts avoiding the collision.
However, these measures evaluate the performance based on the systems behavior before the start of the collision avoidance behavior. Therefore, this cannot be directly applicable to proactive navigation systems which do not perform the collision avoidance in the traditional way.

The **trajectory quality** evaluation is the most addressed problem since it applies to all autonomous navigation systems regardless of the environment and context. Te main aspects addressed in this regard are the smoothness and efficiency of the resulting trajectory. A smooth trajectory limits abrupt changes in direction and speed. Therefore, many works, as [Bai+15] and [Luo+18], uses the acceleration/deceleration of the

system as a smoothness measure. Moreover, the efficiency of a trajectory is usually measured in terms of the travelled distance [Bai+15], or the travel time [MVL07] or the goal reaching rate [Luo+18]. Other works suggest adapting the previous measures to relative terms. For example, [Pas20] compares the trajectory to the optimal trajectory in terms of the travelled distance and time.
All the previous trajectory quality metrics are valid to evaluate the performance of AV navigation. However, the case of a vehicle includes the special property of possibly having passengers on-board. The specific trajectory that the vehicle adapts will have consequences of the safety and comfort of its passengers. This is an important issue in AV performance validation which needs to be addressed with the appropriate performance metrics.

Finally, the comfort of humans navigating around the vehicle is crucial given that it determines the social acceptance of autonomous vehicles. However, **Pedestrian comfort** is a newly addressed topic in the literature, specially for the case of autonomous vehicles. [MMH17] studies the comfort of a pedestrian for a pedestrian-wheelchair interaction in a corridor. The work suggests estimating the comfort based on the deviation from the ideal location within the corridor (i.e. optimal trajectory deviation).

In the following we present a set of performance metrics suitable for the case of shared spaces navigation, with the success/fail criteria adapted for the case of autonomous vehicles.

6.3 Motion Safety Metrics

6.3.1 Collision Detection

The main indices used to validate the motion safety around pedestrians are derived from analysing the collisions occurring in the simulations. A collision is detected in the simulation when an overlap occurs between the footprints of both the pedestrian and the vehicle. As explained in Section 2.7.2, the footprint of a pedestrian in the 2D plane is considered circular with a radius R_{ped}. Whereas, the footprint of the rectangular AV is approximated with the outer Löwner-John ellipse of the rectangle [Joh14].

The *Collisions Rate* is an important factor in estimating the safety of the navigation policy. A near-zero collision rate is required to validate the navigation. However, when looking at the collision rate in a simulated world it is important to evaluate if this collision could actually occur in the real world. An *Unrealistic Collisions Rate* can be detected in the simulator that could not lead to an actual collision in real life. An example of this is

shown in Fig. 6.1a where the vehicle is static and a pedestrian walks into the side of the vehicle. This case is detected as a collision in the simulator whereas in real-life this is highly unlikely to happen and such a situation would mean, for example, that a distracted person bumped into a parking vehicle which is not considered an accident and cannot be avoided in the navigation algorithm. To assist if a collision is realistic or not, a velocity obstacle based collision analysis is performed.

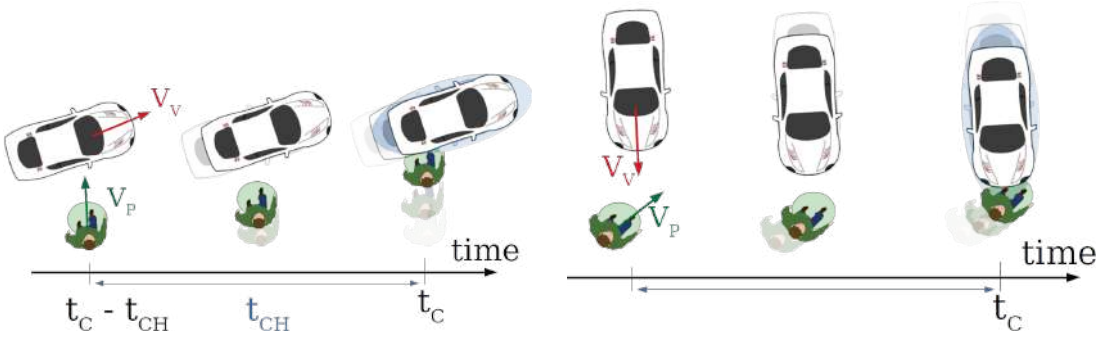

(a) UnRealistic Collision **(b)** Realistic Collision

Fig. 6.1.: Two collisions detected at time t_C and the state of the AV and the pedestrian in the previous t_{CH} period

6.3.2 Velocity Obstacle Based Collision Analysis

The Velocity Obstacle (VO) is a known method in robotics used for motion planning. The method allows to calculate the set of robot velocities that can lead to a collision with another moving obstacle, or what is referred to as the collision cone. When planning a trajectory, the velocity command is selected outside the collision cone for obstacle avoidance [FS98].

The idea of the **VO-based Collision Analysis** is to examine the AV's velocity commands during the time period proceeding the collision with a pedestrian. If the AV's velocity belongs to the pedestrian's collision cone, then the collision is considered "Realistic". Otherwise, the collision is considered "Unrealistic" as the AV is moving away from the pedestrian and the pedestrian still collided with the AV. One main limitation of the VO method is that it assumes a circular shape in the 2D plane for both of the colliding objects. Since the footprint of the vehicle can be approximated with the smallest enclosing ellipse, then an ellipse-based velocity obstacle method (EBVO) is applied to derive the collision cone [JL14].

Approximate AV footprint

One main limitation of the VO method is that it assumes a circular shape in the 2D plane for both of the colliding objects. However, assuming a circular footprint for the rectangular AV would result in large errors. Therefore, the footprint of the vehicle is approximated with the minimum number of enclosing circles (Fig. 6.2a) [ZS10]. Algorithm 2 shows how the approximated footprint C_{fp} of the AV with a pose $(x_o(t), y_o(t), \theta_V(t))$ is obtained in the local frame of the AV then in the global frame using the transformation matrix R_L^G:

$$R_L^G(t) = \begin{bmatrix} \cos(\theta_V(t)) & -\sin(\theta_V(t)) & x_o(t) \\ \sin(\theta_V(t)) & \cos(\theta_V(t)) & y_o(t) \\ 0 & 0 & 1 \end{bmatrix} \tag{6.1}$$

Once the set of footprint circles is obtained, the VO-based analysis is applied to each circle and the collision is considered realistic if any of the circles of the set yields a positive result (Algorithm 3).

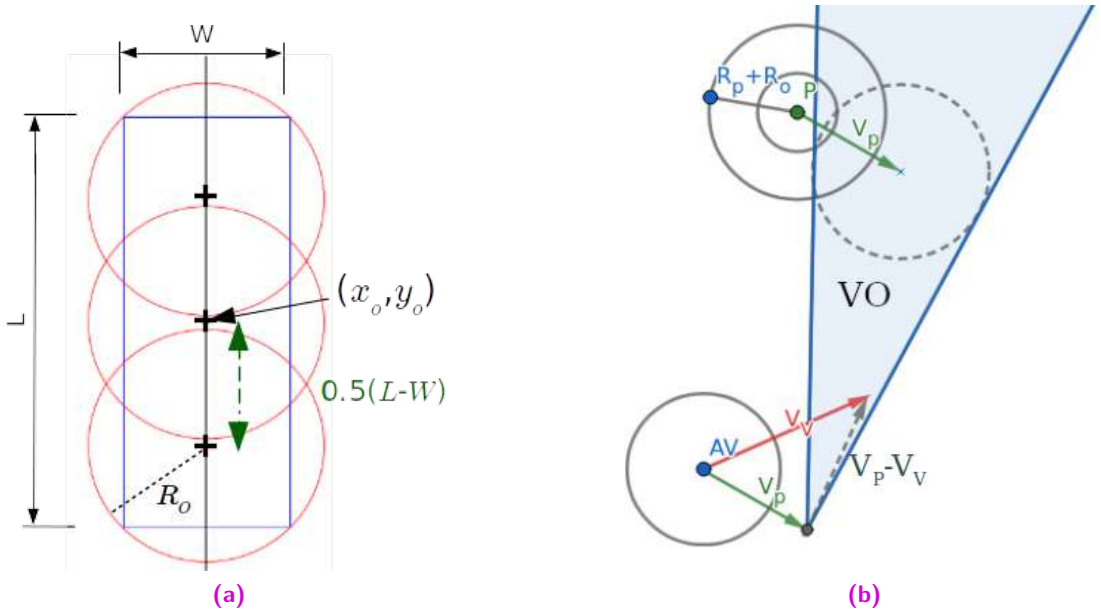

Fig. 6.2.: (a) Circular approximation of the AV footprint (Algorithm 2), (b) VO method applied to one part of the AV footprint

6.3.3 Pedestrian-Vehicle Time To Collision Based Danger Estimate

Time To Collision (TTC) is one of the most used road safety time-based indicators. TTC refers to the time remaining before a collision occurs between two bodies if they continue

Algorithm 2. AV Footprint Circular Approximation

Input: AV centers of mass: $X_V(t) = (x_o(t), y_o(t))$, and orientation $\theta_V(t)$, AV dimensions: Length L_V, Width W_V
Output: $C_{fp}(t) = \cup_{i \in \mathbf{N}_+}(c_i(t), R_i) \in \mathbf{R}^2 \times \mathbf{R}_+$

Set: $L_T \leftarrow L_V$, $i \leftarrow 0$
while $L_T > W_V$ **do**
  $c_i^l \leftarrow (\frac{L_V - W_V}{2}, 0)$ ▷ Frontal circle (AV frame)
  $c_{i+1}^l \leftarrow (-\frac{L_V - W_V}{2}, 0)$ ▷ Rear circle (AV frame)
  $i \leftarrow i + 2$
  $L_T \leftarrow L_V - W_V$
end while
$c_i \leftarrow (x_o(t), y_o(t))$ ▷ Middle circle (AV frame)
$C_{fp} \leftarrow \{(R_L^G(t)c_j^l(t), \frac{\sqrt{2}}{2}W_V) : \ 0 \leq j \leq i\}$ ▷ Transform to global frame

moving on the same direction and speed. TTC is usually used to estimate the rear-end collisions between vehicles on roads [Nas+13]. Improvements on the TTC calculations are proposed in the literature to cover more divers collision angles between two vehicles [JNG13]. Computing TTC for two bodies depends on the considered geometric shape of their footprints, and the simplest case is considering circular footprints [HLG14].
Assuming the following configuration at time t_k: a pedestrian j with a position (x_j, y_j) and velocity $\boldsymbol{V_j} = (V_j, \theta_j)$, and a vehicle with a position (x_V, y_V) and velocity $\boldsymbol{V_V} = (V_V, \theta_V)$. If the footprints for both the pedestrian and the vehicle are circular with radius R_{ped}, R_{veh} respectively. Then, the estimated time to collision TTC is found by solving the following equation:

$$\begin{aligned}[(x_V + TTC.V_V cos\theta_V) - (x_j + TTC.V_j cos\theta_j)^2 \\ + [(y_V + TTC.V_V sin\theta_V) - (y_j + TTC.V_j sin\theta_j)]^2 = (R_{ped} + R_{veh})^2\end{aligned} \tag{6.2}$$

If the root to this equation is not real, then a collision cannot occur and $TTC \to +\infty$. Otherwise, TTC is the minimum positive root of the equation.

Pedestrian-Vehicle TTC

Since the circular case is the simplest to calculate, [HLG14] suggests starting with this case to estimate if a collision is possible. Then, if TTC is found in the circular case, a more accurate footprint is considered to estimate TTC.

Algorithm 3. VO-Based Collision Analysis

Input:

- Time step: t_k, Collision time horizon: t_{CH}
- $\{X_V(t), V_V(t), X_P(t), V_P(t)\}$: $t \in [t_C - t_{CH}, t_C]$

Output: Collision Type: $IsReal \in \{0, 1\}$

for $(c_i(t), R_i) \in C_{fp}$ **do** ▷ AV footprint circles
  $t_s \leftarrow t_C - t_{CH}$
  $Center \leftarrow c_i(t_s) - X_P(t_s)$
  $D_C \leftarrow D(Center, R_i + R_{fp})$ ▷ Collision disk
  while $t_s \leq t_C$ **do**
    if $t_s * (V_P(t_s) - V_V(t_s)) \in D_C$ **then**
      return 1
    end if
    $t_s \leftarrow t_s + t_k$
  end while
end for
return 0

To compute the pedestrian-vehicle TTC a similar method to [HLG14] is applied. In a first step, circular footprints are considered to both the pedestrian and the vehicle. The radius of the vehicle's radius footprint is:

$$R_{veh} = \frac{1}{2}\sqrt{\left(\frac{L_V}{2}\right)^2 + \left(\frac{W_V}{2}\right)^2} \tag{6.3}$$

where L_V, W_V are the dimensions of the rectangular vehicle.

Then we estimate if a collision is geometrically possible based on the current positions and orientations of the pedestrian and the vehicle. If the interaction between the pedestrian and the vehcile is not frontal or back interaction (i.e. $\theta_V \neq \theta_j \pm \pi$) , then a collision is possible at a point (x_+, y_+): (Fig. 6.3):

$$\begin{aligned} x_+ &= \frac{(y_V - y_j) - (x_V tan\theta_V - x_j tan\theta_j)}{tan\theta_j - tan\theta_V} \\ y_+ &= \frac{(x_V - x_j) - (y_V cot\theta_V - y_j cot\theta_j)}{cos\theta_j - cos\theta_V} \end{aligned} \tag{6.4}$$

In the case of a frontal/back interaction, a collision is still possible if the lateral displacement between the pedestrian and the vehicle is less than the sum of footprint radius:

$$|y_j^v| \leq (R_{ped} + R_{veh})^2 \tag{6.5}$$

with y_j^v the y coordinate of pedestrian j in the vehicle's local coordinates frame.

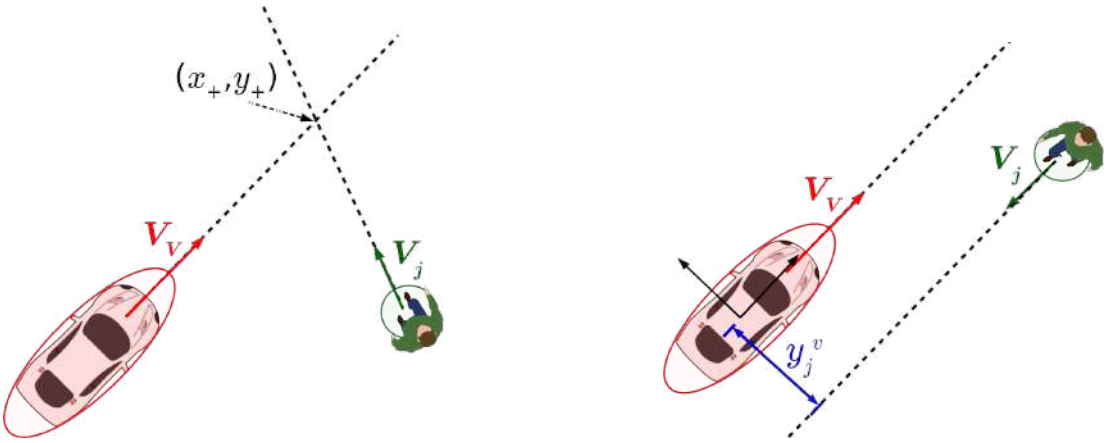

(a) Non frontal/back interaction **(b)** Frontal interaction

Fig. 6.3.: Pedestrian-vehicle possible collision point

If this first test yields a possible collision, we start by checking the possibility of collision with the circular case. If a collision is possible with the circular case as well, the approximate footprint of the vehicle with multiple circles is estimated as in Algorithm 2. The circular check is repeated for each circle in the approximate vehicle footprint set. If one or more of the footprint's circles yields a possible collision, then TTC is the minimum found time among the possible values.

Pedestrian-Vehicle TTC-based danger estimate

TTC is measured if the two agents (pedestrian and vehicle) could reach a possible future collision point with the exact time. [JNG13] suggests that a danger can be detected when the two agents reach the collision point with a close time difference and not necessarily the same time. Assuming TTC_{ped}, TTC_{veh} to be the time needed for the pedestrian and the vehicle to reach the collision point, respectively. Then the TTC-based danger can be estimated as:

$$\begin{aligned} TTC_{Danger} &= \frac{1}{|\alpha| + 1} \in [0, 1] \\ \alpha &= TTC_{ped} - TTC_{veh} \end{aligned} \tag{6.6}$$

If the previous TTC algorithm yields an exact possible TTC value, then $TTC_{ped} = TTC_{veh}$ and $TTC_{Danger} = 1$. If a collision is not immanent and an exact TTC is not

found, then TTC_{ped}, TTC_{veh} are found as the time needed to reach the collision point (x_+, y_+) with the same current speed for the pedestrian and the vehicle:

$$TTC_{ped} = \frac{\sqrt{(x_j - x_+)^2 + (y_j - y_+)^2} - R_{ped}}{V_j}$$
$$TTC_{veh} = \frac{\sqrt{(x_V - x_+)^2 + (y_V - y_+)^2} - R_{veh}}{V_V} \tag{6.7}$$

The algorithm for calculating the pedestrian-vehicle time to collision TTC and the TTC-based danger estimate is summarized in the flowchart in Fig. 6.4

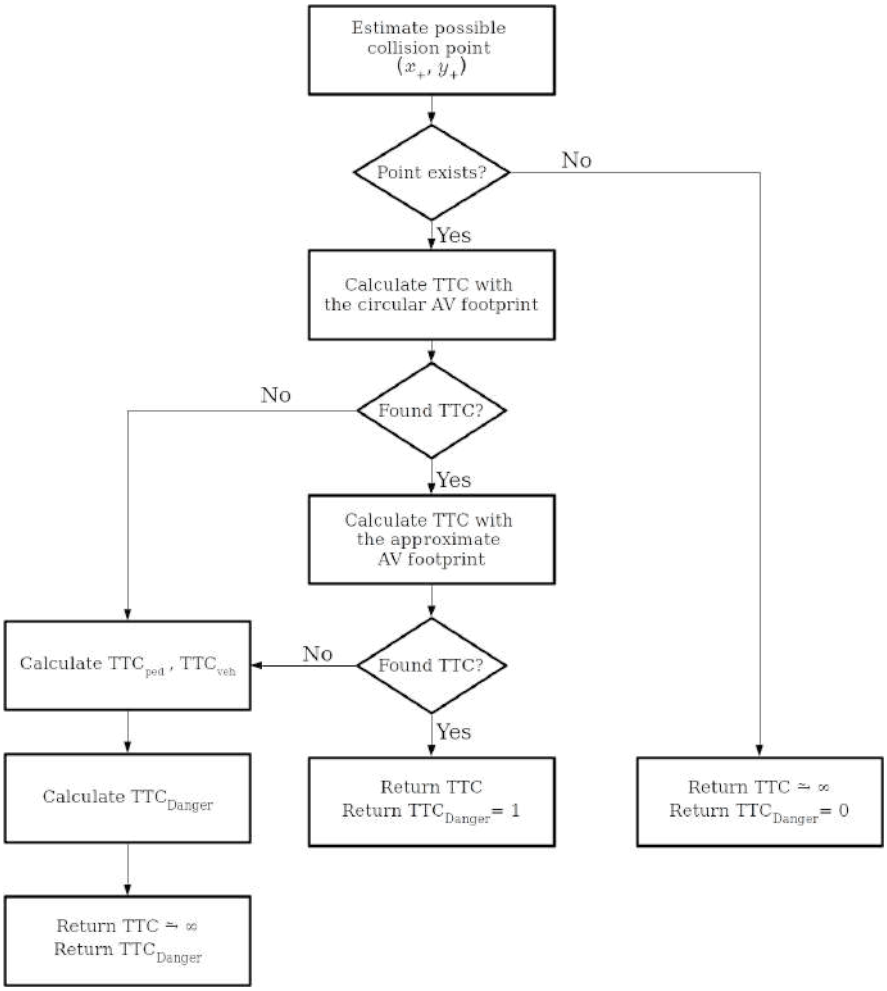

Fig. 6.4.: Pedestrian-vehicle TTC and TTC-based danger calculation

6.4 Trajectory Quality Metrics

A trajectory is a sequence of sample points of the 2D path, ordered by time stamps. Let T_V be the trajectory of the vehicle consisting of M sample points over a time period $[t_0, t_0 + T_F]$, then:

$$T_V = \{(\boldsymbol{X_i}, t_i) : \boldsymbol{X_i} = [x_i, y_i] \in \mathbb{R}^2,\ t_i \in [t_0, t_0 + T_F]\} :\ i \leq M \in \mathbb{N}_+ \tag{6.8}$$

Estimating the quality of a vehicle's trajectory involves three main aspects: the energy cost of the trajectory, its efficiency and the comfort of the vehicle's passengers during such a trajectory.

6.4.1 Trajectory Energy Cost

The energy cost of a trajectory is the cost of following the trajectory's maneuvers and speed variations. In other words, the energy cost is a measure of the trajectory's smoothness. This energy is estimated using two metrics: the **Path Energy** [BN90] which is based on the change of heading during the trajectory, and the **Dynamic Trajectory Energy** [Xu+12] which is a speed-based energy estimate.

The path energy measures the smoothness of the path by evaluating the average sharpness of the path maneuvers. While, the dynamic energy measures the average instantaneous variation of the speed from the average. The equivalent path energy E_P of a trajectory T_V are evaluated as:

$$E_P = \frac{1}{M} \sum_{j=1}^{M} \left(\frac{y_j - y_{j-1}}{x_j - x_{j-1}} \right)^2 \tag{6.9}$$

$E_P \in \mathbb{R}_+$ increases when a path contains more frequent and sharp maneuvers ($E_P = 0$ for a straight path). The main limitation in using the previous path energy measure is that it is not estimated in relative terms. Meaning, that a reference range of accepted values is required to estimate the quality of a trajectory using this measure. Therefore, we estimated the value of E_P for a number of reference paths. Tab. 6.1 shows the resulting values of E_P for straight lanes, lane change, roundabout and u-turn paths. Fig. 6.5 shows an illustration of some of the previous paths shapes. As a result of the tested paths energy values , we consider a trajectory with $E_P \leq 25$ to be of good quality and the quality of the trajectory increases for lesser path energy values.

Path	Path Equation	Parameters Value	E_P
Straight Lane	$y = ax + b$	$\forall a, b$	0
Lane Change (Quintic)	$y = \sum_{i=0}^{5} a_i x^i$	$e_L = 3.7$, $L_H = 1$	19
		$e_L = 3.7$, $L_H = 5$	0.5
		$e_L = 3.7$, $L_H = 10$	0.2
Roundabout (Circle)	$y^2 + x^2 = R^2$	$\forall R$	25
U-turn	$y = ax^2$	$a = 0.1$	4.5
		$a = 0.3$	43
	$y = ax^4$	$a = 0.001$	24

Tab. 6.1.: Path energy estimation for different types of vehicle paths

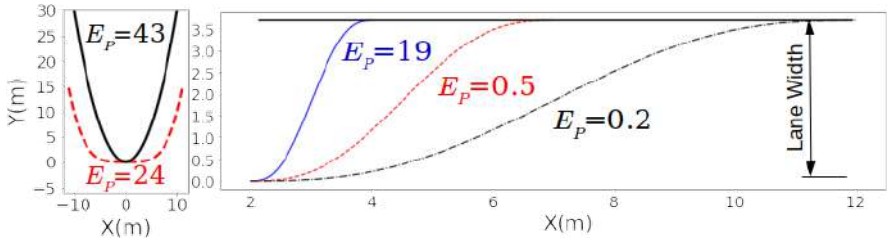

Fig. 6.5.: Examples of path energy for lane change and U-turn

The limit accepted value for E_P is selected based on the working scenario. For example, in the case of uni-directional road driving where the vehicle is not supposed to do any 180^o turns, the limit value can be selected around 0.5 to ensure a low-energy lane changes. Whereas, this limit is set higher in scenarios where the vehicle is supposed to go on roundabouts or make u-turns.

On the other hand, the dynamic trajectory energy $E_T \in \mathbb{R}_+$ is evaluated as:

$$E_T = \frac{1}{M} \sum_{j=0}^{M} \left(\frac{v_{perf} - v(j)}{v_{perf}} \right)^2 \tag{6.10}$$

$$v(j) = \sqrt{\dot{x}^2(j) + \dot{y}^2(j)} : \; v_{perf} = max_j v(j) \tag{6.11}$$

where E_T increases when the trajectory consists of large instantaneous velocity variations and $E_T = 0$ for a constant velocity trajectory. Smaller E_T values yield smoother trajectories.

6.4.2 Trajectory's Efficiency

The efficiency of the trajectory can be expressed in distance or time terms [Xu+12]. Firstly, the **Relative Traveled Distance** (C_L) measures the length of the traveled path relative to the shortest distance path between the start and goal points:

$$C_L = \frac{\sum_{i=0}^{M} D(X_{i+1} - Xi)}{D(X_M, X_0)} \tag{6.12}$$

$$D(X_2, X_1) = \sqrt{(x_2 - x_1)^2 + (y_2 - y_1)^2} \tag{6.13}$$

Secondly, the **Relative Time To Goal** (TT_G) measures the traveled time relative to the time to reach the goal on the average speed:

$$TT_G = \frac{(t_M - t_0) \times v_{avg}}{D(X_M, X_0)} \tag{6.14}$$

In more efficient trajectories, the length of the traveled distance is close to the shortest path distance corresponding to the optimal path between the goal and the start points in a dynamic obstacle free case $C_L \xrightarrow{1}$. Moreover, more efficient trajectories do not contain large time delays, i.e. $TT_G \leq 1$.

6.4.3 Passengers' Comfort

Assessing passengers' comfort along a trajectory is a problem specific to vehicles navigation. The trajectory itself entails information on the comfort of the vehicle's passengers, which is an important part of the trajectory quality validation. This problem drew the attention of researchers with the growing applications of autonomous navigation. Works in the domain started considering the passengers' comfort aspect when developing a trajectory planning method [WCM18; BMS19]. A recent case study shows that passengers comfort is mainly related to their experience of the centripetal force [GC21]. Meaning that passengers experienced more discomfort when passing small radius curves with high speed. Therefore, the average **Centripetal Acceleration** (a_C) is used as a passengers' comfort measure:

$$a_C = \frac{1}{M} \sum_{i=0}^{M} v^2(i)\kappa(i) \tag{6.15}$$

where $\kappa(i)$ is the curvature of the path at point i. The results of the study in [GC21] recommends different a_C values depending on the driving speed range. For the case of

shared space (speed $\leq 20km/h$), $a_C \leq 1$ is recommended for a very comfortable driving and at least $a_C \leq 1.75$ for an acceptable comfort level.

6.5 Pedestrians Comfort Metrics

Providing a comfortable experience for pedestrians in shared spaces is an important milestone to successfully integrate AV in daily life. Conducting a survey experiment is one way of estimating pedestrian comfort. However, it is essential to provide measures capable of approximately estimating pedestrian comfort in simulations as well. The first metric used to evaluate the pedestrian comfort during the interaction with the AV is the **Uncomfortableness Index** $\bar{I}_{ucf}$ suggested in [Hel+01]. This index is an average value which reflects the degree and frequency of the linear velocity change a pedestrian experienced during the navigation. Let N be the total number of pedestrians in a simulation with a duration $[t_0, t_0 + T_F]$, then the uncomfortableness index is evaluated as:

$$\bar{I}_{ucf} = \frac{1}{N} \sum_{i=1}^{N} \frac{\bar{y}_i}{\bar{h}_i} \tag{6.16}$$

$$\bar{h}_i = \tfrac{1}{T_F} \textstyle\sum_{t=t_0}^{t_0+T_F} v_i^2(t) \quad \bar{y}_i = \tfrac{1}{T_F} \textstyle\sum_{t=t_0}^{t_0+T_F} (v_i(t) - \bar{g}_i)^2$$
$$\bar{g}_i = \tfrac{1}{T_F} \textstyle\sum_{t=t_0}^{t_0+T_H} v_i(t) \tag{6.17}$$

where $\bar{h}_i$, $\bar{y}_i$ are the mean square velocity and the deviation of the average velocity of agent i respectively, and $\bar{g}_i$ the average velocity of agent i over the simulation period.

Moreover, pedestrians are known to accelerate/decelerate heavily when detecting danger [Tek16]. However, it is more relevant to the pedestrian-vehicle interaction to consider the behavior at the min approach distance (MAD) to the vehicle. Therefore, the pedestrian min. approach acceleration during the navigation is used as a metric of pedestrian comfort. Moreover, the vehicle's behavior at the MAD contains information on the resulting pedestrian comfort.

Assuming d^i_{min}, t^i_{MAD} is the vehicle's min approach distance and time to pedestrian i during the interaction, respectively. Then the **Vehicle's Average Min. Approach Acceleration**:

$$a^V_{MAD} = \frac{1}{N} \sum_{i=1}^{N} a_v(t^i_{MAD}) \tag{6.18}$$

Similarly, the **Pedestrian Min. Approach Acceleration**:

$$a^P_{MAD} = \frac{1}{N}\sum_{i=1}^{N} a_i(t^i_{MAD}) \tag{6.19}$$

where a_v, a_i are the AV and the pedestrian i linear acceleration, respectively.

To evaluate the success/fail criteria for the previous comfort metrics a reference data is required. The goal is to analyse the pedestrian behavior and the values of these metrics in comfortable interactions with a vehicle. These values can then be used as our success criteria. To do so we use the pedestrian-vehicle interaction data that we presented earlier in 3.5. This dataset includes a number of interactions between a vehicle and a group of pedestrians in different scenarios (frontal, lateral, etc). The recorded interactions was split into two parts: one with an aggressive behavior on the driver's side where pedestrians experienced some levels of discomfort, and one part with a more yielding driving patterns. Since we wish to maintain the pedestrian comfort during the navigation, we use the values of the previous metrics calculated for the yield mode as reference values as shown in Table 6.2.

Parameter	Scenario	Behaviour	Mean	Max	Std. Dev.
$\bar{I}_{ucf}$	All	Aggressive	3.7	8.6	2.2
		Yield	1.2	5.6	2.0
a^V_{MAD}	All	Aggressive	0.18	1.19	0.20
		Yield	0.14	0.44	1.30
a^P_{MAD}	Lateral	Aggressive	0.08	1.00	0.14
		Yield	0.06	0.36	0.11
	Frontal/Back	Aggressive	0.12	1.33	0.22
		Yield	0.11	2.26	0.31
	Shared Space	Aggressive	0.08	0.40	0.10
		Yield	0.08	0.33	0.09

Tab. 6.2.: Collected PVI data statistics relative to pedestrian comfort

6.6 Conclusion

Performance validation of autonomous navigation systems in shared spaces requires an adapted set of performance metrics, specially in the case of AV navigation. The selected set of performance metrics is trajectory-based and is designed to validate: the motion safety, the trajectory quality and both the pedestrians and the passengers comfort.

Let N be the total number of simulated tests, Assuming a simulation s contains $N_{RC}(s)$ realistic collisions, $A(s)$ pedestrians, and T_V the trajectory of the vehicle:

$$T_V = \{(\boldsymbol{X_i}, t_i) : \boldsymbol{X_i} = [x_i, y_i] \in \mathbb{R}^2,\ t_i \in [t_0, t_0 + T_F]\} :\ i \leq M \in \mathbb{N}_+ \tag{6.20}$$

then the performance metrics computed for a simulation s can be summarized in Tables 6.3, 6.4 and 6.5. Where the success criteria for N simulations can be compared with the statistical distribution of each metric.

Trajectory Energy		
Metric	Definition	Success Criteria
Path Energy	$E_P = \frac{1}{M}\sum_{j=1}^{M}\left(\frac{y_j - y_{j-1}}{x_j - x_{j-1}}\right)^2$	One-Way Road $E_P \leq 0.5$ Round-about/ U-turn $E_P \leq 25$
Dynamic Energy	$E_T = \frac{1}{M}\sum_{j=0}^{M}\left(\frac{v_{perf} - v(j)}{v_{perf}}\right)^2$ $v(j) = \sqrt{\dot{x}^2(j) + \dot{y}^2(j)}$: $v_{perf} = \max_j v(j)$	$E_T \leq 1$
Trajectory Efficiency		
Relative Traveled Distance	$C_L = \frac{\sum_{i=0}^{M} D(X_{i+1} - Xi)}{D(X_M, X_0)}$ $D(X_2, X_1) = \sqrt{(x_2 - x_1)^2 + (y_2 - y_1)^2}$	$C_L \to 1$
Relative Time To Goal	$TT_G = \frac{(t_M - t_1) \times v_{avg}}{D(X_M, X_1)}$	$TT_G \leq 1$
Passengers' Comfort		
Centripetal Acceleration	$a_C = \frac{1}{M}\sum_{i=0}^{M} v^2(i)\kappa(i)$	$a_C \leq 1.75$

Tab. 6.3.: Performance metrics for validating the trajectory quality around pedestrians

Motion Safety		
Metric	Definition	Success Criteria
Realistic Collisions Rate	$N_{RC}\% = \frac{1}{N}\sum_{s=1}^{N} N_{RC}(s) \times 100\%$	$N_{RC}\% \rightarrow 0$

Tab. 6.4.: Performance metrics for validating the motion safety around pedestrians

Pedestrians' Comfort			
Metric		Definition	Success
Uncomfortableness Index		$\bar{I}_{ucf} = \frac{1}{A(s)}\sum_{i=1}^{A(s)} \frac{\bar{y}_i}{\bar{h}_i}$ $\bar{h}_i = \frac{1}{T_F}\sum_{t=t_0}^{t_0+T_F} v_i^2(t)$ $\bar{y}_i = \frac{1}{T_F}\sum_{t=t_0}^{t_0+T_F} (v_i(t) - \bar{g}_i)^2$ $\bar{g}_i = \frac{1}{T_F}\sum_{t=t_0}^{t_0+T_H} v_i(t)$	$\bar{I}_{ucf} \leq 5.6$
Average Min. Approach Acceleration	Vehicle	$a_{MAD}^{V} = \frac{1}{A(s)}\sum_{i=1}^{A(s)} a_v(t_{MAD}^i)$	$a_{MAD}^{V} \leq 0.44 m/s^2$
	Pedestrian	$a_{MAD}^{P} = \frac{1}{A(s)}\sum_{i=1}^{A(s)} a_i(t_{MAD}^i)$	Lateral: $a_{MAD}^{P} \leq 0.36 m/s^2$ Frontal: $a_{MAD}^{P} \leq 2.26 m/s^2$

Tab. 6.5.: Performance metrics for validating the motion safety around pedestrians

7 Implementation and Performance Evaluation

This chapter includes the implementation of the proactive navigation framework in its three parts: the pedestrian cooperative behavior prediction system (in Ch. 3), the proactive longitudinal velocity and steering control system (in Ch. 4), and the manoeuvring system using the proactive dynamic channel method presented in Ch. 5. The proactive navigation system is implemented under ROS and tested with SPACiSS [Pré21] simulator. A diverse group of simulations is run and the performance is evaluated using the statistical performance metrics presented in Ch. 6. Furthermore, the Risk-RRT planning method is implemented and the performance of the system with the two methods is compared.

7.1 Testing Environments

Once the proactive navigation system is designed, it is crucial to run a sufficient number of tests using a virtual environment which simulates pedestrians in a shared space as accurately as possible. This is due to the difficulty of designing and deploying real-life experiments which include pedestrian-vehicle interaction. These experiments are not only difficult to establish but also dangerous due to the high risk of operating a heavy and potentially harmful robot such as an AV around humans. Therefore, it is necessary to have realistic simulators for shared spaces to test such a system in complete safety and repeatedly. The reliability of the simulator is a key point in the development process, as the simulated tests will serve as the bases to moving towards real-life experimentation.

Several simulators have been created in the recent past years for the purpose of developing and testing autonomous vehicles systems. However, there are no global simulators and the choice of the simulator depends on the goal and the targeted scenarios. The goal being the tested sub-system, as the navigation system, the lower-level vehicle control, the visual perception, etc. The targeted testing environment/scenarios also affect the choice of the simulator. One simulator might be good for driving testing on highways, while another can be targeting urban areas.

To test the proactive navigation system in a shared space, the simulator should be able to capture both the vehicle model and the pedestrians behaviors, as well as, the interaction dynamics between the two. Moreover, the simulator should reflect the existing diversity in pedestrians behaviors and include the ability to build realistic scenes with various interaction scenarios and testing parameters.

CARLA [Dos+17], PORCA [Luo+18] and SUMMIT [Cai+20] are few of the well-know open-source simulators for urban environments. CARLA targets urban areas and it is suitable for the training and validation of autonomous driving systems. PORCA is build on a pedestrian extension of the Optimal Reciprocal Collision Avoidance (ORCA) method, and it allows to simulate high density crowds in shared spaces. SUMMIT supports a wide range of applications, including perception, vehicle control and planning, and end-to-end learning. However, it is based on the same motion model for all road users and does not provide a specialized pedestrian model.

The simulator used to test the navigation method in this work is SPACiSS [Pré21] simulator which is based on PEDSIM library [Glo12] with the addition of the PVI, therefore it is suitable for simulating pedestrian crowds in shared spaces.

7.2 Reference Comparison Method: Risk-RRT

Risk-RRT is a risk guided search algorithm which integrates a collision risk assessment with the classic Rapidly-exploring Random Trees (RRT) non-convex space search [Ful+10]. RRT is an incremental space search method developed in the late 90s [LaV98]. This method has been widly used in robotic motion planning as it easily handles nonholonomic and kinodynamic constraints. Many variants and improvements of this method have been introduced over the years [NKH16]. Risk-RRT was one of these improvements which was introduced to handle dynamic environments and implemented to produced more human-friendly motion [Chi+16; CWM18].

In Risk-RRT, the configuration-time space is given a probabilistic representation. The moving obstacles are modeled using Gaussian Processes and a probabilistic prediction of their future trajectories is performed. The uncertainty in the static environment is represented with an occupancy grid. Afterwards, a probabilistic risk of collision is estimated for each path based on the probability of occupations of the surface swept by the robot motion along the path. Then a search similar to RRT is performed, where the weights of the nodes are adapted to account for the risk of collision. Finally, the decisions in Risk-RRT are updated in real-time.

This method is implemented under ROS for comparison purposes. The method is selected as the proposed risk improved probabilistic framework is designed for dynamic environment. In the following, we analyse the performance results for our proactive framework in comparison with the Risk-RRT method.

7.3 System Implementation

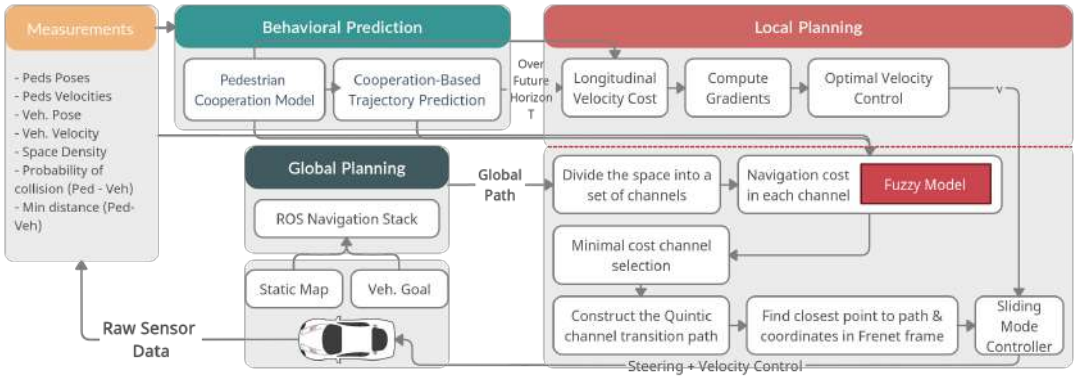

Fig. 7.1.: The proactive navigation framework structure

The proactive navigation system is implemented under ROS in combination with a global path planner. Fig. 7.1 shows the structure of the implemented system regardless of the used simulation tool. First, the space state measurements and semantics are extracted from the raw sensor data. This includes the pedestrian tracking information (pedestrians positions, velocities, orientations) and the vehicle's pose and velocity, as well. This part is assumed to be treated by an external system or provided directly by the respective simulation tool. Furthermore, other enquired space measurements are computed using the space state information. These measurements include the inputs required by the proactive systems such as the space density, the distances between the pedestrians and the vehicle, the probabilities of collisions, etc. The second step is the behavioral prediction of the tracked pedestrians. The pedestrian cooperation model presented in Ch. 3 is run to compute the cooperation factor of each pedestrian. The estimated cooperation for each pedestrian is used to predict the future trajectory using the cooperation-based trajectory planning model in Ch. 3. The predicted pedestrian behavior is then used for the local planning system for both the longitudinal and lateral control. Using the cascading architecture, first the proactive longitudinal control is computed using the controller presented in Ch. 4. Then, using this control along with the estimated cooperative pedestrians behavior in the space, the global path of the vehicle is locally modified. This global path is provided by an external path planner,

which is the ROS Navigation Stack in the case of the SPACiSS simulator, for example. The local modification of the global path and the lateral control of the vehicle is done using the proactive dynamic channel system presented in Ch. 5. Finally, the resulting speed and steering controls are provided to the vehicle model in the simulator and the corresponding effect on the space dynamic is re-measured.

7.4 Evaluating the Performance with SPACiSS

SPACiSS is a kinematic simulator which does not consider the vehicle's dynamics. The vehicle used in the simulator has the dimensions and visual representation of the Renault ZOE vehicle with an underlying bicycle model. The particle interest of using this simulator came from the possibility of testing the navigation around a crowd of pedestrians which can perceive and react to the vehicle. Fig. 7.2 shows the overall structure of the system under ROS.

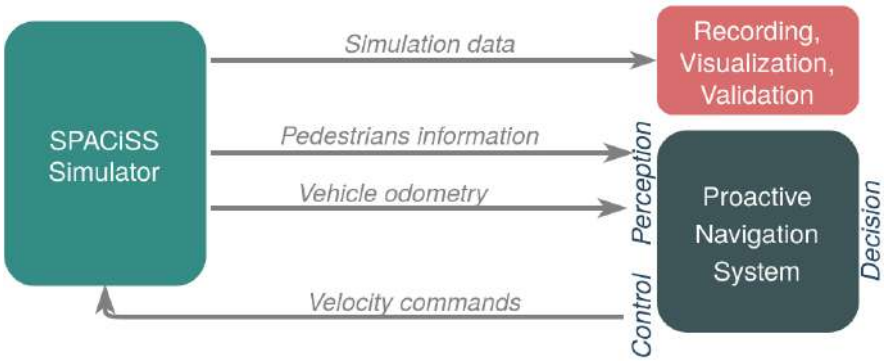

Fig. 7.2.: System structure with SPACiSS simulator under ROS

7.4.1 Tests Design

To test and validate the proactive navigation around pedestrians, we selected one test environment $E = \{e_1\}$ $(K = 1)$ which represents a shared space with no specific assign pedestrian or vehicle areas. This means that the space does not contain any road, sidewalks, pedestrian crossings, traffic signals, .. etc. The space is bounded by two side barriers which can represent a parking lot or a shared business area like the Exhibition Road in London for example. The dimensions of the environment and the possible entry/exit points are shown on Fig. 7.3 for a frontal and a lateral crossing scenarios.

The navigation is tested in environment e_1 in 7 different different interaction scenarios: Frontal Crossing, Back Crossing, Frontal-Back Crossing, Lateral Crossing, Bi-Lateral

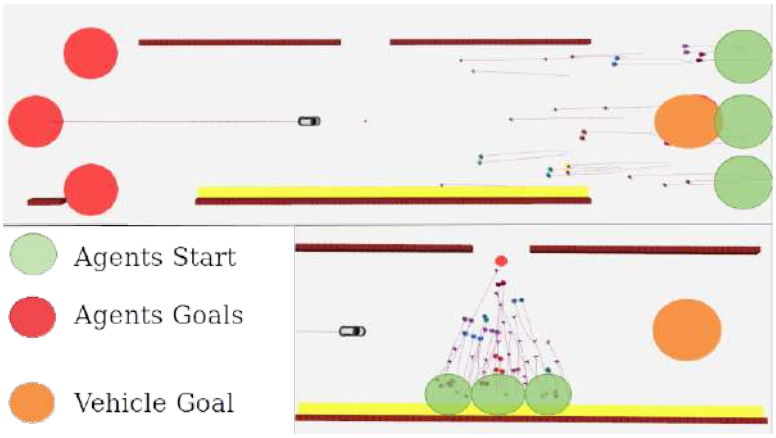

Fig. 7.3.: Simulation space structure on SPACiSS

Crossing, 45^o Uni-Directional Crossing, 45^o Bi-Directional Crossing. The AV's goal in all scenarios is to cross the shared space, while the possible pedestrian start/goal points vary based on the scenario. The start and goal points of all agents (pedestrians and AV) are shown on Fig. 7.4 for each scenario.

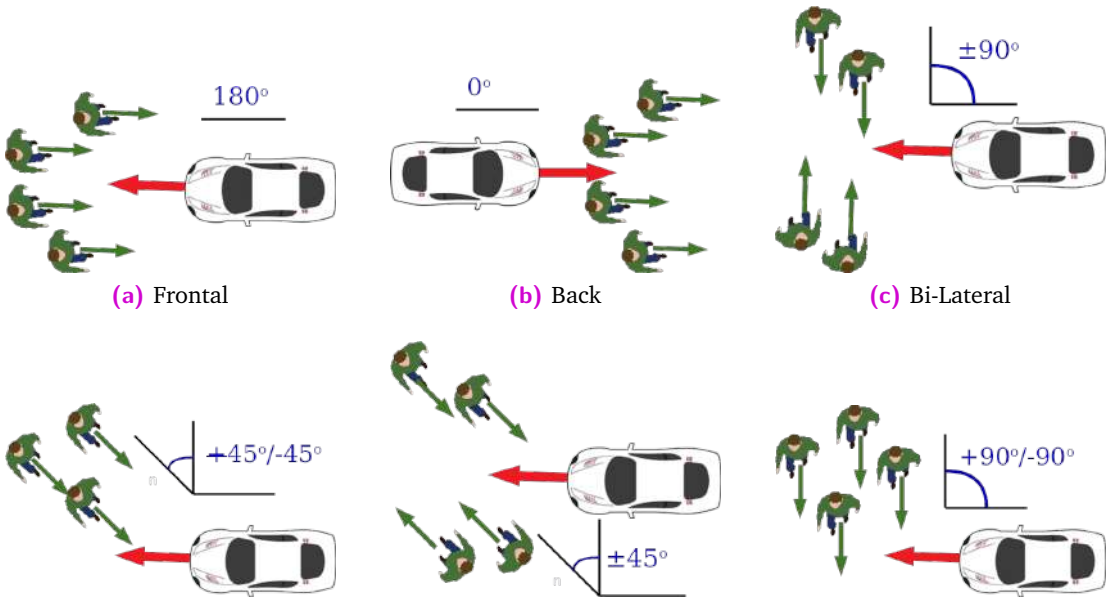

(a) Frontal **(b)** Back **(c)** Bi-Lateral

(d) 45^o (Uni-directional) **(e)** 45^o (Bi-directional) **(f)** Lateral

Fig. 7.4.: PVI scenarios definition based on the interaction angle

The variable test parameters set includes the space density, the space sparsity (or the distribution of the pedestrians in the space) and the existence of pedestrian groups in the space. The density of the space is measured as the average percentage of the occupied space by pedestrians during the simulation. Whereas, the space sparsity is estimated with a Gini Index which measures the distribution of pedestrians among the interaction

space partitions [GMD16]. Let $[t_0, t_0 + T_F]$ be the simulation period, A the area of the shared space (m^2), and $N(t)$ be the total number of pedestrians in the space at time t. Then, the average pedestrian density and sparsity are measured as follows:

$$D = \frac{1}{T_F} \sum_{t=t_0}^{t_0+T_F} \frac{N(t)}{A} \quad (\text{pedestrian}/m^2) \tag{7.1}$$

$$GI = \frac{1}{T_F} \sum_{t=t_0}^{t_0+T_F} \sum_{j=1}^{N(t)} \frac{|1 - N_j(t)|}{N(t) + 1} \times 100\% \tag{7.2}$$

where the interaction space is first divided into a grid of $N(t)$ equal cells. Then, N_j is the number of pedestrians in a cell j of the grid. For example, if the distribution of the pedestrians in the space is homogeneous, then there is one pedestrian in each of the equal grid cells, yielding $GI = 0\%$. Two examples of a pedestrian distribution with the corresponding GI vales are shown in Fig. 7.5. We can notice here that larger GI values means that more pedestrian free navigation options exist in the space. Whereas, smaller GI values means that the pedestrians occupy the space in a more homogeneous way which can yield the navigation more challenging with higher densities.

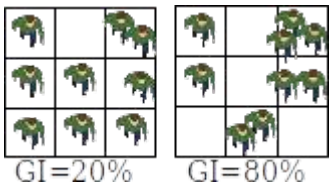

Fig. 7.5.: Two examples of the GI calculation to estimate the sparsity

Other test parameters which are required to define the scenario but have been set to a constant value, along with the values of the variable test parameters are the following:

- Constants: AV max speed $5.5m/s$, Pedestrian max speed $6.5m/s$,
- Variables: pedestrian density $D \in [0.003, 0.56]$ ped/m^2, pedestrian distribution (Sparsity) $GI \in [6, 34]\%$.

Every simulation is run with 20 repetitions, with 8 different values for the pair (D, GI) to have finally a total of 2280 test simulation.

Fig. 7.6 and Fig. 7.7 show six examples of the resulting trajectories in the XY-Plane for the pedestrians and the AV in different testing scenarios. In the following, we analyse the test simulations based on the statistical results relative to the motion safety, the quality of the produced vehicle trajectory and the pedestrians comfort around the AV.

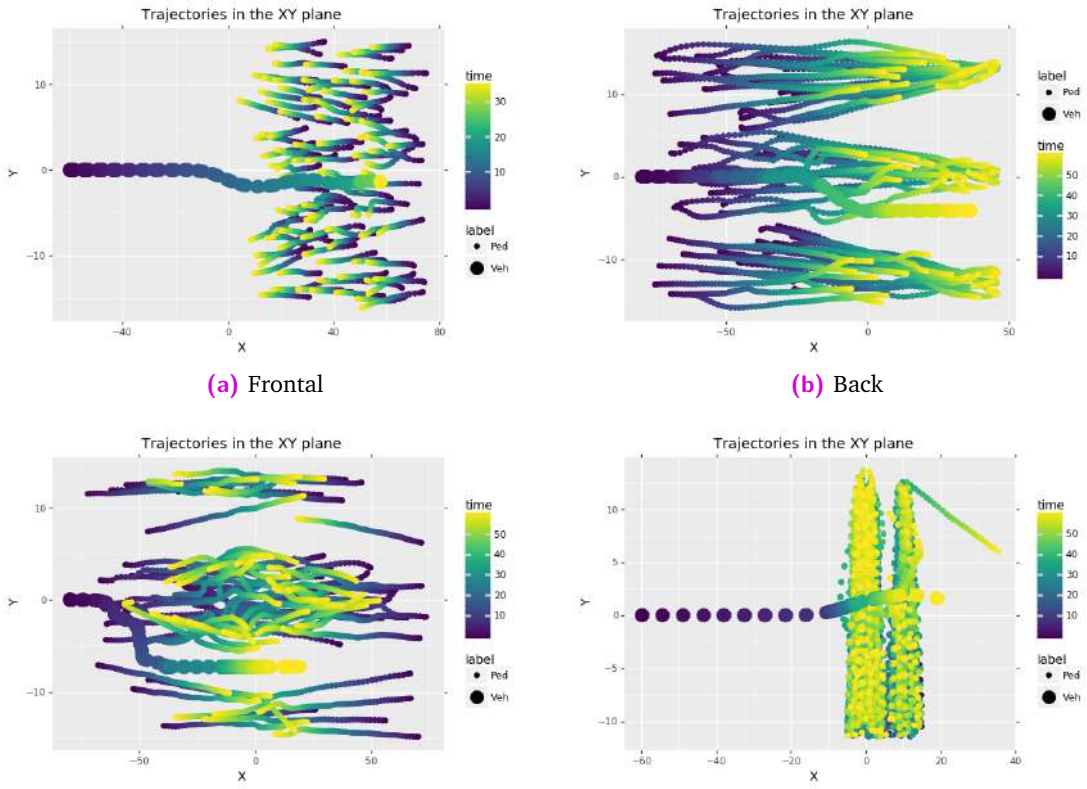

(a) Frontal (b) Back

(c) Frontal-Back (d) Lateral

Fig. 7.6.: The PVI trajectories visualization in XY-Plane in frontal, lateral and back crossing scenarios

7.4.2 Motion Safety - Collisions Analysis

A collision is detected in a simulation when an overlap occurs between the footprint of the vehicle and that of a pedestrian, as shown in Sec. 6.3.1. The corresponding collisions in each of the test simulations are counted and a VO-based collision analysis (Sec. 6.3.2) is performed on each detected collision. This analysis was developed after observing some faulty behaviors in the simulator. The goal is to get a realistic estimate of the safety of the navigation without over penalizing the system due to collisions with an external cause. To make this point more clear, an example of what is detected as an unrealistic collision is shown in Fig. 7.8. The figure shows four snapshots of the simulation at four consecutive time instants around the moment when a collision is detected with the highlighted pedestrian. This collision is qualified as unrealistic, as the pedestrian ran to collision with the vehicle from the side and the vehicle did not take any velocity command to collide with this pedestrian. By counting the collisions occurring in each test simulation and performing the VO-based collision analysis, we can get the both **Realistic Collision Rate** and the **Unrealistic Collision Rate**. Overall,

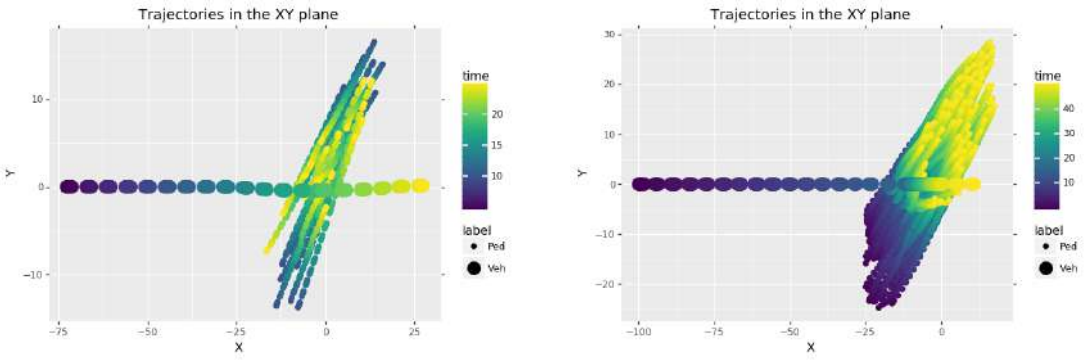

(a) 45^o Bi-directional **(b)** 45^o uni-directional

Fig. 7.7.: The PVI trajectories visualization in XY-Plane in the 45^o crossing scenarios

we get a collision rate of 3.085 collisions per simulation, of which 2.877 collisions are qualified as unrealistic and 0.208 collisions are realistic collisions. To investigate the interactions where more collisions are occurring, the two rates are computed for each interaction type, as shown in Fig. 7.9. We can see from the detailed collision rates, that we got a very low realistic collision rates for the frontal and lateral crossing scenarios, which are the scenarios used to obtain the used behavioral model. This rate increases when incorporating a bi-directional movement for the pedestrians in the lateral scenario. The rate also increases when back crossing a pedestrian crowd. This is a particular case that requires an incorporation of the perception range of a pedestrian which is present in the simulator but not treated in our navigation system. When moving from the two basic crossing scenarios to a crossing with a different interaction angle such as the 45^o crossing, we notice an increase in the realistic collision rate. Specially for the more complicated case when a bi-directional movement in combined with the new interaction angle (45^o Bi). Therefore, it is important to consider a wider range of interaction angles when training or calibrating an interaction model. This in terms require a more rich and diverse sets of PVI data to be recorded either in controlled laboratory experiments or in real-life interactions.

7.4.3 Trajectory Quality

The resulting vehicle trajectory in each simulation is qualified by analysing the corresponding energy cost, the efficiency in terms of the traveled distance and the traveled time, and the passengers comfort using the centripetal acceleration as explained in Sec. 6.4. Tab. 7.1 shows the corresponding performance metrics values to the set of testing simulations across all scenarios, density and sparsity levels. The statistical results

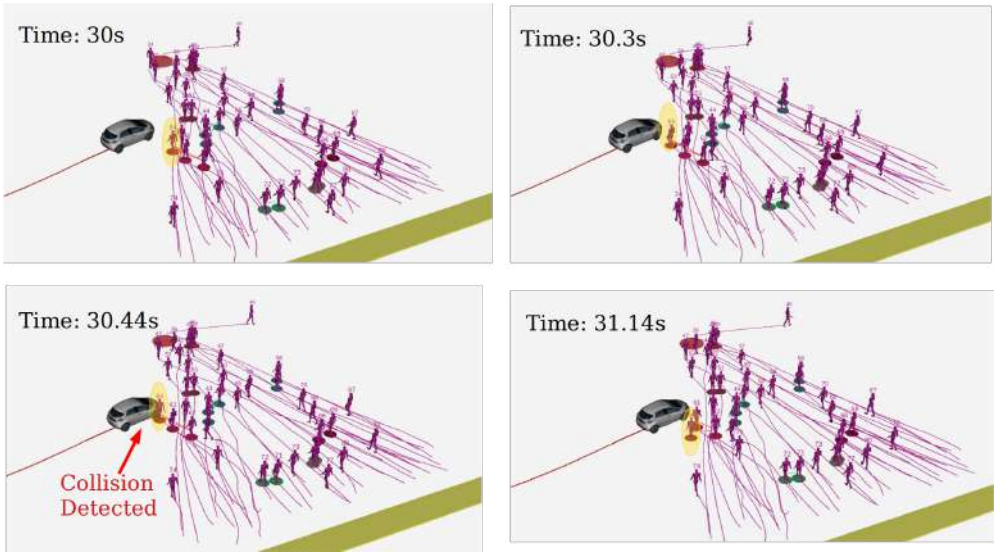

Fig. 7.8.: Four snapshots from a simulation on SPACiSS where an unrealistic collision is detected with the highlighted pedestrian

for each metric are shown with: the average and max values across all simulations (Mean/Max), the max value for 75% of the simulations, and the standard deviation of the values (Std. Dev.). Moreover, the success criteria found in Ch. 6 are shown for each metric.

Trajectory Energy Cost						
Metric		Mean	Max	75%	Std. Dev.	Success Criterion
Path Energy	E_P	**0.14**	1.10	**0.16**	0.06	≤ 0.5
Trajectory Energy	E_T	0.13	**0.23**	0.17	0.05	≤ 1
Trajectory Efficiency						
Metric		Mean	Max	75%	Std. Dev.	Success Criterion
Relative Traveled Distance	C_L	**1.12**	1.36	**1.13**	0.02	$\rightarrow 1$
Relative Time To Goal	TT_G	**0.55**	2.14	**0.78**	0.35	≤ 1
Passengers' Comfort						
Metric		Mean	Max	75%	Std. Dev.	Success Criterion
Centripetal Acceleration	a_C	**0.17**	**1.29**	**0.24**	0.17	≤ 1.75

Tab. 7.1.: Trajectory quality metrics statistical results

Firstly, the navigation system resulted in low energy cost both in terms of the manoeuvring (path energy) and the linear velocity (trajectory energy). The values of the

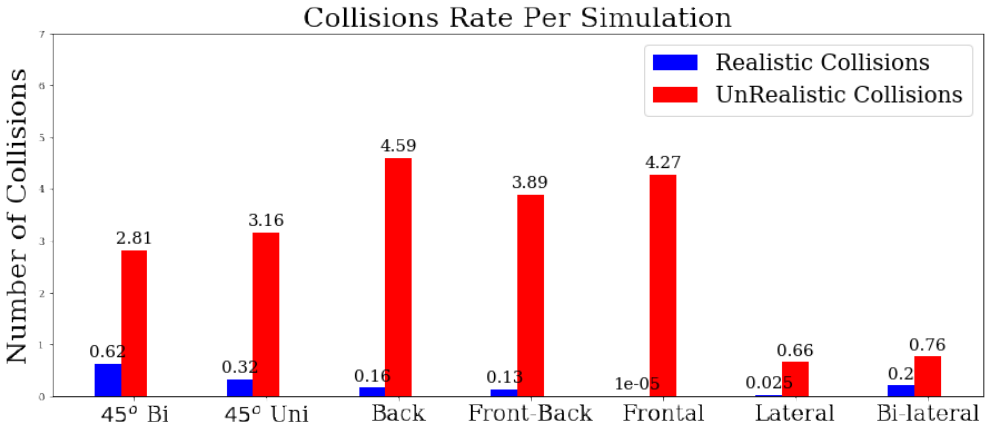

Fig. 7.9.: Detected collision rate in each scenario type in the test simulations on SPACiSS

trajectory energy E_T are all within the desired low limit to maintain a smooth linear velocity variations. Although the maximum value of the path energy E_P is a little higher than the desired limit, most of its values fall in a very low acceptable energy range. Secondly, the resulting trajectories are efficient in terms of the traveled distance. We can notice that C_L takes values close to 1, which means that the vehicle did not deviate very far from its optimal path. Whereas for the efficiency in terms of the traveled time, we can see that the larger part of the test simulations did not have large time delays and only a small portion had larger time delays with TT_G reaching over double the max desired value. Finally, the values of the centripetal acceleration of the vehicle along its traveled trajectory was overall within the desired range to maintain a comfortable ride for any potential passengers.

7.4.4 Pedestrian Comfort

The trajectory information for both the pedestrians and the vehicle in a test simulation is used to estimate the pedestrian comfort during the interaction with the vehicle. As explained in Sec. 6.5, this can be analysed using the average uncomfortableness index ($\bar{I}_{ucf}$) and both the pedestrian and the vehicle average acceleration at the minimum approach distance (a^V_{MAD} and a^P_{MAD}). In a similar manner to the previously presented trajectory metrics results, Tab. 7.2 shows the statistical results corresponding to the pedestrian comfort metrics.

The average uncomfortableness index across the test simulations had an average of 2.69 with maximum values reaching 8.6 which exceeds the desired limit of 5.6. However, the majority of the samples (75%) had values well within the desired range with a maximum of 3.89. To further examine the cases leading to higher level of discomfort for

Pedestrian Comfort							
Metric		Scenario	Mean	Max	75%	Std. Dev.	Success Criterion
Uncomfortableness Index	$\bar{I}_{ucf}$	All	**2.69**	8.60	**3.89**	1.80	$\leq$ 5.60
Vehicle MAD Acceleration	a^V_{MAD}	All	**0.02**	0.76	**0.12**	0.07	$\leq$ 0.44
Ped. MAD Acceleration	a^P_{MAD}	Frontal	0.36	**0.57**	0.39	0.05	$\leq$ 2.26
		Lateral	0.39	**0.48**	0.42	0.05	$\leq$ 0.36

Tab. 7.2.: Pedestrian comfort metrics statistical results

the pedestrian, we can analyse the distribution of the values along the different scenarios and the different pedestrian densities. Fig. 7.10 shows the histogram of the average uncomfortableness index for the different testing scenarios. We can see from the figure that the higher levels of discomfort are mostly resulting in lateral and bi-lateral crossing scenarios. Furthermore, Fig. 7.11 shows the uncomfortableness index values against the pedestrian density of each testing scenario. We can clearly notice here a correlation between the two where the uncomfortableness index increases in general for higher levels of pedestrian density. In our tests, the lateral and bi-lateral cases presented the most dense interaction, therefore leading to higher levels of discomfort. The defined desired limit of the uncomfortableness index is completely maintained for interactions with pedestrian densities reaching $0.2ped/m^2$. The index also remains close to the desired range for densities up to $0.3ped/m^2$. Beyond this density limit, the navigation policy is bound to produce higher levels of undesired pedestrian discomfort.

Furthermore, the behavior of both the vehicle and the pedestrians at the minimum approach distance is an indicator to the resulting pedestrian comfort. The vehicle acceleration at the MAD a^V_{MAD} was well within the desired acceleration limit for most cases. The maximum value for 75% of the simulations is $0.12m/s^2$ which is much lower than the acceptable max limit defined for a comfortable navigation ($0.44m/s^2$). Whereas, the maximum value for the values can reach $0.76m/s^2$ for some simulations. It is worth noting that (unlike the uncomfortableness index) these values that exceeded the defined limit did not result due to higher pedestrian density. On the contrary, the highest a^V_{MAD} values exceeding the defined limit resulted for densities lower than $0.1ped/m^s$. Whereas, the system maintained low levels of MAD acceleration with the highest densities, as shown in Fig. 7.12. Moreover, the previous correlation between

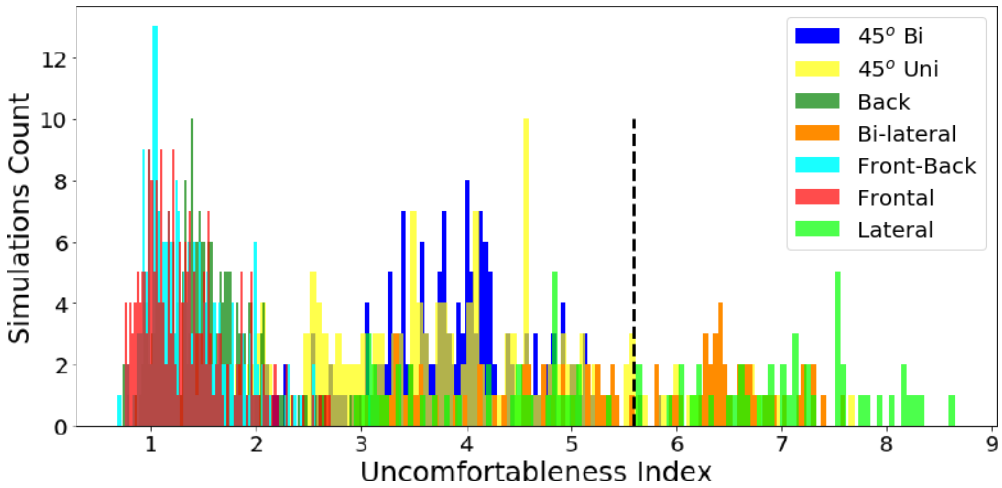

Fig. 7.10.: Histogram of the average uncomfortableness index ($\bar{I}_{ucf}$) across the tests

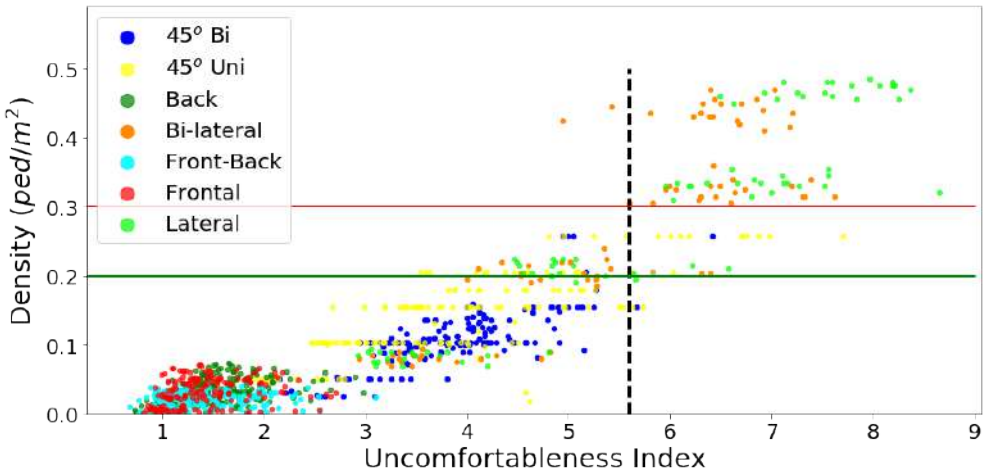

Fig. 7.11.: The pedestrian density Vs. average uncomfortableness index ($\bar{I}_{ucf}$) across the test simulations

the metric and the pedestrian density is not noticed here. The higher values of vehicle acceleration at the minimum approach distance in lower densities means that the navigation system is deciding to take more aggressive actions when working with lower pedestrian densities.

Finally, the pedestrian acceleration at the minimum approach distance a^P_{MAD} was very close to the desired range for the lateral crossing scenarios. Whereas for the frontal crossing cases, it is observed that the values of the observed acceleration for the pedestrians is much lower than the observed limit recorded in real interactions. This can be due to the difference in the behavioral model between the observed behaviors and the model considered in the simulator. In our observations, pedestrians had higher acceleration levels at very close distances of the vehicle in the frontal case during yielding

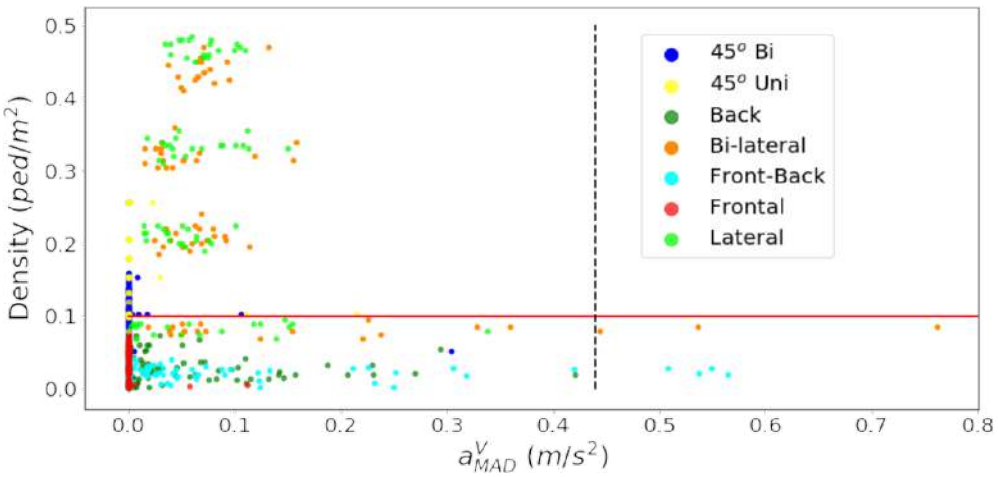

Fig. 7.12.: The pedestrian density Vs. the vehicle MAD acceleration across the test simulations

driving patterns. Whereas, such behavior may not be included in the pedestrians model used in the simulator.

7.4.5 Comparison with Risk Rapidly-exploring Random Trees

A group of tests is selected and ran twice. In the first run, the navigation of the vehicle is done using the developed proactive navigation framework. We refer to the results of this run with PDC. Whereas in the second run, the navigation is done using the Risk-RRT method presented in Sec. 7.2. The selected test group included a total of 840 simulations for each run (520 frontal crossing and 320 lateral crossing) with over $10K$ pedestrian trajectories. The tests are selected to scan the same previous range of variable density and sparsity, and with the same fixed parameter values. Tab. 7.3 shows the results in both the lateral and frontal scenarios for our method (PDC) and the Risk-RRT method.

Firstly, the results of the collisions tests are shown for the **pedestrian safety** analysis. Additionally, the **success rate** for each method is shown, which is the percentage of simulations where the vehicle reached its goal destination within the simulation period. There is a significant improvement in terms of the navigation success (in both scenarios) when using the proactive framework. The Risk-RRT method is noticed to fail in planning a trajectory in many interaction scenarios due to its reactive and uncooperative nature. The vehicle was noted to freeze in many cases, specially with higher densities. Whereas, using the developed proactive system, the vehicle anticipates the pedestrian cooperation and succeeds to find a valid solution. This is done while maintaining a better pedestrian safety than the Risk-RRT. Using the proactive system, the vehicle was adapting its behavior in critical situation resulting in no frontal collisions

Collisions Test				Success
Method		Rate	Speed	Rate
PDC	Frontal	**0.0008**	**0.25m/s**	**98%**
	Lateral	0.020	**0.65m/s**	**78%**
Risk-RRT	Frontal	0.001	$3.13m/s$	22%
	Lateral	**0.012**	$2.36m/s$	8.3%

		$\bar{I}_{ucf}$		E_P	
Method		Mean	Max	Mean	Max
PDC	Frontal	**3.07**	**5.37**	0.18	0.53
	Lateral	6.46	10.31	0.16	0.49
Risk-RRT	Frontal	4.32	6.86	0.02	0.15
	Lateral	**5.64**	**8.78**	0.01	0.05

Tab. 7.3.: Pedestrians Safety and Comfort Results

and low collision speed. Moreover, a low collision rate is detected in the frontal crossing coupled with a high success rate. In the lateral crossing, a slightly higher collision rate is detected in our method. Noting that the collision rates displayed in the table are those of realistic collisions. This is done to eliminate the collisions caused by simulator from the comparison.

For the **pedestrian comfort**, the proactive system provoked less pedestrian discomfort in the frontal crossing scenario that the Risk-RRT. Whereas, less levels of discomfort are experienced with the Risk-RRT for the lateral crossing scenario. For the **path smoothness**, in our method the path energy E_P falls in a low energy range, which shows that the smooth steering adapted in our method allowed to produce smooth trajectories in both the frontal and lateral interactions. The Risk-RRT freezes in many cases, which results in a very low path energy.

Finally, in the lateral crossing for Risk-RRT, a slightly lower collision rate and lower pedestrian uncomfortableness are detected. However, this result is coupled with a very low success rate ($< 10\%$) which means that the vehicle, in most cases, did not succeed to insert itself in the pedestrian crowd.

7.5 Conclusion

The proposed proactive navigation system was integrated and implemented in its entirety in this chapter. The system was implemented under ROS and tested using a kinematic

simulator for pedestrian crowds in shared spaces with a vehicle (SPACiSS simulator). A diverse group of PVI scenarios is run to evaluate the performance of the system. The tests included seven different interaction scenarios: frontal, back, frontal-back, lateral, bi-lateral and 45^o crossing both uni and bi-directional. The tests also spanned a wide range of various pedestrian densities and with different space configurations. The performance of the system was evaluated using the performance metrics introduced in the previous chapter (Ch. 6) to evaluate the safety of the motion, the quality of the produced vehicle trajectory and the comfort of the pedestrians around the vehicle during the interaction. Furthermore, the performance of the system was compared with a reference reactive navigation method which is the Risk Rapidly-exploring Random Trees (Risk-RRT). This method was selected as the RRT method is a well known and tested method, and the Risk-RRT improves over the classical RRT to handle dynamic environments.

The simulations results showed the system is capable of navigating dense and complex environments while producing smooth trajectories and maintaining the pedestrians safety and comfort. Moreover, the proposed proactive framework showed a significant advantage when compared the the reactive Risk-RRT method. The system showed a much higher success rate in crossing the pedestrian crowds, as compared to the Risk-RRT which failed to navigate and resulted in the freezing of the vehicle in many scenarios. Although the proposed framework showed major improvement over a reactive system, several points of improvement can be identified to account for the detected limitations.

The lowest collision rates of the system were detected in the frontal and lateral crossing scenarios. Whereas, higher rates resulted for in the back crossing, frontal-back crossing and the bi-lateral crossing scenarios. The highest collision rates of the system were detected in the 45^o crossing scenarios (uni and bi-directional). We believe that this performance can be improved by improving the pedestrian cooperation-based behavioral model used within the proactive system. This is because the model itself was obtained using PVI data in frontal and lateral crossing scenarios. Therefore, an interaction with an angle between the vehicle and the pedestrians was not considered. Rather, only the limit cases for this interaction angle was considered for the lateral and frontal cases. This consideration clearly did not generalize well to the rest of the interaction angles between the two limits, such as the 45^o crossing. Furthermore, considering the back crossing interaction needs an additional part in both the behavioral model and the planning/control system to deal with the perception range of a pedestrian. This was not considered in the actual configuration and the pedestrian is assumed to have an equal 360^o perception at all time, which is not the case in real life or in the testing simulator.

Overall, the system produced smooth and high efficiency trajectories for the vehicle while maintaining the pedestrians comfort. This is thanks to the proactive dynamic channel

method for the lateral control which drives the system in appropriate directions where more cooperative pedestrians and less densities are expected to exist, while not straying far away from the pre-planned trajectory. This efficiency is also thanks to the proactive longitudinal controller which anticipates the pedestrians cooperation and avoids large time delays or the freezing of the vehicle.

8 Conclusion and Future Prospects

Autonomous navigation in close proximity with pedestrians is a highly challenging task, specially for a bigger sized and potentially harmful robot such as an autonomous vehicle. However, developing autonomous navigation solutions capable of navigating around pedestrians is becoming increasingly more interesting to researchers and stockholders in the field. This is mainly motivated by the vision of green modern cities where the traditional street structure is replaced by more livable and pedestrian-friendly spaces shared between vehicles and more vulnerable road users (Fig. 8.1a). Indeed this vision of shared spaces within our city centers is not a future fantasy, but a plan already in action. This direction of city planning can be seen in many cities across Europe and the world (Fig. 8.1b). Unless autonomous driving solutions are capable of navigating shared spaces safely and efficiently, such technologies would not be able to thrive in the future. Moreover, autonomous navigation solutions that are functional in such spaces can lead to a major improvement in urban life style and city design. Only then we will be able to expand the scope of these green and shared spaces over our cities, while providing transport options that are safe, efficient and equally accessible to all.

(a) Shared spaces vision in city planning [Ham08] **(b)** London's Exhibition Road shared space

Fig. 8.1.: Shared spaces: future and current spaces

However, current autonomous driving solutions and technologies are not targeting this sort of environments. The main direction in autonomous driving is focused on cities

that are designed for vehicles with roads infrastructure and working scenarios which sparsely interact with pedestrians. Therefore, the current technologies are not suitable for unstructured, shared and pedestrian-populated spaces. Furthermore, there is an obvious gap between where the planning of cities is heading, and where the technology for AVs is focused.

This vision of shared spaces in city planning and the need for autonomous driving solutions in such spaces were the main motivation for this thesis, as part of the ANR project HIANIC. The main goal of the work was to develop a navigation framework suitable for an autonomous vehicle navigating a space shared with pedestrians. The challenges in achieving such a goal are not confined to finding a solution, they start with the formulation of the problem as well. The performance of the final solution remains limited by the aspects taken into consideration when designing this solution. When developing our framework, we explored the different behavioral aspects which are necessary for a safe and socially acceptable navigation around pedestrians. The main drive of the solution was the natural behavior of drivers and even pedestrians when navigating and interacting with each other. We explored a diverse range of works on robot social navigation and navigation in dynamic and pedestrian-populated environments. The ideas present in these works along with their limitations motivated our proposed *Proactive Navigation Framework*.

We argued along this thesis that the lack of proactivity is a main source of limitation in many existing works in the literature. Where the drawback of the develop method is the result of ill-defined problem. The main point of limitation that was observed globally is designing strictly reactive navigation solutions and expecting the system to perform in a social and natural way. We discussed this idea back in **Chapters 1 and 2** with several examples demonstrating that a proactive behavior is a natural behavior deployed by humans. Therefore, a natural navigation policy requires this behavioral aspect to be included in the system. Furthermore, when it comes to shared tasks, a proactive behavior is necessary for the success of a task between two peers. The absence of proactivity and a strictly reactive behavior would always lead to a master/slave relationship during the shared task. This is not always desirable, which is the case for navigation tasks around pedestrians in shared spaces. We discussed in **Chapter 2** how the navigation in such scenarios is considered a shared task between the vehicle and the surrounding pedestrians. A task of pooling and sharing the navigation resources (space and time) between the vehicle and the pedestrians. A shared task that requires an interaction between the two, which we called Pedestrian-Vehicle Interaction (PVI) as a sub-category of Human-Robot Interaction (HRI). Therefore, in order for the navigation to succeed in this peer-to-peer shared task, the vehicle must participate in the navigation space as an active agent and not merely react to the surrounding events. Furthermore,

we demonstrated with several examples how the absence of proactivity can lead to the failure of the navigation in cases where either the pedestrians are navigating in close proximity or the complexity of the space exceeds a certain limit. In such cases, a reactive policy would be over penalizing to the system and can lead to the failure of the navigation and the freezing of the vehicle.

The proposed proactive navigation framework is build on the idea of human cooperation. The system exploits the cooperation of pedestrians and influences their trajectories to facilitate the navigation of the vehicle. This is done while maintaining the pedestrian safety and comfort. The developed system is composed of three main parts. The first part is responsible of predicting the pedestrians reactions and behavior around the vehicle. Whereas, the two other parts are the systems to control the longitudinal and lateral movement of the vehicle.

The developed pedestrian behavioral model which was discussed in **Chapter 3**, is a cooperation-based model. The cooperation in this context is defined as the pedestrian's tendency to modify its optimal trajectory to facilitate the movement of the vehicle. The proposed model is composed of two layers. In the first layer, the pedestrian cooperation around the vehicle is estimated with a time-varying scalar based on the state of the space, the behavior of the vehicle and the state of the pedestrian. This cooperation estimation is then used as an input to the second layer to predict the short-term future trajectory of the pedestrian. The model was designed using social concepts and calibrated using real-life recorded pedestrian to vehicle interactions. Basing the behavioral model on the concept of cooperation was essential to exploit it in the proactive navigation system. In this context, proactivity can be defined as equivalent to taking an action which increases the pedestrian cooperation along the interaction.

The possibility of deploying a proactive robotic behavior on the vehicle side was first explored using only the longitudinal control in **Chapter 4**. To develop a proactive longitudinal controller, the lateral control was assumed to be provided by a higher level system. The goal was to explore navigating even dense environments not by modifying the vehicle's direction but by influencing the surrounding agents and behaving proactivly. The proposed controller was designed to maximize the pedestrians cooperation while maintaining an appropriate safety margin. The longitudinal system was implemented using the developed cooperation-based trajectory planning model to simulate the pedestrian crowd (Fig. 8.2). The implementation of this system on its own resulted in an important improvement over reactive controllers which leads to the freezing of the system in many cases. This demonstrated that a proactive influence is indeed possible even with the longitudinal control on its own.

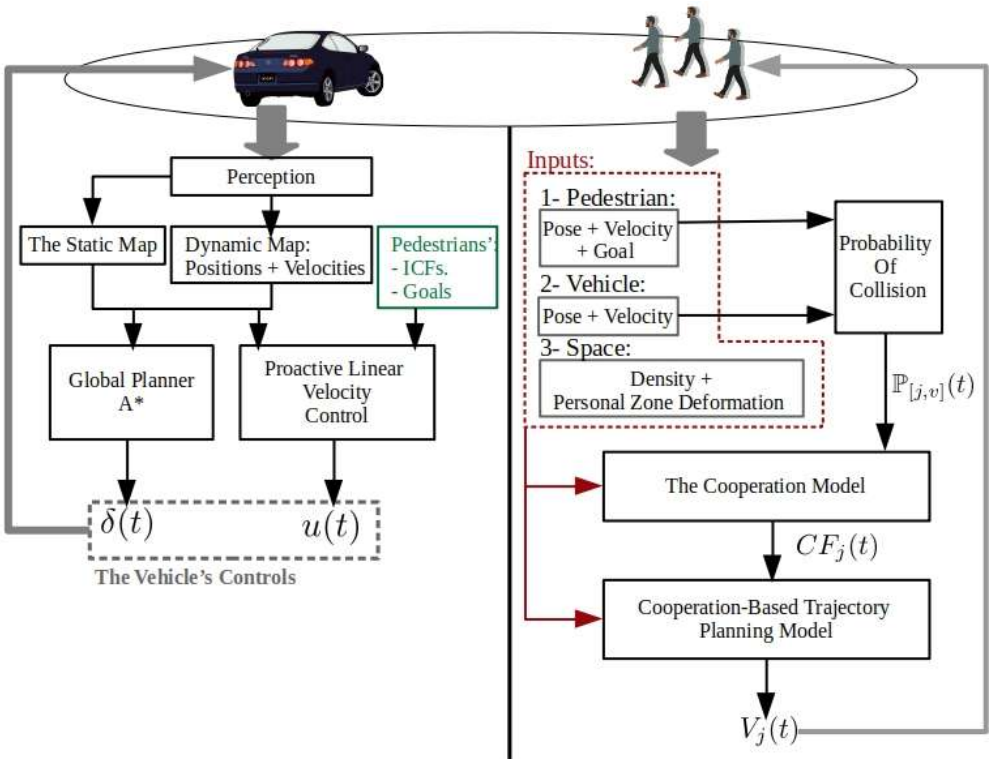

Fig. 8.2.: The longitudinal proactive controller implementation summary

The longitudinal control was used as an input to the lateral control system proposed in **Chapter 5**. The system was based on the idea of proactive exploration of the space in combination with a dynamic channel method. The proactive exploration means that more navigation options are considered which are not necessarily pedestrian-free. This is done by dividing the space into a set of navigation channel. Then estimating the state of each channel based on its current pedestrian density, future predicted density and the cooperation of pedestrians within it. Using this estimate along with its distance relative to the vehicle and to the global path, the cost of navigating in each channel is estimated. This is done using a proposed fuzzy model for the cost estimation. After considering all the possible navigation options and their respective costs, the channel with the lowest costs is selected as the goal destination. The transition to the goal channel is done using a Qunitic path to ensure a smooth transition similar to the lane change manoeuvre (Fig. 8.3). This ensures the legibility of vehicle movement, as such behavior is often performed by experienced drivers on roads. The proposed system allowed us to explore the possibility of proactivity by controlling the steering of the vehicle. This allows the vehicle to find the best possible navigation direction and avoid the freezing when an obstacle free path does not exist.

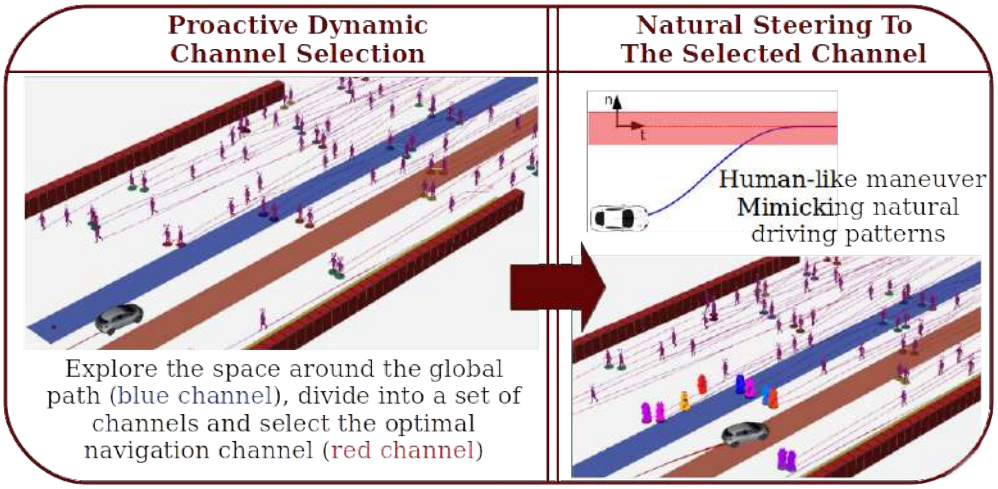

Fig. 8.3.: The proactive dynamic channel method summary

The issue of evaluating the system performance was discussed in **Chapter 6**. The different aspects of the performance to be evaluated is summarized in three main category. The first is the safety of the vehicle's motion around the pedestrians. This can be evaluated using the collision rate and the time to collision during an interaction. Furthermore, a collision analysis based on the velocity obstacle method was presented to qualify the cause of a collision occurring in a simulation. The second category is the trajectory quality which includes its smoothness, efficiency and the comfort of a passenger along this trajectory. The third and final category is the comfort of the pedestrians around the vehicle. Appropriate performance metrics were suggested for each category. Moreover, the success/fail criterion for each metric was presented.

The three parts of the proactive navigation system were integrated and implemented under ROS in **Chapter 7**. The system was tested in a diverse group of interaction scenarios with variable pedestrian density and sparsity. The proactive system was also compared with the reactive Risk-RRT method. The performance in the simulation was evaluated using the previously presented performance metrics.

Finally, we can summarized the main conclusions of the work in the following points:

- A proactive behavior is necessary for a robotic system to navigate socially and naturally among pedestrian crowds. Proactivity was approached in this work as the way of increasing pedestrian cooperation. The system implementation presents a proof of concept of the defined proactivity. The results proved the possibility of applying a proactive control during navigation and influencing pedestrian behavior in a desired manner.

- Cooperation is a natural behavior deployed by humans, and considering this aspect in the navigation is essential for its success. Pedestrians have a tendency to alter their trajectories and cooperate in different degrees depending on their state and on the specific interaction. Therefore, it is important to understand the degree to which a pedestrian is willing to cooperate and exploit this cooperation during the navigation. Furthermore, building a behavioral model based on the concept of cooperation is essential for a cooperative and proactive navigation framework. Understanding what vehicle behaviors stimulate more cooperation on the pedestrian side can be one of the keys to a proactive navigation system.

- There is an imperative requirement for reliable PVI simulators for the development of social and safe autonomous navigation system. The navigation system must be tested intensively in simulation before letting this potentially harmful robot (the AV) operate around humans. Moreover, appropriate performance evaluation metrics must be considered to evaluate the different aspects of the navigation.

- The proactive framework allows the system to navigate complex spaces much more efficiently and improves the success rate of the navigation significantly. The results of the integrated proactive navigation framework implementation in chapter 7 proved the efficiency of the system and its improvement over reactive navigation systems. However, the performance of the navigation system is bound to be more limited when the complexity of the space increases. The efficiency in terms of the traveled time and a high level of pedestrian comfort cannot be maintained beyond a certain level of pedestrian density. This level was close to $0.3ped/m^2$ according to our analysis.

In this work we managed to suggest a first implementation of a proactive navigation framework around pedestrians. However, the system still has some limitations and would benefit from future development. These limitations combined with the premise of the HIANIC project on human inspired navigation in crowds, creates the opportunity for multiple extensions and future prospects. We can summarize the main points on future improvements in the following:

- The proactive navigation framework presented in this thesis was tested and evaluated in a simulated PVI environment under ROS. The next step is implementing the system on an automated vehicle and evaluating the performance in real-time testing. This can be done in the future by benefiting from the ICARs simulator which is a ROS-based self-driving cars testing platform developed by the LS2N[1] laboratory. The main benefit of ICARs is its multiple working modes options. In the

[1]Le Laboratoire des Sciences du Numérique de Nantes, `https://www.ls2n.fr/`

Simulation Mode, the dynamics of the vehicle have been accurately implemented using experimental data obtained with a physical car. This mode simulates the vehicle's sensors such as GPS, IMU, LiDAR and cameras. After testing the navigation system using this mode, the *Real Time Mode* can be run on-board of the self driving car using the exact same architecture.

- The cooperation-based behavioral model proposed in this work can benefit from multiple improvements. The perception range of a pedestrian, the possibility of a distraction and weather the pedestrian perceived the AV or not should be included in the model. Moreover, currently the model is based only on spatio-temporal information. However, the model can benefit from integrating other sources of information of the pedestrian state such as the body pose, gaze, facial and body gestures. These information sources can be merged with the suggested model as a way of estimating what we called the inner cooperation factor. Furthermore, the navigation system can be significantly improved if more diverse PVI data is considered in the development of the model, which leads us to our second point.

- There is an obvious lack in the collected PVI data globally. It is imperative to have more diverse PVI data to understand pedestrian behavior around vehicles in different situations and against different drivers and driving patterns. This can either be real-life recorded data for natural interactions, or designed experiments with prepared volunteers. However, both methods are challenging. The first due to the privacy and consent of the recorded individuals. The latter due to the challenge in designing the experiment itself and the challenge of obtaining natural behaviors from volunteers conscious to the experiment. This takes us to the third point on the importance of collaborating with the social sciences in this domain.

- The collaboration with social and cognitive sciences can be of great benefit to the development of proactive and socially-aware navigation systems. This collaboration can take place in two stages of the work. The first is PVI data collection for understanding and modeling the pedestrian behavior. We have seen from our own experiment the difficulty in obtaining free and natural trajectories from the volunteers who in most cases would behave in a preconceived manner. Therefore, it is important to have experts preparing volunteers to eliminate their basis from natural behavior as much as possible. The second stage of the collaboration can take part when evaluating the system performance in real experimentation around pedestrians. In this stage, the goal of the collaboration would be to estimate the safety and comfort of the pedestrians and even the passenger during the navigation.

- The proposed proactive navigation system was focused on the interactions with pedestrians and did not consider dealing with static obstacles. The static obstacles are assumed to be treated by the global path planner. However, it is important to include the sensor-based static obstacles avoidance in the proposed lateral controller using the proactive dynamic channel method. This can be done by first modifying the navigation cost model of a dynamic channel to include an additional cost caused by the existence of a static obstacle in the channel. This would be a very important cost in some cases. If the size of this obstacle is big enough, then it can eliminate the containing channel from the navigation options all together (Fig. 8.4a). The sensor-based treatment of static obstacles can also be included in the path generation layer after selecting a goal channel. This can either be by maintaining an exact Quintic transition path but modifying its look-ahead distance to avoid an obstacle of the way. Meaning to make the Quintic extend shorter to pass before a static obstacle, as shown in Fig. 8.4b for example. This can also be done by a modification of the Quintic or considering a different transition shape. However, this part would require more in depth study to generate smooth and legible trajectory around the pedestrians with the existence of static obstacles.

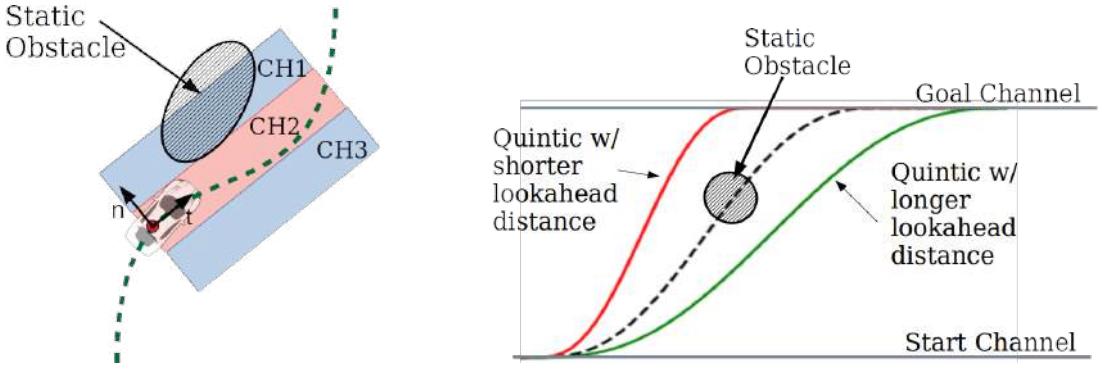

(a) A static obstacle can eliminate channel $CH1$ from the navigation options

(b) Modifying the Quintic transition (dashed black) to avoid the static obstacle

Fig. 8.4.: Targeting static obstacle in the PDC method

- The proposed proactive framework can be integrated with a reactive driving system under a global structure for decision making. The switching between the two systems can be made based on the perceived situation. The system can switch to highly reactive (slave) mode when perceiving an external agent with high priority such as an ambulance vehicle for example. Similarly the system can be switched to a highly proactive mode in case of passenger emergency for example. This can also be approached by defining different levels of control proactivity instead of the binary (reactive/proactive). This new proposed proactivity factor can be modeled and estimated in the interaction scenarios based on the state of the space.

- An extension of this work can be made to treat unmodeled or hazardous pedestrian behaviors in shared spaces. Furthermore, more social influence can be integrated in the work to consider diverse social relationships, such as dealing with pedestrian groups or couples. This is to maintain the highest possible levels of pedestrians comfort and ensure the social acceptance of the autonomous vehicle.
- A clear intention communication on the vehicle's side is a very critical point to the success of the proactive navigation. This has been discussed through the lateral and longitudinal commands to produce legible motion. However, this aspect can also be supported by a visual/audible communication system implemented on board of the vehicle. This system should be linked to the navigation system through an action interpretation layer to further communicate the vehicle's proactivity to its surroundings.

Finally, throughout this thesis we sat out to solve the problem of social and natural autonomous navigation in shared spaces by deploying a proactive robotic behavior. We managed to propose a first implementation for a proactive navigation framework. This implementation showed very promising results and significant improvements over the solutions based on reactive concepts. This enables us to solve the navigation problem around pedestrians from a different perspective. A perspective based on engaging the vehicle (or the robot) more actively in the navigation space by perceiving intentions, expecting cooperation and influencing other agents. This can transform the way autonomous vehicles or mobile robots function and increase their efficiency and social awareness. We hope that the concepts and methods presented in this thesis could open the door to more developments in the domain of social navigation and enable more beneficial mobile robot applications to function safely around humans.

Bibliography

[AA20] Abughalieh, K. M. and Alawneh, S. G. “Predicting Pedestrian Intention to Cross the Road”. In: *IEEE Access* 8 (2020), pp. 72558–72569. DOI: 10.1109/ACCESS.2020.2987777.

[Abd54] Abdel-Aty, S. “Approximate formulae for the percentage points and the probability integral of the non-central $\chi 2$ distribution”. In: *Biometrika* 41 (1954), pp. 538–540.

[ABM11] Adouane, L., Benzerrouk, A., and Martinet, P. “Mobile Robot Navigation in Cluttered Environment using Reactive Elliptic Trajectories”. In: *18th IFAC World Congress*. Milano, Italy, Sept. 2011. URL: https://hal.archives-ouvertes.fr/hal-01714859.

[ABO99] Ackermann, J., Bünte, T., and Odenthal, D. “Advantages Of Active Steering For Vehicle Dynamics Control”. In: *32nd International Symposium on Automotive Technology and Automation*. Jan. 1999, pp. 263–270.

[Adm18] Administration, T. N. H. T. S. *Critical Reasons for Crashes Investigated in the National Motor Vehicle Crash Causation Survey*. Tech. rep. COM-HS-812-506. U.S. Department of Transportation, NHTSA, Mar. 2018, p. 3.

[Ado16] Adouane, L. *Autonomous Vehicle Navigation: From Behavioral to Hybrid Multi-Controller Architectures*. Taylor & Francis CRC Press, Apr. 2016. URL: https://hal.archives-ouvertes.fr/hal-01711776.

[Aje+20] Ajeil, F. H., Ibraheem, I. K., Azar, A. T., and Humaidi, A. J. “Grid-Based Mobile Robot Path Planning Using Aging-Based Ant Colony Optimization Algorithm in Static and Dynamic Environments”. In: *Sensors* 20.7 (2020), pp. 1880–1906. ISSN: 1424-8220. DOI: 10.3390/s20071880. URL: https://www.mdpi.com/1424-8220/20/7/1880.

[Amo+11] Amouri, L., Novales, C., Poisson, G., Njah, M., Jallouli, M., and Derbel, N. “DVZ-based Obstacle Avoidance Control of a Wheelchair Mobile Robot”. In: *IEEE Intemational Conference on Mechatronics*. Istanbul, Turkey, Apr. 2011, pp. 911–915. URL: https://hal.archives-ouvertes.fr/hal-00630139.

[AOB14] Attia, R., Orjuela, R., and Basset, M. “Nonlinear cascade strategy for longitudinal control in automated vehicle guidance”. In: *Control Engineering Practice* 29 (Mar. 2014), pp. 225–234. DOI: 10.1016/j.conengprac.2014.02.003. URL: https://hal.archives-ouvertes.fr/hal-00955162.

[AS20] Alsaleh, R. and Sayed, T. “Modeling pedestrian-cyclist interactions in shared space using inverse reinforcement learning”. In: *Transportation Research Part F: Traffic Psychology and Behaviour* 70 (2020), pp. 37–57. ISSN: 1369-8478. DOI: https://doi.org/10.1016/j.trf.2020.02.007. URL: https://www.sciencedirect.com/science/article/pii/S1369847819306552.

[Bai+15] Bai, H., Cai, S., Ye, N., Hsu, D., and Lee, W. S. “Intention-aware online POMDP planning for autonomous driving in a crowd”. en. In: *IEEE International Conference on Robotics and Automation (ICRA)*. Seattle, WA, USA: IEEE, May 2015, pp. 454–460. ISBN: 978-1-4799-6923-4.

[Bai+21] Bailey, J. P., Nash, A., Tovey, C. A., and Koenig, S. “Path-Length Analysis for Grid-Based Path Planning”. In: *Artificial Intelligence* (2021), pp. 560–571. ISSN: 0004-3702. DOI: https://doi.org/10.1016/j.artint.2021.103560. URL: https://www.sciencedirect.com/science/article/pii/S0004370221001119.

[Bar+17] Barabas, I., Todoruţ, A., Nicolae, C., and Molea, A. “Current challenges in autonomous driving”. In: *IOP Conference Series: Materials Science and Engineering* 252 (Oct. 2017), p. 012096. DOI: 10.1088/1757-899X/252/1/012096.

[Bar+18] Bartolini, G., Fridman, L., Pisano, A., and Usai, E. (*Modern Sliding Mode Control Theory*. Vol. 375. Springer Lecture Notes in Control and Information Sciences, Apr. 2018.

[Bel+19] Bellet, T., Cunneen, M., Mullins, M., Murphy, F., Pütz, F., Spickermann, F., Braendle, C., and Baumann, M. F. “From semi to fully autonomous vehicles: New emerging risks and ethico-legal challenges for human-machine interactions”. In: *Transportation Research Part F: Traffic Psychology and Behaviour* 63 (2019), pp. 153–164. ISSN: 1369-8478. DOI: https://doi.org/10.1016/j.trf.2019.04.004. URL: http://www.sciencedirect.com/science/article/pii/S1369847818308556.

[Ber+04] Bertozzi, M., Broggi, A., Fascioli, A., Tibaldi, A., Chapuis, R., and Chausse, F. “Pedestrian localization and tracking system with Kalman filtering”. In: *IEEE Intelligent Vehicles Symposium, 2004*. 2004, pp. 584–589. DOI: 10.1109/IVS.2004.1336449.

[BK21] Brik, B. and Ksentini, A. “Toward Optimal MEC Resource Dimensioning for a Vehicle Collision Avoidance System: A Deep Learning Approach”. In: *IEEE Network* 35.3 (2021), pp. 74–80. DOI: 10.1109/MNET.011.2000577.

[BL01] Bullo, F. and Lynch, K. “Kinematic controllability for decoupled trajectory planning in underactuated mechanical systems”. In: *IEEE Transactions on Robotics and Automation* 17.4 (2001), pp. 402–412. DOI: 10.1109/70.954753.

[BMM05] Blanc, G., Mezouar, Y., and Martinet, P. “Indoor Navigation of a Wheeled Mobile Robot along Visual Routes”. In: *Proceedings of the 2005 IEEE International Conference on Robotics and Automation*. 2005, pp. 3354–3359. DOI: 10.1109/ROBOT.2005.1570628.

[BMM06] Blanc, G., Mezouar, Y., and Martinet, P. “A Path Planning Strategy For Obstacle Avoidance”. In: *Proceedings of the Third International Conference on Informatics in Control, Automation and Robotics*. Vol. 2. INSTICC. SciTePress, 2006, pp. 438–444. ISBN: 978-972-8865-60-3. DOI: 10.5220/0001211604380444.

[BMS19] Bae, I., Moon, J., and Seo, J. “Toward a Comfortable Driving Experience for a Self-Driving Shuttle Bus”. In: *Electronics* 8.9 (2019), pp. 943–956. ISSN: 2079-9292. DOI: 10.3390/electronics8090943. URL: https://www.mdpi.com/2079-9292/8/9/943.

[BN90] Bruckstein, A. M. and Netravali, A. N. “On minimal energy trajectories”. In: *Computer Vision, Graphics, and Image Processing* 49.3 (1990), pp. 283–296. ISSN: 0734-189X. DOI: https://doi.org/10.1016/0734-189X(90)90105-5.

[Boo20] Books, E. S. *Ageing Europe - looking at the lives of older people in the EU*. Tech. rep. 978-92-76-21520-2. European Commission, Nov. 2020, p. 52.

[BR82] Boyd, R. and Richerson, P. J. “Cultural transmission and the evolution of cooperative behavior”. In: *Human Ecology* 10.3 (Sept. 1982), pp. 325–351. ISSN: 1572-9915. DOI: 10.1007/BF01531189. URL: https://doi.org/10.1007/BF01531189.

[Bri+21] Brito, B., Everett, M., How, J. P., and Alonso-Mora, given=Javier, giveni=J., givenun=0. “Where to go next: Learning a Subgoal Recommendation Policy for Navigation Among Pedestrians”. In: *CoRR* abs/2102.13073 (2021). arXiv: 2102.13073. URL: https://arxiv.org/abs/2102.13073.

[Cai+20] Cai, P., Lee, Y., Luo, Y., and Hsu, D. “SUMMIT: A Simulator for Urban Driving in Massive Mixed Traffic”. In: *IEEE International Conference on Robotics and Automation (ICRA)*. 2020, pp. 4023–4029.

[Ccr20] Communication from the commission to the European parliament the council, t. E. e., committee, social, and regions, the committee of the. *Stepping up Europe’s 2030 climate ambition Investing in a climate-neutral future for the benefit of our people*. Tech. rep. COM/2020/562 final. Brussels: European Commission, Sept. 2020, p. 26.

[CFD21] Cornes, F., Frank, G., and Dorso, C. “Microscopic dynamics of the evacuation phenomena in the context of the Social Force Model”. In: *Physica A: Statistical Mechanics and its Applications* 568 (2021). ISSN: 0378-4371. DOI: https://doi.org/10.1016/j.physa.2021.125744. URL: https://www.sciencedirect.com/science/article/pii/S0378437121000169.

[CG76] Caudill, R. J. and Garrard, W. L. “Vehicle-Follower, Longitudinal Control for Automated Transit Vehicles”. In: *IFAC Proceedings Volumes* 9.4 (1976). IFAC/IFIP/IFORS 3rd International Symposium on Control in Transportation Systems, Columbus, Ohio, 9-13 August, pp. 195–209. ISSN: 1474-6670. DOI: https://doi.org/10.1016/S1474-6670(17)67295-1. URL: https://www.sciencedirect.com/science/article/pii/S1474667017672951.

[CH99] Connolly, T. and Hedrick, J. “Longitudinal Transition Maneuvers in an Automated Highway System”. In: *Journal of Dynamic Systems Measurement and Control-transactions of The Asme* 121 (1999), pp. 471–478.

[Cha11] Chan, F. K. “Miss distance–generalized variance non-central chi distribution”. In: *AAS/AIAA Space Flight Mechanics Meeting*. 2011, pp. 11–175.

[Che+17] Chen, L., Bai, X.-Z., Liang, Y.-G., and Li, K. “Calculation of Collision Probability”. In: *Orbital Data Applications for Space Objects*. Springer, Dec. 2017, pp. 135–183. ISBN: 978-981-10-2962-2. DOI: 10.1007/978-981-10-2963-9_5.

[Che+21] Cheng, H., Johora, F., Sester, M., and J.P., M. “Trajectory Modelling in Shared Spaces: Expert-Based vs. Deep Learning Approach?” In: *Swarup S., Savarimuthu B.T.R. (eds) Multi-Agent-Based Simulation XXI. Lecture Notes in Computer Science* 12316 (May 2021).

[Chi+16] Chi, W., Kono, H., Tamura, Y., Yamashita, A., Asama, H., and Meng, M. Q.-H. "A human-friendly robot navigation algorithm using the risk-RRT approach". In: *IEEE International Conference on Real-time Computing and Robotics (RCAR)*. 2016, pp. 227–232. DOI: 10.1109/RCAR.2016.7784030.

[Clo+06] Clodic, A., Fleury, S., Alami, R., Chatila, R., Bailly, G., Brethes, L., Cottret, M., Danes, P., Dollat, X., Elisei, F., Ferrane, I., Herrb, M., Infantes, G., Lemaire, C., Lerasle, F., Manhes, J., Marcoul, P., Menezes, P., and Montreuil, V. "Rackham: An Interactive Robot-Guide". In: *The 15th IEEE International Symposium on Robot and Human Interactive Communication*. Sept. 2006, pp. 502–509. DOI: 10.1109/ROMAN.2006.314378.

[CMF19] Camara, F., Merat, N., and Fox, C. W. "A heuristic model for pedestrian intention estimation". In: *IEEE Intelligent Transportation Systems Conference (ITSC)*. Auckland, New Zealand, 2019, pp. 3708–3713. DOI: 10.1109/ITSC.2019.8917195.

[CN21] Cherubini, A. and Navarro-Alarcon, D. "Sensor-Based Control for Collaborative Robots: Fundamentals, Challenges, and Opportunities". In: *Frontiers in Neurorobotics* 14 (Jan. 2021), pp. 113–127. ISSN: 1662-5218. DOI: 10.3389/fnbot.2020.576846. URL: https://www.frontiersin.org/article/10.3389/fnbot.2020.576846.

[CS19] Costa, M. and Silva, M. "A Survey on Path Planning Algorithms for Mobile Robots". In: Gondomar, Portugal, Apr. 2019, pp. 1–7. DOI: 10.1109/ICARSC.2019.8733623.

[CSB96] Canudas de Wit, C., Siciliano, B., and Bastin, G. *Theory of Robot Control*. Springer Communications and Control Engineering, 1996.

[CT94] Chee, W. and Tomizuka, M. "Lane Change Maneuver of Automobiles for The Intelligent Vehicle and Highway System (IVWS)". In: *American Control Conference. Baltimore, Maryland* (June 1994), pp. 3586–3587.

[Cun+15] Cunningham, A. G., Galceran, E., Eustice, R. M., and Olson, E. "MPDM: Multipolicy decision-making in dynamic, uncertain environments for autonomous driving". In: *IEEE International Conference on Robotics and Automation (ICRA)*. Seattle, WA, USA, 2015, pp. 1670–1677. DOI: 10.1109/ICRA.2015.7139412.

[Cun+20] Cunningham, A., Galceran, E., Mehta, D., Ferrer, G., Eustice, R., and E., O. *MPDM: Multi-policy Decision-Making from Autonomous Driving to Social Robot Navigation. In: Waschl H., Kolmanovsky I., Willems F. (eds) Control Strategies for Advanced Driver Assistance Systems and Autonomous Driving Functions. Lecture Notes in Control and Information Sciences*. Springer, Cham., 2020. URL: https://hal.archives-ouvertes.fr/hal-01711776.

[CWM18] Chi, W., Wang, J., and Meng, M. Q.-H. "Risk-Informed-RRT*: A Sampling-based Human-friendly Motion Planning Algorithm for Mobile Service Robots in Indoor Environments". In: *IEEE International Conference on Information and Automation (ICIA)*. 2018, pp. 1101–1106. DOI: 10.1109/ICInfA.2018.8812396.

[CZ01] Cacitti, A. and Zapata, R. "Reactive behaviours of mobile manipulators based on the DVZ approach". In: *IEEE International Conference on Robotics and Automation (ICRA)*. Vol. 1. May 2001, pp. 680–685. DOI: 10.1109/ROBOT.2001.932629.

[Din+21] Ding, Y., Zhuang, W., Wang, L., Liu, J., Guvenc, L., and Li, Z. “Safe and optimal lane-change path planning for automated driving”. In: *Proceedings of the Institution of Mechanical Engineers, Part D: Journal of Automobile Engineering* 235.4 (2021), pp. 1070–1083. DOI: 10.1177/0954407020913735.

[Dom+16] Dominguez, S., Ali, A., Garcia, G., and Martinet, P. “Comparison of lateral controllers for autonomous vehicle: Experimental results”. In: *IEEE 19th International Conference on Intelligent Transportation Systems (ITSC)*. 2016, pp. 1418–1423. DOI: 10.1109/ITSC.2016.7795743.

[Dos+17] Dosovitskiy, A., Ros, G., Codevilla, F., Lopez, A., and Koltun, V. “CARLA: An Open Urban Driving Simulator”. In: *Proceedings of the 1st Annual Conference on Robot Learning*. 2017, pp. 1–16.

[DT17a] Deo, N. and Trivedi, M. M. “Learning and predicting on-road pedestrian behavior around vehicles”. In: *IEEE 20th International Conference on Intelligent Transportation Systems (ITSC)*. 2017, pp. 1–6. DOI: 10.1109/ITSC.2017.8317865.

[DT17b] Dey, D. and Terken, J. “Pedestrian Interaction with Vehicles: Roles of Explicit and Implicit Communication”. In: *Proceedings of the 9th International Conference on Automotive User Interfaces and Interactive Vehicular Applications*. AutomotiveUI ’17. Oldenburg, Germany: Association for Computing Machinery, 2017, pp. 109–113. ISBN: 9781450351508. DOI: 10.1145/3122986.3123009. URL: https://doi.org/10.1145/3122986.3123009.

[Dur+16] Durupınar, F., Güdükbay, U., Aman, A., and Badler, N. I. “Psychological Parameters for Crowd Simulation: From Audiences to Mobs”. In: *IEEE Transactions on Visualization and Computer Graphics* 22.9 (Sept. 2016), pp. 2145–2159. ISSN: 2160-9306. DOI: 10.1109/TVCG.2015.2501801.

[Ebe06] Eberly, D. “Distance from a Point to an Ellipse, an Ellipsoid, or a Hyperellipsoid”. In: 2006.

[Env04] Environment, D.-G. for. *Reclaiming city streets for people Chaos or quality of life?* Tech. rep. 92-894-3478-3. European Commission, Sept. 2004, p. 52.

[ET21] Engineering, R. C. of and Technology. *The Future of Driving*. Tech. rep. COM/2020/562 final. Ohio University, Mar. 2021, p. 3.

[Fan+05] Fang, H., Lenain, R., Thuilot, B., and Martinet, P. “Trajectory tracking control of farm vehicles in presence of sliding”. In: *IEEE/RSJ International Conference on Intelligent Robots and Systems*. 2005, pp. 58–63. DOI: 10.1109/IROS.2005.1545226.

[Fan+19] Fan, T., Cheng, X., Pan, J., Long, P., Liu, W., Yang, R., and Manocha, D. “Getting Robots Unfrozen and Unlost in Dense Pedestrian Crowds”. In: *IEEE Robotics and Automation Letters* 4 (2019), pp. 1178–1185.

[Far+17] Farina, F., Fontanelli, D., Garulli, A., Giannitrapani, A., and Prattichizzo, D. “Walking Ahead: The Headed Social Force Model”. In: *PLOS ONE* 12.1 (Jan. 2017), pp. 1–23. DOI: 10.1371/journal.pone.0169734. URL: https://doi.org/10.1371/journal.pone.0169734.

[FFB19] Filimonov, A., Filimonov, N., and Barashkov, A. “Construction of Potential Fields for the Local Navigation of Mobile Robots”. In: *Optoelectronics, Instrumentation and Data Processing* 55 (July 2019), pp. 371–375. DOI: 10.3103/S8756699019040071.

[FK12] Fraichard, T. and Kuffner, J. “Guaranteeing Motion Safety for Robots”. In: *Autonomous Robots* 32.3 (Apr. 2012), pp. 173–175. DOI: 10.1007/s10514-012-9278-z.

[FL20] Fraichard, T. and Levesy, V. “From Crowd Simulation to Robot Navigation in Crowds”. In: *IEEE Robotics and Automation Letters* 5.2 (2020), pp. 729–735. DOI: 10.1109/LRA.2020.2965032.

[FR11] Friesen, A. and Rao, R. “Gaze Following as Goal Inference: A Bayesian Model”. In: *Cognitive Science* 33 (2011), pp. 2457–2462.

[Fra+20] Fransen, K., van Eekelen, J., Pogromsky, A., Boon, M., and Adan, I. “A dynamic path planning approach for dense, large, grid-based automated guided vehicle systems”. In: *Computers Operations Research* 123 (2020), pp. 105046–105056. ISSN: 0305-0548. DOI: https://doi.org/10.1016/j.cor.2020.105046. URL: https://www.sciencedirect.com/science/article/pii/S0305054820301635.

[Fra07] Fraichard, T. “A Short Paper about Motion Safety”. In: *IEEE International Conference on Robotics and Automation*. Rome, Italy, 2007, pp. 1140–1145. DOI: 10.1109/ROBOT.2007.363138.

[Fre52] Frenet, M. “Sur les courbes à double courbure”. In: *Toulouse. Abstract in Journal de Mathématiques Pures et Appliquées* 17 (1852).

[FS14a] Ferrer, G. and Sanfeliu, A. “Proactive kinodynamic planning using the Extended Social Force Model and human motion prediction in urban environments”. In: *IEEE/RSJ International Conference on Intelligent Robots and Systems*. Sept. 2014, pp. 1730–1735. DOI: 10.1109/IROS.2014.6942788.

[FS14b] Ferrer, G. and Sanfeliu, A. “Proactive kinodynamic planning using the Extended Social Force Model and human motion prediction in urban environments”. In: *IEEE/RSJ International Conference on Intelligent Robots and Systems*. 2014, pp. 1730–1735. DOI: 10.1109/IROS.2014.6942788.

[FS98] Fiorini, P. and Shiller, Z. “Motion Planning in Dynamic Environments Using Velocity Obstacles”. In: *The International Journal of Robotics Research* 17.7 (1998), pp. 760–772. DOI: 10.1177/027836499801700706.

[FSL07a] Fulgenzi, C., Spalanzani, A., and Laugier, C. “Dynamic Obstacle Avoidance in uncertain environment combining PVOs and Occupancy Grid”. In: *IEEE International Conference on Robotics and Automation*. Rome, Italy, Apr. 2007, pp. 1610–1616. DOI: 10.1109/ROBOT.2007.363554.

[FSL07b] Fulgenzi, C., Spalanzani, A., and Laugier, C. “Dynamic Obstacle Avoidance in uncertain environment combining PVOs and Occupancy Grid”. In: *IEEE International Conference on Robotics and Automation*. Rome, Italy, Apr. 2007, pp. 1610–1616. DOI: 10.1109/ROBOT.2007.363554.

[Ful+08] Fulgenzi, C., Tay, C., Spalanzani, A., and Laugier, C. “Probabilistic navigation in dynamic environment using Rapidly-exploring Random Trees and Gaussian processes”. In: *IEEE/RSJ International Conference on Intelligent Robots and Systems*. 2008, pp. 1056–1062. DOI: 10.1109/IROS.2008.4650959.

[Ful+10] Fulgenzi, C., Spalanzani, A., Laugier, C., and Tay, C. *Risk based motion planning and navigation in uncertain dynamic environment*. Research Report. Oct. 2010, p. 14. URL: https://hal.inria.fr/inria-00526601.

[Gal+17] Galceran, E., Cunningham, A. G., Eustice, R., and Olson, E. “Multipolicy decision-making for autonomous driving via changepoint-based behavior prediction: Theory and experiment”. In: *Autonomous Robots* 41 (July 2017), pp. 1367–1382.

[Gal19] Galvani, M. “History and future of driver assistance”. In: *IEEE Instrumentation Measurement Magazine* 22.1 (2019), pp. 11–16. DOI: 10.1109/MIM.2019.8633345.

[Gar+17] Garrell, A., Villamizar, M., Moreno-Noguer, F., and Sanfeliu, A. “Teaching Robot’s Proactive Behavior Using Human Assistance”. In: *International Journal of Social Robotics* 9 (2017), pp. 231–249.

[GC21] García, R. Y. and Cárdenas, D. “Passengers comfort in horizontal curves on mountain roads: A field study using lateral accelerations”. In: *Revista Facultad de Ingenieria* 98 (Mar. 2021), pp. 94–103. DOI: 10.17533/udea.redin.20200578.

[Gér+08] Gérin-Lajoie, M., Richards, C. L., Fung, J., and McFadyen, B. J. “Characteristics of personal space during obstacle circumvention in physical and virtual environments”. In: *Gait Posture* 27.2 (2008), pp. 239–247. ISSN: 0966-6362. DOI: https://doi.org/10.1016/j.gaitpost.2007.03.015. URL: https://www.sciencedirect.com/science/article/pii/S0966636207001026.

[GL94] Godbole, D. and Lygeros, J. “Longitudinal control of the lead car of a platoon”. In: *IEEE Transactions on Vehicular Technology* 43.4 (1994), pp. 1125–1135. DOI: 10.1109/25.330177.

[Glo12] Gloor, C. *Pedsim: Pedestrian crowd simulation homepage*. 2012. URL: http://pedsim.silmaril.org.

[GMD16] Goswami, S., Murthy, C., and Das, A. “Sparsity Measure of a Network Graph: Gini Index”. In: *Information Sciences* 462 (Dec. 2016). DOI: 10.1016/j.ins.2018.05.044.

[GN11] Graubner, R. and Nixdorf, E. *Biomechanical Analysis ofthe Sprint and Hurdles Events at the 2009 IAAF WorldChampionships in Athletics*. http://www.meathathletics.ie/devathletes/pdf/Biomechanics%20of%20Sprints.pdf. 2011.

[Gra+19] Graf, U., Borges, P., Hernández, E., Siegwart, R., and Dubé, R. “Optimization-Based Terrain Analysis and Path Planning in Unstructured Environments”. In: *International Conference on Robotics and Automation (ICRA)*. Montreal, QC, Canada, 2019, pp. 5614–5620. DOI: 10.1109/ICRA.2019.8794331.

[GS07] Goodrich, M. and Schultz, A. “Human-Robot Interaction: A Survey”. In: *Foundations and Trends in Human-Computer Interaction* 1 (Jan. 2007), pp. 203–275. DOI: 10.1561/1100000005.

[Guy+11] Guy, S. J., Kim, S., Lin, M. C., and Manocha, D. "Simulating Heterogeneous Crowd Behaviors Using Personality Trait Theory". In: *Proceedings of the 2011 ACM SIGGRAPH/Eurographics Symposium on Computer Animation*. SCA '11. Vancouver, British Columbia, Canada: ACM, 2011, pp. 43–52. ISBN: 978-1-4503-0923-3. DOI: 10.1145/2019406.2019413. URL: http://doi.acm.org/10.1145/2019406.2019413.

[Hal66] Hall, E. T. *The hidden dimension: man's use of space in public and private*. The Bodley Head Ltd, London, 1966.

[Ham08] Hamilton-Baillie, B. "Towards shared space". In: *Urban Design International* 13 (Sept. 2008), pp. 130–138. DOI: 10.1057/udi.2008.13.

[Has+15] Hashimoto, Y., Gu, Y., Hsu, L.-T., and Kamijo, S. "Probability estimation for pedestrian crossing intention at signalized crosswalks". In: *IEEE International Conference on Vehicular Electronics and Safety (ICVES)*. Yokohama, Japan, 2015, pp. 114–119. DOI: 10.1109/ICVES.2015.7396904.

[Hed+91] Hedrick, J., Mcmahon, D., Narendran, V., and Darbha, S. "Longitudinal Vehicle Controller Design for IVHS Systems". In: vol. 3. July 1991, pp. 3107–3112. DOI: 10.23919/ACC.1991.4791980.

[Hei+17] Heilig, M., Hilgert, T., Mallig, N., Kagerbauer, M., and Vortisch, P. "Potentials of Autonomous Vehicles in a Changing Private Transportation System – a Case Study in the Stuttgart Region". In: *Transportation Research Procedia* 26 (2017). Emerging technologies and models for transport and mobility, pp. 13–21. ISSN: 2352-1465. DOI: https://doi.org/10.1016/j.trpro.2017.07.004. URL: https://www.sciencedirect.com/science/article/pii/S2352146517308633.

[Hel+01] Helbing, D., Molnár, P., Farkas, I. J., and Bolay, K. "Self-Organizing Pedestrian Movement". In: *Environment and Planning B: Planning and Design* 28.3 (2001), pp. 361–383. DOI: 10.1068/b2697.

[HLG14] Hou, J.-S., List, G., and Guo, X.-c. "New Algorithms for Computing the Time-to-Collision in Freeway Traffic Simulation Models". In: *Computational Intelligence and Neuroscience* 384 (Dec. 2014), pp. 761047–761055.

[HM95] Helbing, D. and Molnár, P. "Social force model for pedestrian dynamics". In: *Phys. Rev. E* 51 (5 May 1995), pp. 4282–4286. DOI: 10.1103/PhysRevE.51.4282. URL: https://link.aps.org/doi/10.1103/PhysRevE.51.4282.

[Hoe11] Hoek, H. "Why Shared Space?:: An Exploration of the Motivations for Shared Space Development in Nine European Cities". In: 2011.

[Hos15] Hossin M, S. M. "A Review on Evaluation Metrics for Data Classification Evaluations". In: *International Journal of Data Mining and Knowledge Management Process* 5.2 (2015), pp. 1–11. ISSN: 2231-007X. DOI: 10.5121/ijdkp.2015.5201.

[HRJ04] Hinds, P. J., Roberts, T. L., and Jones, H. "Whose Job Is It Anyway? A Study of Human–Robot Interaction in a Collaborative Task". In: *Human-Computer Interaction* 19 (2004).

[HRO97] Hatipolglu, C., Redmill, K., and Ozguner, U. “Steering and lane change: a working system”. In: *Proceedings of Conference on Intelligent Transportation Systems*. 1997, pp. 272–277. DOI: 10.1109/ITSC.1997.660487.

[HTV95] Hedrick, J., Tomizuka, M., and Varaiya, P. “Control Issues in Automated Highway Systems”. In: *Control Systems, IEEE* 14 (Jan. 1995), pp. 21–32. DOI: 10.1109/37.334412.

[HYH18] Hwang, C., Yang, C., and Hung, J. Y. “Path Tracking of an Autonomous Ground Vehicle With Different Payloads by Hierarchical Improved Fuzzy Dynamic Sliding-Mode Control”. In: *IEEE Transactions on Fuzzy Systems* 26.2 (2018), pp. 899–914. DOI: 10.1109/TFUZZ.2017.2698370.

[IA17] Iryo-Asano, M. and Alhajyaseen, W. K. “Modeling pedestrian crossing speed profiles considering speed change behavior for the safety assessment of signalized intersections”. In: *Accident Analysis Prevention* 108 (2017), pp. 332–342. ISSN: 0001-4575. DOI: https://doi.org/10.1016/j.aap.2017.08.028. URL: https://www.sciencedirect.com/science/article/pii/S0001457517303081.

[Int18] International, S. *Automated Driving – Levels of Driving Automation are Defined in New SAE International Standard J3016*. Tech. rep. July 2018, p. 2.

[Jin+20] Jing, P., Xu, G., Chen, Y., Shi, Y., and Zhan, F. “The Determinants behind the Acceptance of Autonomous Vehicles: A Systematic Review”. In: *Sustainability* 12.5 (2020). ISSN: 2071-1050. URL: https://www.mdpi.com/2071-1050/12/5/1719.

[JL14] Jeon, J. and Lee, B. “Ellipse-based velocity obstacles for local navigation of holonomic mobile robot”. In: *Electronics Letters* 50.18 (2014), pp. 1279–1281. DOI: https://doi.org/10.1049/el.2014.1592. eprint: https://ietresearch.onlinelibrary.wiley.com/doi/pdf/10.1049/el.2014.1592. URL: https://ietresearch.onlinelibrary.wiley.com/doi/abs/10.1049/el.2014.1592.

[JNG13] Jiménez, F., Naranjo, J., and García, F. “An Improved Method to Calculate the Time-to-Collision of Two Vehicles”. In: *International Journal of Intelligent Transportation Systems Research* 11 (2013), pp. 34–42.

[Joh14] John, F. “Extremum Problems with Inequalities as Subsidiary Conditions”. In: *Traces and Emergence of Nonlinear Programming*. Ed. by G. Giorgi and T. H. Kjeldsen. Basel: Springer Basel, 2014, pp. 197–215. ISBN: 978-3-0348-0439-4. DOI: 10.1007/978-3-0348-0439-4_9. URL: https://doi.org/10.1007/978-3-0348-0439-4_9.

[JSM20] Jin, W., Salaris, P., and Martinet, P. “Proactive-Cooperative Navigation in Human-Like Environment for Autonomous Robots”. In: *ICINCO 2020 - 17th International Conference on Informatics in Control, Automation and Robotics*. Paris / Online, France, July 2020. URL: https://hal.archives-ouvertes.fr/hal-02899758.

[Jun+16] Juniastuti, S., Fachri, M., Nugroho, S. M. S., and Hariadi, M. “Crowd navigation using leader-follower algorithm based Reciprocal Velocity Obstacles”. In: *International Symposium on Electronics and Smart Devices (ISESD)*. Bandung, Indonesia, 2016, pp. 148–152. DOI: 10.1109/ISESD.2016.7886709.

[KA17] Khambhaita, H. and Alami, R. “A Human-Robot Cooperative Navigation Planner”. In: *Proceedings of the Companion of the 2017 ACM/IEEE International Conference on Human-Robot Interaction*. HRI ’17. Vienna, Austria: ACM, 2017, pp. 161–162. ISBN: 978-1-4503-4885-0. DOI: 10.1145/3029798.3038374. URL: http://doi.acm.org/10.1145/3029798.3038374.

[Kap+13] Kaparias, I., Bell, M. G. H., Dong, W., Sastrawinata, A., Singh, A., Wang, X., and Mount, B. “Analysis of Pedestrian–Vehicle Traffic Conflicts in Street Designs with Elements of Shared Space”. In: *Transportation Research Record: Journal of the Transportation Research Board* 2393.1 (Jan. 2013), pp. 21–30. ISSN: 0361-1981, 2169-4052.

[Kha80] Khatib, O. “Real-time obstacle avoidance for manipulators and mobile robots”. In: *International Journal of Robotics Research* 5 (Jan. 1980), pp. 90–98.

[KI93] Kosko, B. and Isaka, S. “Fuzzy Logic”. In: *Scientific American* 269.1 (1993), pp. 76–81. ISSN: 00368733, 19467087. URL: http://www.jstor.org/stable/24941550.

[KJD18] Kocić, J., Jovičić, N., and Drndarević, V. “Sensors and Sensor Fusion in Autonomous Vehicles”. In: *The 26th Telecommunications Forum (TELFOR)*. 2018, pp. 420–425. DOI: 10.1109/TELFOR.2018.8612054.

[Kru+13] Kruse, T., Pandey, A. K., Alami, R., and Kirsch, A. “Human-Aware Robot Navigation: A Survey”. In: *Robotics and Autonomous Systems* 61.12 (Dec. 2013), pp. 1726–1743. URL: https://hal.archives-ouvertes.fr/hal-01684295.

[KS20] Kibalov, V. and Shipitko, O. “Safe Speed Control and Collision Probability Estimation Under Ego-Pose Uncertainty for Autonomous Vehicle”. In: *IEEE 23rd International Conference on Intelligent Transportation Systems (ITSC)*. 2020, pp. 1–6. DOI: 10.1109/ITSC45102.2020.9294531.

[KZ86] Kant, K. and Zucker, S. “Toward Efficient Trajectory Planning: The Path-Velocity Decomposition”. In: *International Journal of Robotic Research - IJRR* 5 (Sept. 1986), pp. 72–89. DOI: 10.1177/027836498600500304.

[Lam+08] Lambert, A., Gruyer, D., Pierre, G. S., and Ndjeng, A. N. “Collision Probability Assessment for Speed Control”. In: *11th International IEEE Conference on Intelligent Transportation Systems*. 2008, pp. 1043–1048. DOI: 10.1109/ITSC.2008.4732692.

[LaV98] LaValle, S. “Rapidly-exploring random trees : a new tool for path planning”. In: *The annual research report* TR 98–11 (1998).

[LH00] Lu, X.-Y. and Hedrick, K. “Longitudinal control algorithm for automated vehicle merging”. In: *Proceedings of the 39th IEEE Conference on Decision and Control*. Vol. 1. 2000, pp. 450–455. DOI: 10.1109/CDC.2000.912805.

[LH99] Lim, E. and Hedrick, J. “Lateral and longitudinal vehicle control coupling for automated vehicle operation”. In: *Proceedings of the American Control Conference (Cat. No. 99CH36251)*. Vol. 5. 1999, pp. 3676–3680. DOI: 10.1109/ACC.1999.782452.

[Li+20a] Li, J., Yao, L., Xu, X., Cheng, B., and Ren, J. “Deep reinforcement learning for pedestrian collision avoidance and human-machine cooperative driving”. In: *Information Sciences* 532 (2020), pp. 110–124. ISSN: 0020-0255. DOI: https://doi.org/10.1016/j.ins.2020.03.105. URL: https://www.sciencedirect.com/science/article/pii/S0020025520302851.

[Li+20b] Li, Z., Liang, H., Zhao, P., Wang, S., and Zhu, H. “Efficent Lane Change Path Planning based on Quintic spline for Autonomous Vehicles”. In: *2020 IEEE International Conference on Mechatronics and Automation (ICMA)*. 2020, pp. 338–344. DOI: 10.1109/ICMA49215.2020.9233841.

[Li+20c] Li, Z., Liang, H., Zhao, P., Wang, S., and Zhu, H. “Efficent Lane Change Path Planning based on Quintic spline for Autonomous Vehicles”. In: *IEEE International Conference on Mechatronics and Automation (ICMA)*. 2020, pp. 338–344. DOI: 10.1109/ICMA49215.2020.9233841.

[LI20] Li, Y. and Ibanez-Guzman, J. “Lidar for Autonomous Driving: The Principles, Challenges, and Trends for Automotive Lidar and Perception Systems”. In: *IEEE Signal Processing Magazine* 37.4 (2020), pp. 50–61. DOI: 10.1109/MSP.2020.2973615.

[Liu+20] Liu, J., Huang, Z., Xu, X., Zhang, X., Sun, S., and Li, D. “Multi-Kernel Online Reinforcement Learning for Path Tracking Control of Intelligent Vehicles”. In: *IEEE Transactions on Systems, Man, and Cybernetics: Systems* (2020), pp. 1–14. DOI: 10.1109/TSMC.2020.2966631.

[LL18] Le, A. and Le, T. “Search-Based Planning and Replanning in Robotics and Autonomous Systems”. In: *Advanced Path Planning for Mobile Entities*. Ed. by R. Róka. Sept. 2018.

[LS13] Lu, D. V. and Smart, W. D. “Towards more efficient navigation for robots and humans”. In: *IEEE/RSJ International Conference on Intelligent Robots and Systems*. Tokyo, Japan, 2013, pp. 1707–1713. DOI: 10.1109/IROS.2013.6696579.

[LT19] Lorenz, O. and Thomas, U. “Real Time Eye Gaze Tracking System using CNN-based Facial Features for Human Attention Measurement”. In: *Proceedings of the 14th International Joint Conference on Computer Vision, Imaging and Computer Graphics Theory and Applications*. Vol. 5. INSTICC. SciTePress, 2019, pp. 598–606. ISBN: 978-989-758-354-4. DOI: 10.5220/0007565305980606.

[Luo+18] Luo, Y., Cai, P., Bera, A., Hsu, D., Lee, W. S., and Manocha, D. “PORCA: Modeling and Planning for Autonomous Driving Among Many Pedestrians”. In: *IEEE Robotics and Automation Letters* 3.4 (Oct. 2018), pp. 3418–3425. ISSN: 2377-3766, 2377-3774. DOI: 10.1109/LRA.2018.2852793.

[Man+97] Mandow, A., Munoz, V., Fernandez, R., and Garcia-Cerezo, A. “Dynamic speed planning for safe navigation”. In: *Proceedings of the IEEE/RSJ International Conference on Intelligent Robot and Systems (IROS)*. Vol. 1. 1997, pp. 231–237. DOI: 10.1109/IROS.1997.649059.

[Mar50] Marcum, J. I. *Table of Q Functions*. Santa Monica, CA: Rand Corporation: U.S. Air Force RAND Research Memorandum M-339, Jan. 1950.

[Mav+21] Mavrogiannis, C. I., Baldini, F., Wang, A., Zhao, D., Trautman, P., Steinfeld, A., and Oh, J. “Core Challenges of Social Robot Navigation: A Survey”. In: *CoRR* abs/2103.05668 (2021). arXiv: 2103.05668. URL: https://arxiv.org/abs/2103.05668.

[May14] Mayne, D. Q. “Model predictive control: Recent developments and future promise”. In: *Automatica* 50.12 (2014), pp. 2967–2986. ISSN: 0005-1098. DOI: https://doi.org/10.1016/j.automatica.2014.10.128. URL: https://www.sciencedirect.com/science/article/pii/S0005109814005160.

[Men95] Mendel, J. “Fuzzy logic systems for engineering: a tutorial”. In: *Proceedings of the IEEE* 83.3 (1995), pp. 345–377. DOI: 10.1109/5.364485.

[MFO16] Mehta, D., Ferrer, G., and Olson, E. “Autonomous navigation in dynamic social environments using Multi-Policy Decision Making”. In: *IEEE/RSJ International Conference on Intelligent Robots and Systems (IROS)* (2016), pp. 1190–1197.

[MG76] Moore, G. T. and Golledge, R. G. *Environmental Knowing: Theories, Research, and Methods*. Stroudsberg, US: Hutchinson and Ross, 1976.

[Mit+20] Mitov, A., Kralev, J., Slavov, T., and Angelov, I. “Design of H-infinity tracking controller for application in autonomous steering of mobile machines”. In: *19th International Scientific Conference Engineering for Rural Development*. May 2020. DOI: 10.22616/ERDev.2020.19.TF209.

[MKV20] McLaren, L., Koutsombogera, M., and Vogel, C. “A Heuristic Method for Automatic Gaze Detection in Constrained Multi- Modal Dialogue Corpora”. In: *11th IEEE International Conference on Cognitive Infocommunications (CogInfoCom)*. Mariehamn, Finland, 2020, pp. 55–60. DOI: 10.1109/CogInfoCom50765.2020.9237883.

[MM14] Moody, S. and Melia, S. “Shared space – research, policy and problems”. In: *Proceedings of the ICE - Transport* 167 (Nov. 2014), pp. 384–392. DOI: 10.1680/tran.12.00047.

[MMH17] Morales, Y., Miyashita, T., and Hagita, N. “Social robotic wheelchair centered on passenger and pedestrian comfort”. In: *Robotics and Autonomous Systems* 87 (2017), pp. 355–362. ISSN: 0921-8890. DOI: https://doi.org/10.1016/j.robot.2016.09.010. URL: https://www.sciencedirect.com/science/article/pii/S092188901630570X.

[MT00] Martinet, P. and Thibaud, C. “Automatic Guided Vehicles: Robust Controller Design in Image Space”. In: *Autonomous Robots* 8.1 (Jan. 2000), pp. 25–42. DOI: 10.1023/A:1008936817917. URL: https://hal.inria.fr/hal-02465656.

[MTK18] Mavrogiannis, C. I., Thomason, W. B., and Knepper, R. A. “Social Momentum: A Framework for Legible Navigation in Dynamic Multi-Agent Environments”. In: *Proceedings of the 2018 ACM/IEEE International Conference on Human-Robot Interaction*. HRI ’18. Chicago, IL, USA: Association for Computing Machinery, 2018, pp. 361–369. ISBN: 9781450349536. DOI: 10.1145/3171221.3171255. URL: https://doi.org/10.1145/3171221.3171255.

[MTM15] Møgelmose, A., Trivedi, M. M., and Moeslund, T. B. "Trajectory analysis and prediction for improved pedestrian safety: Integrated framework and evaluations". In: *IEEE Intelligent Vehicles Symposium (IV)*. 2015, pp. 330–335. DOI: 10.1109/IVS.2015.7225707.

[Mül+08] Müller, J., Stachniss, C., Arras, K., and Burgard, W. "Socially Inspired Motion Planning for Mobile Robots in Populated Environments". In: Jan. 2008.

[MV21] Mendzina, E. and Vugule, K. "Importance and planning of pedestrian streets in urban environment". In: *Landscape architecture and art* 16 (Apr. 2021), pp. 80–86. DOI: 10.22616/j.landarchart.2020.16.08.

[MVL07] Muñoz, N. D., Valencia, J. A., and Londoño, N. "Evaluation of Navigation of an Autonomous Mobile Robot". In: *Proceedings of the 2007 Workshop on Performance Metrics for Intelligent Systems*. PerMIS '07. Washington, D.C.: Association for Computing Machinery, 2007, pp. 15–21. ISBN: 9781595938541.

[Nas+13] Naseralavi, S., Nadimi, N., Saffarzadeh, M., and Mamdoohi, A. R. "A general formulation for time-to-collision safety indicator". In: *Proceedings of the ICE - Transport* 166 (Oct. 2013), pp. 294–304. DOI: 10.1680/tran.11.00031.

[NKH16] Noreen, I., Khan, A., and Habib, Z. "Optimal Path Planning using RRT* based Approaches: A Survey and Future Directions". In: *International Journal of Advanced Computer Science and Applications* 7.11 (2016). DOI: 10.14569/IJACSA.2016.071114. URL: http://dx.doi.org/10.14569/IJACSA.2016.071114.

[Now06] Nowak, M. A. "Five Rules for the Evolution of Cooperation". In: *Science* 314.5805 (Dec. 2006), pp. 1560–1563. ISSN: 0036-8075. DOI: 10.1126/science.1133755. eprint: https://science.sciencemag.org/content/314/5805/1560.full.pdf. URL: https://science.sciencemag.org/content/314/5805/1560.

[NS92] Nagel, K. and Schreckenberg, M. "A cellular automaton model for freeway traffic". In: *Journal de Physique I* 2.12 (1992), pp. 2221–2229. DOI: 10.1051/jp1:1992277. URL: https://hal.archives-ouvertes.fr/jpa-00246697.

[NSB16] Narayanan, V. K., Spalanzani, A., and Babel, M. "A semi-autonomous framework for human-aware and user intention driven wheelchair mobility assistance". In: *IEEE/RSJ International Conference on Intelligent Robots and Systems (IROS)*. 2016, pp. 4700–4707. DOI: 10.1109/IROS.2016.7759691.

[Oli+20] Oliveira, R., Ljungqvist, O., Lima, P. F., and Wahlberg, B. "Optimization-Based On-Road Path Planning for Articulated Vehicles". In: *CoRR* abs/2001.06827 (2020). arXiv: 2001.06827. URL: https://arxiv.org/abs/2001.06827.

[Pad+16] Paden, B., Čáp, M., Yong, S. Z., Yershov, D., and Frazzoli, E. "A Survey of Motion Planning and Control Techniques for Self-Driving Urban Vehicles". In: *IEEE Transactions on Intelligent Vehicles* 1.1 (2016), pp. 33–55. DOI: 10.1109/TIV.2016.2578706.

[Pas+14] Pasteau, F., K. Narayanan, V., Babel, M., and Chaumette, F. "A visual servoing approach for autonomous corridor following and doorway passing in a wheelchair". In: *Robotics and Autonomous Systems* 75 (Sept. 2014), pp. 28–40. DOI: 10.1016/j.robot.2014.10.017.

[Pas20] Pascucci, F. “A microsimulation based method to evaluate shared space performances”. PhD thesis. Braunschweig, Germany: Technische Universität Braunschweig, 2020.

[Pol+17] Polack, P., Altché, F., Novel, B., and La Fortelle, A. de. “The kinematic bicycle model: A consistent model for planning feasible trajectories for autonomous vehicles?” In: *IEEE Intelligent Vehicles Symposium (IV)*. June 2017, pp. 812–818. DOI: 10.1109/IVS.2017.7995816.

[Pou+17] Pourseif, T., andani, M. taheri, Ramezani, Z., and Pourgholi, M. “Model Reference Adaptive Control for Robot Tracking Problem: Design Performance Analysis”. In: *International Journal of Control Science and Engineering* 7 (Jan. 2017), pp. 18–23. DOI: 10.5923/j.control.20170701.03.

[Pré21] Prédhumeau, M. “Simulating Realistic Pedestrian Behaviors in the Context of Autonomous Vehicles in Shared Spaces: Doctoral Consortium”. In: *Proc. of the 20th International Conference on Autonomous Agents and Multiagent Systems (AAMAS 2021)*. Jan. 2021.

[Ran+19] Randhavane, T., Bera, A., Kubin, E., Wang, A., Gray, K., and Manocha, D. “Pedestrian Dominance Modeling for Socially-Aware Robot Navigation”. In: *CoRR* abs/1810.06613 (May 2019), pp. 5621–5628. arXiv: 1810.06613. URL: http://arxiv.org/abs/1810.06613.

[Ras+19] Rasouli, A., Kotseruba, I., Kunic, T., and Tsotsos, J. K. “PIE: A Large-Scale Dataset and Models for Pedestrian Intention Estimation and Trajectory Prediction”. In: *Proceedings of the IEEE/CVF International Conference on Computer Vision (ICCV)*. Seoul, South Korea, Oct. 2019. ISBN: 978-1-7281-4804-5.

[Rid+18a] Ridel, D., Rehder, E., Lauer, M., Stiller, C., and Wolf, D. “A Literature Review on the Prediction of Pedestrian Behavior in Urban Scenarios”. In: *IEEE 21st International Conference on Intelligent Transportation Systems (ITSC)*. Maui, HI, USA, 2018, pp. 3105–3112. DOI: 10.1109/ITSC.2018.8569415.

[Rid+18b] Ridel, D., Rehder, E., Lauer, M., Stiller, C., and Wolf, D. “A Literature Review on the Prediction of Pedestrian Behavior in Urban Scenarios”. In: *2018 21st International Conference on Intelligent Transportation Systems (ITSC)*. 2018, pp. 3105–3112. DOI: 10.1109/ITSC.2018.8569415.

[RKS18] Radmanesh, M., Kumar, M., and Sarim, M. “Grey wolf optimization based sense and avoid algorithm in a Bayesian framework for multiple UAV path planning in an uncertain environment”. In: *Aerospace Science and Technology* 77 (2018), pp. 168–179. ISSN: 1270-9638. DOI: https://doi.org/10.1016/j.ast.2018.02.031. URL: https://www.sciencedirect.com/science/article/pii/S1270963817308994.

[Rob+16] Robicquet, A., Sadeghian, A., Alahi, A., and Savarese, S. “Learning Social Etiquette: Human Trajectory Understanding In Crowded Scenes”. In: *Computer Vision (ECCV)*. Ed. by B. Leibe, J. Matas, N. Sebe, and M. Welling. Cham: Springer International Publishing, 2016, pp. 549–565. ISBN: 978-3-319-46484-8.

[Roe+12] Roesmann, C., Feiten, W., Woesch, T., Hoffmann, F., and Bertram, T. "Trajectory modification considering dynamic constraints of autonomous robots". In: *7th German Conference on Robotics (ROBOTIK)*. Munich, Germany, 2012, pp. 1–6.

[Ros+19] Rosique, F., Navarro, P. J., Fernández, C., and Padilla, A. "A Systematic Review of Perception System and Simulators for Autonomous Vehicles Research". In: *Sensors* 19.3 (2019). ISSN: 1424-8220. DOI: 10.3390/s19030648. URL: https://www.mdpi.com/1424-8220/19/3/648.

[Ros00] Ross, T. J. "Membership Functions, Fuzzification and Defuzzification". In: *Fuzzy Systems in Medicine, Studies in Fuzziness and Soft Computing. Physica, Heidelberg*. Vol. 41. 2000. DOI: https://doi.org/10.1007/978-3-7908-1859-8_3.

[RS12] Rios, L. and Sahinidis, N. "Derivative-free optimization: A review of algorithms and comparison of software implementations". In: *Journal of Global Optimization* 56 (Nov. 2012), pp. 1247–1293. DOI: 10.1007/s10898-012-9951-y.

[RSL11] Rios-Martinez, J., Spalanzani, A., and Laugier, C. "Understanding human interaction for probabilistic autonomous navigation using Risk-RRT approach". In: *IEEE/RSJ International Conference on Intelligent Robots and Systems*. 2011, pp. 2014–2019. DOI: 10.1109/IROS.2011.6094496.

[RSL15] Rios-Martinez, J., Spalanzani, A., and Laugier, C. "From Proxemics Theory to Socially-Aware Navigation: A Survey". In: *International Journal of Social Robotics* (Apr. 2015). DOI: 10.1007/s12369-014-0251-1. URL: https://hal.inria.fr/hal-01067278.

[Rud+20] Rudenko, A., Palmieri, L., Herman, M., Kitani, K. M., Gavrila, D. M., and Arras, K. O. "Human motion trajectory prediction: a survey". In: *The International Journal of Robotics Research* 39.8 (2020), pp. 895–935. DOI: 10.1177/0278364920917446.

[Sat+20] Sathyamoorthy, A. J., Patel, U., Guan, T., and Manocha, D. *Frozone: Freezing-Free, Pedestrian-Friendly Navigation in Human Crowds*. 2020. arXiv: 2003.05395 [cs.RO].

[Sch18] Schofield, R. T. "Potential Fields Navigation of Lifeguard Assistant Robot for Mass Marine Casualty Response". MA thesis. Undergraduate Research Scholars Program: Texas AM University, May 2018.

[SD90] Sheikholeslam, S. and Desoer, C. A. "Longitudinal Control of a Platoon of Vehicles". In: *American Control Conference*. 1990, pp. 291–296. DOI: 10.23919/ACC.1990.4790743.

[Sem+19] Semmens, R., Martelaro, N., Kaveti, P., Stent, S., and Ju, W. "Is Now A Good Time An Empirical Study of Vehicle Driver Communication Timing". In: *ACM CHI Conference on Human Factors in Computing Systems*. Glasgow, UK, May 2019. DOI: 10.1145/3290605.3300867.

[SF09] Schmidt, S. and Färber, B. "Pedestrians at the kerb – Recognising the action intentions of humans". In: *Transportation Research Part F: Traffic Psychology and Behaviour* 12.4 (2009), pp. 300–310. ISSN: 1369-8478. DOI: https://doi.org/10.1016/j.trf.2009.02.003. URL: https://www.sciencedirect.com/science/article/pii/S1369847809000102.

[SFA21] Singamaneni, P. T., Favier, A., and Alami, R. "Human-Aware Navigation Planner for Diverse Human-Robot Contexts". In: *CoRR* abs/2106.09971 (2021). arXiv: 2106.09971. URL: https://arxiv.org/abs/2106.09971.

[Sha+20] Shan, Y., Zheng, B., Chen, L., Chen, L., and Chen, D. "A Reinforcement Learning-Based Adaptive Path Tracking Approach for Autonomous Driving". In: *IEEE Transactions on Vehicular Technology* 69.10 (2020), pp. 10581–10595. DOI: 10.1109/TVT.2020.3014628.

[Sha12] Shan, C. "Learning Human Emotion from Body Gesture". In: *Encyclopedia of the Sciences of Learning*. Ed. by N. M. Seel. Boston, MA: Springer US, 2012, pp. 1887–1889. ISBN: 978-1-4419-1428-6. DOI: 10.1007/978-1-4419-1428-6_1905. URL: https://doi.org/10.1007/978-1-4419-1428-6_1905.

[Shi+17] Shi, W., Alawieh, M. B., Li, X., and Yu, H. "Algorithm and hardware implementation for visual perception system in autonomous vehicle: A survey". In: *Integration* 59 (2017), pp. 148–156. ISSN: 0167-9260. DOI: https://doi.org/10.1016/j.vlsi.2017.07.007. URL: https://www.sciencedirect.com/science/article/pii/S0167926017303218.

[Ski16] Skinner Rachel, B. N. *Making better places: Autonomous vehicles and future opportunities*. Tech. rep. WSP Parsons Brinckerhoff & Farrells, 2016.

[SMT20] Sinapayen, L., Masumori, A., and Takashi, I. *Reactive, Proactive, and Inductive Agents: An evolutionary path for biological and artificial spiking networks*. 2020.

[SN08] Sakurama, K. and Nakano, K. "Leader-Following Formation Navigation for Multiple Robots with Collision Avoidance". In: *IFAC Proceedings Volumes* 41.2 (2008). 17th IFAC World Congress, pp. 12099–12104. ISSN: 1474-6670. DOI: https://doi.org/10.3182/20080706-5-KR-1001.02049. URL: https://www.sciencedirect.com/science/article/pii/S1474667016409158.

[Ste+16a] Stein, P., Spalanzani, A., Santos, V., and Laugier, C. "Leader following: A study on classification and selection". In: *Robotics and Autonomous Systems* 75 (2016). Assistance and Service Robotics in a Human Environment, pp. 79–95. ISSN: 0921-8890. DOI: https://doi.org/10.1016/j.robot.2014.09.028. URL: https://www.sciencedirect.com/science/article/pii/S0921889014002139.

[Ste+16b] Stein, P., Spalanzani, A., Santos, V., and Laugier, C. "Leader following: A study on classification and selection". In: *Robotics and Autonomous Systems* 75 (2016). Assistance and Service Robotics in a Human Environment, pp. 79–95. ISSN: 0921-8890. DOI: https://doi.org/10.1016/j.robot.2014.09.028. URL: https://www.sciencedirect.com/science/article/pii/S0921889014002139.

[Ste+19] Stern, R. E., Chen, Y., Churchill, M., Wu, F., Delle Monache, M. L., Piccoli, B., Seibold, B., Sprinkle, J., and Work, D. B. "Quantifying air quality benefits resulting from few autonomous vehicles stabilizing traffic". In: *Transportation Research Part D: Transport and Environment* 67 (2019), pp. 351–365. ISSN: 1361-9209. DOI: https://doi.org/10.1016/j.trd.2018.12.008. URL: https://www.sciencedirect.com/science/article/pii/S1361920918304383.

[Sto18] Stowers, D. T. “Creating Legible Robotic Motion via Local Planning”. MA thesis. Georgia Institute of Technology, Apr. 2018.

[SU16] Swikir, A. and Utkin, V. “Chattering analysis of conventional and super twisting sliding mode control algorithm”. In: *2016 14th International Workshop on Variable Structure Systems (VSS)*. 2016, pp. 98–102. DOI: 10.1109/VSS.2016.7506898.

[Sun+21] Sun, X., Deng, S., Zhao, T., and Tong, B. “Motion planning approach for car-like robots in unstructured scenario”. In: *Transactions of the Institute of Measurement and Control* (Mar. 2021). DOI: 10.1177/0142331221994393. eprint: https://doi.org/10.1177/0142331221994393. URL: https://doi.org/10.1177/0142331221994393.

[SW14] Savkin, A. V. and Wang, C. “Seeking a path through the crowd: Robot navigation in unknown dynamic environments with moving obstacles based on an integrated environment representation”. In: *Robotics and Autonomous Systems* 62.10 (2014), pp. 1568–1580. ISSN: 0921-8890. DOI: https://doi.org/10.1016/j.robot.2014.05.006. URL: https://www.sciencedirect.com/science/article/pii/S0921889014000955.

[SXV20] Smith, J. S., Xu, R., and Vela, P. “egoTEB: Egocentric, Perception Space Navigation Using Timed-Elastic-Bands”. In: *IEEE International Conference on Robotics and Automation (ICRA)*. Paris, France, 2020, pp. 2703–2709. DOI: 10.1109/ICRA40945.2020.9196721.

[Tek16] Teknomo, K. “Microscopic Pedestrian Flow Characteristics: Development of an Image Processing Data Collection and Simulation Model”. In: *CoRR* 29 (2016).

[Thu+04] Thuilot, B., Bom, J., Marmoiton, F., and Martinet, P. “Accurate automatic guidance of an urban electric vehicle relying on a kinematic GPS sensor”. In: *IFAC Proceedings Volumes* 37.8 (2004). IFAC/EURON Symposium on Intelligent Autonomous Vehicles. Lisbon, Portugal, pp. 155–160. ISSN: 1474-6670. DOI: https://doi.org/10.1016/S1474-6670(17)31968-7. URL: https://www.sciencedirect.com/science/article/pii/S1474667017319687.

[Tik43] Tikhonov, A. N. “On the stability of inverse problems”. In: *Doklady Akademii Nauk SSSR* 39 (5) (1943), pp. 195–198.

[TK10] Trautman, P. and Krause, A. “Unfreezing the robot: Navigation in dense, interacting crowds”. In: *IEEE/RSJ International Conference on Intelligent Robots and Systems*. 2010, pp. 797–803. DOI: 10.1109/IROS.2010.5654369.

[TP20] Trautman, P. and Patel, K. “Real Time Crowd Navigation from First Principles of Probability Theory”. In: *Proceedings of the Thirtieth International Conference on Automated Planning and Scheduling, Nancy, France, October 26-30, 2020*. Ed. by J. C. Beck, O. Buffet, J. Hoffmann, E. Karpas, and S. Sohrabi. AAAI Press, 2020, pp. 459–468. URL: https://aaai.org/ojs/index.php/ICAPS/article/view/6741.

[TS16] Tageldin, A. and Sayed, T. “Developing evasive action-based indicators for identifying pedestrian conflicts in less organized traffic environments: Developing Evasive Action-Based Indicators”. In: *Journal of Advanced Transportation* 50.6 (Oct. 2016), pp. 1193–1208. ISSN: 01976729. (Visited on 01/06/2021).

[Urd+07] Urdiales, C., Poncela, A., Sanchez-Tato, I., Galluppi, F., Olivetti, M., and Sandoval, F. “Efficiency based reactive shared control for collaborative human/robot navigation”. In: *IEEE/RSJ International Conference on Intelligent Robots and Systems*. 2007, pp. 3586–3591. DOI: 10.1109/IROS.2007.4399288.

[Vas16] Vasquez, D. “Novel planning-based algorithms for human motion prediction”. In: *IEEE International Conference on Robotics and Automation (ICRA)*. 2016, pp. 3317–3322. DOI: 10.1109/ICRA.2016.7487505.

[Vic+17] Victerpaul, P., Devaraj, S., Subbiah, J., and Jayabala, P. “Path planning of autonomous mobile robots: A survey and comparison”. In: *Journal of Advanced Research in Dynamical and Control Systems* 9.12 (Jan. 2017), pp. 1535–1565.

[VMO17a] Vemula, A., Muelling, K., and Oh, J. “Modeling cooperative navigation in dense human crowds”. In: *IEEE International Conference on Robotics and Automation, Singapore*. May 2017, pp. 1685–1692. DOI: 10.1109/ICRA.2017.7989199.

[VMO17b] Vemula, A., Muelling, K., and Oh, J. “Modeling cooperative navigation in dense human crowds”. In: *IEEE International Conference on Robotics and Automation (ICRA)* (2017), pp. 1685–1692.

[Völ+16] Völz, B., Behrendt, K., Mielenz, H., Gilitschenski, I., Siegwart, R., and Nieto, J. “A data-driven approach for pedestrian intention estimation”. In: *IEEE 19th International Conference on Intelligent Transportation Systems (ITSC)*. Rio de Janeiro, Brazil, 2016, pp. 2607–2612. DOI: 10.1109/ITSC.2016.7795975.

[Wan+13] Wang, Z., Mülling, K., Deisenroth, M. P., Amor, H. B., Vogt, D., Schölkopf, B., and Peters, J. “Probabilistic movement modeling for intention inference in human–robot interaction”. In: *The International Journal of Robotics Research* 32.7 (2013), pp. 841–858. DOI: 10.1177/0278364913478447. eprint: https://doi.org/10.1177/0278364913478447. URL: https://doi.org/10.1177/0278364913478447.

[WCM18] Wang, Y., Chardonnet, J.-R., and Merienne, F. “Speed Profile Optimization for Enhanced Passenger Comfort: An Optimal Control Approach”. In: *21st International Conference on Intelligent Transportation Systems (ITSC)*. Maui, HI, USA, 2018, pp. 723–728. DOI: 10.1109/ITSC.2018.8569420.

[XP20] Xu, S. and Peng, H. “Design, Analysis, and Experiments of Preview Path Tracking Control for Autonomous Vehicles”. In: *IEEE Transactions on Intelligent Transportation Systems* 21.1 (2020), pp. 48–58. DOI: 10.1109/TITS.2019.2892926.

[Xu+12] Xu, W., Wei, J., Dolan, J. M., Zhao, H., and Zha, H. “A real-time motion planner with trajectory optimization for autonomous vehicles”. In: *IEEE International Conference on Robotics and Automation (ICRA)*. Saint Paul, MN, USA, 2012, pp. 2061–2067. DOI: 10.1109/ICRA.2012.6225063.

[Xu+19] Xu, B., Li, J., Wong, Y., Kankanhalli, M. S., and Zhao, Q. *Interact as You Intend: Intention-Driven Human-Object Interaction Detection*. 2019. arXiv: 1808.09796 [cs.CV].

[Yan+19] Yang, D., Li, L., Redmill, K., and Ozguner, U. “Top-view Trajectories: A Pedestrian Dataset of Vehicle-Crowd Interaction from Controlled Experiments and Crowded Campus”. In: *IEEE Intelligent Vehicles Symposium (IV)* (June 2019), pp. 899–904. DOI: 10.1109/ivs.2019.8814092. URL: http://dx.doi.org/10.1109/IVS.2019.8814092.

[Yaq+20] Yaqoob, I., Khan, L. U., Kazmi, S. M. A., Imran, M., Guizani, N., and Hong, C. S. “Autonomous Driving Cars in Smart Cities: Recent Advances, Requirements, and Challenges”. In: *IEEE Network* 34.1 (2020), pp. 174–181. DOI: 10.1109/MNET.2019.1900120.

[Ye+19] Ye, H., Jiang, H., Ma, S., Tang, B., and Wahab, L. “Linear model predictive control of automatic parking path tracking with soft constraints”. In: *International Journal of Advanced Robotic Systems* 16.3 (2019), pp. 1–13. DOI: 10.1177/1729881419852201.

[Yim+20] Yimer, T. H., Wen, C., Yu, X., and Jiang, C. *A Study of the Minimum Safe Distance between Human Driven and Driverless Cars Using Safe Distance Model*. 2020. arXiv: 2006.07022 [cs.RO].

[YOR18] Yang, D., Ozguner, U., and Redmill, K. “Social Force Based Microscopic Modeling of Vehicle-Crowd Interaction”. In: *IEEE Intelligent Vehicles Symposium (IV)*. Changshu, China, June 2018, pp. 1537–1542. DOI: 10.1109/IVS.2018.8500499.

[YT16] Yadron, D. and Tynan, D. *Tesla driver dies in first fatal crash while using autopilot mode*. Ed. by T. Guardian. [Online; posted 1st Jul 2016]. July 2016. URL: https://www.theguardian.com/technology/2016/jun/30/tesla-autopilot-death-self-driving-car-elon-musk.

[Zad65] Zadeh, L. “Fuzzy sets”. In: *Information and Control* 8.3 (1965), pp. 338–353. ISSN: 0019-9958. DOI: https://doi.org/10.1016/S0019-9958(65)90241-X. URL: https://www.sciencedirect.com/science/article/pii/S001999586590241X.

[Zen+19] Zeng, D., Yu, Z., Xiong, L., Zhao, J., Zhang, P., Li, Z., Fu, Z., Yao, J., and Zhou, Y. “A Novel Robust Lane Change Trajectory Planning Method for Autonomous Vehicle”. In: *IEEE Intelligent Vehicles Symposium (IV)*. 2019, pp. 486–493. DOI: 10.1109/IVS.2019.8814151.

[Zha+12] Zhao, P., Chen, J., Song, Y., Tao, X., Xu, T., and Mei, T. “Design of a Control System for an Autonomous Vehicle Based on Adaptive-PID”. In: *International Journal of Advanced Robotic Systems* 9 (July 2012), pp. 44–55. DOI: 10.5772/51314.

[Zha+17] Zhang, X., Zhang, X., Wang, Y., and Yu, H. “Extended social force model-based mean shift for pedestrian tracking under obstacle avoidance”. In: *IET Computer Vision* 11.1 (2017), pp. 1–9. DOI: https://doi.org/10.1049/iet-cvi.2016.0022. eprint: https://ietresearch.onlinelibrary.wiley.com/doi/pdf/10.1049/iet-cvi.2016.0022. URL: https://ietresearch.onlinelibrary.wiley.com/doi/abs/10.1049/iet-cvi.2016.0022.

[Zho+19] Zhong, Y., Guo, L., Zhang, Y., Liu, Q., and Chen, H. “Optimal Lane Change Control of Intelligent Vehicle Based on MPC”. In: *Chinese Control And Decision Conference (CCDC)*. 2019, pp. 1468–1473. DOI: 10.1109/CCDC.2019.8833003.

[Zho+21] Zhou, R., Cui, Y., Wang, Y., and Jiang, J. “A modified social force model with different categories of pedestrians for subway station evacuation”. In: *Tunnelling and Underground Space Technology* 110.3 (Apr. 2021). ISSN: 0886-7798. DOI: https://doi.org/10.1016/j.tust.2021.103837. URL: https://www.sciencedirect.com/science/article/pii/S0886779821000286.

[Zie+17] Ziebinski, A., Cupek, R., Grzechca, D., and Chruszczyk, L. “Review of advanced driver assistance systems (ADAS)”. In: *AIP Conference Proceedings* 1906.1 (2017), p. 120002. DOI: 10.1063/1.5012394.

[ZLC18] Zhang, H.-y., Lin, W.-m., and Chen, A.-x. “Path Planning for the Mobile Robot: A Review”. In: *Symmetry* 10.10 (2018), pp. 450–467. ISSN: 2073-8994. DOI: 10.3390/sym10100450. URL: https://www.mdpi.com/2073-8994/10/10/450.

[ZLT94] Zapata, R., Lépinay, P., and Thompson, P. “Reactive behaviors of fast mobile robots”. In: *Journal of Robotic Systems* 11.1 (1994), pp. 13–20. DOI: 10.1002/rob.4620110104. eprint: https://onlinelibrary.wiley.com/doi/pdf/10.1002/rob.4620110104. URL: https://onlinelibrary.wiley.com/doi/abs/10.1002/rob.4620110104.

[ZMK21] Zafar, M., Mohanta, J., and Keshari, A. “GWO-Potential Field Method for Mobile Robot Path Planning and Navigation Control”. In: *Arabian Journal for Science and Engineering volume* 55 (46 2021), pp. 8087–8104. DOI: 10.1007/s13369-021-05487-w.

[ZS10] Ziegler, J. and Stiller, C. “Fast collision checking for intelligent vehicle motion planning”. In: *IEEE Intelligent Vehicles Symposium (IV)*. La Jolla, CA, USA, 2010, pp. 518–522. DOI: 10.1109/IVS.2010.5547976.

[ZWT12] Zhou, B., Wang, X., and Tang, X. “Understanding collective crowd behaviors: Learning a Mixture model of Dynamic pedestrian-Agents”. In: *IEEE Conference on Computer Vision and Pattern Recognition*. Providence, RI, USA, 2012, pp. 2871–2878. DOI: 10.1109/CVPR.2012.6248013.

A

Collected Pedestrian-Vehicle Interaction Data: Visualization

This appendix includes a visualization of the recorded trajectories during the experiment performed at the parking lot of the LS2N lab on the École Centrale de Nantes campus (Sec. 3.5). Seventeen volunteers interact with a Renault Fluence vehicle with a driver behind the wheel, during the experiment. The data is collected on board of the vehicle using a perception system consisting of: 4 Camera, 1 Velodyne (VLP-16), 1 IMU and 1 GPS.

The experiment is comprised of 5 different interaction scenarios: Frontal, Back, Frontal-Back, Lateral, Bi-lateral and Shared Space scenarios. Each volunteer is given a start and goal point in the space and is asked to move in a free and natural way. The driver is asked to move to a goal point as well with one of two driving patterns: an aggressive driving pattern and a more yielding driving pattern where the priority is given to the pedestrians.

In the following we presented the recorded trajectories in the XY plane for both the vehicle and the pedestrians in the different interaction scenarios. The driving behavior adapted in each scenarios (Yielding or Aggressive) is indicated below each figure.

Firstly, the three recorded bi-lateral crossing scenarios are shown in Fig. A.1 – Fig. A.3.

Secondly, the five recorded uni-lateral crossing scenarios are shown in Fig. A.4 – Fig. A.8.

Thirdly, the nine recorded frontal crossing scenarios are shown in Fig. A.9 – Fig. A.17.

Fourthly, the two recorded back crossing scenarios are shown in Fig. A.18 and Fig. A.19.

Then, the two recorded frontal-back crossing scenarios are shown in Fig. A.20 and Fig. A.21.

Finally, the five recorded shared space scenarios are shown in Fig. A.22 – Fig. A.26.

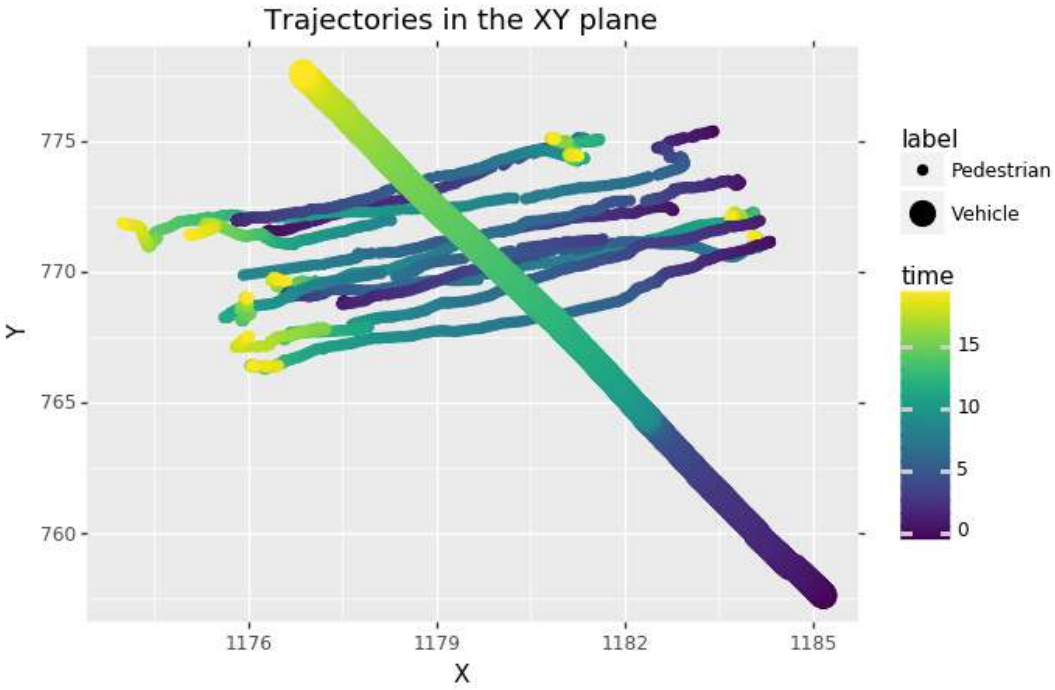

Fig. A.1.: Bi-Lateral Crossing 1: Yielding Driver

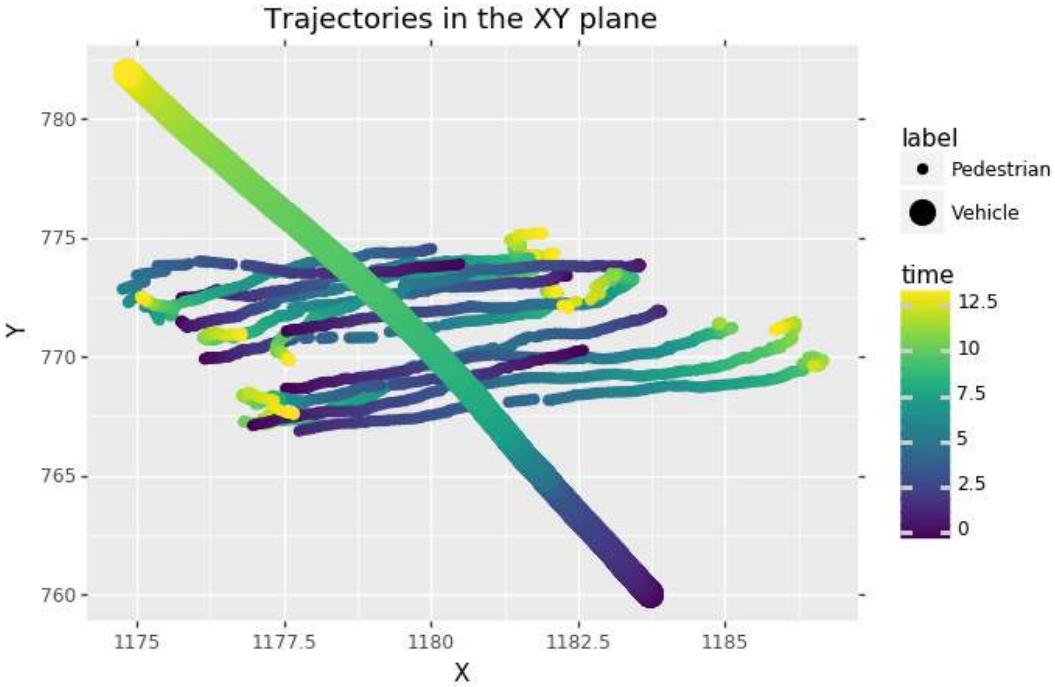

Fig. A.2.: Bi-Lateral Crossing 2: Aggressive Driver

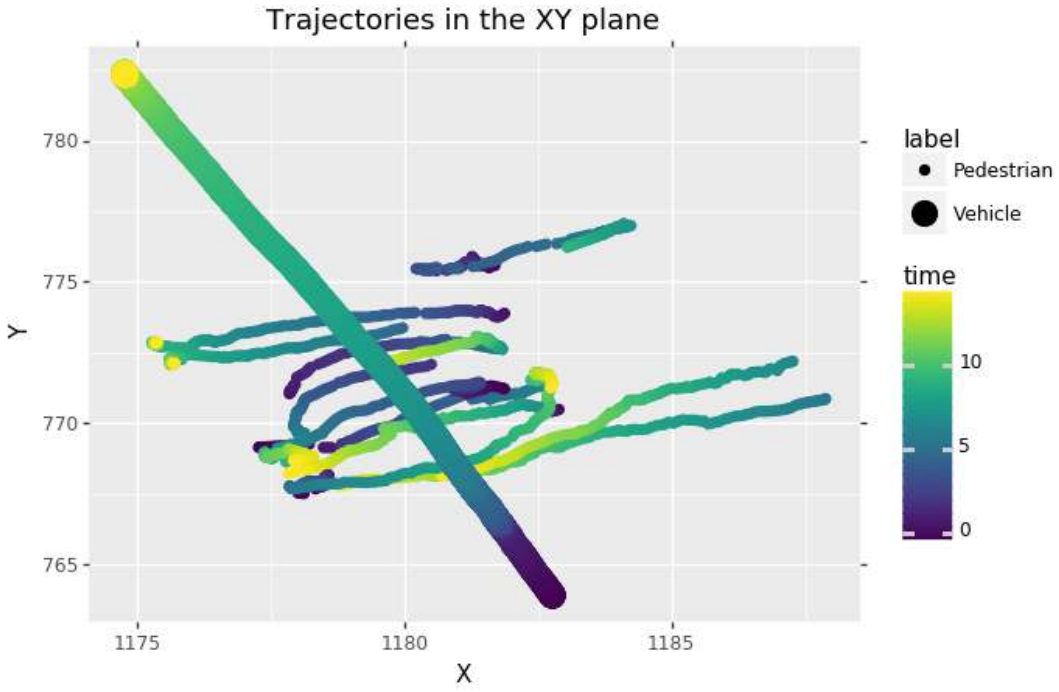

Fig. A.3.: Bi-Lateral Crossing 3: Aggressive Driver

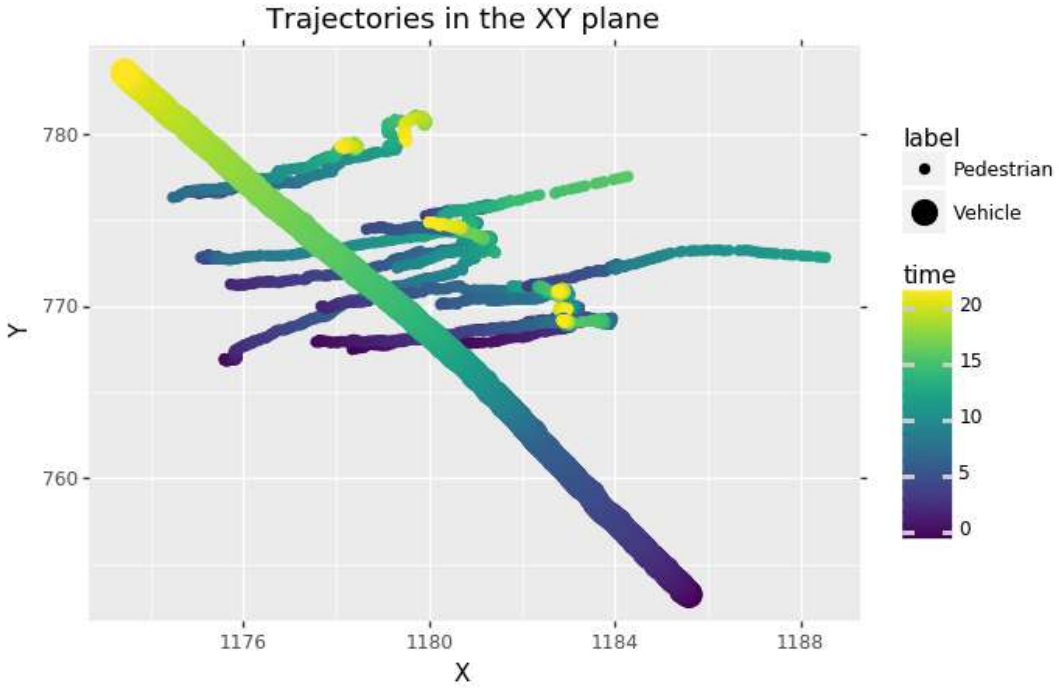

Fig. A.4.: Lateral Crossing 1: Yielding Driver

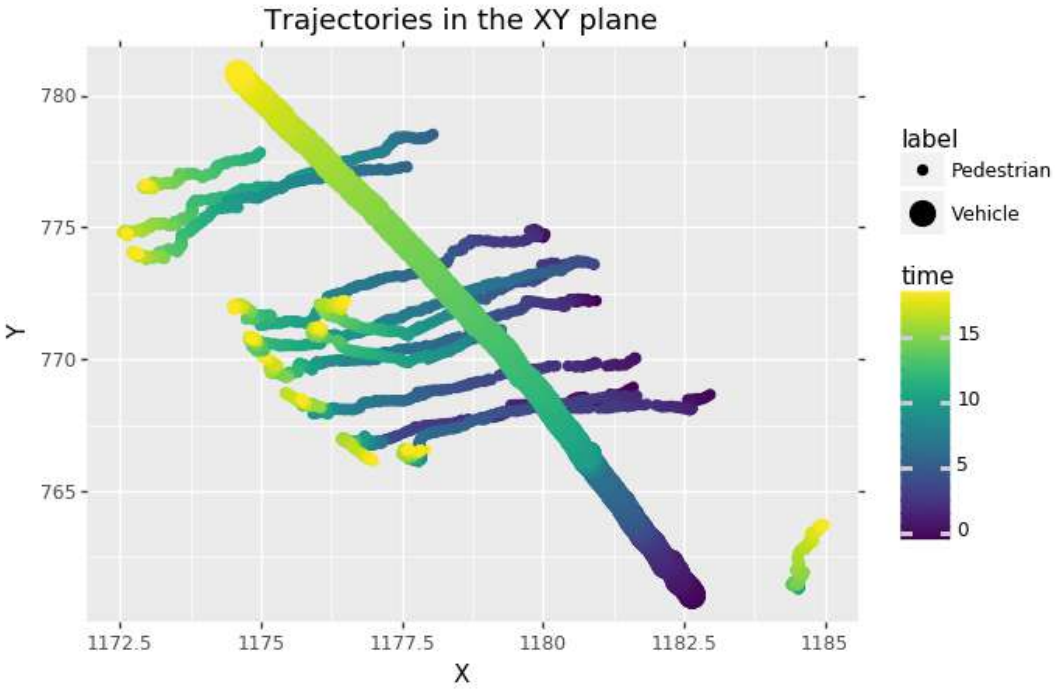

Fig. A.5.: Lateral Crossing 2: Aggressive Driver

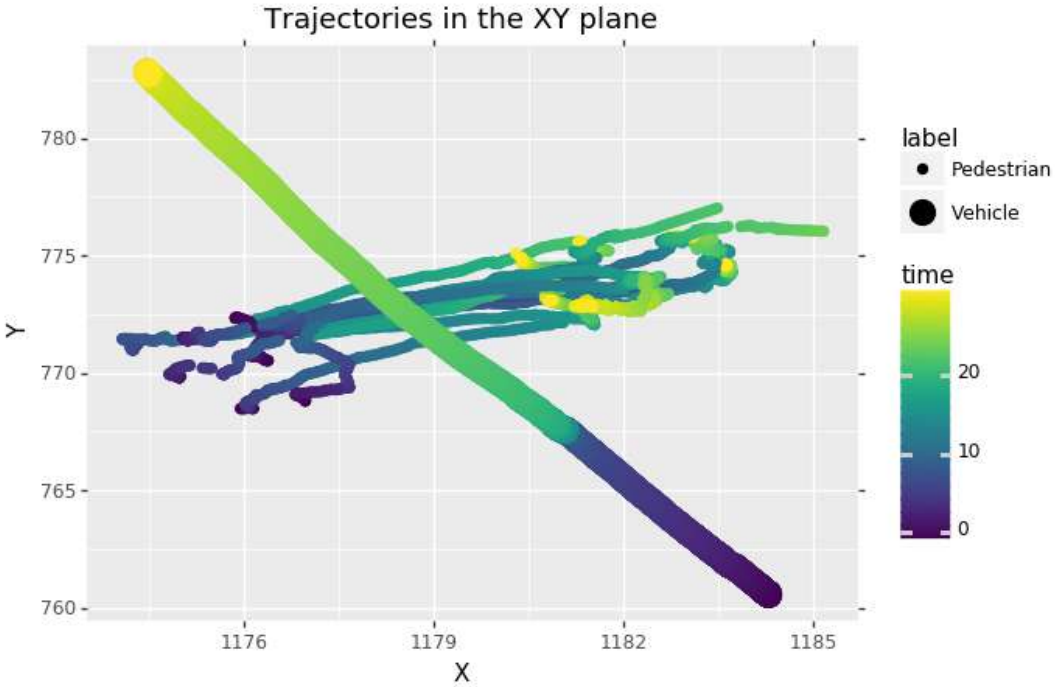

Fig. A.6.: Lateral Crossing 3: Yielding Driver

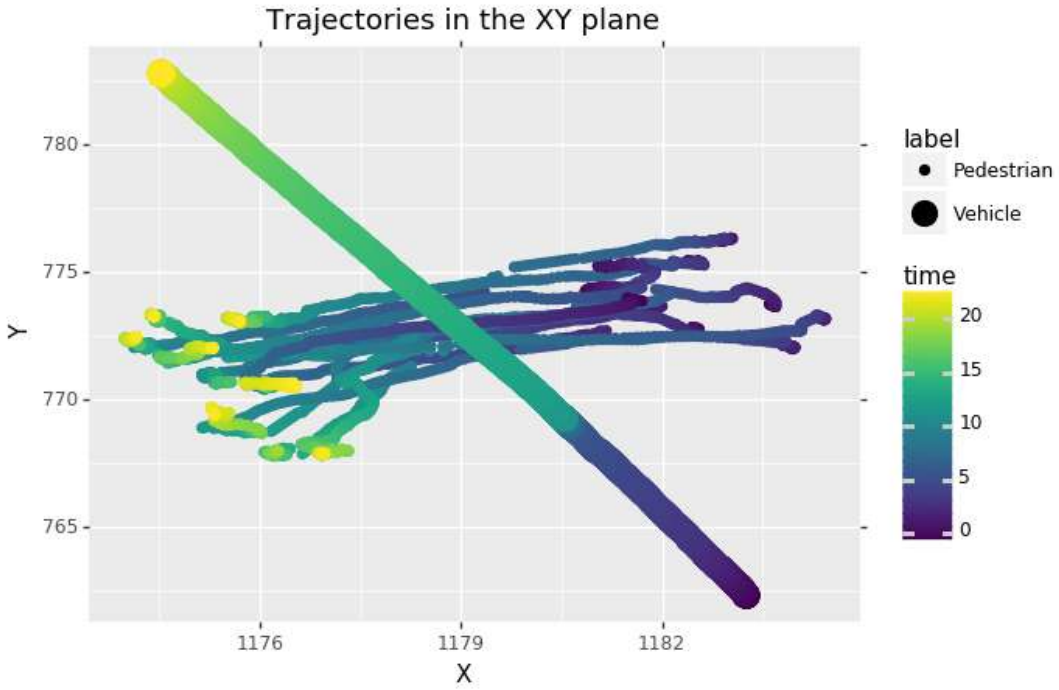

Fig. A.7.: Lateral Crossing 4: Aggressive Driver

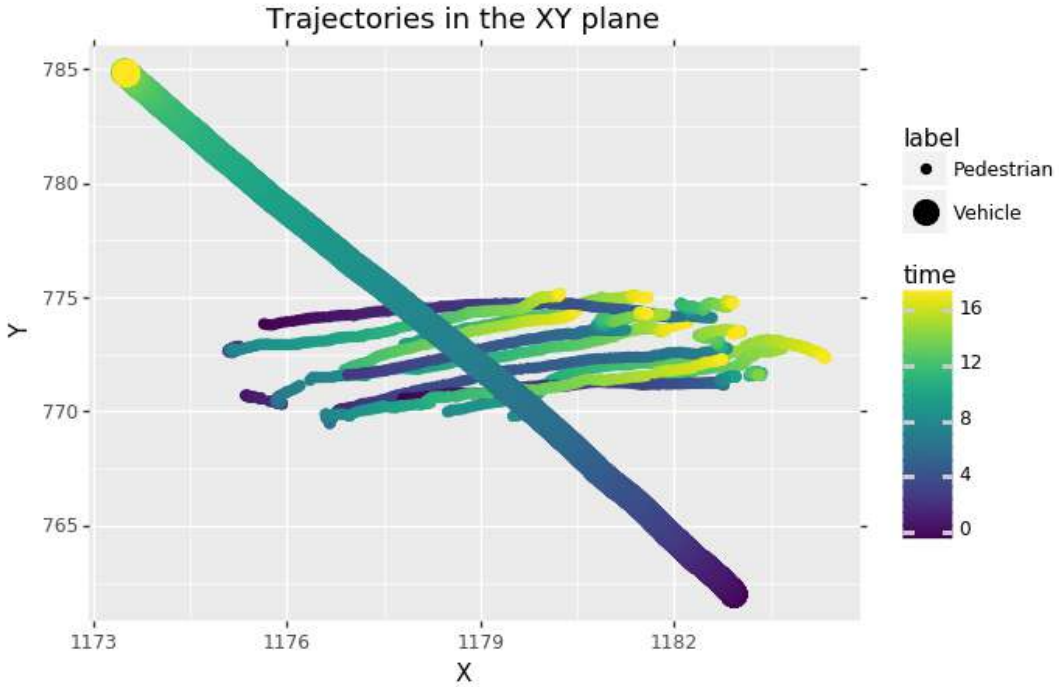

Fig. A.8.: Lateral Crossing 5: Aggressive Driver

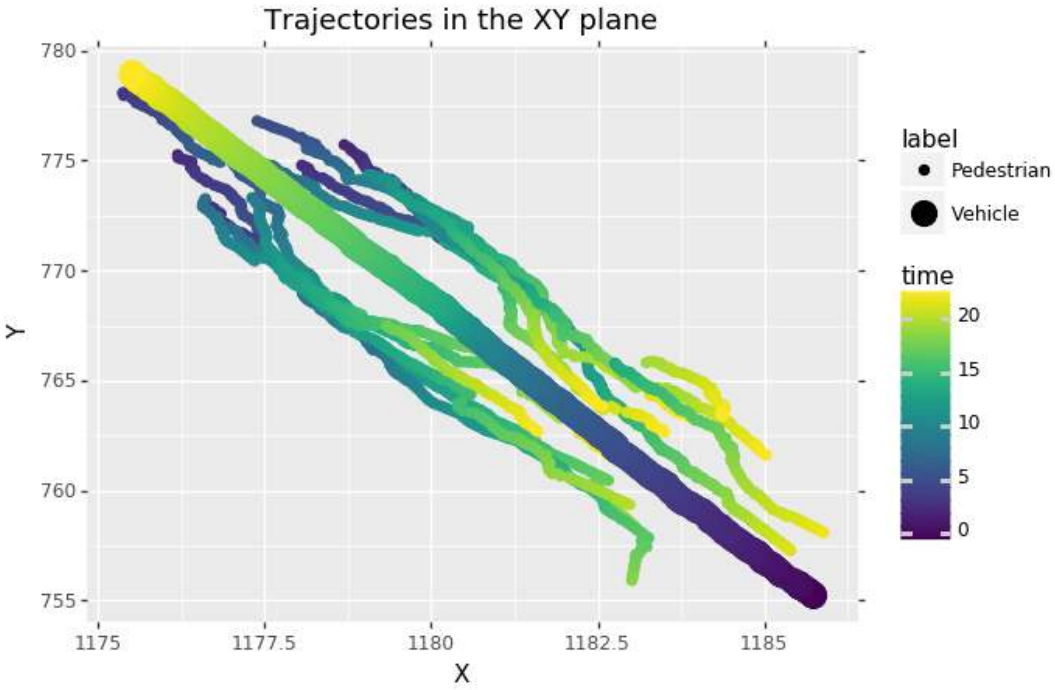

Fig. A.9.: Frontal Crossing 1: Aggressive Driver

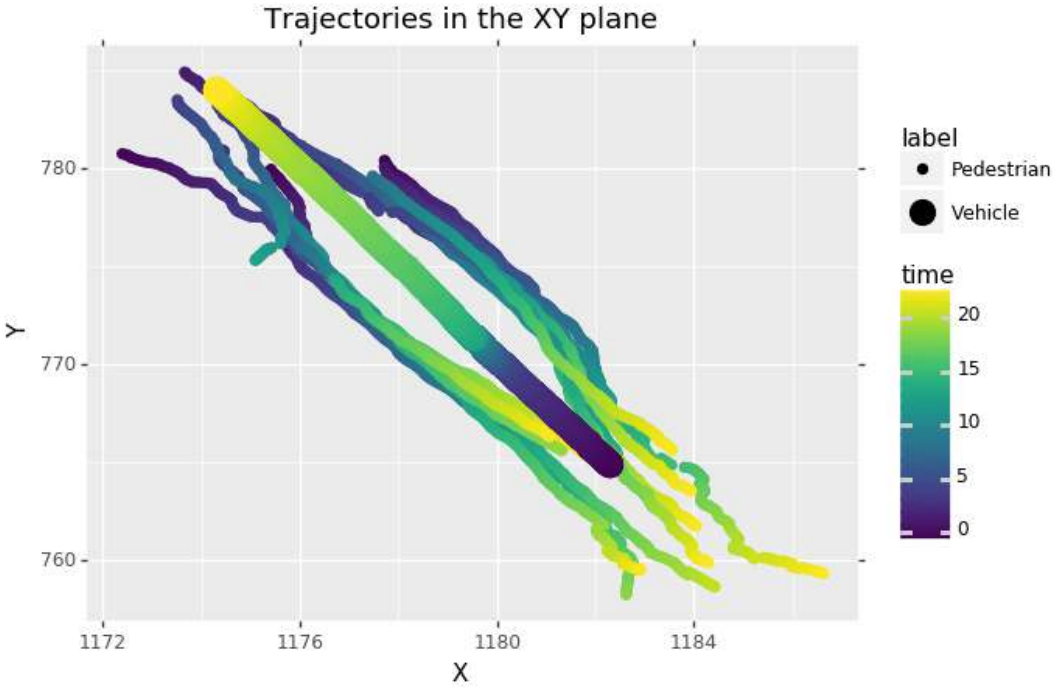

Fig. A.10.: Frontal Crossing 2: Yielding Driver

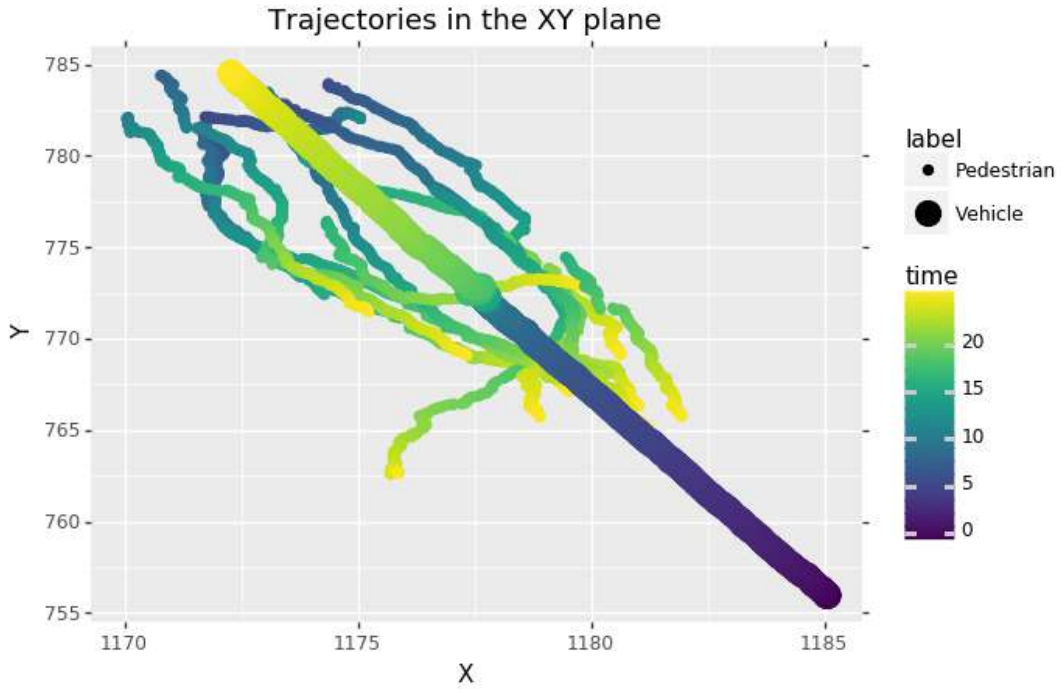

Fig. A.11.: Frontal Crossing 3: Aggressive Driver

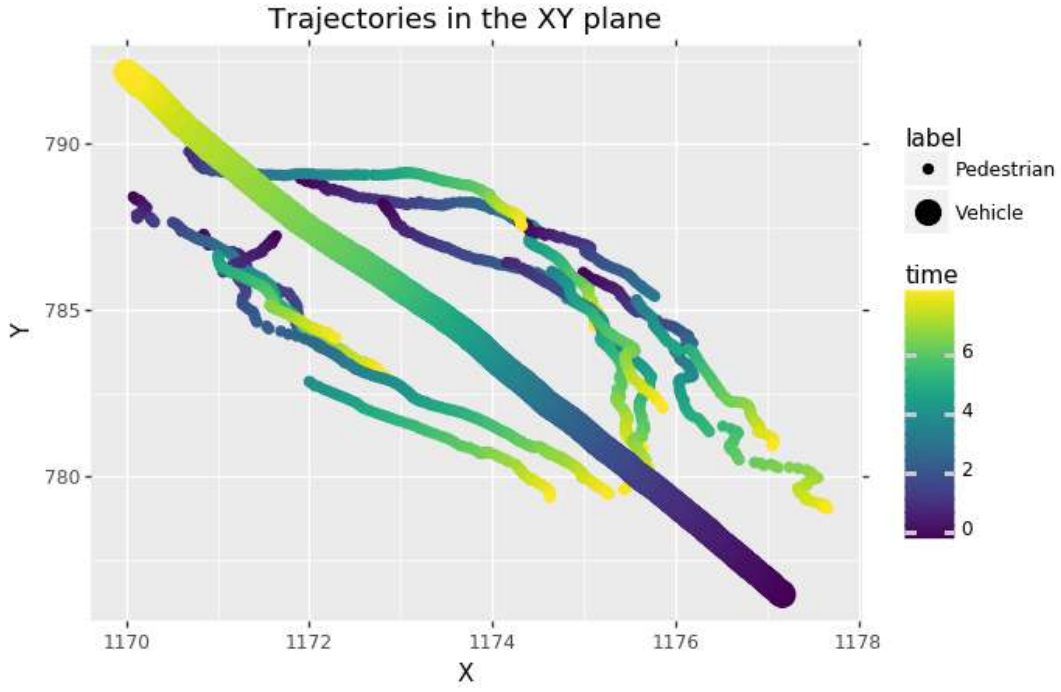

Fig. A.12.: Frontal Crossing 4: Aggressive Driver

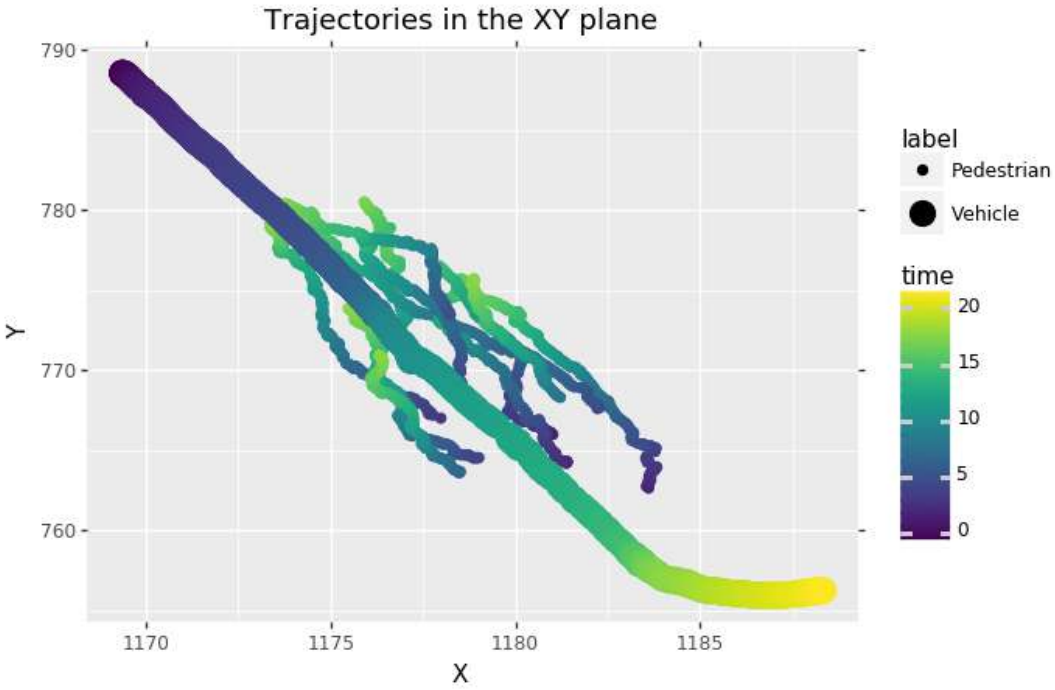

Fig. A.13.: Frontal Crossing 5: Aggressive Driver

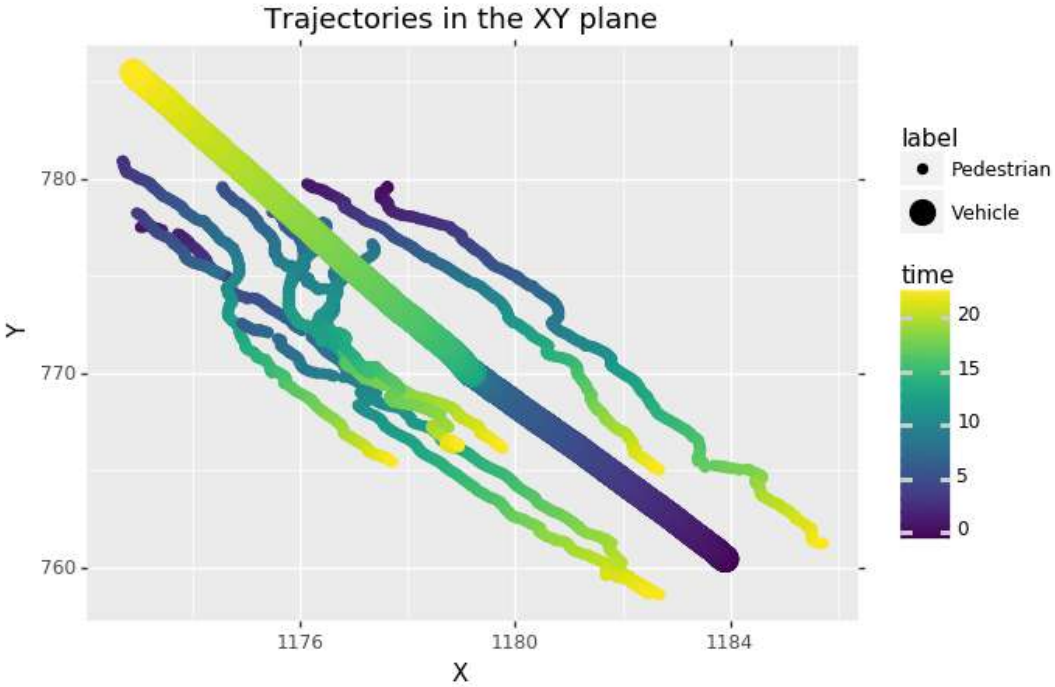

Fig. A.14.: Frontal Crossing 6: Yielding Driver

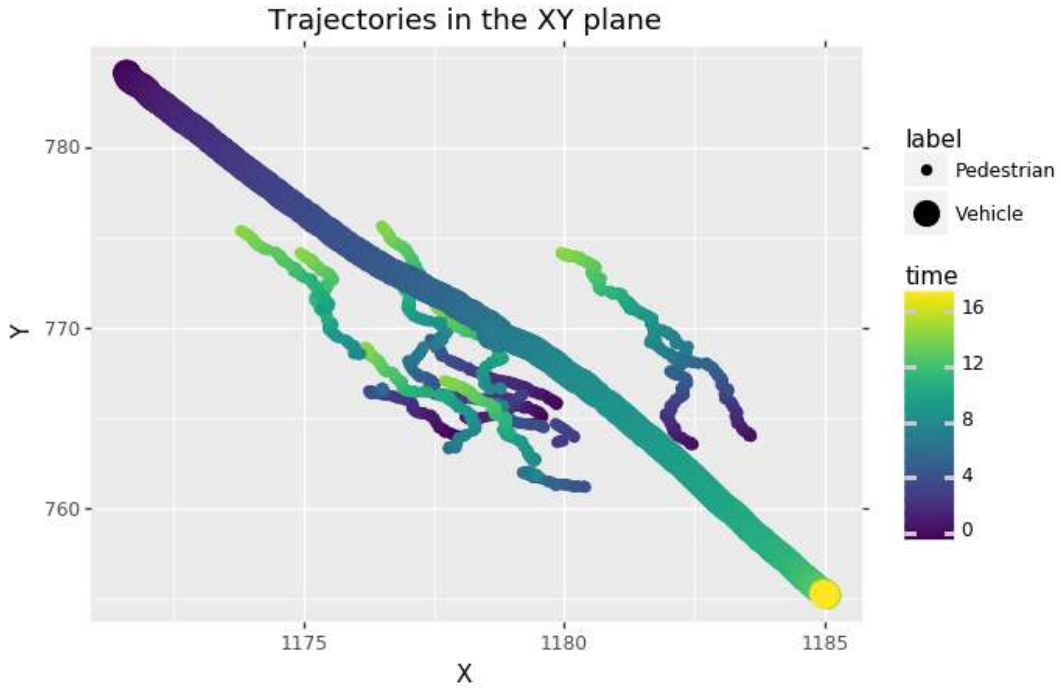

Fig. A.15.: Frontal Crossing 7: Aggressive Driver

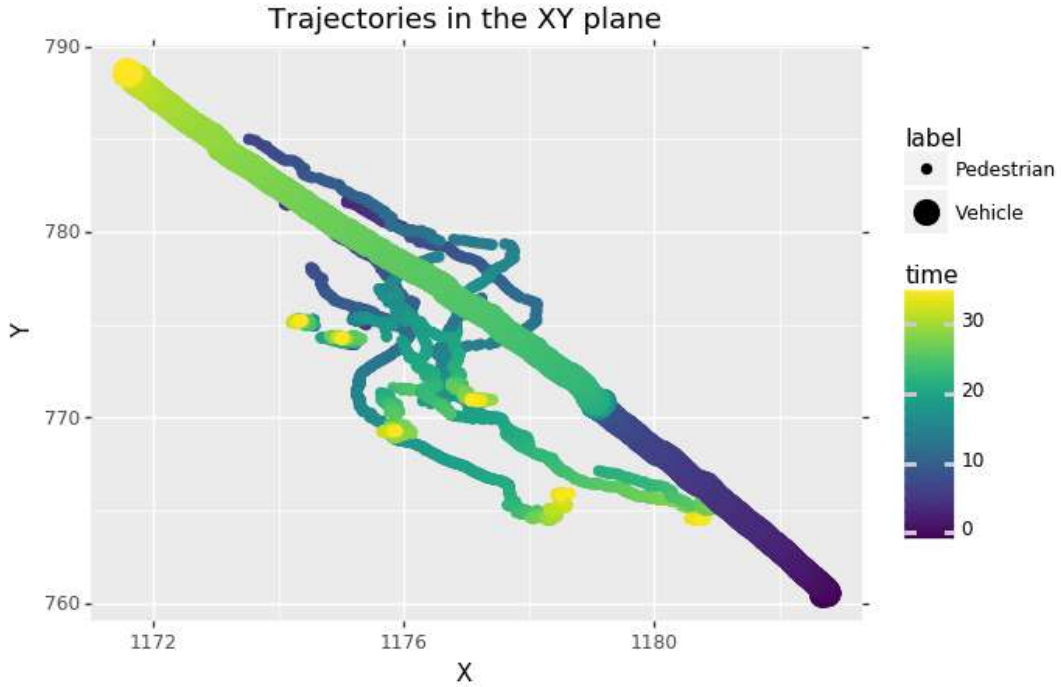

Fig. A.16.: Frontal Crossing 8: Yielding Driver

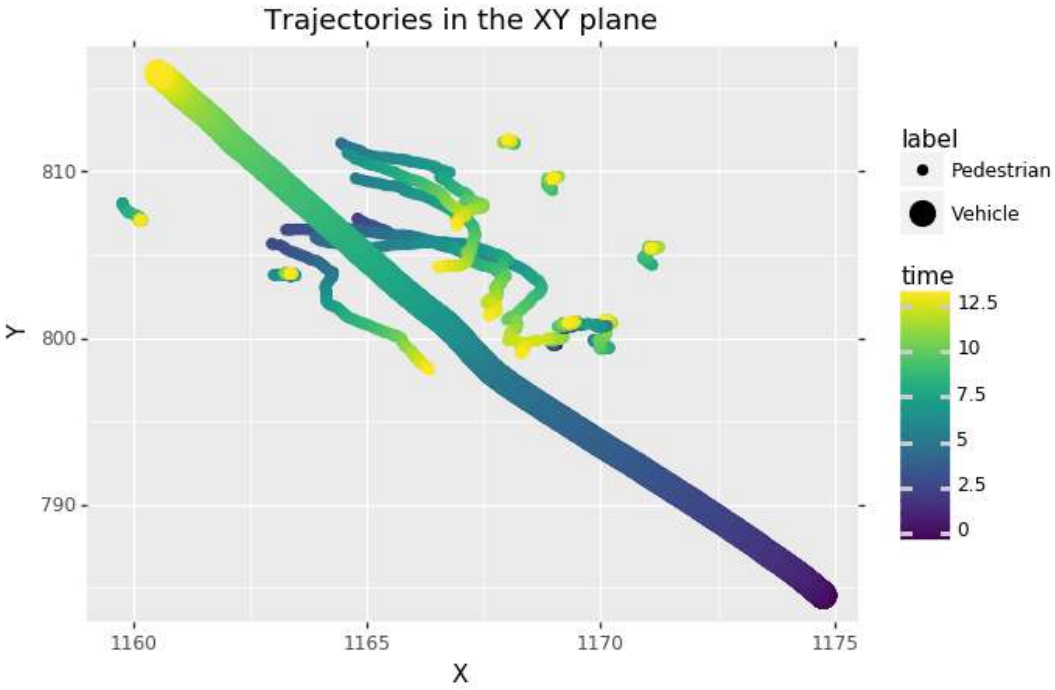

Fig. A.17.: Frontal Crossing 9: Aggressive Driver

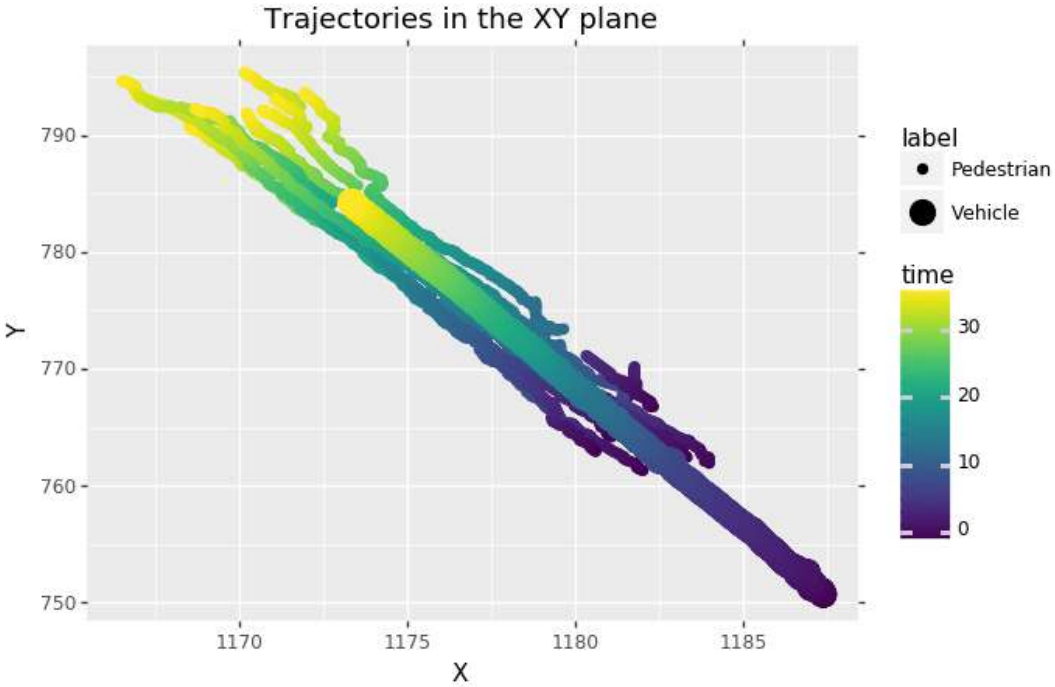

Fig. A.18.: Back Crossing 1: Yielding Driver

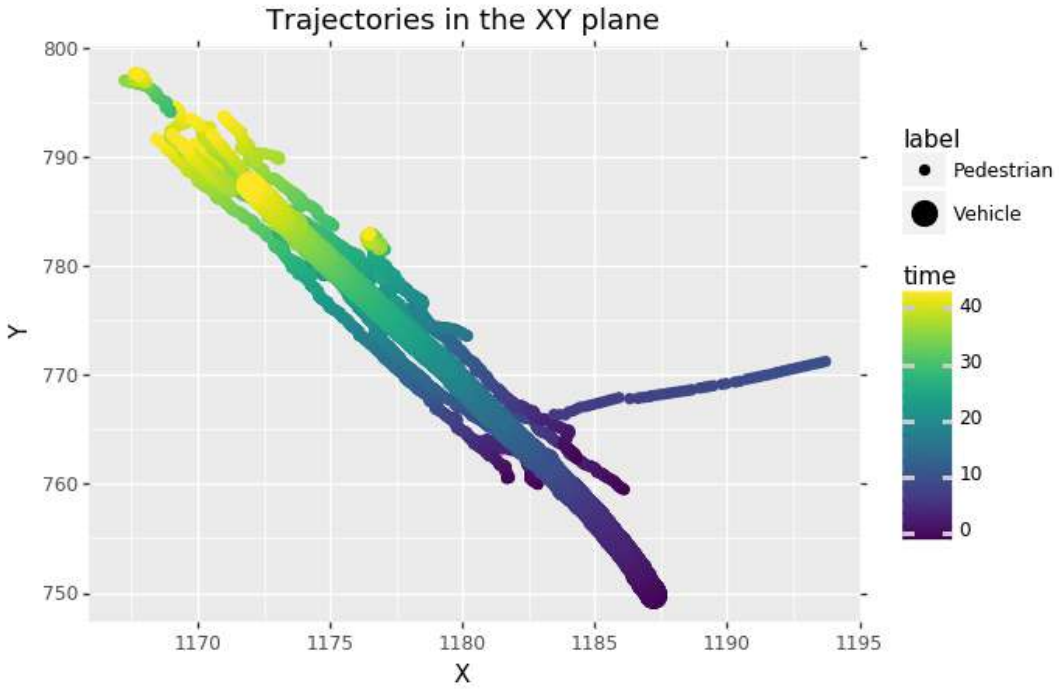

Fig. A.19.: Back Crossing 2: Aggressive Driver

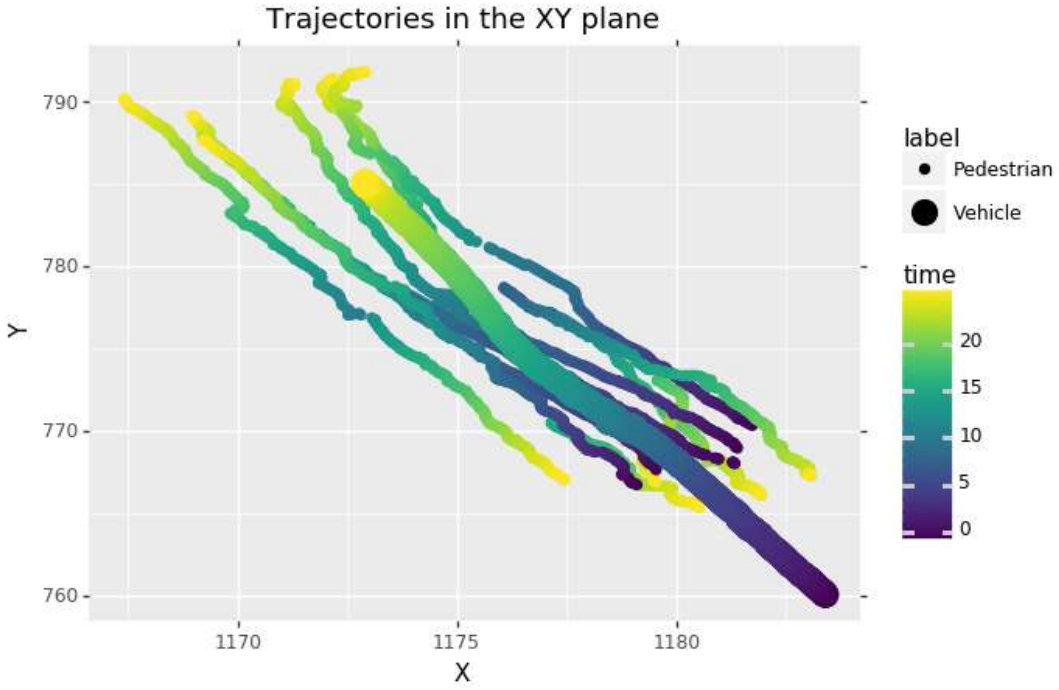

Fig. A.20.: Frontal-Back Crossing 1: Yielding Driver

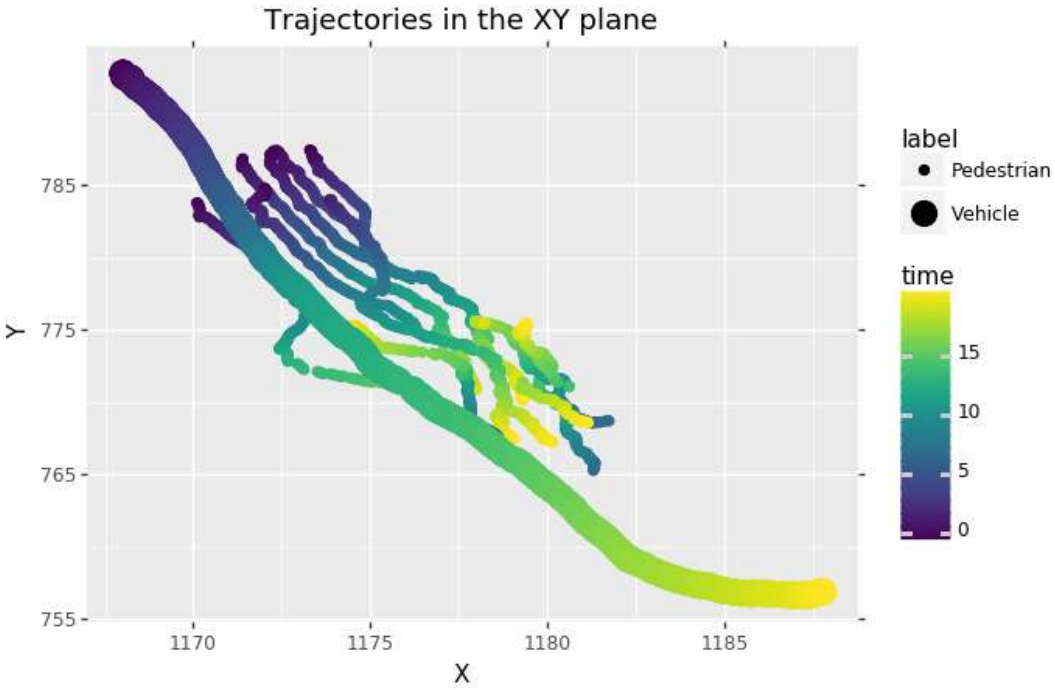

Fig. A.21.: Frontal-Back Crossing 2: Aggressive Driver

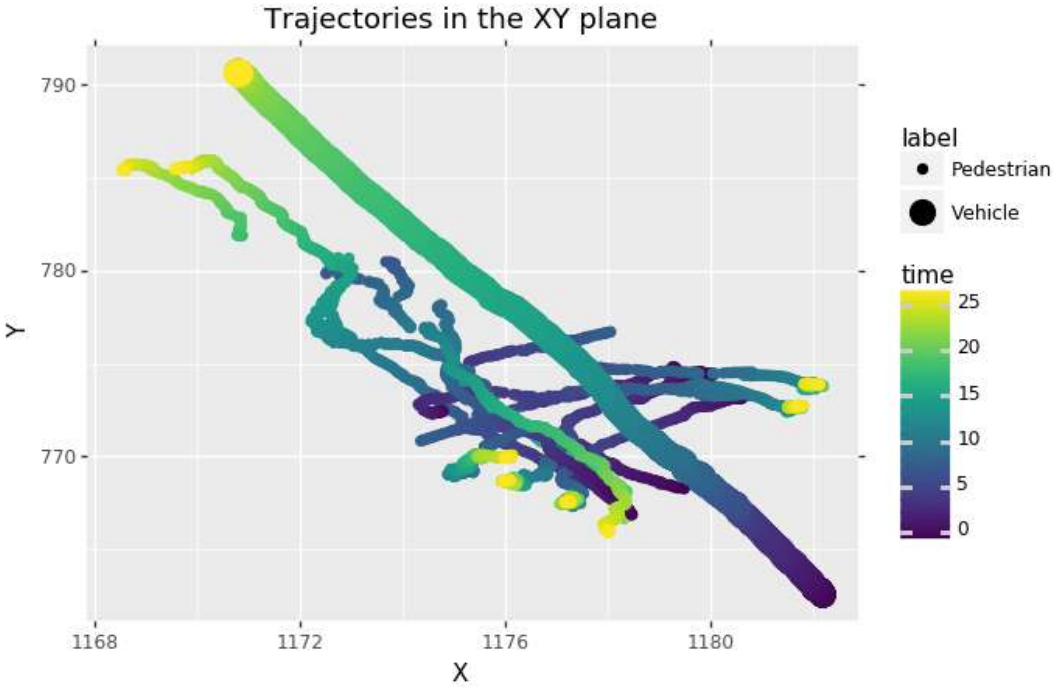

Fig. A.22.: Shared Space 1: Yielding Driver

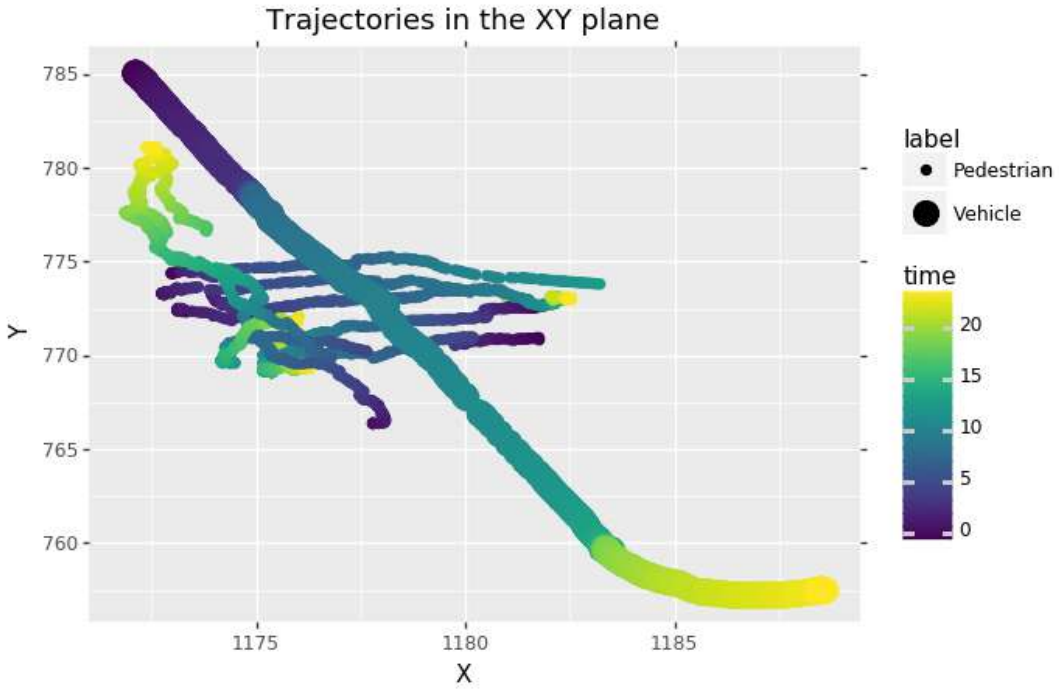

Fig. A.23.: Shared Space 2: Aggressive Driver

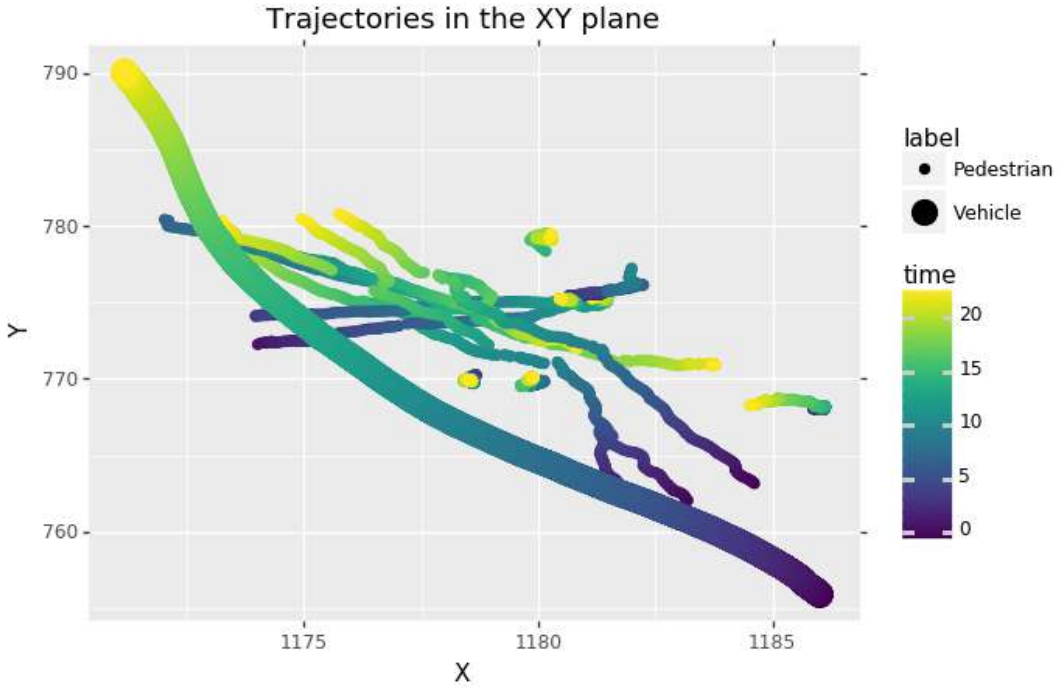

Fig. A.24.: Shared Space 3: Yielding Driver

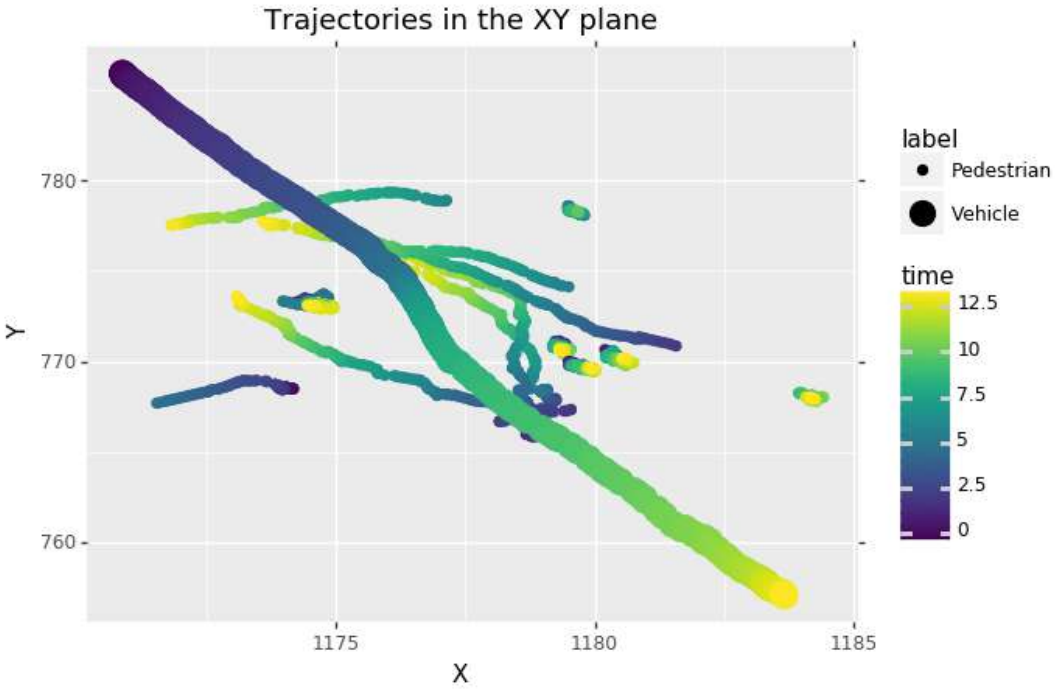

Fig. A.25.: Shared Space 4: Aggressive Driver

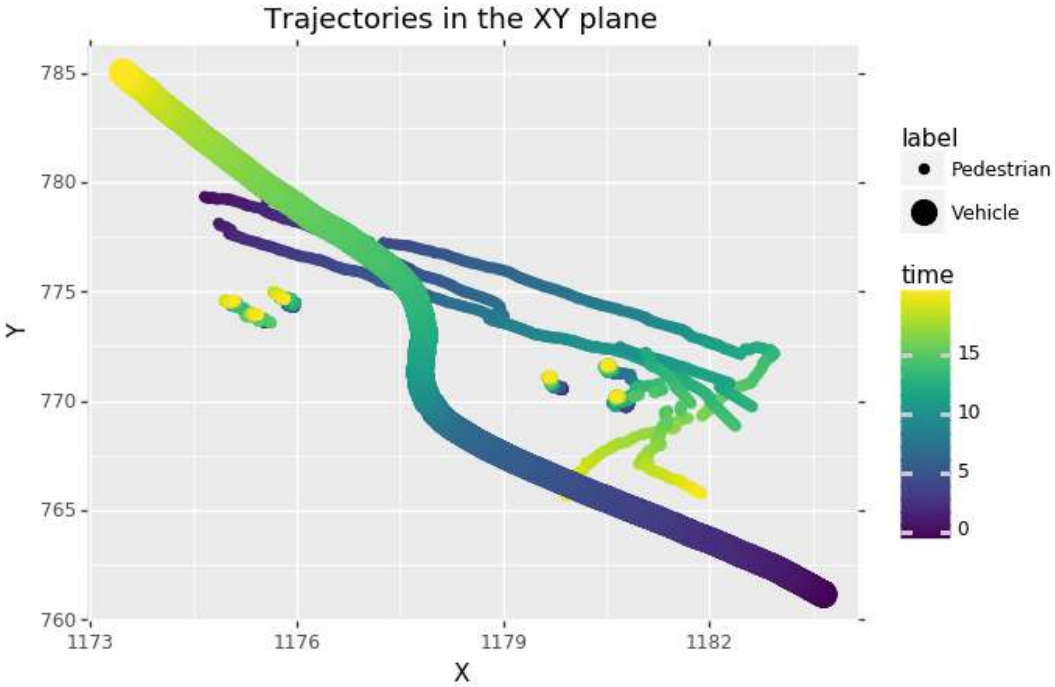

Fig. A.26.: Shared Space 5: Yielding Driver

B Collected Pedestrian-Vehicle Interaction Data: Statistics

This appendix includes the statistics of the recorded data during the experiment performed at the parking lot of the LS2N lab on the École Centrale de Nantes campus (Sec. 3.5 and Appendix A).

Seventeen volunteers interact with a Renault Fluence vehicle with a driver behind the wheel, and the data is collected on board of the vehicle. The experiment is comprised of 5 different interaction scenarios: Frontal, Back, Frontal-Back, Lateral, Bi-lateral and Shared Space scenarios. Each volunteer is given a start and goal point in the space and is asked to move in a free and natural way. The driver is asked to move to a goal point as well with one of two driving patterns: an aggressive driving pattern and a more yielding driving pattern where the priority is given to the pedestrians.

In the following, we show the key observed statistics for both the vehicle trajectory data and the pedestrians trajectories data.

B.1 Vehicle Statistics

Firstly, the linear velocity of the vehicle at the minimum approach distance to each pedestrian in each interaction. This is done by computing the distance between the vehicle and the pedestrians throughout each interaction. Then, the point of minimum approach distance is found for each pedestrian in each interaction, and the linear velocity of the vehicle at this point is what we refer to as the minimum approach distance. The previous method results for one value of the minimum approach speed for each pedestrian. These values of the vehicle speed are gathered based on the driving pattern (aggressive or yield). Finally, the corresponding histogram of the values with respect to the pedestrian count shown in Fig. B.1, where no obvious distinction was found between the two driving modes in terms of the speed.

Secondly, the vehicle's maximum linear acceleration value is computed for each recorded interaction. These values are gathered based on the driving mode and the corresponding histogram is plotted with respect to the recorded interactions count (Fig. B.3). The

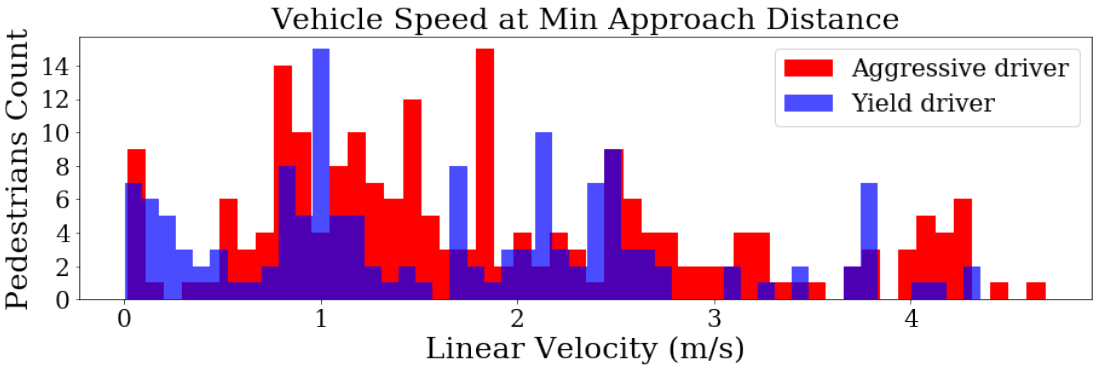

Fig. B.1.: Histogram of the recorded vehicle speed at the minimum approach distance of the pedestrians

figure shows larger values of the maximum vehicle acceleration in the aggressive driving mode, on average, as compared to the yielding mode.

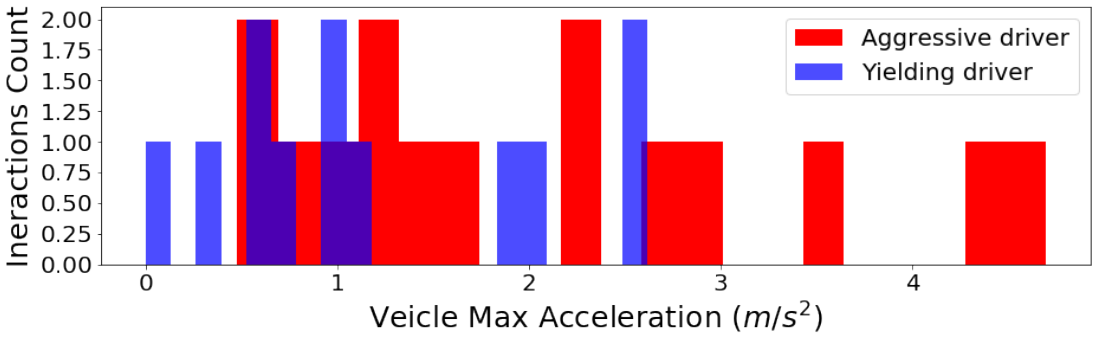

Fig. B.2.: Histogram of the recorded max vehicle acceleration in all interactions

Finally, the max linear acceleration value of the vehicle is computed for each recorded interaction. The values are gathered based on the driving mode and on the interaction type: lateral (uni and bi), frontal and back or shared space. This results in six categories. The mean value for the max acceleration values in each each category is computed. The resulting mean vehicle max acceleration points are shown on Fig. B.3. We notice that the vehicle achieves higher levels of acceleration in the aggressive mode. However, the difference in acceleration between the two modes becomes much smaller in the frontal and back interactions.

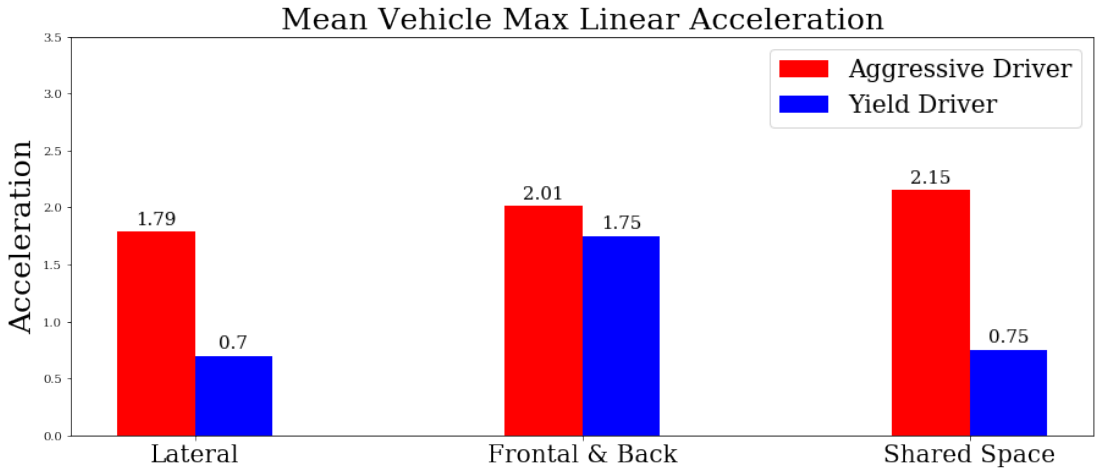

Fig. B.3.: Recorded mean value for the vehicle's max acceleration in an interaction across the different interaction types and driving modes

B.2 Pedestrian Statistics

Firstly, the speed of the pedestrians during the interactions are examined. Fig. B.4 shows the histogram on the average pedestrians speed, whereas, Fig. B.5 shows the histogram of the maximum speed for each pedestrian in each interaction. The pedestrians maintain on average lower speed in the yielding driving mode. However, the do reach similar levels of maximum speeds during one point of the interaction in both modes.

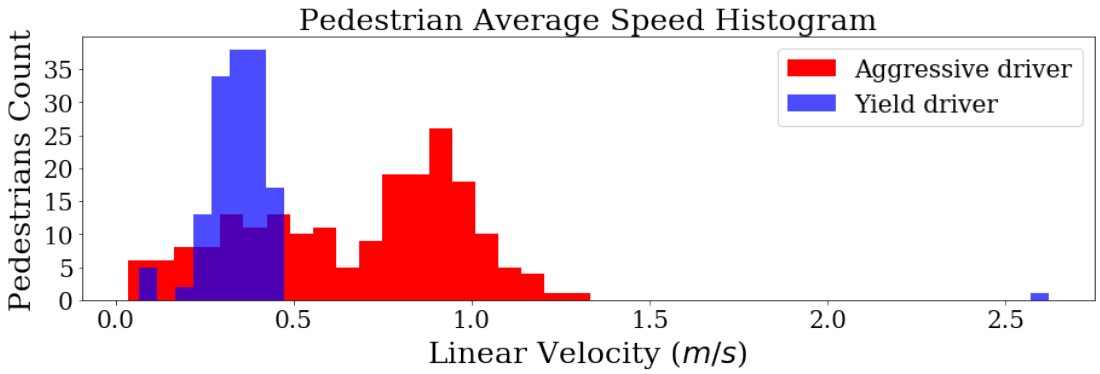

Fig. B.4.: Histogram of the average pedestrian speed in the collected data

Secondly, the recorded values of pedestrian acceleration is observed. Fig. B.6 shows the histogram of the average acceleration value for each pedestrian in each interaction, and Fig. B.8 shows the histogram of the maximum acceleration value for each pedestrian in each interaction. Moreover, Fig. B.8 shows the pedestrian acceleration values at the vehicle's minimum approach distance. The previous values were all gathered based on

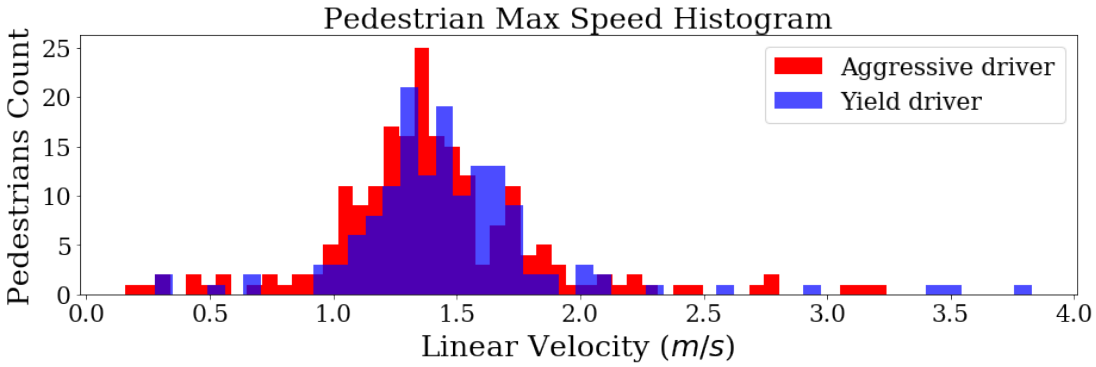

Fig. B.5.: Histogram of the maximum pedestrian speed in the collected data

the driving mode. However, no significant difference was noted between the two modes, other than a number of higher acceleration values reached with the yielding mode.

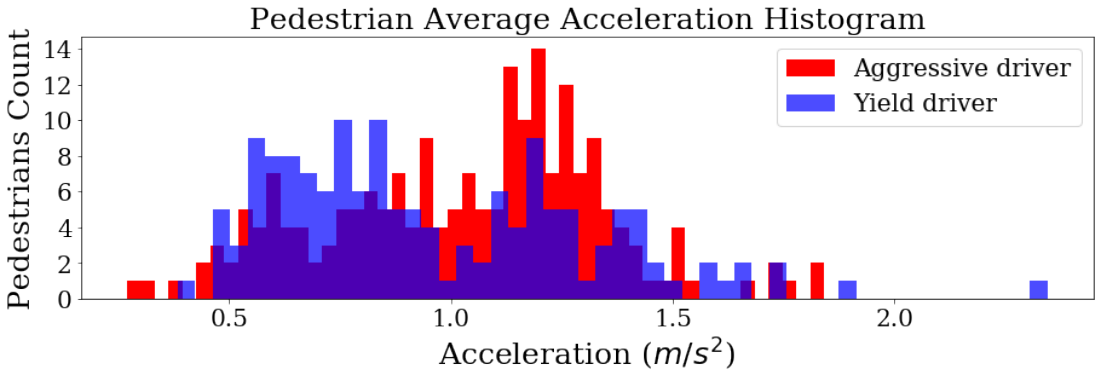

Fig. B.6.: Histogram of the average pedestrian acceleration in the collected data

Finally, the distance left between the pedestrians and the vehicle is analysed. Fig. B.9 shows the histogram of the vehicle's minimum approach distance to each pedestrian in each interaction, and Fig. B.10 shows the histogram of the average overall distance left between the vehicle and each pedestrian during each interaction. The vehicle can be in very close proximity to the pedestrian ($\leq 0.1m$) even in the yielding mode. However, the pedestrians do maintain larger minimum approach distances to the vehicle in the aggressive mode.

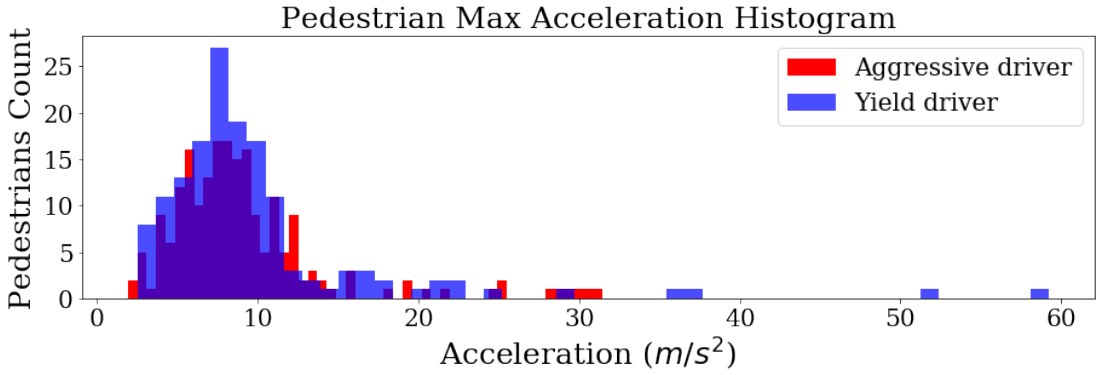

Fig. B.7.: Histogram of the maximum pedestrian speed in the collected data

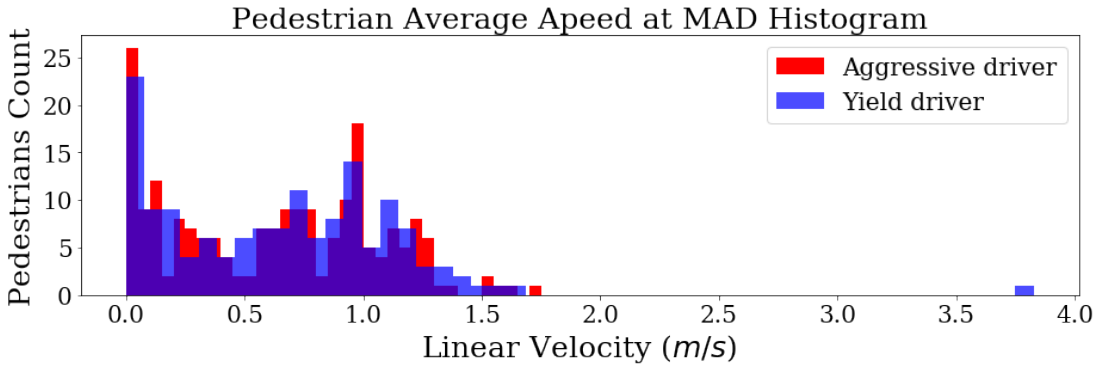

Fig. B.8.: Histogram of the average pedestrians' minimum approach speed in the collected data

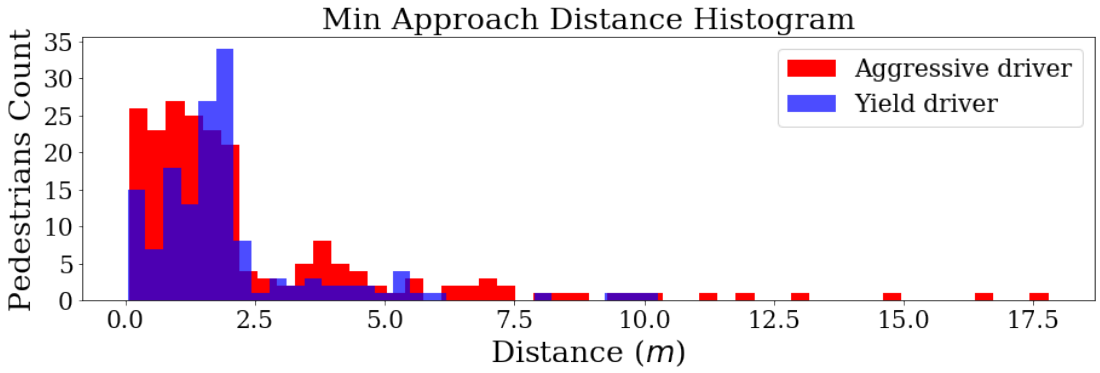

Fig. B.9.: Histogram of the minimum approach distance in the collected data

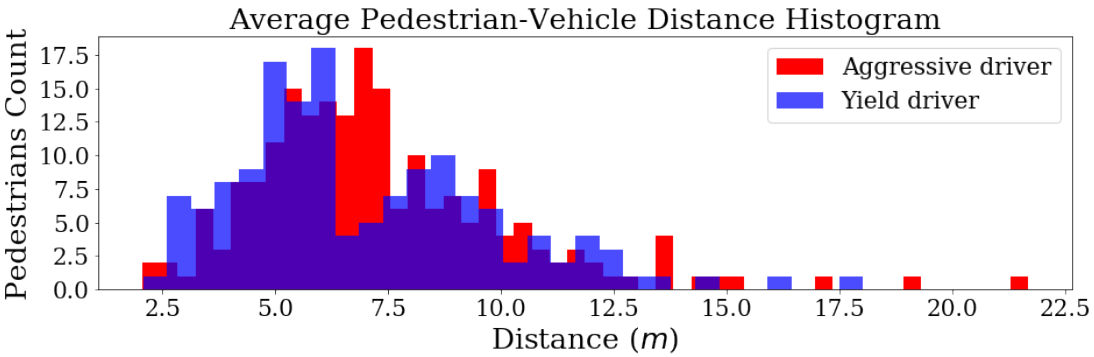

Fig. B.10.: Histogram of the average pedestrian-vehicle distance in the collected data

C Pedestrian Behavioral Model Results

The appendix includes a more detailed visualization of the output of the pedestrian cooperation behavioral model proposed in Chapter 3 and in Sec. 3.4.1. In the following we explore the result of the trajectory prediction when applied to two scenarios of the VCI-CITR[1] data-set: one bi-lateral and one frontal crossing. The prediction is done over a future prediction horizon of $5s$

C.1 Lateral Crossing Results

Fig. C.1 and Fig. C.2 show an example of the trajectory prediction model output using the generalized cooperation model in a bi-lateral crossing scenario. On Fig. C.1 the real trajectories from the data-set are shown with a black contouring circles, whereas, the predicted trajectory in shown without a contour. The starting point for the vehicle and for each agent is marked with a red "X" mark. Moreover, a unique ID is given to each pedestrian. To better examine the prediction quality, the respective linear velocity and orientation estimation are shown on Fig. C.2 for each pedestrian during the interaction. Where the number on each sub-figure corresponds to the unique pedestrian ID given on Fig. C.1. The model manages to capture similar speed and orientation patterns for the pedestrians. An inverse orientation estimation is noted in many cases, however, with a similar orientation pattern.

[1] https://github.com/dongfang-steven-yang/vci-dataset-citr

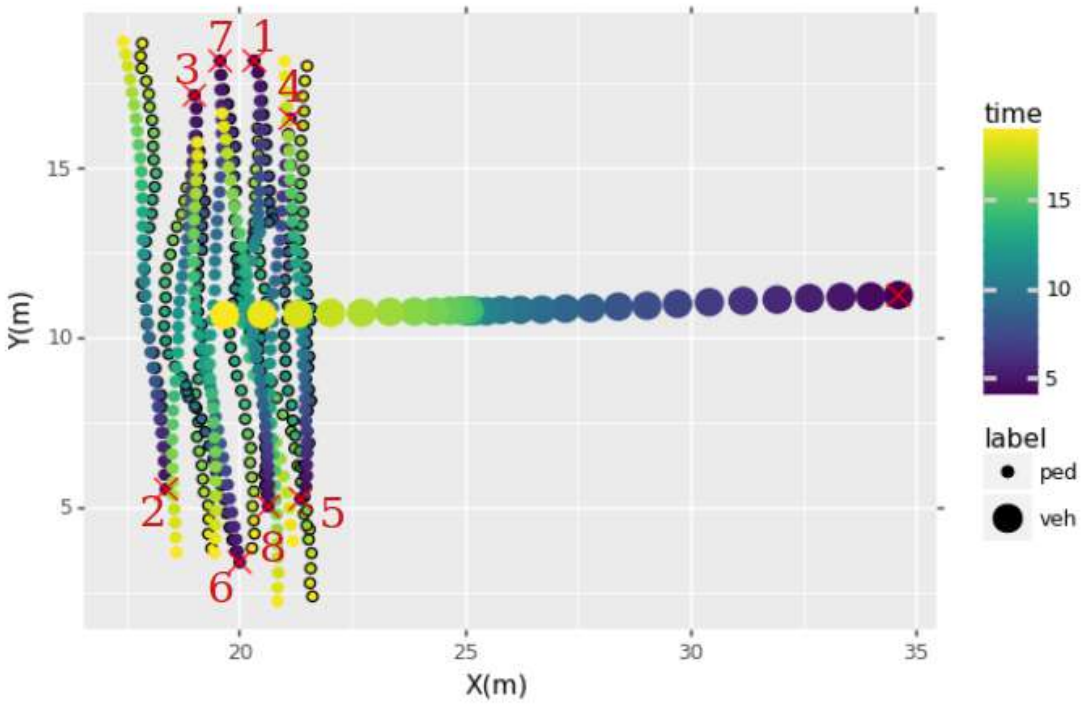

Fig. C.1.: Trajectory prediction model output in a bi-lateral interaction scenario. Black contour: Real. No contour: Predicted. X: starting point

C.2 Frontal Crossing Results

Similarly to the lateral case, we show the prediction results for one of the frontal interaction cases. Fig. C.3 and Fig. C.4 show an example of the trajectory prediction model output using the generalized cooperation model in a frontal crossing scenario. The figures shows the predicted trajectory for each pedestrian and the corresponding linear speed and orientation estimation errors.

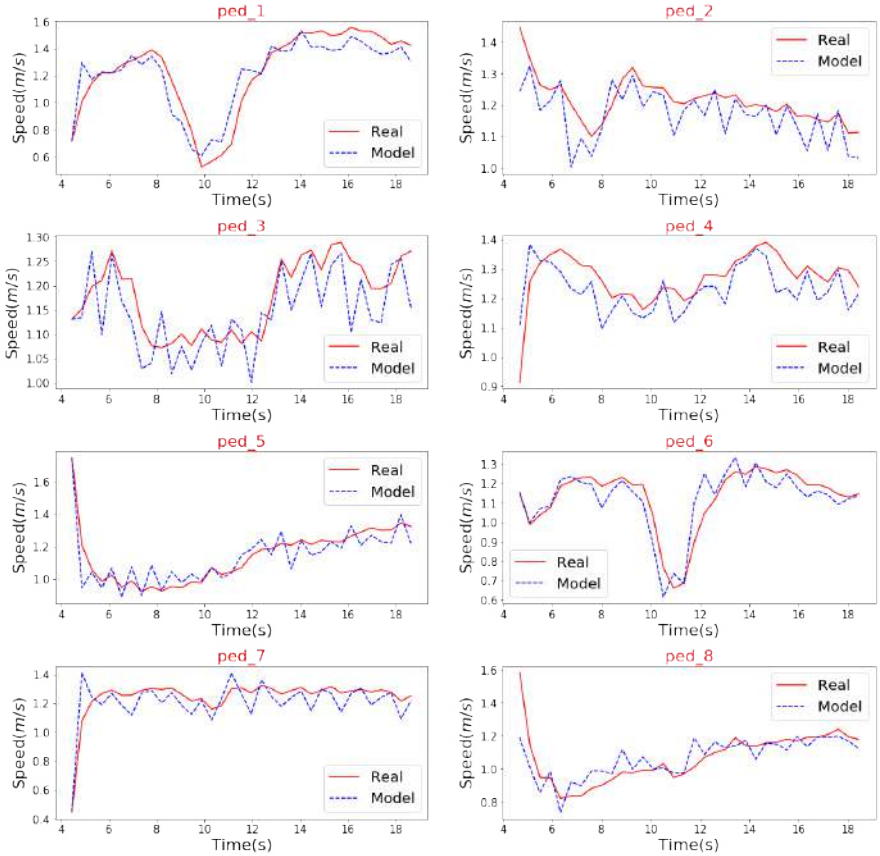

(a) Linear velocity estimation error for each pedestrian

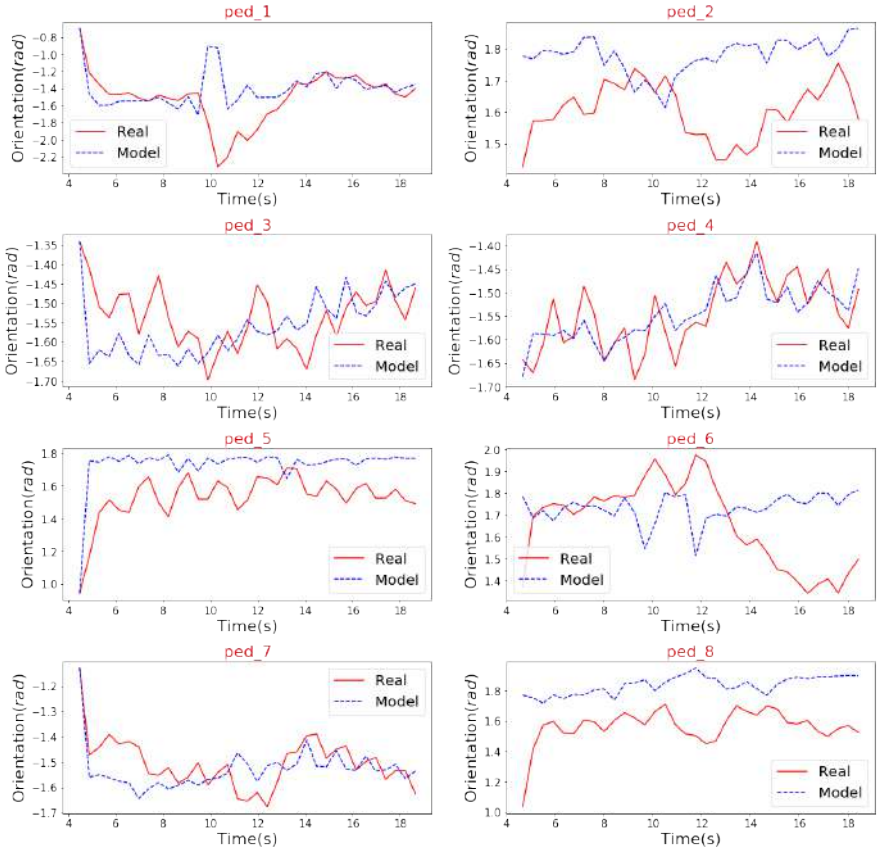

(b) Orientation estimation error for each pedestrian

Fig. C.2.: Trajectory prediction error corresponding to the trajectories in Fig. C.1

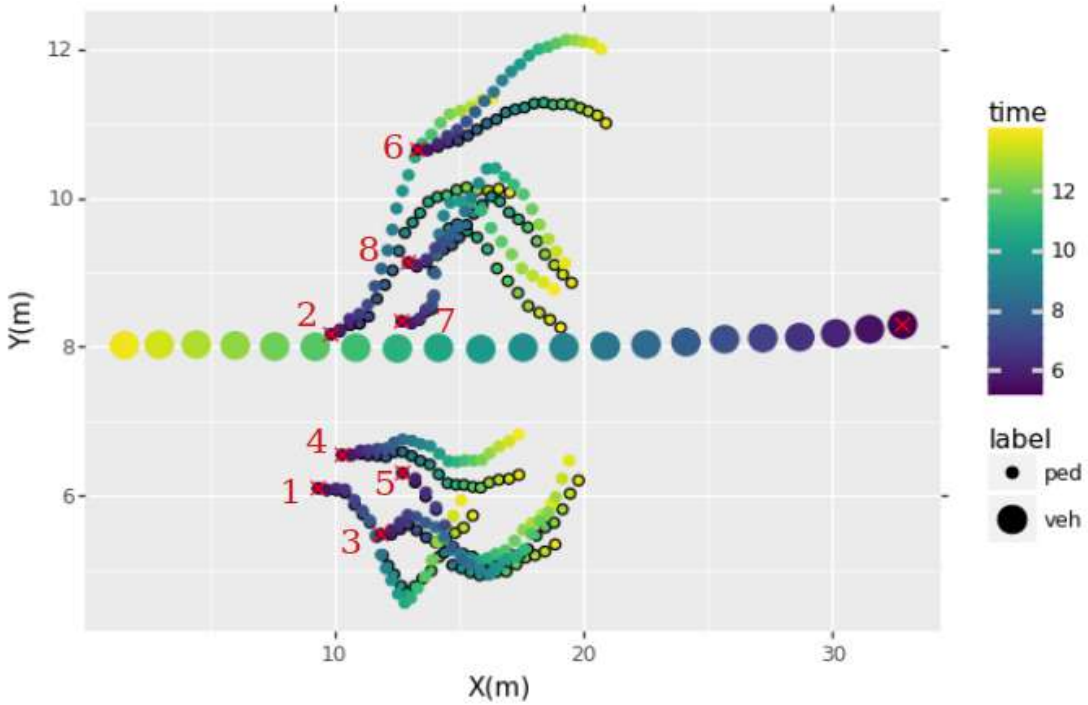

Fig. C.3.: Trajectory prediction model output in a frontal interaction scenario. Black contour: Real. No contour: Predicted. X: starting point

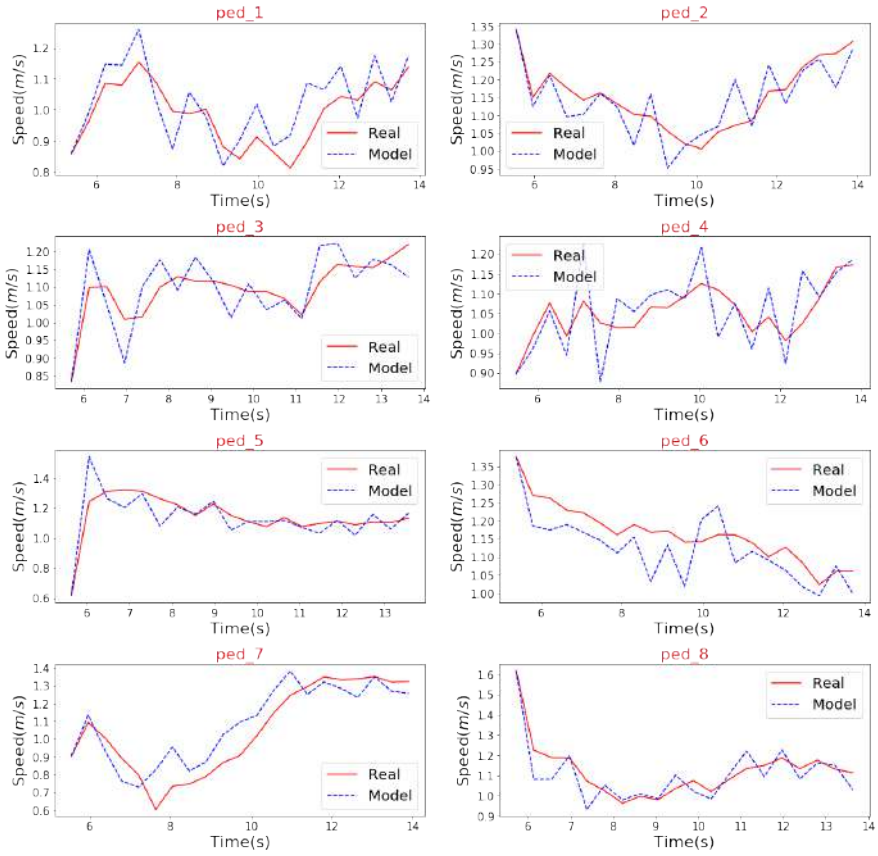

(a) Linear velocity estimation error for each pedestrian

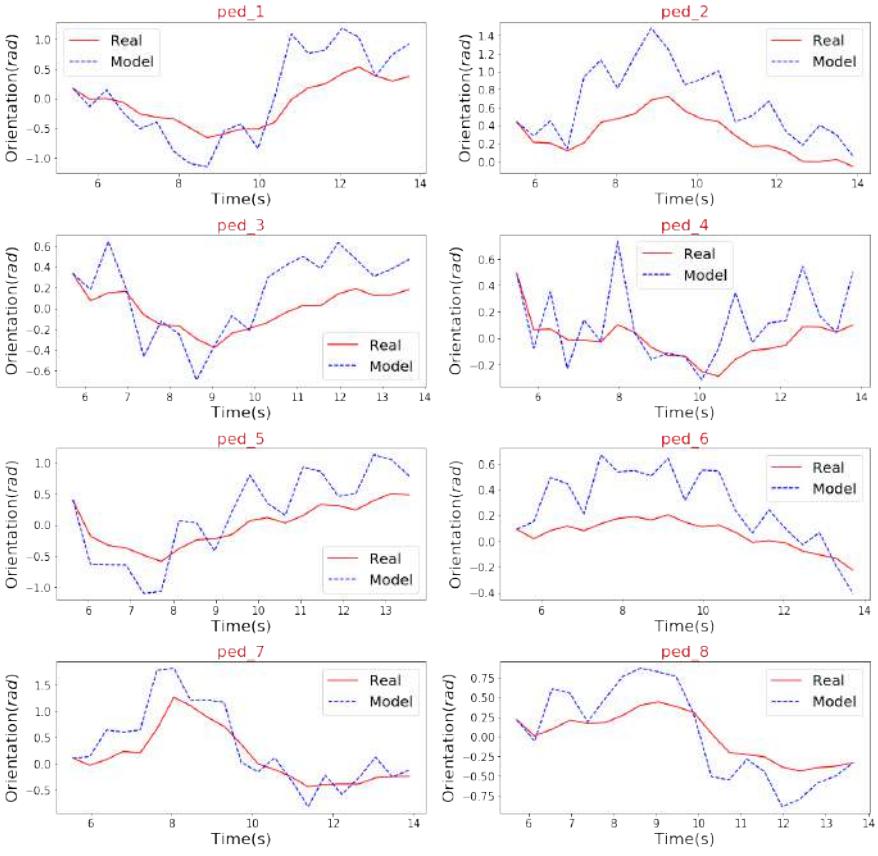

(b) Orientation estimation error for each pedestrian

Fig. C.4.: Trajectory prediction error corresponding to the trajectories in Fig. C.3

D

Deriving The Trajectory Prediction Error Gradient

Assuming a pedestrian j in interaction with the vehicle, where the pedestrian and the vehicle models are as in 2.7.2. The pedestrian cooperation based trajectory planning model (in 3) can be written as:

$$\boldsymbol{V_j}(t) = C_1 P_m^j(t) + C_2 \tag{D.1}$$

where $\boldsymbol{V_j}(t)$ is the velocity vector:

$$\boldsymbol{V_j}(t) = [V_j(t), \angle \boldsymbol{V_j}(t)]^T \tag{D.2}$$

and:

$$P_m^j(t) = \begin{bmatrix} CF_j(t).I_V^j(t) \\ CF_j(t).\Theta_V^j(t) \\ [1 - CF_j(t)].\Theta_{goal}^j(t) \\ [1 - CF_j(t)].D_{goal}^j(t) \\ I_P^j(t) \\ \theta_P^j(t) \end{bmatrix} \tag{D.3}$$

$$C_1 = [C_1[0], C_1[1]]$$
$$C_2 = [C_2[0], C_2[1]]^T$$

with $C_1[0] = [c_{00}, ..., c_{04}]$ and $C_1[1] = [c_{10}, ..., c_{14}]$. and the pedestrian generalized cooperation model is written as:

$$CF_j(t) = a_0 \mathbb{P}_{[j,veh]}(t) + a_1 \mathcal{D}^j(t) + a_2 I_P^j(t) + a_3 \frac{V_m^a(t)}{V_{Pmax}} + ICF \tag{D.4}$$

where ICF is the inner cooperation factor we aim to update online by minimizing the trajectory prediction error.

Assuming $\boldsymbol{V_j^{real}}(t)$ and $\boldsymbol{V_j^{pred}}(t)$ are the observed and predicted velocity of agent j at time t, then the trajectory prediction error over a time window $[t_0, t_0 + t_k]$ can be written as:

$$J_{pred}(t_k) = \frac{1}{t_k} \int_{t=t_0}^{t_k} \left(\boldsymbol{V_j^{real}}(t) - \boldsymbol{V_j^{pred}}(t)\right)^T A_J \left(\boldsymbol{V_j^{real}}(t) - \boldsymbol{V_j^{pred}}(t)\right) dt \tag{D.5}$$

where A_j is a diagonal matrix:

$$A_j = \begin{bmatrix} \frac{1}{V_{max}} & 0 \\ 0 & \frac{1}{2\pi} \end{bmatrix} \tag{D.6}$$

and $V_{max} = 5.5m/s$ is the maximum allowed velocity for the vehicle.

Therefor, the gradient of the trajectory prediction with respect to ICF can be written as:

$$\nabla J_{pred}(t_k) = \frac{2}{t_k} \int_{t=t_0}^{t_k} A_J \left(\boldsymbol{V_j^{real}}(t) - \boldsymbol{V_j^{pred}}(t)\right) \left(\frac{\partial \boldsymbol{V_j^{pred}}(t)}{\partial ICF}\right)^T dt \tag{D.7}$$

By substituting the partial derivative of the predicted velocity from the cooperation model, we get:

$$\nabla J_{pred}(t_k) = \frac{2}{t_k} \int_{t=t_0}^{t_k} A_J \left(\boldsymbol{V_j^{real}}(t) - \boldsymbol{V_j^{pred}}(t)\right) \left(C_s.P_s^j(t)\right)^T dt \tag{D.8}$$

with:

$$C_s = \begin{bmatrix} c_{00} & c_{01} & -c_{02} & -c_{03} \\ c_{10} & c_{11} & -c_{12} & -c_{13} \end{bmatrix} \tag{D.9}$$

$$P_s^j(t) = \begin{bmatrix} I_V^j(t) \\ \Theta_V^j(t) \\ \Theta_{goal}^j(t) \\ D_{goal}^j(t) \end{bmatrix} \tag{D.10}$$

E

Deriving The Model Gradients For Computing The Proactive Longitudinal Velocity Control

Assuming a pedestrian j in interaction with the vehicle, where the pedestrian and the vehicle models are as in 2.7.2. The pedestrian cooperation model, and the pedestrian linear velocity from the cooperation based trajectory planning model (in 3) can be written as:

$$CF_j(t) = a_0 \mathbb{P}_{[j,veh]}(t) + a_1 \mathcal{D}^j(t) + a_2 I_P^j(t) + a_3 \frac{V_m^a(t)}{V_{Pmax}} + B \tag{E.1}$$

$$V_j(t) = C_1[0] P_m^j(t) + C_2[0] \tag{E.2}$$

where:

$$P_m^j(t) = \begin{bmatrix} CF_j(t).I_V^j(t) \\ CF_j(t).\Theta_V^j(t) \\ [1 - CF_j(t)] .\Theta_{goal}^j(t) \\ [1 - CF_j(t)] .D_{goal}^j(t) \\ I_P^j(t) \\ \theta_P^j(t) \end{bmatrix} \tag{E.3}$$

and $C_1[0] = [c_{00}, ..., c_{04}]$, $C_2[0] \in \mathbb{R}$.

The gradients of both the pedestrian cooperation and velocity can be obtained assuming that: When a pedestrian is inside the vehicle's influence zone, the effect of the surrounding pedestrians on the pedestrian behavior is much smaller than the effect of the vehicle.

Assuming $u(t)$ is the longitudinal velocity control of the vehicle. Using the previous assumption, we can write:

$$\partial_u CF_j(t) = a_0 \partial_u \mathbb{P}_{[j,veh]}(t) + \frac{a_3}{V_{Pmax}} \partial_u V_j(t-1) \tag{E.4}$$

therefore the gradient of the cooperation can be written as in (4.23)

$$\boxed{\begin{aligned}&\partial_u CF_j(t) = \mathbf{F}_2\left(\partial_u \mathbb{P}_{[j,veh]}(t), \partial_u V_j(t-1)\right)\\&\mathbf{F}_2 :\ \mathbb{R}^2 \to \mathbb{R}\\&\mathbf{F}_2\left(\partial_u \mathbb{P}_{[j,veh]}(t), \partial_u V_j(t-1)\right) = a_0 \partial_u \mathbb{P}_{[j,veh]}(t) + \frac{a_3}{V_{Pmax}} \partial_u V_j(t-1)\end{aligned}} \tag{E.5}$$

To express the gradient of the pedestrian's linear velocity as in (4.22), let's write the gradients of the vehicle influence parameters (deformation and deformation angle). We have the deformation of the cooperation zone due to vehicle intrusion is written as:

$$I_V^j(t) = \frac{1}{2\pi} \int_{\alpha=0}^{2\pi} \frac{R_C - d(\alpha, t)}{R_C} d\alpha \tag{E.6}$$

where $d(\alpha, t)$ is the deformation radius at angle α and time t which is proportional to the minimum distance between the pedestrian and the vehicle:

$$d(\alpha, t) = d_k D_j^{min}(\alpha, t) :\ d_k \in \mathbb{R}_+^* \tag{E.7}$$

Moreover, the cooperation zone weighted deformation angle is defined as:

$$\Theta_V^j(t) = \frac{\frac{1}{2\pi} \int_{\alpha=0}^{2\pi} (R_C - d(\alpha, t))\, \alpha d\alpha}{I_V^j(t)} \tag{E.8}$$

The gradients of the two previous parameters are:

$$\partial_u I_V^j(t) = \frac{1}{2\pi} \int_{\alpha=0}^{2\pi} \frac{-d_k \partial_u D_j^{min}(\alpha, t)}{R_C} d\alpha \tag{E.9}$$

$$\partial_u \Theta_V^j(t) = \frac{1}{2\pi} \frac{I_V^j(t) \int_{\alpha=0}^{2\pi} \left(-d_k \partial_u D_j^{min}(\alpha, t)\right) \alpha d\alpha - \partial_u I_V^j(t) \int_{\alpha=0}^{2\pi} (R_C - d(\alpha, t))\, \alpha d\alpha}{\left(I_V^j(t)\right)^2} \tag{E.10}$$

Therefore, we can write:

$$\boxed{\begin{aligned}&\partial_u I_V^j(t) = g_1(\partial_u D_j^{min})\\&g_1 :\ \mathbb{R} \to \mathbb{R}\\&g_1(\partial_u D_j^{min}) = \frac{1}{2\pi} \int_{\alpha=0}^{2\pi} \frac{-d_k \partial_u D_j^{min}(\alpha, t)}{R_C} d\alpha\end{aligned}}$$

and

$$\partial_u \Theta_V^j(t) = g_2(\partial_u D_j^{min})$$
$$g_2 : \mathbb{R} \to \mathbb{R}$$
$$g_2(\partial_u D_j^{min}) = \frac{1}{2\pi} \frac{I_V^j(t) \int_{\alpha=0}^{2\pi} \left(-d_k \partial_u D_j^{min}(\alpha, t)\right) \alpha d\alpha - g_1(\partial_u D_j^{min}) \int_{\alpha=0}^{2\pi} (R_C - d(\alpha, t)) \alpha d\alpha}{\left(I_V^j(t)\right)^2}$$

By substituting this along with (E.4) in (E.2), we can write:

$$\begin{aligned}\partial_u V_j(t) =& CF(t) \left[a_0 g_1(\partial_u D_j^{min}(t)) + c_{01} g_2(\partial_u D_j^{min}(t))\right] \\ &+ [a_0 \partial_u \mathbb{P}_{[j,veh]}(t) + \frac{a_3}{V_{Pmax}} \partial_u V_j(t-1)][c_{00} I_V^j(t) + c_{01} \Theta_V^j(t)]\end{aligned}$$

which is equivalent to the writing in (4.22):

$$\partial_u V_j(t) = \mathbf{F}_1 \left(\partial_u V_j(t-1), CF_j(t), \partial_u \mathbb{P}_{[j,v]}(t), \partial_u D_j^{min}(t)\right)$$
$$\mathbf{F}_1 : \mathbb{R}^4 \to \mathbb{R}$$
$$\mathbf{F}_1 \left(\partial_u V_j(t-1), CF_j(t), \partial_u \mathbb{P}_{[j,v]}(t), \partial_u D_j^{min}(t)\right) = CF(t) \left[a_0 g_1(\partial_u D_j^{min}(t)) + c_{01} g_2(\partial_u D_j^{min}(t))\right]$$
$$+ [a_0 \partial_u \mathbb{P}_{[j,veh]}(t) + \frac{a_3}{V_{Pmax}} \partial_u V_j(t-1)][c_{00} I_V^j(t) + c_{01} \Theta_V^j(t)]$$

F SMC for Quintic path following

F.1 Vehicle Model (Reminder)

Let (O, X_G, Y_G) be the global Cartesian Coordinates map frame. Two additional local coordinate frames are used in this work (Fig. F.1). The first is the the vehicle's local Cartesian Coordinates frame $(O_V, \vec{X_V}, \vec{Y_V})$, where O_V is the center of mass of the vehicle and $\vec{x_V}$ is in the direction of the longitudinal velocity of the vehicle $\vec{v}$. The second local frame is a Frenet frame [Fre52]. this frame can be computed analytically at arbitrary points along a curve, which makes it convenient for path tracking applications. The Frenet frame is defined by the tangential and normal vectors at a certain point of a reference curve. To use Frenet frame with degenerate curves (straight paths for example), the tangential is defined in the same direction of the path in this case. In the following: the symbols X^g, X^v and $X^{\mathcal{F}_\mathbf{C}}$ denotes the coordinates of a point X expressed in the global frame, the vehicle frame and the Frenet frame of a curve $\mathbf{C}$ respectively.

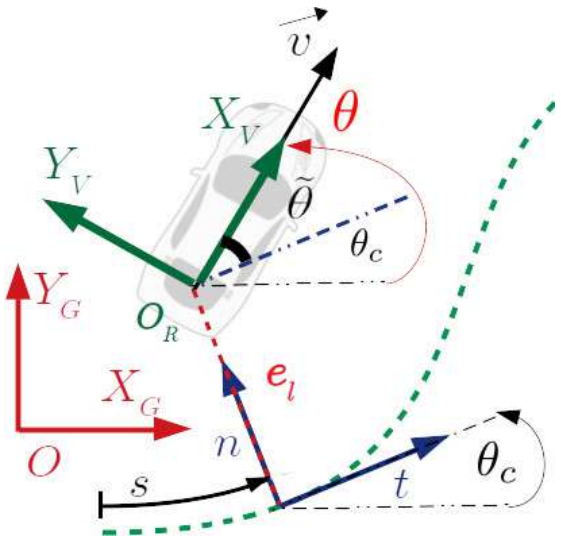

Fig. F.1.: Vehicle local frame and the Frenet frame

The vehicle model used in this work is a kinematic bicycle model expressed in the Frenet frame, with a zero slip assumption. This model is convenient since the navigation among pedestrians imposes low velocities and acceleration limits on the vehicle [Pol+17]. As shown in Figure **??**.a, the vehicle model is defined in the Frenet frame of a path $\mathbb{C}$

using the the lateral displacement of the vehicle and the traveled path length (e_l and s respectively), and heading error angle $\tilde{\theta}$. The heading error is the difference between the vehicle heading respect to the global frame $\theta = (\widehat{X_G, X_V})$ and $\theta_c = (\widehat{X_G, t})$ the heading angle of the tangential vector of the frame. Assuming O_R to be the center of the rear axis, the vehicle model can be written at O_R as follows: [CSB96]

$$\dot{s} = v\cos(\tilde{\theta})\frac{1}{1 - e_l\kappa(s)} \qquad \dot{e}_l = v\sin(\tilde{\theta}) \tag{F.1}$$

$$\dot{\tilde{\theta}} = w - v\cos(\tilde{\theta})\frac{\kappa(s)}{1 - e_l\kappa(s)} \qquad \dot{v} = a \tag{F.2}$$

where $\kappa(s)$ is the curvature of the path, and $w = \frac{v}{L}\tan(\delta)$ (L is the length of the vehicle and δ is the steering control input).

F.2 SMC implementation

To implement the SMC, we start by defining a tracking error to the selected Quintic transition path (e_q). Then, a sliding surface is designed using this tracking error. Finally, the local steering control is derived by insuring the closed-loop stability of the system.

Firstly, the model of the vehicle is expressed in the Frenet frame of the goal channel. Since the goal channel has zero curvature we can write the vehicle kinematics as follows:

$$\dot{s} = v\cos(\tilde{\theta}) \qquad \dot{e}_l = v\sin(\tilde{\theta}) \tag{F.3}$$

$$\dot{\tilde{\theta}} = w = \frac{v}{L}\tan(\delta) \qquad \dot{v} = a \tag{F.4}$$

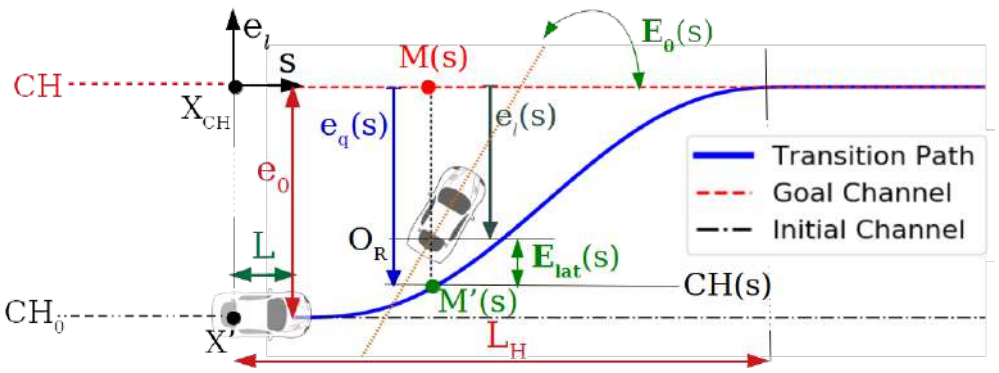

Fig. F.2.: Quintic path tracking errors

Two tracking errors are used. One lateral displacement error and another heading error. These two heading errors can be written with respect to the vehicle model in the Frenet frame of the goal channel $\mathcal{F}_C$ as follows:

$$E_{lat}(s) = e_l(s) - e_q(s) \tag{F.5}$$

$$E_\theta(s) = \tilde{\theta}(s) \tag{F.6}$$

and the global tracking error is written as:

$$E(s) = E_{Lat}(s) + d_s E_\theta(s) \quad : d_s \in \mathbb{R}_+^* \tag{F.7}$$

Since the relative input-output degree of our system is two, a first degree sliding surface σ is selected:

$$\sigma = \left(\frac{d}{dt} + \lambda\right) E(s) \tag{F.8}$$

$$= \underbrace{\dot{E}_{Lat}(s) + \lambda E_{Lat}(s)}_{\sigma_{Lat}} + d_s \underbrace{\left[\dot{E}_\theta(s) + \lambda E_\theta(s)\right]}_{\sigma_\theta} \tag{F.9}$$

where $\lambda \in \mathbb{R}_+^*$ defines the unique pole of the reduced dynamics system resulting in the closed loop. The control required to reach the goal state ($E(s) = 0, \dot{E}(s) = 0$) is composed of two parts. These two modes are an equilibrium control which drives the system to the sliding surface (δ_{eq}), and a sliding control δ_s. The sliding control part keeps the system close to the sliding surface until the goal state is reached.

The previous equilibrium control is achieved when σ is constant:

$$\delta_{eq} = \delta|_{\dot{\sigma}=0} \tag{F.10}$$

$$\dot{\sigma} = 0 => \dot{\sigma}_{Lat} = -d_s \dot{\sigma}_\theta \tag{F.11}$$

$$\dot{\sigma}_{Lat} = \dot{E}_{Lat}(s) + \lambda \ddot{E}_{Lat}(s) \tag{F.12}$$

$$\dot{E}_{Lat}(s) = \underbrace{v \sin(\tilde{\theta})}_{\dot{e}_l(s)} - \underbrace{\dot{s} \frac{\partial e_q(s)}{\partial s}}_{\partial_s e_q} \tag{F.13}$$

let's use: $\partial_s e_q = \frac{\partial e_q(s)}{\partial s}$. we have:

$$\dot{s} = v\cos(\tilde{\theta}) \tag{F.14}$$

Therefore:

$$\boxed{\dot{E}_{Lat}(s) = v\left[\sin(\tilde{\theta}) - \cos(\tilde{\theta})\partial_s e_q(s)\right]} \tag{F.15}$$

Now let's compute $\ddot{E}_{Lat}(s)$:

$$\ddot{E}_{Lat}(s) = a\left[\sin(\tilde{\theta}) - \cos(\tilde{\theta})\partial_s e_q(s)\right] + v.w\left[\cos(\tilde{\theta}) + \sin(\tilde{\theta})\partial_s e_q(s)\right] - v\cos(\tilde{\theta})\partial_s^2 e_q(s)\dot{s} \tag{F.16}$$

then:

$$\boxed{\ddot{E}_{Lat}(s) = \sin(\tilde{\theta})\left[a + v.w.\partial_s e_q(s)\right] + \cos(\tilde{\theta})\left[vw - a\partial_s e_q(s)\right] + v^2\cos^2(\tilde{\theta})\partial_s^2 e_q(s)} \tag{F.17}$$

and $\dot{\sigma}_{Lat}$:

$$\begin{aligned}\dot{\sigma}_{Lat} &= w.\lambda.v\left[\cos(\tilde{\theta}) + \partial_s e_q \sin(\tilde{\theta})\right] \\ &+ \underbrace{\sin(\tilde{\theta})\left[v + \lambda a\right] - \cos(\tilde{\theta})\partial_s e_q(s)\left[v + \lambda a\right] + \lambda v^2\cos^2(\tilde{\theta})\partial_s^2 e_q(s)}_{G_1(a,v,\tilde{\theta},s,\lambda)}\end{aligned} \tag{F.18}$$

then:

$$\boxed{\dot{\sigma}_{Lat} = w.K_0(\tilde{\theta}, s, \lambda) + G_1(a, v, \tilde{\theta}, s, \lambda)} \tag{F.19}$$

with:

$$\boxed{K_0(\tilde{\theta}, s, \lambda) = \lambda.v\left[\cos(\tilde{\theta}) + \partial_s e_q \sin(\tilde{\theta})\right]} \tag{F.20}$$

and:

$$\boxed{G_1(a, v, \tilde{\theta}, s, \lambda) = \sin(\tilde{\theta})\left[v + \lambda a\right] - \cos(\tilde{\theta})\partial_s e_q(s)\left[v + \lambda a\right] + \lambda v^2\cos^2(\tilde{\theta})\partial_s^2 e_q(s)} \tag{F.21}$$

Now lets find $\dot{\sigma}_\theta$:

$$\dot{\sigma}_\theta = \dot{E}_\theta(s) + \lambda\ddot{E}_\theta(s) \tag{F.22}$$

since: $E_\theta = \tilde{\theta}$, then:

$$\dot{E}_\theta(s) = \dot{\tilde{\theta}} = w \tag{F.23}$$

$$\ddot{E}_\theta(s) = \dot{w} \tag{F.24}$$

Then:

$$\boxed{\dot{\sigma}_\theta = w + \lambda\dot{w}} \tag{F.25}$$

Now to find the equilibrium control it is enough to plug the results we obtained in the following equation:

$$\delta_{eq} = \delta|_{\dot{\sigma}=0} \tag{F.26}$$

$$\begin{aligned} &\dot{\sigma}_{Lat} + d_s\dot{\sigma}_\theta = 0 \\ &K_0(\tilde{\theta}, s, \lambda)w + G_1(a, v, \tilde{\theta}, s, \lambda) + d_s w + \lambda d_s \dot{w} = 0 \end{aligned} \tag{F.27}$$

$$\boxed{\left[K_0(\tilde{\theta}, s, \lambda) + d_s\right] w + \lambda d_s.\dot{w} = -G_1(a, v, \tilde{\theta}, s, \lambda)} \tag{F.28}$$

with the assumption: $\dot{\delta} << 1$:

$$\begin{aligned} w &= \frac{v}{L}\tan(\delta) \\ \dot{w} &= \frac{a}{L}\tan(\delta) \end{aligned} \tag{F.29}$$

Then:

$$\tan(\delta_{eq})\left[v.K_0(\tilde{\theta}, s, \lambda) + d_s.(v + \lambda.a)\right] = -L.G_1(a, v, \tilde{\theta}, s, \lambda) \tag{F.30}$$

then the equilibrium control:

$$\boxed{\delta_{eq} = \tan^{-1}\left(\frac{-L.G_1(a, v, \tilde{\theta}, s, \lambda)}{v.K_0(\tilde{\theta}, s, \lambda) + d_s(v + \lambda.a)}\right)} \tag{F.31}$$

with the constraint:

$$v.K_0(\tilde{\theta}, s, \lambda) + d_s(v + \lambda.a) \neq 0 \tag{F.32}$$

Noting that if the vehicle is stationary $v = 0 \rightarrow a = 0$ we get a singularity of the system where the steering cannot be derived using the previous controller and in this case we use $\delta_{eq} = 0$.

Several methods are used in the literature to derive the sliding mode control part. To avoid the chattering phenomena which occurs in simpler first order SMC, we use the "Super Twisting" second order algorithm [SU16]. The "Super Twisting" can be seen as a nonlinear version of the classic PI controller, where the sliding control is chosen as:

$$\begin{aligned} &\delta_s = -\gamma_1\sqrt{|\sigma|}sign(\sigma) + c \\ &\text{with: } \dot{c} = -\gamma_0 sign(\sigma) \end{aligned} \tag{F.33}$$

with the constants: $\gamma_1 = U, \gamma_0 = 1.1U$, where $U \in \mathcal{R}_+$ is a constant to be tuned. Finally, given an initial state of the vehicle (s, e_l, θ, v, a) and a goal channel C, the steering control is computed as:

$$\delta = \delta_{eq} + \delta_s \tag{F.34}$$

Parameters Values

G

In the following table we display the values of all the parameters used in this work. This includes both the models and the controllers paramerters.

General Parameters	
Parameter	Value
V_{max}	$5.5m/s$
V_{Pmax}	$6.5m/s$
T_F	$60s$
T_h	$10s$
L	$4m$
W	$2m$
L_V	$4.4m$
W	$2.2m$
R_{ped}	$0.3m$
R_P	$2m$
R_C	$10m$
Φ	[0.449, -0.952, 0.0476, -0.460]
$[\alpha_1, \alpha_2, \alpha_3]$	[0.04, 0.2, 1]
$[\beta_0, \beta_1, \beta_2]$	[1, 0.06, 0.12]
L_H	$10v$
d_s	2
λ	10
U	10